DISSERTATION

ANTIBACTERIAL GROWTH EFFECTS AND SPECIATION OF SEVERAL VANADIUM SALTS AND COMPLEXES

Submitted by

Zeyad Kamal Arhouma

Graduate Degree Program in Cell and Molecular Biology

In partial fulfillment of the requirements

For the Degree of Doctor of Philosophy

Colorado State University

Fort Collins, Colorado

Summer 2023

Doctoral Committee:

Advisor: Debbie C. Crans

Dean Crick
Deborah Roess
Mary Jackson

ABSTRACT

ANTIBACTERIAL GROWTH EFFECTS AND SPECIATION OF SEVERAL VANADIUM SALTS AND COMPLEXES

Vanadium (V) is a first-row transition metal ion that acts as a phosphatase inhibitor with a wide variety of biochemical and physiological functions. The ability of vanadium to form stable polyoxovanadates (POVs) and organometallic complexes has attracted attention for studying the properties and effects of these compounds in various biological systems. In my research, I used the bacterium species *Mycobacterium smegmatis* (*M. smeg*), which has undergone reclassification and is now classified as *Mycolicibacterium smegmatis*. Despite the taxonomic change, both the previous and current classifications use the same abbreviation, *M. smeg*. I also carried out some studies in *Mycobacterium tuberculosis (M. tb).* In my work, I explored the properties of several types of vanadium compounds including salts, oxometalates, and coordination complexes to investigate how they impact cellular growth.

The first chapter of this thesis focuses on determining the growth inhibitory effects of decavanadate (V_{10}) and rapidly exchanging oxovanadates on the growth of two mycobacterial species: *M. tb* and *M. smeg*. Speciation analysis, utilizing ^{51}V NMR spectroscopy, was employed to document that one specific oxometalate exhibits greater potency as a growth inhibitor for these mycobacterial species compared to other oxovanadates, indicating selectivity in its cellular interaction.

Oxometalates have been involved in numerous applications in biological and medical studies, including their ability in addressing the phase-problem in X-ray crystallography of the ribosome. This study investigated the effect of different vanadate salts on the growth of *M. smeg* and *M. tb*, highlighting the critical role of speciation in the observed growth inhibition. Specifically, the large orange-colored sodium decavanadate ($V_{10}O_{28}^{6-}$) anion was found to be a stronger growth inhibitor for these bacteria compared to the colorless oxovanadate derived from sodium metavanadate. The ^{51}V NMR spectroscopy and speciation calculations were employed to monitor the vanadium(V) speciation in the growth media and its conversion among species under growth conditions. Our results show that the decavanadate was 200-20 times more potent in inhibiting growth dependent the consideration of molecules or total vanadium content.

The findings presented in this work are particularly important in the context of the numerous applications of polyoxometalates in biological and medical studies.

The second chapter focuses on investigating the inhibitory effects of two monosubstituted decavanadates (V_{10}): monoplatino(IV)nonavanadate(V) ($[H_2Pt^{IV}V_9O_{28}]^{5-}$, V_9Pt), and by Mo^{IV} in monomolybdo(VI)nonavanadate(V) ($[Mo^{VI}V_9O_{28}]^{5-}$,V_9Mo) on the growth of *M. smeg*. The inhibitory effects of V_9Pt and V_9Mo were examined against the growth of *M. smeg* with EC_{50} values of 0.0048 mM and 0.015 mM, respectively. These values were compared to the reported inhibitory value of decavanadate ($[V_{10}O_{28}]^{6-}$/$[HV_{10}O_{28}]^{5-}$, V_{10}) on *M. smeg* (EC_{50} = 0.0037 mM). Time-dependent ^{51}V NMR spectroscopic studies were carried out for all three polyanions in aqueous solution, biological medium (7H9), and heated and non-heated supernatant. These studies aimed to evaluate their stability in their respective media, monitor their hydrolysis over time to form different oxovanadates, and calculate the corresponding EC_{50} values. The results presented in this study indicate that the two related derived decavanadate derivatives (V_9Pt and V_9Mo) and

V_{10} exhibited greater potency as growth inhibitors of *M. smeg,* compared to monomeric vanadate (V_1). The spectroscopic characterization conducted in the growth medium led to the conclusion that both the decavanadate structure and its properties play significant roles in their growth effects.

In the **third chapter** in this thesis, we investigated the growth effects of an anticarcinogenic non-toxic Schiff base oxidovanadium(V) complex (N-(salicylideneaminato)-N′-(2-hydroxyethyl) ethane-1,2-diamine) coordinated to the 3,5-di-tert-butylcatecholato ligand on a representative bacterium, *M. smeg*.. In addition, we synthesized a series of the Schiff base V-complexes based on previously reported methods and examined the effect of complexes as well as the free catecholates on the bacterial growth. To determine the inhibition activity of these complexes on *M. smeg*., the biological studies were complemented by spectroscopic studies using UV-Vis spectrophotometry and NMR spectroscopy. These spectroscopic studies determine which complexes remained intact under biologically relevant conditions. In this work, we examine (1) the growth effects of Schiff base oxidovanadium complexes coordinated to a catechol, (2) the growth effects of the respective free catecholates on *M. smeg.,* and (3) the effects of the scaffold. These studies allowed us to demonstrate that some metal coordination complex exhibited greater potency than the ligand alone under biological conditions, whereas others showed greater effects of the free catecholate ligand and in one case the effects were similar of complex and catecholate ligand. The findings from these studies revealed that the observed effects of the Schiff base V-catecholate complex were influenced by the properties of the catechol, including toxicity, hydrophobicity, and steric factors.

Finally, the **fourth chapter** of this thesis presents preliminary research data on the antimicrobial effects of two pseudospherical mixed-valence polyoxovanadates (MV-POVs), namely $K(NH_4)_4[H_6PV^{IV}_2V^{V}_{12}O_{42}]\cdot 11H_2O$ (**V_{14}**) and $(Me_4N)_6[V^{IV}_8V^{V}_7O^{36}(Cl)]$ (**V_{15}**) on the growth of *M. smeg*. These MV-POVs showed complex effects on cell growth, as many of these

systems are not stable under biological conditions. To investigate the vanadium(V) speciation in aqueous solutions and growth media, as well as to monitor any conversion among species under growth conditions, ^{51}V NMR spectroscopy was employed. The ^{51}V NMR spectra revealed some hydrolysis and more extensive oxidation of vanadium(IV) in V_{14} compared to V_{15} in both aqueous solutions and media. The studies show that both MV-POVs are effective growth inhibitors.

The combined findings from the studies described in all the chapters of this thesis indicate that the stability of the vanadium compound and its structure plays a significant role in the ability of the vanadium complexes to inhibit bacterial growth. These studies highlight the importance of speciation in the biological activity of vanadium complexes.

ACKNOWLEDGEMENTS

I would like to thank many people for their support and assistance. I wish to thank my advisor **Dr. Debbie C. Crans** for her countless hours of responding, reading, encouraging, and most of all patience throughout the entire process. Your guidance has brought me to this place, and I would not be here without you. A special thanks goes to my committee members who were more than generous with their expertise and advice for doing my PhD study and research.

I would especially like to thank my wife and my children who have been extremely supportive of me throughout this entire process and has made countless sacrifices to help me get to this point. Thank you for being there for me all the time. Additionally, I would especially like to thank my parents, my parents in low, my siblings, my friends deserve special thanks for their continued support and encouragement.

I would also like to thank my lab members for their assistance and for their time for pointing me in the right direction on my projects. I would like to thank Dr. Carol Wilusz, Director, Program in Cell and Molecular Biology for her support and providing any assistance requested.

I want to extend my thanks to my country Libya, University of Benghazi, and my advisor at University of Benghazi Dr. Abdulla Ibrahim for their generous support.

PREFACE

This dissertation thesis was submitted for the degree of Doctor of Philosophy in Cellular and Molecular Biology at the Colorado State University in Fort Collins, CO. The literature reviews and research presented in this document was conducted under the supervision of Dr. Debbie C. Crans in the Chemistry Department, Colorado State University.

The major part of this dissertation thesis is original work and copied from the three papers reported in peer reviewed journals: **1)** Samart N, **Arhouma Z**, Kumar S, Murakami HA, Crick DC, and Crans DC. Decavanadate inhibits mycobacterial growth more potently than other oxovanadates. *Frontiers in chemistry* 2018, (6),519. doi: 10.3389/fchem.2018.00519; **2)** Kostenkova K, **Arhouma Z**, Postal K, Rajan A, Kortz U, Nunes GG, Crick DC, and Crans DC. Pt^{IV}-or Mo^{VI}-substituted decavanadates inhibit the growth of Mycobacterium smegmatis. *Journal of Inorganic Biochemistry*, 2021, 217, 111356; **3)** **Arhouma Z**, Murakami HA, Koehn JT, Li X, Roess DA, Crick DC, and Crans DC. Exploring Growth of *Mycobacterium smegmatis* Treated with Anticarcinogenic Vanadium Compounds. *Inorganics* 2022,10(4):50. https://doi.org/10.3390/inorganics10040050. The 4th chapter is part of a publication that is still to be reported: Postal K, **Arhouma Z**, Feng Z, Li X, Crick DC, Nunes GG, and Crans DC. Speciation studies and growth inhibition of *Mycobacteria* by mixed valence polyoxometalates: phosphotetradecavanadate and chloropentadecavanadate 2023.

DEDICATION

I dedicate my dissertation work to my lovely family, wife and my kids who have been my best supportive during this journey. A special feeling of gratitude to my loving parents, my father Kamal (who passed away and was hoping to attend this moment), my mother Nadia and my wife's family because without them, I would not have reached this place. I also dedicate this dissertation to my siblings and many friends who have supported me throughout my study. I will always appreciate all they have done. Also, my sincere thanks and appreciation to my advisor Dr. Debbie Crans who always believed in me.

TABLE OF CONTENTS

Chapter 3: Exploring Growth of *Mycobacterium Smegmatis* Treated with Anticarcinogenic Vanadium-Compounds

LIST OF TABLES

LIST OF FIGURES

Chapter 1: Decavanadate Inhibits Mycobacterial Growth More Potently Than Other Oxovanadates

1.1. Introduction

Polyoxometalates (POMs) are a class of compounds that have been investigated in a range of biological and biomedical systems, as their effects in cell culture studies and *in vivo* suggest that these compounds have potential for use as therapeutic agents (Moskovitz and Group, 1988; Hill et al., 1990; Rhule et al., 1998; Aureliano and Crans, 2009; Fraqueza et al., 2012; Aureliano et al., 2013, 2016; Wang et al., 2013; Aureliano and Ohlin, 2014; Leon et al., 2014; Kioseoglou et al., 2015; Shah et al., 2015; Sun et al., 2016; Fu et al., 2018; Gumerova et al., 2018).

Decavanadate is a homopolyoxometalate anion, and one of the POMs that has been reported to have known biological effects, as documented by studies reported with cells as well as with isolated enzyme systems. (Pluskey et al., 1996; Aureliano and Crans, 2009; Zhai et al., 2009; Fraqueza et al., 2012; Turner et al., 2012; Aureliano et al., 2013; Kioseoglou et al., 2013; Aureliano, 2014, 2016; Aureliano and Ohlin, 2014). Protein crystal structures have been reported for some protein-POM complexes such as those reported between the ribosome and a Dawson oxometallate (Weinstein et al., 1999; Auerbach-Nevo et al., 2005; Bashan and Yonath, 2008; Noeske et al., 2015). Other protein-POM complexes include protein complexes with smaller oxometalates such as decavanadate (Winkler et al., 2017). The limited stability of decavanadate at neutral pH would suggest that hydrolysis intermediates may form and generate stable complexes with proteins or cellular components. Speciation studies are important in this regard, and different species and possibilities must be considered when investigating the mode of action

of systems that are not thermodynamically stable (Aureliano and Crans, 2009; Levina et al., 2017a). Even if the speciation is characterized, the active species and mode of action of these complex systems can be non-trivial to interpret (Willsky et al., 1984b, 1985, 2011; Delgado et al., 2005; Crans et al., 2011; Postal et al., 2016; Jakusch and Kiss, 2017). However, a wide range of activities have been reported depending on the protein, biological system, or specific vanadium species (Crans, 2000; Crans et al., 2013; Correia et al., 2015; Postal et al., 2016). Recently, it has become clear that compound uptake is critical to the mode of action because many vanadium compounds are modified during the uptake process (Pessoa and Tomaz, 2010; Crans et al., 2011; Le et al., 2017; Levina et al., 2017a). In the case of a large anion such as decavanadate, the question is simply whether the species is too large to enter through protein channels and thus must be taken up through endocytosis or passive transport mechanisms. The alternative possibility is that the uptake is of the smaller vanadium oxovanadates, such as monomeric vanadate, which then oligomerizes to form decavanadate inside the cell. The formation of decavanadate has been demonstrated in yeast (*S. cerevisiae*) and thus makes this anion a desirable system to understand in greater detail (Willsky et al., 1984b, 1985).

Vanadium is a first-row transition metal ion and is in the group of transition metals that can form POMs (Baes, 1976; Chasteen, 1983; Vilas Boas and Costa Pessoa, 1987; Pope and Müller, 1991; Rehder, 1991; Crans et al., 2004, 2017). Vanadium is particularly prone to forming homopolyoxometalate ions as well (Baes, 1976; Aureliano and Crans, 2009). Indeed, pure crystalline metavanadate and orthovanadate upon dissolution will form several oxovanadate species containing vanadate monomer, V_1, vanadate dimer, V_2, vanadate tetramer, V_4, vanadate pentamer, V_5 and decavanadate, V_{10} (Pettersson et al., 1983, 1985; Crans et al., 1990), **Figure 1.1**.

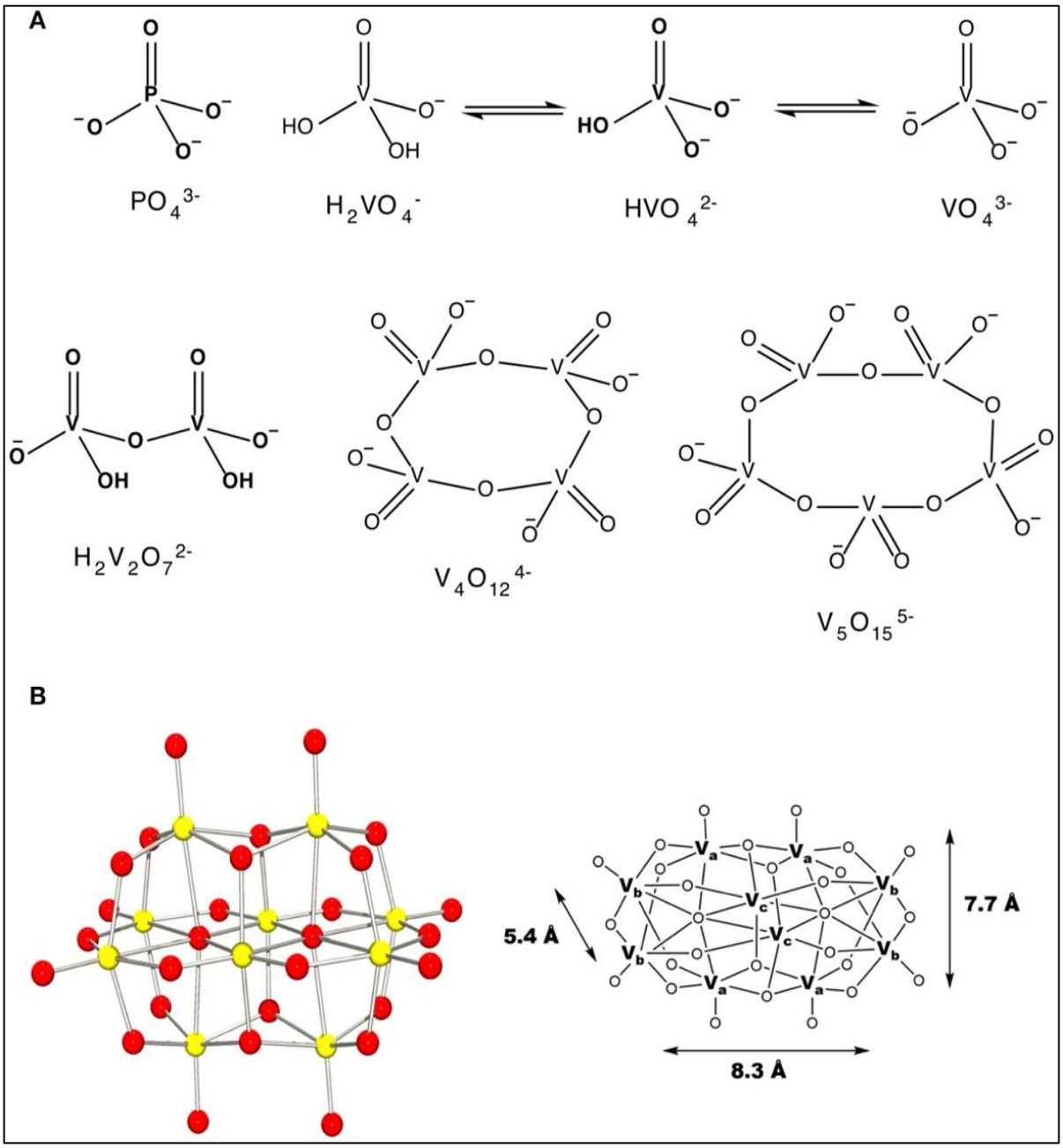

Figure 1.1. The schematic structures of **(A)** monomeric vanadate, monomeric and polymeric vanadate series **(B)** X-ray structure of V_{10} and the three different types of vanadium atoms in this complex ion with indicated dimensions (Evans, 1966). This figure was adapted with permission from Aureliano and Ohlin (2014), Crans et al. (2017).

Some of these species have been characterized using X-ray crystallography and have been found to interconvert in aqueous solution (Evans, 1966; Crans et al., 1990). However, the specifics of the reactions and their conditions vary. For example, vanadate and oligomeric species

containing 2, 4, and 5 vanadium atoms are colorless and rapidly convert at neutral pH, **Figure 1.1A** (Crans et al., 1990). In contrast, decavanadate will form rapidly at acidic pH, but it is only kinetically stable at neutral pH, **Figure 1.1B** (Baes, 1976; Pope and Müller, 1991; Aureliano and Crans, 2009; Crans et al., 2017). Indeed, the kinetic studies have shown that decamer formation is a rapid process and much faster than the $V10$ decomposition in both neutral and basic solution (Clare et al., 1973a,b; Druskovich and Kepert, 1975; Comba and Helm, 1988; Kustin, 2015; Crans et al., 2017). The decomposition pathways investigated follow several different mechanisms and are dependent on the concentrations of H^+ and OH^- and the other counter ions present in solution (Clare et al., 1973a,b; Druskovich and Kepert, 1975; Comba and Helm, 1988; Kustin, 2015).

Information is needed describing how decavanadate interacts with membrane interfaces and cellular systems, including how decavanadates biological activities compare to monomeric vanadate. Specifically, an attractive alternative mode of action to simple decavanadate binding would be the direct delivery of a vanadium atom from decavanadate to a biomolecule resulting in the dissolution of the decavanadate cluster. The X-ray characterization of decavanadate shows that its dimensions are 5.4 Å × 7.7 Å × 8.3 Å, **Figure 1.1** (Evans, 1966), a large size that cannot be accommodated by many biological transport channels. Therefore, any uptake of decavanadate is likely to be through endocytosis or a passive mechanism. An attractive alternative mode of uptake would involve dissolution of the cluster by direct delivery of vanadium atoms, for example, into a system such as a protein. However, such a mechanism is more difficult to investigate and will require more information regarding the potential interactions of the anion with ligands and interfaces. We have been addressing related questions for some time (Crans et al., 2017) and exploring the interactions of $V10$ with interfaces (Baruah et al., 2006; Crans et al., 2006, 2017; Samart et al., 2014; Sanchez-Lombardo et al., 2016). Indeed, more information is needed to be

able to characterize the process of how the decavanadate converts to the vanadate monomer and smaller clusters, but such processes undoubtedly involve the molecular association of structures that form in solution.

The work presented in this manuscript compares the effect of decavanadate and oxovanadates on two mycobacterial species. The results of this comparison are related to the questions of uptake of vanadate and will form the background information on which it will be possible to begin to address issues regarding potential delivery of V-atoms as well as uptake of decavanadate compared to monomeric and oligomeric vanadate.

Mycobacteria are particularly resistant to hydrophilic drug penetration, and thus studies with these organisms are of general interest. There have been several studies documenting the possibility that vanadium may affect growth of the bacteria, whether in a stimulatory of inhibitory manner; however, these studies did not consider the speciation of the studied compounds in growth media and in the biological context of the cells. For example, previous studies have been carried out investigating the effects of the simple salt vanadate on the cell growth of mycobacteria in the presence and absence of Tween-80 (Costello and Hedgecock, 1959). These studies investigated the possibility that vanadium may be stimulatory to growth because it would be able to replace Fe^{2+} , Fe^{3+} , or biologically active Mo-atoms (Turian, 1951). Dose response curves reported in cultures in the presence of added metavanadate gave complete growth inhibition observed at 5.0 μg/mL V-atom for *M. tb* (H37Rv), at 10 μg/mL V-atom for *Mycobacterium butyricum*, at 50 μg/mL V-atom for *Mycobacterium phlei*, but even at 200μg/mL V-atom *M. smeg* was not completely inhibited (Costello and Hedgecock, 1959).

Additionally, studies have been carried out on vanadium coordination complexes and their effect on the growth of mycobacteria (Maiti and Ghosh, 1989; David et al., 2005; Correia et al.,

2014; Gajera et al., 2015). The studies explore the possibility that a known drug, or drug derivative complexes binding to vanadium, may exert a greater synergetic activity (Correia et al., 2014; Gajera et al., 2015). For example, in a series of hydroxyquinoline (Correia et al., 2014), fluoroquinoline (Gajera et al., 2015) and acid hydrazides (Martins et al., 2015) vanadium(V) complex studies, the complexes were found with micromolar inhibitory potency against *M. tb*. In other systems the vanadium complex was found to have little if any effect on the growth of the bacterium (Maiti and Ghosh, 1989; Gajera et al., 2015). Additionally, a series of vanadium thiosemicarbazone and hydroquinoline complexes tested against *M. tb* were found to have micromolar inhibition constant against growth, but the ligand was more potent than the complex (Correia et al., 2014; Gajera et al., 2015). In these cases, complexation to the vanadium protected the bacterium. Combined these studies demonstrate that vanadium compounds may be inhibitory or protective, depending on the environment and ligands that may be complexed to it, and thus it is of interest to investigate the effects of simple vanadium complexes prior to formation of a coordination complex.

In this work, we determine the effects of decavanadate and the rapidly exchanging oxovanadates on the growth of two mycobacterial species: *Mycobacterium tuberculosis* mc^2 6230 (*M. tb*) and *Mycobacterium smegmatis* mc^2 155 (*M. smeg*). It is important to note that the bacterium *M. smeg* which was previously characterized as a mycobacterium has been reclassified as a Mycolicibacterium. Both classifications, however, use the abbreviation *M. smeg* (Ghielmetti and Giger, 2020; Scalese et al., 2022; Yamada et al., 2018). These studies directly compare the effects of the two vanadium salt species and in doing so, will allow researchers to address the issue of whether such oxometalate species exert different effects, possibly due to uptake or conversion of the salt under physiological conditions. In our studies with *M. smeg* and *M. tb*, it was discovered

that decavanadate undergoes hydrolysis forming monomeric vanadate in the presence of the cells, suggesting some type of interaction with the bacterial cells or with the material excreted by the bacterial cells. Comparison of metavanadate and decavanadate demonstrates that these two oxovanadate species have very different effects on the growth of these mycobacterial species and depending on species, the potency varies.

1.2. Materials and Methods

1.2.1. Materials

Sodium metavanadate (99.9% $NaVO_3$) was purchased from Sigma-Aldrich, hydrochloric acid (36.5–38%, HCl) and citric acid (99% $C_6H_8O_7$) were purchased from Fischer. Deuterium oxide (D_2O, 99.9%) was purchased from Cambridge Isotope Laboratories, Inc. All reagents and other chemicals were purchased from Sigma-Aldrich. Vanadium complexes were prepared according to literature (Samart et al., 2014; Sanchez- Lombardo et al., 2016).

1.2.2. Preparation of Stock Solutions for NMR Spectroscopy Evaluation

1.2.2.1. Vanadate

Colorless stock solutions of sodium metavanadate ($NaVO_3$, 100 mM) were prepared in deuterium oxide (D_2O). The suspension was heated to dissolve the solid, the solution was cooled to room temperature and then the pH was measured (~ pH 7–8) (Crans et al., 1990).

1.2.2.2. Decavanadate

An orange-red solution of sodium decavanadate ($Na_6V_{10}O_{28}$, 100 mM) was prepared from $NaVO_3$ (1.00 M, 1.22 g). Sodium metavanadate solutions were prepared directly by addition of solid $NaVO_3$ to D_2O and heating the solution to dissolve the solid. Once the solution was clear, the pH was adjusted to 4.5–5.8 using 6 M DCl (DCl was prepared from 12 M HCl by the addition of D_2O) resulting in an orange-colored solution. The V_{10} content in this solution was verified using

^{51}V NMR spectroscopy and assuming the vanadium was all present as V(V) the concentration of each oxovanadate could be calculated from the integration of the spectra (Crans et al., 1990).

1.2.2.3. Citric Acid and V-Citrate Complex Solutions

Stock solutions of citric acid (100 mM, pH 2.33) were prepared in deuterium oxide (D_2O). The vanadium-citrate complexes were prepared by adding equimolar amounts of citric acid and vanadium. The solution was diluted to form solutions with 75, 50, 10, and 5.0 mM vanadium(V).

1.2.2.4. Preparation of Stock Solution to Cell Culture Studies

Stock solutions of vanadate and vanadium complexes were prepared in double distilled water (DI H_2O), 7H9 media or in 100% DMSO depending on the solubility of these complexes. Specifically, metavanadate, orthovanadate or decavanadate were prepared in double distilled water. Isoniazid (INH) was dissolved in sterile distilled water and used as a positive control.

1.2.3. Nuclear Magnetic Resonance (NMR) Measurements

All ^{51}V NMR spectroscopy measurements were taken on a Bruker spectrometer at 78.9 MHz for ^{51}V (400 MHz for ^{1}H). The chemical shifts were obtained using external reference for ^{51}V NMR of Na_3VO_4 (100 mM, pH 12.9, signals at −535 (V_1) and −559 ppm (V_2)). The samples were prepared fresh to form vanadium-citrate complexes in media and the composition was investigated as a function of time with experiments carried out at time points: 0, 1, 5, and 24 h.

Speciation of vanadium was calculated using the integration of the vanadium peak(s) within the ^{51}V NMR spectra. The concentration of each species was determined using the known added concentration [assuming all vanadium is in the form of V(V)] (Crans et al., 1990), the integration of the vanadium peak(s) in the spectrum and by using the mole fractions for each signal, the concentration of each species could be calculated as shown in **Table 1.1**.

Table 1.1. Formation constants of Vanadate species in a 0.6M NaCl system.

(p, q)	log β	Formula	Extended formula
BINARY SYSTEM (H^+-$H2VO_4^-$) REF (2)			
−1, 1	−7.92	HVO_4^{2-}	$(H^+)_{-1}(H_2VO_4^{2-})$
−2, 2	−15.17	$V_2O_7^{4-}$	$(H^+)_{-2}(H_2VO_4^{2-})_2$
−1, 2	−5.25	$HV_2O_7^{3-}$	$(H^+)_{-1}(H_2VO_4^{2-})_2$
0, 2	2.77	$H_2V_2O_7^{2-}$	$(H_2VO_4^{2-})_2$
−2, 4	−8.88	$V_4O_{13}^{6-}$	$(H^+)_{-2}(H_2VO_4^{2-})_4$
−1, 4	0.22	$HV_4O_{13}^{5-}$	$(H^+)_{-1}(H_2VO_4^{2-})_4$
0, 4	10.0	$V_4O_{12}^{4-}$	$(H_2VO_4^{2-})_4$
0, 5	12.4	$V_5O_{15}^{5-}$	$(H_2VO_4^{2-})_5$
4, 10	52.1	$V_{10}O_{28}^{6-}$	$(H^+)_4(H_2VO_4^{2-})_{10}$
5, 10	58.1	$HV_{10}O_{28}^{5-}$	$(H^+)_5(H_2VO_4^{2-})_{10}$
6, 10	61.9	$H_2V_{10}O_{28}^{4-}$	$(H^+)_6(H_2VO_4^{2-})_{10}$
7, 10	63.5	$H_3V_{10}O_{28}^{3-}$	$(H^+)_7(H_2VO_4^{2-})_{10}$
2, 1	6.96	VO_2^+	$(H^+)_2(H_2VO_4^{2-})_{10}$
(p, q, r)	**log β**	**Formula**	**Extended formula**
TERNARY SYSTEM (H^+-$H_2VO_4^{2-}C_6H_5O_7^{3-}$) REF (3)			
1, 0, 1	5.217	Cit^{2-}	$(H^+)(Cit^{3-})$
2, 0, 1	9.298	Cit^-	$(H^+)_2(Cit^{3-})$
3, 0, 1	12.067	Cit	$(H^+)_3(Cit^{3-})$
1, 2, 1	12.84	$(H^+)(H_2VO_4^{2-})_2(Cit^{3-})$	
2, 2, 1	19.68	$(H^+)_2(H_2VO_4^{2-})_2(Cit^{3-})$	
3, 2, 1	24.12	$(H^+)_3(H_2VO_4^{2-})_2(Cit^{3-})$	
3, 1, 1	18.35	$(H^+)_3(H_2VO_4^{2-})(Cit^{3-})$	
2, 1, 1	14.1	$(H^+)_2(H_2VO_4^{2-})(Cit^{3-})$	
4, 2, 2	31.3	$(H^+)_4(H_2VO_4^{2-})_2(Cit^{3-})_2$	
5, 2, 2	35.3	$(H^+)_5(H_2VO_4^{2-})_2(Cit^{3-})_2$	
6, 2, 2	39.2	$(H^+)_6(H_2VO_4^{2-})_2(Cit^{3-})_2$	
(p, q, r)	**log β**	**Formula**	**Extended formula**

(p, q)	log β	Formula	Extended formula
TERNARY SYSTEM (H^+-$H_2VO_4^{2-}$ $H_2PO_4^-$) REF (4)			
−2, 0, 1	−17.650	POO_4^{3-}	$[(H^+)_{-2}(H_2PO_4^-)]^{3-}$
−1, 0, 1	−6.418	$H\ PO_4^{2-}$	$[(H^+)_{-1}(H_2\ PO_4^-)]^{2-}$
1, 0, 1	1.772	H_3PO_4	$[(H^+)(H_2\ PO_4^-)]$
9, 14, 1	90.7	$H_3PV_{14}O_{42}^{6-}$	$[(H^+)_9\ (H_2VO_4^{2-})_{14}\ (PO_4^-)]^{6-}$
10, 14, 1	94.84	$H_4PV_{14}O_{42}^{5-}$	$[(H^+)_{10}\ (H_2VO_4^{2-})_{14}\ (H_2\ PO_4^-)]^{5-}$
11, 14, 1	96,41	$H_5PV_{14}O_{42}^{4-}$	$[(H^+)_{11}\ (H_2VO_4^{2-})_{14}\ (H_2\ PO_4^-)]^{4-}$

1.2.4. Speciation Analysis

The interpretation of the ^{51}V NMR spectral data was supplemented by speciation calculations based on constants measured previously (Pettersson et al., 1983; Ehde et al., 1989; Selling et al., 1994). The species distribution diagrams were calculated by using HySS 2009 software (Alderighi et al., 1999; Carsella et al., 2017) and known speciation constants of the system at hand (Pettersson et al., 1983; Ehde et al., 1989; Selling et al., 1994). The citrate and the phosphate concentrations found in the Middlebrook 7H9 broth medium supplemented with 5% BSA, 2% dextrose, 5% catalase (ADC) enrichment, glycerol (0.2%, v/v), and Tween 80 (0.05%, v/v) were 0.48 and 24 mM, respectively (Bbl*tm*, 2018).

The vanadium concentrations that were investigated were concentrations of 5, 3.3, and 10 mM. The speciation diagrams were constructed using the following equilibrium reactions for the binary H^+-$H_2VO_4^{2-}$ system [see equation (1)] (Pettersson et al., 1983), and two ternary system, H^+-$H_2VO_4^{2-}$-$C_6H_5O_7^{3-}$ and H^+-$H_2VO_4^{2-}$-$H_2PO_4^-$ [see equation (2) (Ehde et al., 1989) and (3) (Selling et al., 1994)]. The alternate formulas were provided in the format of the equations provided for comparison.

$$p\mathrm{H^+} + q\mathrm{H_2VO_4^-} \leftarrow (\mathrm{H^+})_p(\mathrm{H_2VO_4^{2-}})_q$$

(Pettersson et al., 1983) (1)

$$\mathrm{pH^+ + qH2VO_4^{2-} + rC6H5O_7^{3-} \leftarrow (H^+)p(H_2VO_4^{2-})q(C_6H5O_7^{3-})_r}$$

(Ehde et al., 1989) (2)

$$\mathrm{pH{+}{+}qH_2VO_4^{2-}{+}rH_2PO_4^- \leftarrow [(H^+)_p(H_2VO_4^{2-})_q(H_2PO_4^-)_r]^{p-q-r}}$$

(Selling et al., 1994) (3)

As described previously, the equations above describe the nature of the complexes that form. For example, HVO_4^{2-} is described as $H_2VO_4^-$ minus H^+ and thus the species is described as (−1,1) where the p being −1 (Pettersson et al., 1983; Ehde et al., 1989).

1.2.5. Bacterial Strains and Culture Conditions

M. smeg were grown in 7H9 Middlebrook Medium supplemented with 0.2% (v/v) glycerol, 10% ADC, 0.05% Tween-80, and incubated at 37°C with shaking for 24 h. The growth of bacteria was monitored to mid-logarithmic growth phase using a spectrophotometer at 600 nm to an optical density of 0.6 (OD_{600nm}) (Bbl^{tm}, 2018). Metavanadate (40 mM, pH 8.6) and decavanadate [100 mM V_{10} (1.0 M V-atoms), pH 3.8] stock solutions and the media with bacteria were added to a 96 well plate in a 3-fold dilution experiment monitored at times 0, 1, 5, and 24 h. The pH of these samples ranged from 5.5 to 6.3 before and after treatment with V-compounds and growth; see spectra for in supplemental for details (Upadhyay et al., 2015).

Culture supernatant after cell growth generated for ^{51}V NMR analysis was prepared by running separate growth experiments for the *M. smeg* experiments with a total volume of 5 mL. At each time point, a 1 mL aliquot was removed for NMR analysis. ^{51}V NMR spectra were run at the time points 0, 1, 5, and 24 h without lock.

M. tb is a nonpathogenic deletion mutant (ΔRD1 ΔpanCD) strain H37Rv that can safely be used in a Biosafety Level 2 conditions (Sambandamurthy et al., 2006). The bacteria were grown in 7H9 Middlebrook medium with the addition of D-pantothenate (24 mg/L) at 37°C to an optical density at 600 nm (OD_{600nm}) of 0.6–0.8. The cultures were diluted and treated with the appropriate metavanadate and decavanadate stock solutions in a 96 well plate in a 3-fold dilution experiment and incubated at 37°C for the duration of the experiment (5–7 days). The pH values of these samples ranged from 5.6 to 6.8 after growth for 5 days; see spectra for details.

^{51}V NMR spectra were acquired on culture supernatant without lock (no D_2O in sample) at the beginning and end of the bacterial growth experiment (0 and 5 days) for *M. tb* growth samples.

1.3. Results

Investigating the effects of both vanadate and decavanadate on mycobacterial growth requires information on the speciation of vanadium under the conditions of the growth assay studies. *M. tb* and *M. smeg* were grown in supplemented Middlebrook 7H9 medium. Some of the components of the medium may form vanadium complexes. The major candidates for complex formation based on literature formation constants are phosphate (Gresser et al., 1986), citrate (Pettersson et al., 1985; Levina et al., 2017a), and amino acids (Crans, 2000; Rehder et al., 2002; Esbak et al., 2009). In the following, we investigated whether these complexes formed in the media, **Figure 1.1**.

1.3.1. Reaction of Vanadate and Decavanadate With Components in Growth Media

^{51}V NMR studies were carried out with vanadate and decavanadate solutions and Middlebrook 7H9 broth medium supplemented with 10% ADC enrichment (5% BSA, 2% dextrose, 5% catalase), glycerol (0.2%, v/v) and Tween 80 (0.05%, v/v). The mycobacteria grow well at pH 6.8, and decavanadate is known to form between pH 3 to 6.5 (Pope and Müller,

1991; Crans et al., 2004; Baruah et al., 2006; Aureliano and Crans, 2009). V_{10} is formed at low pH values and the V_{10} hydrolyzes at neutral pH. When V_{10} is added to the growth media the pH was increased from pH 7.6 to 6.5/7 by the buffering capacity of the growth media and there is a potential for hydrolysis of V_{10}. Importantly, little hydrolysis is observed in growth media in the absence of mycobacteria. NMR spectra were recorded at a range of pH values because the reactions of vanadate are very sensitive to pH (see **Appendix I; Figure A1.S1**); however, the spectra shown in **Figures 1.2** and **1.3** are those of direct relevance to observation and assignment of the species that form in the growth media. Importantly, all the spectra are referenced against a reference sample (labeled Ref. in **Figure 1.3**, containing 100 mM Na_3VO_4).

In **Figure 1.2**, we show the spectra of decavanadate under various conditions. First, we show the spectrum of the stock solution at pH 3.1 with the three characteristic signals for the three different V-atoms in the V_{10} molecule. Next, we show two spectra with added citrate at two concentrations at pH 2.8 and 2.2 where the decavanadate will form VCit complex (two signals at −548 and −552 ppm). The next three spectra at higher pH values are shown first in the presence of phosphate (P_i), demonstrating that the signals for V_{10} shifts as the pH increases from 3 to 6.9. As shown in the final two spectra in **Figure 1.2**, V_{10} in the presence of media that contains both citrate and P_i did not form any other V-products when all V-atoms are in the form of V_{10}.

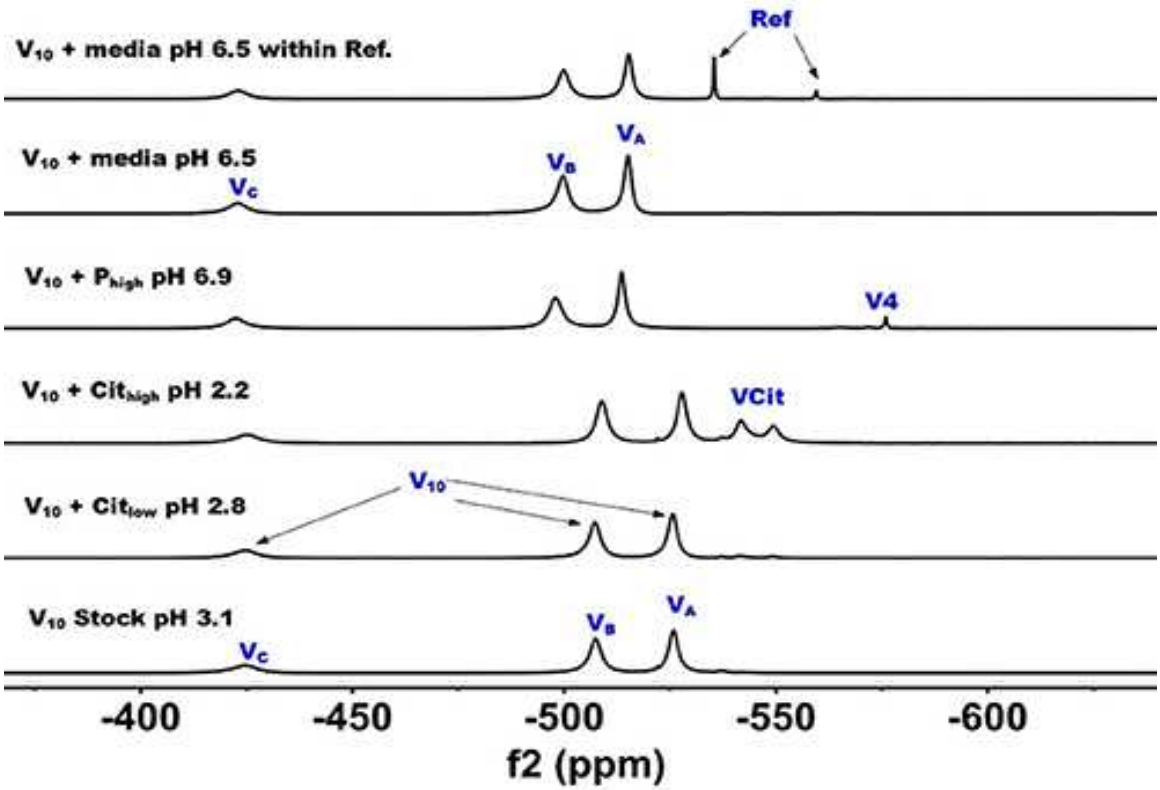

Figure 1.2. ^{51}V NMR (78.9 MHz) spectra are shown of solution of decavanadate (10 mM V_{10}, 100 mM V-atoms). The samples are from the bottom up diluted V_{10} stock solution (100 mM V-atom) at pH 3.1; 10 mM V_{10} in the presence of 0.48 mM and 0.97 mM citrate at pH 2.8 and 2.2, respectively; 10 mM V_{10} in the presence of 24 mM Pi at pH 6.9; and finally 10 mM V10 in the presence of Middlebrook 7H9 broth medium supplemented with 10% ADC enrichment (5% BSA, 2% dextrose, 5% catalase), glycerol (0.2%, v/v) and Tween 80 (0.05%, v/v) recorded both in the absence and the presence of a capillary reference of 100 mM Na_3VO_4.

The spectrum of V_{10} in media is shown both in the presence and absence of a capillary tube filled with Na_3VO_4 and used to reference the spectra (**Figure 1.2**). All the NMR spectra were referenced in this manner and the other NMR spectra are provided in Appendix I (**Figure A1.S2 and A1.S3**). In summary, these spectra shown that when vanadium is present in the form of V_{10}, other vanadium species do not form in the cell media.

The spectra shown in **Figure 1.2** demonstrated that the V_{10} is stable in the growth media, which is consistent with studies in yeast media reported previously (Willsky et al., 1984a, 1985). The data shown in **Figure 1.2** demonstrated that at pH 2, the V_{10} forms complexes with citrate but as the pH increased to near neutral pH, V_{10} did not form such products with growth media

components (Ehde et al., 1989; Zhou et al., 1999; Crans, 2000; Kaliva et al., 2002, 2003; Chen et al., 2007, 2014; Lodyga-Chruscinska et al., 2008).

In contrast, when V_{10} is converted to the oxovanadates or V_1 is the starting form at vanadium, the VCit and PV complexes are formed (this is generally observed in solutions at neutral or more basic pH values, **Figure 1.3**). However, if the pH of the growth media decreases (that is the acidity increase and pH value decrease), V_{10} hydrolyzes and forms oxometalates that are able to react with media components (see **Figures 1.2, 1.3**).

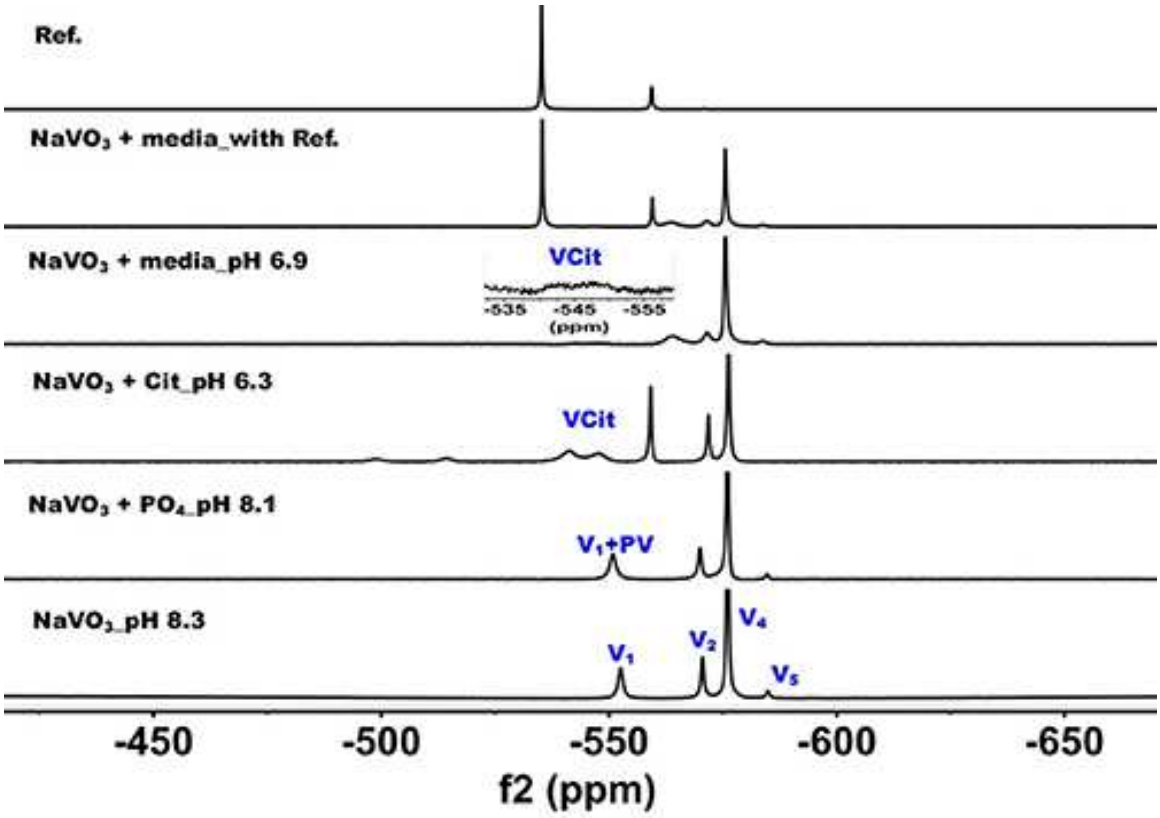

Figure 1.3. ^{51}V NMR (78.9 MHz) spectra are shown of solution of colorless oxovanadate (40 mM V_1, 40 mM V-atoms). The samples are from the bottom up diluted V_1 stock solution (40 mM V-atom) at pH 8.3; 10 mM V_{10} in the presence of 24 mM P_i at pH 8.1; 10 mM V_{10} in the presence of 0.48 mM citrate at pH 6.3, and finally 10 mM V_{10} in the presence of Middlebrook 7H9 broth medium supplemented with 10% ADC enrichment (5% BSA, 2% dextrose, 5% catalase), glycerol (0.2%, v/v) and Tween 80 (0.05%, v/v) recorded both in the absence and the presence of a capillary reference of 100mM Na_3VO_4. The spectrum labeled Reference is of the capillary reference alone (top spectrum). The key to the signals: V-oligomers, V_1 monomer; V_2, dimer; V_4, tetramer; V_5, pentamer; VCit, V-citrate complex; PV, vanadate-phosphate complex.

The spectra of solutions from metavanadate ($NaVO_3$) containing vanadate monomer and other oxovanadates prepared in aqueous solution and in media are shown in **Figure 1.3**. Since vanadate solutions contain rapidly converting species (Crans et al., 1990) and the composition depends on pH and concentration, the species present is dependent on the solution composition. The first spectrum shows a solution containing the interconverting oxovanadates, V_1, V_2, V_4, and V_5. In the presence of P_i and at slightly lower pH value, the V_1 signal shifted and the linewidth increased, which is indicative of the formation of a vanadate-phosphate complex (abbreviated PV on the spectra in **Figure 1.2**) (Gresser et al., 1986; Andersson et al., 2005). Although there are no X-ray structures for these species, the Gresser-Tracey team proposed that there is both a vanadium species that is four or five-coordinate and octahedral based on the chemistry shifts). The formation of the PV species (Gresser et al., 1986; Andersson et al., 2005) is rapid on the NMR time scale, and thus results in shifting of the vanadate monomer (V_1) signal in place of observing two separate signals one for V_1 and one for PV. As the pH decreased to 6.3, V_1 protonates and the monomer signal shifts to about−560 ppm.

At these higher pH values, the VCit complex is found to form in solutions containing both V_1 and citrate. Many different VCit complexes are known, however, the broad doublet signal observe for the VCit could be several structures as described in the literature (Ehde et al., 1989; Zhou et al., 1999; Crans, 2000; Kaliva et al., 2002, 2003; Chen et al., 2007, 2014; Lodyga-Chruscinska et al., 2008). The final spectra show the addition of the vanadate stock solution to media, which at pH 6.9 results in a solution that contains a signal of V_1 and PV, V_2, and V_4 and a trace of V_5. The amount of VCit formed is low and it is difficult to see the signal from in the normal growth media spectrum, so we used an increased amplification to show the VCit signal and part of such spectrum is shown in the spectral insert.

In summary, if the growth of the mycobacteria is conducted near pH 6.8, the speciation of vanadium (V) will readily reach thermodynamic control. Solutions prepared from $NaVO_3$ will contain little to no V_{10} and solutions containing V_{10} will be relatively stable. Therefore, growth studies will be carried out with either V_1 or V_{10} species, and it will be possible to determine if there is a difference in the growth effects on mycobacteria by these two species. That is the growth effects of the V_1 with the oligomeric oxovanadates and V_{10} are measured in media with known vanadium speciation and under conditions where it is possible to observe the effect of each species.

1.3.2. Growth Inhibition Experiments of Vanadate Monomer and Decavanadate

Growth inhibition experiments were designed to measure the effects of V_{10} and V_1 each on *M. tb* mc^2 6230 and *M. smeg* mc^2 155. The measurements monitor growth using absorbance at 600 nm and the concentration of the vanadium compound was changing with 3-fold dilution experiments. In this manner, the growth of the bacteria was measured over a 2,000-fold range of concentrations of vanadium compound and the results with the *M. tb* are shown in **Figure 1.4**, and the EC_{50} (concentration of compound where growth is reduced by half) value calculated for the V_1 experiment was 2.0 mM (2.0 mM V-atoms) and for the V_{10} experiment 29 μM (0.29 mM V-atoms, **Table 1.2**).

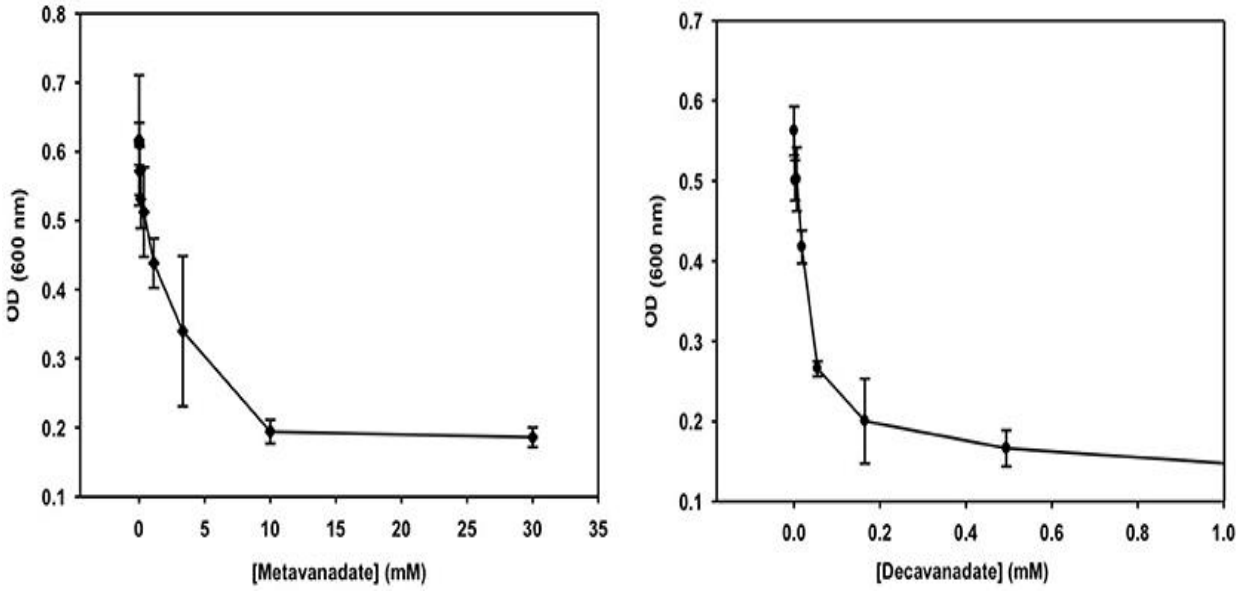

Figure 1.4. The growth curve is shown for treatment with vanadate (left, prepared from a 40 mM colorless metavanadate solution) and decavanadate [right, prepared from a 100 mM orange decavanadate solution (1.0 M V-atoms) on *M. tb*]. Data in all panels represent error bars of the standard deviation for triplicate measurements.

Table 1.2. The EC_{50} values for V_1 and V_{10} treated *Mycobacterium tuberculosis* and *smegmatis*.

	EC50 (*M. tb*) (mM)	**Stand. error**	**EC50 (*M. tb*) (mM V-atoms)**	**Stand. error**	**EC50 (*M. smeg*) (mM)**	**Stand. error**	**EC50 (*M. smeg*) (mM V-atoms)**	**Stand. error**
V_1	2.0	0.43	2.0	0.43	0.19	0.07	0.19	0.07
V_{10}	0.029	0.005	0.29	0.05	0.0037	0.0004	0.037	0.004

These results show that V_{10} is a more potent inhibitor than V_1 by a factor of 100 in terms of concentration and a factor of 10 in terms of concentration of V-atoms. This result demonstrates that the large V_{10} anion is more inhibitory than the V_1 atom even when counting for the fact that there are 10 V-atoms in each V_{10} species. As discussed below, ^{51}V NMR spectroscopy was used to examine the speciation in the solutions and verify that the V_{10} solution indeed contained V_{10} (see below for details).

The growth effects were also measured for *M. smeg* mc^2 155 for both V_{10} and V_1 (data not shown). Similarly, the EC_{50} values were calculated for the V_1 experiment to be 190 μM (0.190

mM V-atoms) and for the V_{10} experiment to be 3.7 μM (0.037 mM V-atoms). These results show that the V_{10} is a more potent inhibitor than V_1, by a factor of 50 in terms of concentration and a factor of 10 in terms of concentration of V-atoms as we also observed for *M. tb*.

These results present evidence that the large compact V_{10}-anion is a stronger inhibitor than V_1 of cell growth of the two mycobacterial strains. The more potent inhibition by V_{10} compared to V_1 shows that the V_{10} is an inhibitor, and that it is not V_1 formed from hydrolyzed V_{10}. However, it should be mentioned that it is solutions of V_{10} that are causing the inhibitory growth effect, and we cannot rule out the possibility that the effect is caused by several species including the hydrolysis products, or some mechanism in which V_{10} delivers the V-atom to the cells. Regardless, these studies demonstrate the effects of simple oxovanadates and the large decavanadate. The fact that V_{10} has a greater effect than V_1 (or 10 V_1 molecules) supports the interpretation that the growth effects observed are not due to V_1 formed from hydrolyzed V_{10}. To support this interpretation, we acquired the ^{51}V NMR spectra of the growth media solutions at various times during the growth experiment.

1.3.3. Speciation Studies in Media of Mycobacteria Treated with Vanadate and Decavanadate

1.3.3.1. ^{51}V NMR Spectra of Media That Have Grown Mycobacteria and Have Been Treated with Metavanadate

^{51}V NMR spectra were recorded at several concentration and time-points in the growth media in which *M. smeg* had grown because as mentioned above the bacteria were subjected to a 2000-fold concentration range. In **Figure 1.5**, we show the ^{51}V NMR spectra recorded at 3.3 mM and 10 mM oxometalates, respectively. Both these series show the presence of the different oxometalates (V_1, V_2 and V_4). In addition, neither series show any evidence for change as the experiment proceeded. This is somewhat surprising, because experiments with other cellular

systems, such as yeast, fungi and red blood cells, all showed significant signs of signal reduction (Willsky et al., 1984b, 1985; Crans et al., 2002; Delgado et al., 2005; Jakusch et al., 2014). Since the V_1 or oxovanadate is not a strong inhibitor of growth, it is possible that the simple vanadate system is not getting into the *M. smeg* cells very effectively.

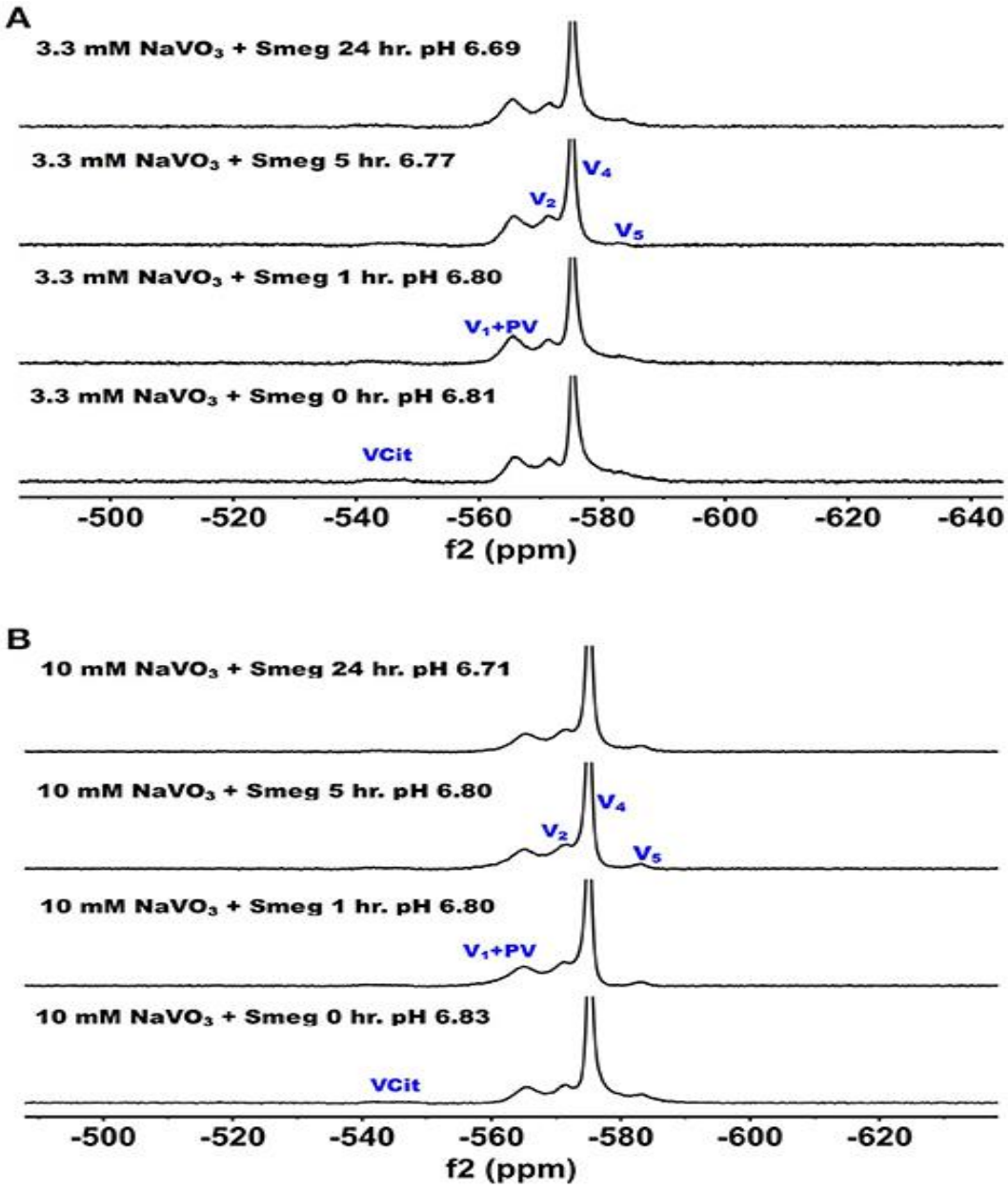

Figure 1.5. The ^{51}V NMR spectra of media in which *M. smeg* had grown at 0, 1, 5, and 24 h time points. Data for two concentrations are shown in **(A)** 3.3 mM V_1 treatment (3.3 mM V-atoms) and **(B)** 10 mM V_1 treatment (10 mM V-atoms). See Figure 3 caption for key to labeling.

1.3.3.2. ^{51}V NMR Spectra of Media in Which Mycobacteria Have Been Treated with Decavanadate

^{51}V NMR spectra were recorded at several concentrations and time-points in the growth media in which *M. smeg* had grown. In **Figure 1.6**, we show the ^{51}V NMR spectra recorded at 3.3 and 10 mM, respectively.

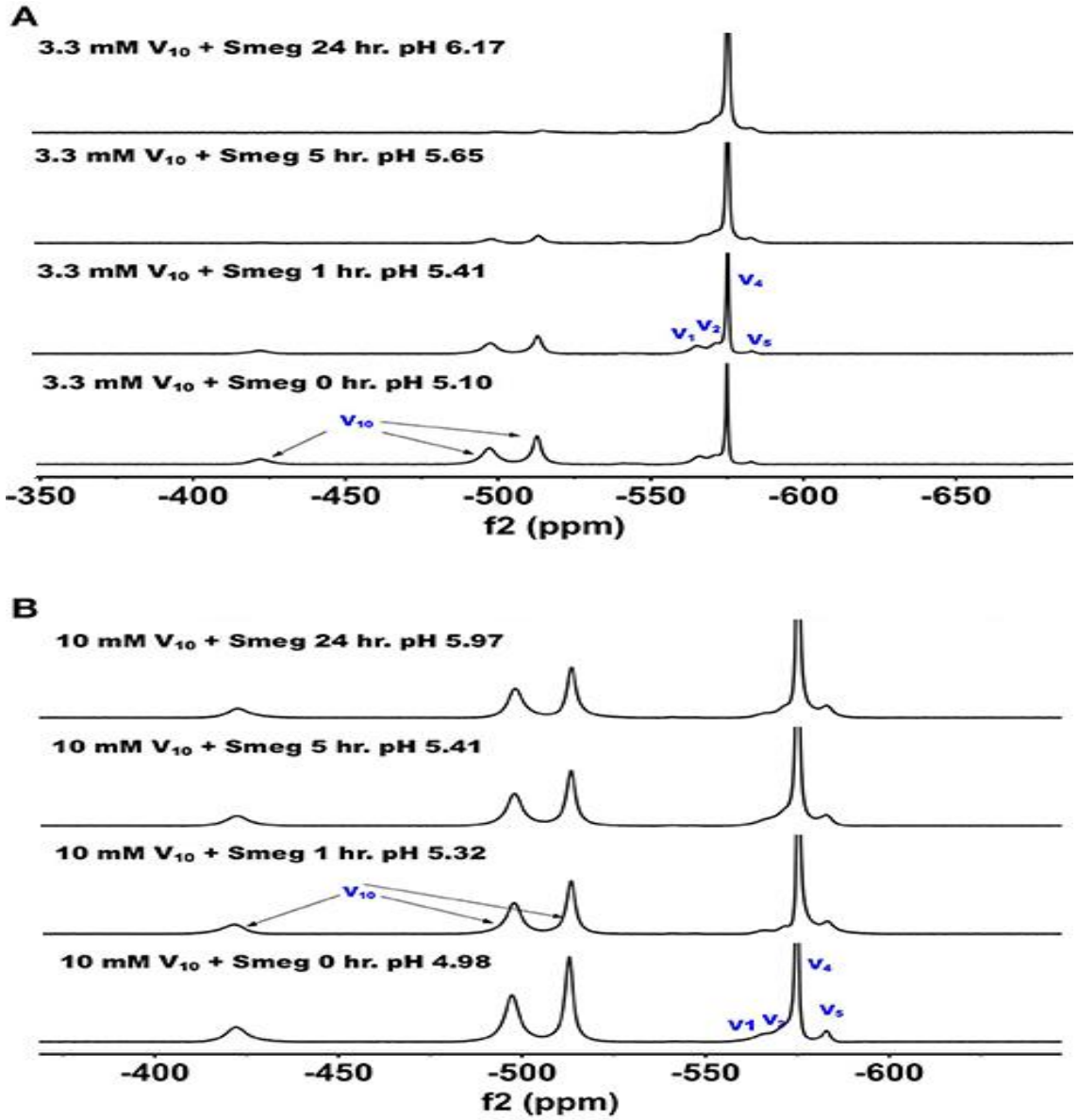

Figure 1.6. The ^{51}V NMR spectra of media in which *M. smeg* had grown at 0, 1, 5, and 24 hr time points. Data for two concentrations are shown in (A) 3.3 mM V_{10} treatment (33 mM V-atoms) and (B) 10 mM V_{10} treatment (100 mM V-atoms).

Both series show the presence of V_{10}. Although the stock solutions and growth media without bacterial cells contains 100% V_{10} (**Figure 1.2**), the addition of growth media containing cells immediately caused some decomposition of V_{10} (**Figure 1.6**).

NMR spectra were recorded multiple times of the 3.3 mM V and resulted in approximately a 1:1 ratio of V_{10} to oxovanadates as determined by integration of the spectra. As shown in **Figure 1.6**, after 1 h the composition of the sample was very similar to the content at the beginning of treatment, whereas at the 5 h time point the V_{10} had decreased significantly and at 24 h very little was left. This demonstrates that the V_{10} is not stable in the media in the presence of the *M. smeg* cells at 33 mM total V-atom concentration even though the pH is between 5.8 and 6.8 which is a pH range where there should not have been any hydrolysis of V_{10} according to the known solution chemistry of V_{10}. However, V_{10} treatment may cause signal reduction, or the V(V) may interact with large structural components in the mycobacterial cells (or their excretion products) and the ^{51}V NMR signal has broadened beyond detection. Precedent for these possibilities has been reported previously (Willsky et al., 1984b, 1985; Crans et al., 2002). In the series of spectra at 10 mM V_{10} in the media, there is less evidence for V_{10} removal is apparent at the different time points. However, when we integrated the signals a slow decrease in the V_{10} signals compared to the oxovanadate signals was clear. The ratio at time zero was 1:0.71, at time 1 h it was 1:1.08; at time 5 h it was 1:1.18 and at 24 h it was 1:1.24. Thus, providing evidence for a slow decrease in V_{10} content as the experiment progressed. This data is consistent with the possibility that there is some reduction of the vanadium from the POM resulting in hydrolysis and formation of the oxovanadates.

To further investigate whether there was any reduction taking place upon vanadium treatment, **Table 1.3** showed the color change in these samples.

Table 1.3. Samples treated with V_{10} and V_1 in 7H9 media, *M. smeg* cultures and supernatant after *M. smeg*. Growth (columns 2, 3, and 4). The yellow or orange V_{10} is shown from the left with 10 and 3.3 mM samples, and the colorless V_1 samples from the left 10 and 3.3 mM in each column. When reduction took place, the green color is evident [vanadium (IV)]. See Appendix I for the pH values of each of these samples (**Figure A1.S4, A1.S5, A1.S6, and Table A1.S1**)

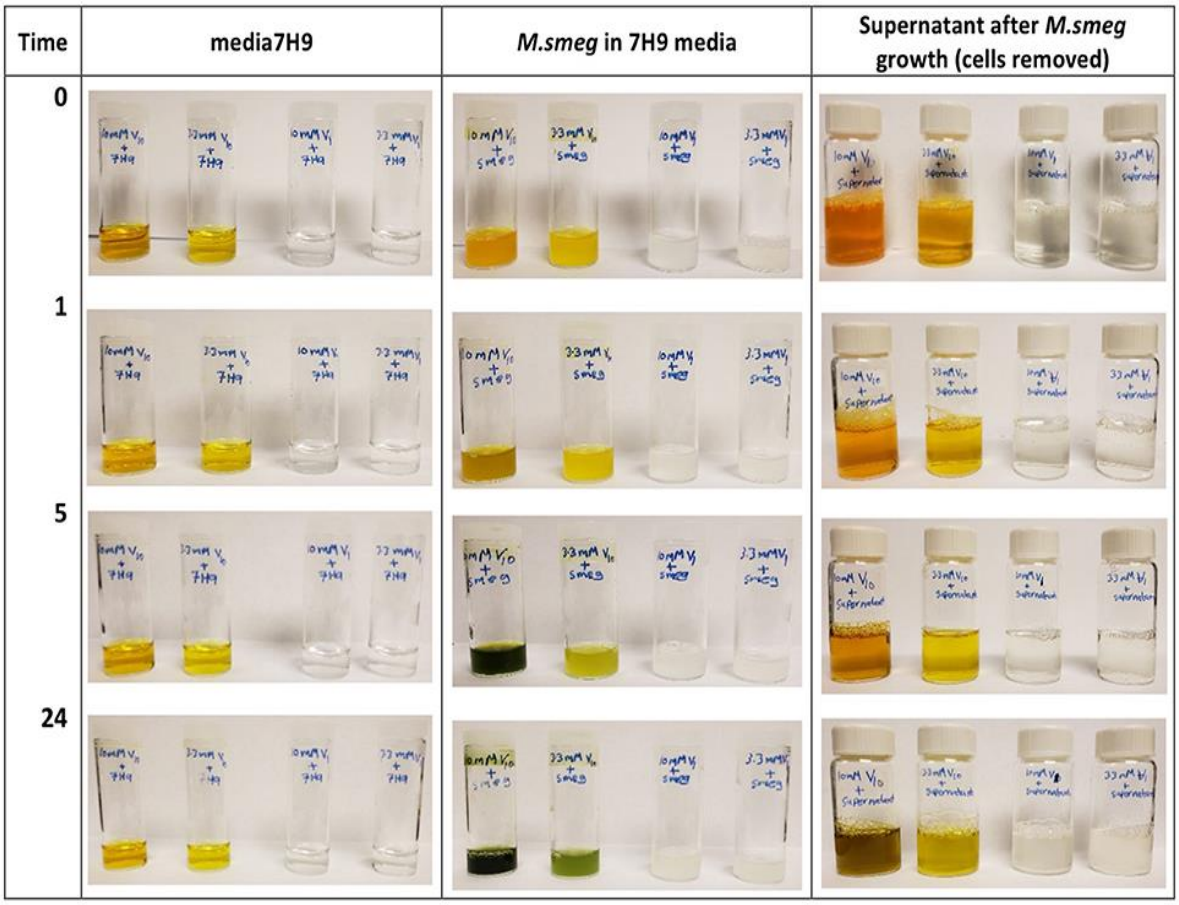

More data and the pH measurements on all the samples shown are provided in Appendix I (**Table A1.S1**), and the pH values are all in the range from 6.1 to 7.4. Vanadium(V) on reduction is known to change from colorless (V_1 oxovanadates) or yellow/orange (V_{10}) to a green color (Crans et al., 2004, 2010, 2013; Pessoa and Tomaz, 2010; Jakusch et al., 2014). The 7H9 media alone did not cause any reduction as evidenced by the media sample maintained the color prior to treatment, **Table 1.3**. All the samples containing media and *M. smegmatis* treated with V_{10} developed a greenish tint as the treatment progressed beyond 5 h time points, whereas the samples treated with V_1 remained colorless, see **Table 1.3**. This is consistent with reduction of

some of the V(V) in the V_{10} salt. Interesting, similar reduction was not observed for the samples treated with the V_1 solutions. These observations are consistent with the selective reduction of the V(V) and that the reduction was more prevalent after longer treatments, higher concentrations of vanadium and V_{10} compared to V_1. Since the reduction only took place in the presence of V_{10}, this anion induced a response that was not induced by V_1. Furthermore, the supernatant of a batch of grown *M. smeg*. bacteria and centrifuging down the bacteria and removing them was collected to investigate if the bacteria excrete a component responsible for the observed reduction. The V_{10} and V_1 samples were added to this supernatant and the data are shown in column 4 in **Table 1.3**. This supernatant also generates the color change from orange to green upon incubation.

This experiment showed that the reduction is something that was induced by a material excreted from the *M. smeg*. cells during growth. This suggest that the reduction is likely to come from the excretion of siderophores (Hider and Kong, 2010) or proteins such as the reported protein tyrosine phosphatases from mycobacteria (Beresford et al., 2009; Dutta et al., 2016). Since we also carried out such studies of supernatant that had been heated (see supplemental material), such a product is either a very heat stable protein or a siderophore-type of material.

Combined these studies show that there is selectivity in the effects of interactions of vanadium with mycobacteria, and that for these systems the most effective form is not the V_1, which is a potent phosphatase inhibitor and a common active form of vanadium. These studies show that the V_{10}, a POM is more potent inhibitor of growth of mycobacteria than the well-known phosphatase inhibitor, V_1. The studies also demonstrate that there is some redox chemistry involved in this process and that the mycobacteria excrete a component that interact with V_{10} and cause the redox chemistry and hydrolysis of the V_{10}. Eventually the V_1 samples would also show

the color change consistent with reduction, but this required growth periods beyond several weeks and this process may be different than the reduction, of V_{10}.

1.3.3.3. Modeling Speciation Vanadium Species Distribution in Mycobacteria Media Added Metavanadate

To quantify the V-species that are present in the growth assay media, we carried out speciation analyses modeling experimentally the distribution of vanadium species in the media. This analysis is based on analyzing solutions containing V-species that are governed by thermodynamics and can be calculated the HySS program (Alderighi et al., 1999). This model can analyze the experimental conditions found in solution prepared by the addition of metavanadate and exposed to the conditions of the cell growth assay. We used the reactions reported previously with regard to the exchange of labile oxovanadates (Pettersson et al., 1983, 1985; Gresser et al., 1986; Ehde et al., 1989; Crans et al., 1990, 2000; Crans, 2000, 2005; Andersson et al., 2005; Baruah et al., 2006; Aureliano and Crans, 2009), the formation of the Vcit complex (Ehde et al., 1989; Crans, 2000), the formation of the PV complex (Gresser et al., 1986; Andersson et al., 2005), and the thermodynamics relating to the decavanadate deprotonation reactions (Crans, 2005; Baruah et al., 2006; Aureliano and Crans, 2009). The known speciation parameters used for vanadate at various pH values were measured in the presence of 0.6 M NaCl to keep the salt concentration constant for all the components in the system. As shown in **Figure 1.5**, the species composition for the conditions of three different concentrations of vanadium (0.0050, 3.3, and 10 mM) are illustrated. As discussed above, the vanadium samples prepared with decavanadate will not contain this speciation distribution because all V(V) was converted to V_{10}. The addition of this solution to the media will only slowly hydrolyze the V_{10} species to the equilibrium oxovanadate mixture if above or near pH 7.

The speciation analysis of the conditions observed in the media with freely exchangeable oxovanadate shown in **Figure 1.3** demonstrate that an observable amount of VCit complex forms. Depending on the concentration of the vanadium, the contribution of VCit is larger percentage-wise at the lower concentrations of vanadate; for example, at 0.005 and 1.0 mM V-atoms at neutral pH the amount is 75–80% (in terms of mole fraction) of VCit complex. In contrast, at 10 mM V-atoms at neutral pH the amount is ~10%. However, if the amounts are calculated, this would correspond to 0.0004, and 1.0 mM VCit complex in the media. These observations are consistent with the very strong formation constant for VCit. The PV complex, however, is much less stable, and even though there is much more phosphate in the assay, the PV complex is only observed in a significant concentration at high V and P_i concentrations (5 and 24 mM, respective). Although the PV complex is only observed in high concentrations at mM V-treatments the shifting of the V_1 signal attests to the presence of the PV adduct in the assays with *M. tb* and *M. smeg*.

The results shown in **Figure 1.7** are in general agreement with the experimental data obtained in **Figures 1.2, 1.3, 1.5, 1.6** with regard to formation of the VCit and PV complexes. **Figure 1.7** shows that there are four different VCit complexes formed at low vanadium concentration, but at higher concentration and in the presence of phosphate two major VCit complexes formed. There are several assumptions on which these estimations are based, including the differences in ionic strengths, the low concentration of the vanadium used, and the fact that some reduction takes place during the growth experiment to be changing the concentrations somewhat of the VCit and PV complexes. Regardless, our general considerations demonstrate that VCit and PV complexes should form as predicted by the speciation analysis (Pettersson et al., 1983; Ehde et al., 1989; Selling et al., 1994) and reflect the equilibrium mixture observed by NMR analysis.

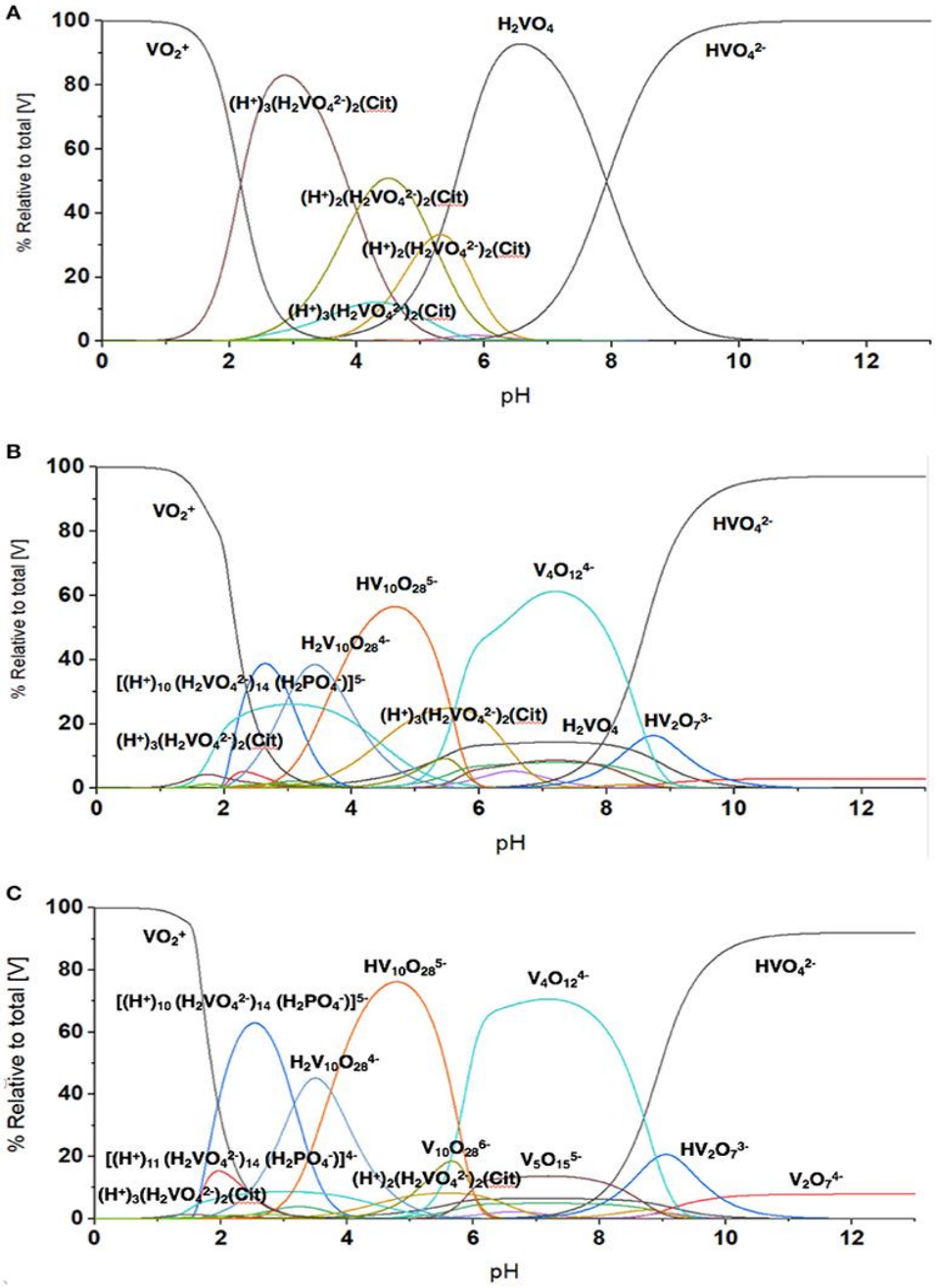

Figure 1.7. The evaluation of the speciation at different vanadium concentration using HySS Program (vs. 2009) (Alderighi et al., 1999). The speciation diagram shown was calculated at several vanadium (V-atom) concentrations in the presence of 0.48 mM citrate and 24 mM phosphate found in the growth media and **(A)** 5.0 μM vanadate, **(B)** 3.3 mM vanadate, and **(C)** 10 mM vanadate. Note, the concentrations of different species regardless of nuclearity are here shown in terms of V-atoms.

1.4. Discussion

Vanadium derivatives have been considered as therapeutic agents since 1899 (Lyonnet et al., 1899; Crans et al., 2018). Recent studies demonstrate that vanadium compounds and salts are effective antidiabetic agents (Sakurai, 2002; Thompson and Orvig, 2006; Kiss et al., 2008; Smith et al., 2008; Thompson et al., 2009; Willsky et al., 2011, 2013; Crans, 2015; Trevino et al., 2015; Boulmier et al., 2017; Levina and Lay, 2017b) but their therapeutic properties have been expanded for these materials to be anticancer agents (Lu and Zhu, 2011; Leon et al., 2017; Medina et al., 2017; Crans et al., 2018), immunotherapy agents (Lu and Zhu, 2011; Selman et al., 2018) as well as treatment for other diseases (Zwolak, 2014; Pessoa et al., 2015).

Many of the compounds are coordination complexes, which form vanadate during processing after administration (Thompson et al., 2009; Willsky et al., 2011). Considering the ease with which vanadium undergoes redox chemistry (Crans et al., 2010), it is known that some of the vanadium is converted from V(V) to lower oxidation states upon administration (Thompson et al., 2009; Willsky et al., 2011). Furthermore, studies were carried out on the salts prior to investigation of coordination complexes (Sakurai et al., 1990; Goldfine et al., 2000; Willsky et al., 2001, 2013; Smith et al., 2008). The biological activity of homo-oxovanadates have been of considerable interest considering the varied biological effects depending on the specific vanadium species (Sakurai et al., 1990; Willsky et al., 2001; Postal et al., 2016). Information on cellular uptake by vanadium species is of interest, and the studies presented here compare the effect of monomeric vanadate and decavanadate. Such direct comparison is important to understand the interconversion between these species, and despite the many reports in the literature (reviewed in Aureliano and Crans, 2009), no similar study showing data for direct comparison between the two different species have been reported.

Cellular studies have been reported in different types of organisms that consider the uptake of vanadate. Willsky reported studies with yeast (Willsky et al., 1984b, 1985; Crans et al., 2002), and concluded that V_1 was the species entering the cells; however, upon entry processing took place; forming decavanadate in the lysosomes, and forming V(IV) through redox processes. The treatment of the yeast cells with vanadate solutions containing mainly vanadate monomer and oligomers is evidenced by ^{51}V NMR spectroscopy and EPR spectroscopy. These studies were very elegant and truly important, because they documented the formation of decavanadate in cells from monomeric vanadate for the first time (Willsky et al., 1984b).

Recently, Zakrzewska and Zivic reported a series of studies in fungi exploring the uptake of both vanadate and V(IV) using ^{51}V and EPR spectroscopy, as well as polarographic studies (Zizic et al., 2013, 2016; Hadzibrahimovic et al., 2017). The initial ^{51}V NMR studies on *Phycomyce blakesleeanus* mycelium were supplemented with polarography, which allowed for the assignment of the signal at −535 ppm accumulating inside the fungi cells to V_1 even though the pH of the system was defined by HEPES buffer at 7.2 where V_1 generally has a peak position at a higher frequency (Zizic et al., 2016). The authors attribute the signal shifting to intracellular complexation of V_1. Alternatively, these observations are consistent with a hydrophobic environment having been reported in some cases to alter composition and speciation and impact the shifting of observed signals. Combined, these studies showed convincingly that the cell wall is not responsible for reduction of vanadate (Hadzibrahimovic et al., 2017) and these studies also confirm that tetrameric vanadate is not able to enter the cells (Zizic et al., 2016) as reported in yeast as well (Crans et al., 2002) (Willsky et al., 1984a,b.)

Cellular studies in mammalian systems have also been carried out, and many of these studies are linked to the stability and speciation of vanadium compounds in blood (Delgado et al.,

2005; Zhang et al., 2006; Li et al., 2009; Jakusch et al., 2011, 2014; Willsky et al., 2013; Sanna et al., 2014, 2017; Jakusch and Kiss, 2017). Although bacterial cells do not contain blood, they do infect mammals and thus the vanadium chemistry in blood is relevant to bacterial infections as well. These studies include detailed investigations into various complexes, and projections based on studies in model systems what would be observed in mammalian systems and *in vivo*. Although such studies remain model studies, they are important because they begin to provide a view of how it will look like in the *in vivo* cells. Studies were also reported by Garner and coworkers using ^{1}H NMR spin echo and ^{51}V NMR spectroscopy to characterize the uptake of vanadate and subsequent reduction to form V(IV) in erythrocytes (Garner et al., 1997). The reduction of the vanadate was attributed to glutathione as demonstrated in a time-dependent response using both ^{51}V NMR and ^{1}H spin echo NMR (Garner et al., 1997). The addition of the blocking agent 4,4′-diisothio-cyanatostilbene-2,2b-disulfonic acid (DIDS) specifically blocks the anion transporter preventing the vanadate from entering the erythrocytes. Adding the blocker prevented vanadate entering, and the depletion of glutathione was arrested. Thus, depletion of intracellular gluthathione could be correlated with entering vanadate and the authors proposed that the reduced vanadium [presumably V(IV)] formed complexed with cellular components, because no or little V(IV) formed (Garner et al., 1997).

These studies stand in direct contrast to studies in which decavanadate is associated with proteins and have been characterized by X-ray crystallography (Winkler et al., 2017). However, consideration of both solution and solid state is necessary to characterize both the effects of decavanadate and simple oxovanadates. The studies shown here demonstrate three important findings. First, the fact that decavanadate is a potent inhibitor of growth of two mycobacterial species and more so than monomeric vanadate, which is a known potent phosphatase inhibitor

(Crans, 2015; Mclauchlan et al., 2015). Indeed, phosphatase inhibition has recently been reported by V_{10} of the Leishmania acid phosphatase as well as earlier reports (Aureliano and Crans, 2009; Dorsey et al., 2018). Second, the fact that monomeric vanadate is not as potent inhibitor for *M. tb and M. smeg*. Third, these studies also demonstrate that under conditions in which the decavanadate would remain stable, in the presence of *Mycobacterium* spp. the decavanadate undergoes hydrolysis. These combined observations suggest that some type of mechanism that involves the bacterium (or something excreted by the bacterium) interacting with the decavanadate and causes the conversion to oxovanadates. This is particularly interesting because similar response is not observed in the media without bacteria.

1.5. Conclusion

The studies presented demonstrate that decavanadate (V_{10}) inhibits the growth of two mycobacterial species, *M. tb* and *M. smeg*, whereas the oxovanadates prepared from $NaVO_3$ inhibit growth with 10-100-fold less potency. The inhibition was observed in media containing citrate and phosphate, resulting in the formation of a VCit complex and PV complexes. However, neither of these complexes appeared to interfere with the observed inhibition for V_{10} and the inhibition by V_1 was still 10-100-fold less. The greater inhibitory selectivity of V_{10} (or a component of V_{10}) result is important because it demonstrates that simple vanadium salts can have different effects on cells, and that a vanadium compound other than the potent phosphatase inhibitor, monomeric vanadate (V_1), can inhibit growth. Importantly, these studies suggest that other oxometalates may have the ability to inhibit growth of mycobacteria and other pathogens.

In addition, these studies demonstrated that mycobacteria or some component excreted by the mycobacteria which catalyzes the hydrolysis of V_{10} and the same effect was not observed in media in the absence of growing cells. This process is particularly interesting because it implies that the

V_{10} interacts with some cell component, possibly through some mechanism involving V_{10} delivering a V-atom to such a cell component. This type of mechanism is novel and further investigation into such process will be of general interest and important for the mode of action of POMs in biological systems.

1.6. References

Alderighi, L., Gans, P., Ienco, A., Peters, D., Sabatini, A., and Vacca, A. (1999). Hyperquad simulation and speciation (HySS): a utility program for the investigation of equilibria involving soluble and partially soluble species. *Coor. Chem. Rev.* 184, 311–318. doi: 10.1016/S0010-8545(98)00 260-4

Andersson, I., Gorzsas, A., Kerezsi, C., Toth, I., and Pettersson, L. (2005). Speciation in the aqueous H+/H_2 VO_4 -H+2 O_2 /phosphate system. *Dalton Trans.* 22, 3658–3666. doi: 10.1039/b508273k

Auerbach-Nevo, T., Zarivach, R., Peretz, M., and Yonath, A. (2005). Reproducible growth of well diffracting ribosomal crystals. *Acta Crystallogr. Sec. D.* 61, 713–719. doi: 10.1107/S0907444905006311

Aureliano, M. (2014). Decavanadate contribution to vanadium biochemistry: *in vitro* and *in vivo* studies. *Inorg. Chim. Acta* 420, 4–7. doi: 10.1016/j.ica.2013.10.010

Aureliano, M. (2016). Decavanadate toxicology and pharmacological activities: V-10 or V-1, both or none? *Oxid. Med. Cell Longev*. 2016:6103457. doi: 10.1155/2016/6103457

Aureliano, M., and Crans, D. C. (2009). Decavanadate (V_{10} O_{28}^{6-}) and oxovanadates: oxometalates with many biological activities. *J. Inorg. Biochem.* 103, 536–546. doi: 10.1016/j.jinorgbio.2008.11.010

Aureliano, M., Fraqueza, G., and Ohlin, C. A. (2013). Ion pumps as biological targets for decavanadate. *Dalton Trans.* 42, 11770–11777. doi:10.1039/c3dt50462j

Aureliano, M., and Ohlin, C. A. (2014). Decavanadate *in vitro* and *in vivo* effects: facts and opinions. *J. Inorg. Biochem.* 137, 123–130. doi: 10.1016/j.jinorgbio.2014.05.002

Aureliano, M., Ohlin, C. A., Vieira, M. O., Marques, M. P. M., Casey, W. H., and De Carvalho, L. (2016). Characterization of decavanadate and decaniobate solutions by Raman spectroscopy. *Dalton Trans.* 45, 7391–7399. doi: 10.1039/C5DT04176G

Baes, C. F. (1976). *The Hydrolysis of Cations.* New York, NY: John Wiley & Sons. Baruah, B., Roden, J. M., Sedgwick, M., Correa, N. M., Crans, D. C., and Levinger, N. E. (2006). When is water not water? Exploring water confined in large reverse micelles using a highly charged inorganic molecular probe. *J. Am. Chem. Soc.* 128, 12758–12765. doi: 10.1021/ja0624319

Bashan, A., and Yonath, A. (2008). The linkage between ribosomal crystallography, metal ions, heteropolytungstates and functional flexibility. *J. Mol. Struct.* 890, 289–294. doi: 10.1016/j.molstruc.2008.03.043

Bbl^{tm}, D. (2018). “Middlebrook 7H9 Broth • Middlebrook 7H9 Broth with Glycerol. Middlebrook 7H9 Broth with Polysorbate 80. Middlebrook ADC Enrichment.” 2nd ed).

Beresford, N., Mulhearn, D., Szczepankiewicz, B., Liu, G., Johnson, M. E., Fordham-Skelton, A., et al. (2009). Inhibition of MptpB phosphatase from Mycobacterium tuberculosis impairs mycobacterial survival in macrophages. *J. Antimicrob. Chemother.* 63. 928–936. doi: 10.1093/jac/dkp031

Boulmier, A., Feng, X. X., Oms, O., Mialane, P., Riviere, E., Shin, C. J., et al. (2017). Anticancer activity of Polyoxometalate-Bisphosphonate complexes: synthesis, characterization, *in vitro* and *in vivo* results. *Inorg. Chem.* 56, 7558–7565. doi: 10.1021/acs.inorgchem.7b01114

Carsella, J. S., Sánchez-Lombardo, I.;, Bonetti, S. J., and Crans, D. C. (2017). Selenium speciation in the Fountain Creek Watershed correlates with water hardness, Ca and Mg levels *Molecules* 22, 708, 1–16. doi: 10.3390/molecules22050708

Chasteen, N. D. (1983). “The biochemistry of vanadium,” in *Copper, Molybendum, and Vanadium in Biological Systems*, eds M. J. Clarke, J. B. Goodenough, J. A. Ibers, C. K. Jørgensen, D. M. P. Mingos, J. B. Neilands, G. A. Palmer, D. Reinen, P. J. Sadler, R. Weiss, and R.J.P. Williams (New York, NY: Springer-Verlag), 105–138. doi: 10.1007/BFb0111304

Chen, C. Y., Chen, M. L., Chen, H. B., Wang, H. X., Cramer, S. P., and Zhou, Z. H. (2014). alpha-Hydroxy coordination of mononuclear vanadyl citrate, malate and S-citramalate with N-heterocycle ligand, implying a new protonation pathway of iron-vanadium cofactor in nitrogenase. *J. Inorg. Biochem.* 141, 114–120. doi: 10.1016/j.jinorgbio.2014.08.003

Chen, C. Y., Zhou, Z. H., Mao, S. Y., and Wan, H. L. (2007). Asymmetric dinuclear hydroxyl and ethoxyl citrato dioxovanadates(V). *J. Coord. Chem.* 60, 1419–1426. doi: 10.1080/00958970601 029420

Clare, B. W., Kepert, D. L., and Watts, D. W. (1973a). Acid decompositon of decavanadate-specific salt effects. *J. Chem. Soc., Dalton Trans.* 22, 2481–2487.

Clare, B. W., Kepert, D. L., and Watts, D. W. (1973b). Kinetic study of the acid decomposition of decavanadate. *J. Chem. Soc. Dalton Trans.* 22, 2479–2487. doi: 10.1039/dt9730002479

Comba, P., and Helm, L. (1988). The solution structure and reactivity of decavanadate. *Helv. Chim. Acta* 71, 1406–1420. doi: 10.1002/hlca.19880710605

Correia, I., Adão, P., Roy, S., Wahba, M., C., M., Maurya, M. R., Marques, F., et al. (2014). Hydroxyquinoline derived vanadium(IV and V) and copper(II) complexes as potential anti-tuberculosis and anti-tumor agents. *J. Inorg. Biochem.* 141, 83–93. doi: 10.1016/j.jinorgbio.2014.07.019

Correia, I., Roy, S., Matos, C. P., Borovic, S., Butenko, N., Cavaco, I., et al. (2015). Vanadium(IV) and copper(II) complexes of salicylaldimines and aromatic heterocycles: Cytotoxicity:

DNA binding and DNA cleavage properties. *J. Inorg. Biochem.* 147, 134–146. doi: 10.1016/j.jinorgbio.2015.02.021

Costello, R. L., and Hedgecock, L. W. (1959). Effect of metavanadate ion on the growth *in vitro* of mycobacterium tuberculosis. *J. Bacteriol.* 77, 794–799.

Crans, D., Yang, L., Haase, A., and Yang, X. (2018). Health benefits of Vanadium and its potential as an anticancer agent. *Met. Ions Life Sci.* 18, 251–279. doi: 10.1515/9783110470734-015

Crans, D. C. (2000). Chemistry and insulin-like properties of vanadium(IV) and vanadium(V) compounds. *J. Inorg. Biochem.* 80, 123–131. doi: 10.1016/S0162-0134(00)00048-9

Crans, D. C. (2005). Fifteen years of dancing with vanadium. *Pure Appl. Chem.* 77, 1497–1527. doi: 10.1351/pac200577091497

Crans, D. C. (2015). Antidiabetic, chemical, and physical properties of organic Vanadates as Presumed transition-state inhibitors for Phosphatases. *J. Org. Chem.* 80, 11899–11915. doi: 10.1021/acs.joc.5b02229

Crans, D. C., Bedi, H. S., Li, S., Zhang, B., Nomiya, K., Kasuga, N. C., et al. and Willsky, G.R. (2002). "Tetravanadate, decavanadate, Keggin and Dawson oxotungstates inhibit growth of S. cerevisiae" in *Polyoxometalate Chemistry for Nano-Composite Design, [Symposium]* (Honolulu, HI), 181–195.

Crans, D. C., Peters, B. J., Wu, W., and Mclauchlan, C. C. (2017). Does Anion- Cation Organization in Na+-containing X-ray crystal structures relate to solution interactions in inhomogeneous nanoscale environments: Sodium- decavanadate in solid state materials, minerals and microemulsions. *Coord. Chem. Rev.* 344, 115–130. doi: 10.1016/j.ccr.2017.03.016

Crans, D. C., Rithner, C. D., Baruah, B., Gourley, B. L., and Levinger, N. E. (2006). Molecular probe location in reverse micelles determined by NMR dipolar interactions. *J. Am. Chem. Soc.* 128, 4437–4445. doi: 10.1021/ja0583721

Crans, D. C., Rithner, C. D., and Theisen, L. A. (1990). Application of time-resolved 51V 2D NMR for quantitation of kinetic exchange pathways between vanadate monomer, dimer, tetramer, and pentamer. *J. Am. Chem. Soc.* 112, 2901–2908. doi: 10.1021/ja0016 4a009

Crans, D. C., Smee, J. J., Gaidamauskas, E., and Yang, L. Q. (2004). The chemistry and biochemistry of vanadium and the biological activities exerted by vanadium compounds. *Chem. Rev.* 104, 849–902. doi: 10.1021/cr020607t

Crans, D. C., Trujillo, A. M., Pharazyn, P. S., and Cohen, M. D. (2011). How environment affects drug activity: localization, compartmentalization and reactions of a vanadium insulin-enhancing compound, dipicolinatooxovanadium(V). *Coord. Chem. Rev.* 255, 2178–2192. doi: 10.1016/j.ccr.2011.01.032

Crans, D. C., Woll, K. A., Prusinskas, K., Johnson, M. D., and Norkus, E. (2013). Metal speciation in health and medicine represented by iron and vanadium. *Inorg. Chem.* 52, 12264–12275. doi: 10.1021/ic4007873

Crans, D. C., Yang, L. Q., Jakusch, T., and Kiss, T. (2000). Aqueous chemistry of ammonium (dipicolinato)oxovanadate(V): the first organic vanadium(V) insulin-mimetic compound. *Inor. Chem.* 39, 4409–4416. doi: 10.1021/ic9908367

Crans, D. C., Zhang, B., Gaidamauskas, E., Keramidas, A. D., Willsky, G. R., and Roberts, C. R. (2010). Is Vanadate reduced by thiols under biological conditions? Changing the redox potential of V(V)/V(IV) by complexation in aqueous solution. *Inor. Chem.* 49, 4245–4256. doi: 10.1021/ic100080k

David, S., Barrosa, V., Cruzb, C., and Delgado, R. (2005). *In vitro* effect of free and complexed indium(III) against Mycobacterium tuberculosis. *FEMS Microbiol. Lett.* 251, 119–124. doi: 10.1016/j.femsle.2005.07.044

Delgado, T. C., Tomaz, A. I., Correia, I., Pessoa, J. C., Jones, J. G., Geraldes, C. F., et al. (2005). Uptake and metabolic effects of insulin mimetic oxovanadium compounds in human erythrocytes. *J. Inorg. Biochem.*, 99, 2328–2339. doi: 10.1016/j.jinorgbio.2005.08.014

Dorsey, B. M., McLauchlan, C. C., and Jones, M. A. (2018). Evidence that speciation of oxovanadium complexes does not solely account for inhibition of Leishmania Acid Phosphatases. *Front. Chem.* 8:109. doi: 10.3389/fchem.2018.00109

Druskovich, D. M., and Kepert, D. L. (1975). Base decomposition of decavanadate. *J. Chem. Soc. Dalton Trans.* 22, 947–851. doi: 10.1039/dt9750000947

Dutta, N. K., He, R., Pinn, M. L., He, Y., Burrows, F., Zhang, Z.- Y., et al. (2016). Mycobacterial protein tyrosine phosphatase A and B inhibitors augment the bactericidal activity of the standard anti- tuberculosis regimen. *ACS Infect. Dis.* 2, 231–239. doi: 10.1021/acsinfecdis.5b 00133

Ehde, P., Andersson, I., and Pettersson, L. (1989). Multicomponent polyanions. 43. A study of aqueous equilibria in the vanadocitrate system. *Acta Chem. Scand.* 43, 136–143. doi: 10.3891/acta.chem.scand.43-0136

Esbak, H., Enyedy, E. A., Kiss, T., Yoshikawa, Y., Sakurai, H., Garribba, E., et al. (2009). Aminoacid-derivatised picolinato-oxidovanadium(IV) complexes: characterisation, speciation and *ex vivo* insulin-mimetic potential. *J. Inorg. Biochem.* 103, 590–600. doi: 10.1016/j.jinorgbio.2008.11.001

Evans, H. T. Jr. (1966). The molecular structure of the isopoly complex ion, decavanadate ($V_{10}O^{6-}$). *Inorg. Chem.* 5, 967–977. doi: 10.1021/ic50040a004 28

Fraqueza, G., De Carvalho, L., Marques, M. P. M., Maia, L., Ohlin, C. A., Casey, W. H., et al. (2012). Decavanadate, decaniobate, tungstate and molybdate interactions with sarcoplasmic reticulum Ca2+-ATPase: quercetin prevents cysteine oxidation by vanadate but does not reverse ATPase inhibition. *Dalton Trans.* 41, 12749–12758. doi: 10.1039/c2dt31688a

Fu, D. Y., Zhang, S. M., Qu, Z. Y., Yu, X. H., Wu, Y. Q., and Wu, L. X. (2018). Hybrid assembly toward enhanced thermal stability of virus-like particles and antibacterial activity of Polyoxometalates. *ACS Appl. Mater. Interf.* 10, 6137–6145. doi: 10.1021/acsami.7b17082

Gajera, S. B., Mehta, J. I., and Patel, M. N. (2015). DNA interaction, cytotoxicity, antibacterial and antituberculosis activity of oxovanadium(IV) complexes derived from ? uoroquinolones and 4-hydroxy-5-((4- hydroxyphenyl) diazenyl)thiazole-2(3H)-thione. *RSC Adv.* 5, 21710–21719. doi: 10.1039/C5RA01222H

Garner, M., Reglinski, J., Smith, W. E., Mcmurray, J., Abdullah, I., and Wilson, R. (1997). A ^{1}H spin echo and ^{51}V NMR study of the interaction of vanadate with intact erythrocytes. *J. Biol. Inorg. Chem.* 2, 235–241. doi: 10.1007/s007750050129

Ghielmetti, G., & Giger, U. (2020). *Mycobacterium avium*: an emerging pathogen for dog breeds with hereditary immunodeficiencies. Curr. Clin. Microbiol. Rep., *7*, 67-80. doi:10.1007/s40588-020-00145-5

Goldfine, A. B., Patti, M.-E., Zuberi, L., Goldstein, B. J., Leblanc, R., Landaker, E. J., et al. (2000). Metabolic effects of vanadyl sulfate in humans with non— insulin-dependent diabetes mellitus: *in vivo* and *in vitro* studies. *Metabolism* 49, 400–410. doi: 10.1016/S0026-0495(00)90418-9

Gresser, M. J., Tracey, A. S., and Parkinson, K. M. (1986). Vanadium(V) oxyanions: the interaction of vanadate with pyrophosphate, phosphate, and arsenate. *J. Am. Chem. Soc.* 108, 6229–6234. doi: 10.1021/ja00280a020

Gumerova, N., Krivosudsky, L., Fraqueza, G., Breibeck, J., Al-Sayed, E., Tanuhadi, E., et al. (2018). The P-type ATPase inhibiting potential of polyoxotungstates. *Metallomics* 10, 287–295. doi: 10.1039/C7MT00279C

Hadzibrahimovic, M., Suznjevic, D., Pastor, F., Antic, T. C., Zizic, M., Zakrzewska, J., et al. (2017). The interactions of vanadate monomer with the mycelium of fungus Phycomyces blakesleeanus: reduction or uptake? *Anton. V. Leeuw. Inter. J. Gen. Mol. Microb.* 110, 365–373. doi: 10.1007/s10482-016- 0808-0

Hider, R. C., and Kong, X. (2010). Chemistry and biology of siderophores. *Nat. Prod. Rep*. 27, 637–657. doi: 10.1039/b906679a

Hill, C. L., Hartnup, M., Faraj, M., Weeks, M., Prosser-Mccartha, C. M., Brown, R. B. Jr., et al. (1990). Polyoxometalates as inorganic anti-HIV-1 compounds. Structure-activity relationships. *Adv. Chemotherapy AIDS*, 33–41.

Jakusch, T., Enyedy, É. A., Kozma, K., Paár, Z., Bényei, A., and Kiss, T. (2014). Vanadate complexes of 3-hydroxy-1, 2-dimethyl-pyridinone: Speciation, structure and redox properties. *Inorg. Chim. Acta* 420, 92–102. doi: 10.1016/j.ica.2013.12.034

Jakusch, T., and Kiss, T. (2017). *In vitro* study of the antidiabetic behavior of vanadium compounds. *Coord. Chem. Rev*. 351, 118–126. doi: 10.1016/j.ccr.2017.04.007

Jakusch, T., Pessoa, J. C., and Kiss, T. (2011). The speciation of vanadium in human serum. *Coord. Chem. Rev.* 255, 2218–2226. doi: 10.1016/j.ccr.2011.02.022

Kaliva, M., Kyriakakis, E., and Salifoglou, A. (2002). Reactivity investigation of dinuclear vanadium(IV,V)-citrate complexes in aqueous solutions. A closer look into aqueous vanadium-citrate interconversions. *Inorg. Chem.* 41, 7015–7023. doi: 10.1021/ic020323r

Kaliva, M., Raptopoulou, C. P., Terzis, A., and Safifoglou, A. (2003). Systematic studies on pH-dependent transformations of dinuclear vanadium(V)- citrate complexes in aqueous solutions - A perspective relevance to aqueous vanadium(V)-citrate speciation. *J. Inorg. Biochem.* 93, 161–173. doi: 10.1016/S0162-0134(02)00563-9

Kioseoglou, E., Gabriel, C., Petanidis, S., Psycharis, V., Raptopoulou, C. P., Terzis, A., et al. (2013). Binary Decavanadate-Betaine composite materials of potential anticarcinogenic activity. *Z. Anorg. Allg. Chem.* 639, 1407–1416. doi: 10.1002/zaac.201300144

Kioseoglou, E., Petanidis, S., Gabriel, C., and Salifoglou, A. (2015). The chemistry and biology of vanadium compounds in cancer therapeutics. *Coord. Chem. Rev.* 301, 87–105. doi: 10.1016/j.ccr.2015.03.010

Kiss, T., Jakusch, T., Hollender, D., Dornyei, A., Enyedy, E. A., Pessoa, J. C., et al. (2008). Biospeciation of antidiabetic VO(IV) complexes. *Coord. Chem. Rev.* 252, 1153–1162. doi: 10.1016/j.ccr.2007.09.011

Kustin, K. (2015). Aqueous vanadium ion dynamics relevant to bioinorganic chemistry: a review. *J. Inorg. Biochem.* 147, 32–38. doi: 10.1016/j.jinorgbio.2014.12.009

Le, M., Rathje, O., Levina, A., and Lay, P. A. (2017). High cytotoxicity of vanadium (IV) complexes with 1, 10-phenanthroline and related ligands is due to decomposition in cell culture medium. *J. Biol. Inorg. Chem.* 22, 663–672. doi: 10.1007/s00775-017-1453-4

Leon, I. E., Cadavid-Vargas, J. F., Di Virgilio, A. L., and Etcheverry, S. B. (2017). Vanadium, Ruthenium and Copper compounds: a new class of Nonplatinum Metallodrugs with Anticancer activity. *Curr. Med. Chem.* 24, 112–148. doi: 10.2174/0929867323666160824162546

Leon, I. E., Porro, V., Astrada, S., Egusquiza, M. G., Cabello, C. I., Bollati-Fogolin, M., et al. (2014). Polyoxometalates as antitumor agents: bioactivity of a new polyoxometalate with

copper on a human osteosarcoma model. *Chem. Biol. Interact.* 222, 87–96. doi: 10.1016/j.cbi.2014.10.012

Levina, A., Crans, D. C., and Lay, P. (2017a). Speciation of metal drugs, supplements and toxins in media and bodily fluids controls *in vitro* activities. *Coord. Chem. Rev.* 352, 473–498. doi: 10.1016/j.ccr.2017. 01.002

Levina, A., and Lay, P. A. (2017b). Stabilities and Biological Activities of Vanadium Drugs: What is the Nature of the Active Species?. *Chem.Asian J.* 12, 1692–1699. doi: 10.1002/asia.201700463

Li, M., Ding, W., Smee, J. J., Baruah, B., Willsky, G. R., and Crans, D. C. (2009). Anti-diabetic effects of vanadium (III, IV, V) - chlorodipicolinate complexes in streptozotocin-induced diabetic rats, *BioMetals* 103, 585–905. doi: 10.1007/s10534-009-9241-4

Lodyga-Chruscinska, E., Sanna, D., Garribba, E., and Micera, G. (2008). Potentiometric, spectroscopic, electrochemical and DFT characterization of oxovanadium(IV) complexes formed by citrate and tartrates in aqueous solution at high ligand to metal molar ratios: the effects of the trigonal bipyramidal distortion in bis-chelated species and biological implications. *Dalton Trans.* 28, 4903–4916. doi: 10.1039/b803520b

Lu, L. P., and Zhu, M. L. (2011). Metal-based inhibitors of protein Tyrosine Phosphatases. *Anti Cancer Agents Med. Chem.* 11, 164–171. doi: 10.2174/187152011794941271

Lyonnet, B., Martz, S., and Martin, E. (1899). L'emploi therapeutique des derives du vanadium. *La Presse Méd.* 1, 191–192.

Maiti, A., and Ghosh, S. (1989). Synthesis and reactivity of the Oxovanadium(IV) Complexes of Two N-O donors and potentiation of the antituberculosis activity of one of them on Chelation to metal ions: part, I. *V. J. Inorg. Biochem.* 36, 131–139. doi: 10.1016/0162-0134(89)80020-0

Martins, P. G., Mori, M., Chiaradia-Delatorre, L. D., Menegatti, A. C., Mascarello, A., Botta, B., et al. (2015). Exploring oxidovanadium (IV) complexes as YopH inhibitors: mechanism of action and modeling studies. *ACS Med. Chem. Lett*. 6, 1035–1040. doi: 10.1021/acsmedchemlett. 5b00267

Mclauchlan, C. C., Peters, B. J., Willsky, G. R., and Crans, D. C. (2015). Vanadium-phosphatase complexes: Phosphatase inhibitors favor the trignonal bipyramidal transition state geometries. *Coord. Chem. Rev.* 301–302, 163–199. doi: 10.1016/j.ccr.2014.12.012

Medina, J. J. M., Naso, L. G., Pérez, A. L., Rizzi, A., Ferrer, E. G., and Williams, P. A. (2017). Antioxidant and anticancer effects and bioavailability studies of the flavonoid baicalin and its oxidovanadium (IV) complex. *J. Inorg. Biochem.* 166, 150–161. doi: 10.1016/j.jinorgbio.2016.11.005

Moskovitz, B. L., and Group, A. T. H.-C. S. (1988). Clinical trial and tolerance of HPA-23 in patients with acquired immunodeficiency syndrome. *Antimicrob. Agents Chemother.* 32, 1300–1303. doi: 10.1128/AAC.32.9.1300

Noeske, J., Wasserman, M. R., Terry, D. S., Altman, R. B., Blanchard, S. C., and Cate, J. H. D. (2015). High-resolution structure of the Escherichia coli ribosome. *Nat. Struct. Mol. Biol.* 22, 336–341. doi: 10.1038/nsmb.2994

Pessoa, J. C., Etcheverry, S., and Gambino, D. (2015). Vanadium compounds in medicine. *Coord. Chem. Rev.* 301, 24–48. doi: 10.1016/j.ccr.2014.12.002

Pessoa, J. C., and Tomaz, I. (2010). Transport of therapeutic Vanadium and Ruthenium complexes by blood plasma components. *Curr. Med. Chem.* 17, 3701–3738. doi: 10.2174/092986710793213742

Pettersson, L., Andersson, I., and Hedman, B. (1985). Multicomponent polyanions. 37. A potentiometric and 51V-NMR study of equilibria in the H^{+}-HVO^{2-} 4 system in 3.0 M-Na(ClO4) medium covering the range 1£-1g[H+]£10. *Chem. Scr.* 25, 309–317.

Pettersson, L., Hedman, B., Andersson, I., and Ingri, N. (1983). Multicomponent polyanions. 34. P potentiometric and 51V NMR study of equilibria in the H+-HVO42- system in the 0.6M Na(Cl) medium covering the range 1£- 1g[H+]£10. *Chem. Scrip.* 22, 254–264.

Pluskey, S., Mahroof-Tahir, M., Crans, D. C., and Lawrence, D. S. (1996). Vanadium oxoanions and cAMP-dependent protein kinase: an anti-substrate inhibitor. *Biochem. J.* 321, 333–339. doi: 10.1042/bj32 10333

Pope, M. T., and Müller, A. (1991). Polyoxometalate chemistry: an old field with new dimensions in several disciplines. *Angew. Chem. Int. Ed. Engl.* 30, 34–48. doi: 10.1002/anie.199100341

Postal, K., Maluf, D. F., Valdameri, G., Rüdiger, A. L., Hughes, D. L., de Sá, E. L., et al. (2016). Chemoprotective activity of mixed valence polyoxovanadates against diethylsulphate in *E. coli* cultures: insights from solution speciation studies. *RSC Adv.* 6, 114955–114866. doi: 10.1039/c6ra15826a

Rehder, D. (1991). The bioinorganic chemistry of vanadium. *Angew. Chem. Int. Ed. Engl. T* 30, 148–167. doi: 10.1002/anie.199101481

Rehder, D., Pessoa, J. C., Geraldes, C., Castro, M., Kabanos, T., Kiss, T., et al. (2002). *In vitro* study of the insulin-mimetic behaviour of vanadium(IV, V) coordination compounds. *J. Biol. Inorg. Chem.* 7, 384–396. doi: 10.1007/s00775-001-0311-5

Rhule, J. T., Hill, C. L., Judd, D. A., and Schinazi, R. F. (1998). Polyoxometalates in medicine. *Chem. Rev.* 98, 327–358. doi: 10.1021/cr960396q

Sakurai, H. (2002). A new concept: the use of vanadium complexes in the treatment of diabetes mellitus. *Chem. Rec.* 2, 237–248. doi: 10.1002/tcr.10029

Sakurai, H., Tsuchiya, K., Nukatsuka, M., Kawada, J., Ishikawa, S., Yoshida, H., et al. (1990). Insulin-mimetic action of vanadyl complexes. *J. Clin. Biochem. Nutr.* 8, 193–200. doi: 10.3164/jcbn.8.193

Samart, N., Saeger, J., Haller, K., Manuel Aureliano, M., and Crans, D. (2014). Interaction of decavanadate with interfaces and biological model membrane systems: characterization of soft oxometalate systems. *J. Mol. Eng. Mat.* 2, 1–21. doi: 10.1142/S2251237314400073

Sambandamurthy, V. K., Derrick, S. C., Hsu, T., Chen, B., Larsen, M. H., Jalapathy, K. V., et al. (2006). Mycobacterium tuberculosis Δ RD1 Δ panCD: a safe and limited replicating mutant strain that protects immunocompetent and immunocompromised mice against experimental tuberculosis. *Vaccine* 24, 6309–6320. doi: 10.1016/j.vaccine.2006.05.097

Sanchez-Lombardo, I., Baruah, B., Alvarez, S., Werst, K. R., Segaline, N. A., Levinger, N. E., et al. (2016). Size and shape trump charge in interactions of oxovanadates with self-assembled interfaces: application of continuous shape measure analysis to the decavanadate anion. *New J. Chem.* 40, 962–975. doi: 10.1039/C5NJ01788B

Sanna, D., Serra, M., Micera, G., and Garribba, E. (2014). Interaction of antidiabetic vanadium compounds with hemoglobin and red blood cells and their distribution between plasma and erythrocytes. *Inorg. Chem.* 53, 1449–1464. doi: 10.1021/ic402366x

Sanna, D., Ugone, V., Micera, G., Bugly,ó, P., Bír,ó, L., and Garribba, E. (2017). Speciation in human blood of Metvan, a vanadium based potential anti-tumor drug. *Dalton Trans.* 46, 8950–8967. doi: 10.1039/C7DT00943G

Scalese, G., Arhouma, Z., Kostenkova, K., Pérez-Díaz, L., Crick, D. C., Gambino, D., & Crans, D. C. (2022). Do bioactive 8-hydroxyquinolines oxidovanadium (IV) and (V) complexes inhibit the growth of *M. smegmatis*? *J. Inorg Biochem*, *237*, 111984. doi:10.1016/j.jinorgbio.2022.111984

Selling, A., Andersson, I., Pettersson, L., and Schramm, C. M., S.L., D., and J.H., G. (1994). Multicomponent Polyanions. 47. The aqueous Vanadophosphate system. *J. Inorg. Chem.* 33, 3141–3150. doi: 10.1021/ic00092a021

Selman, M., Rousso, C., Bergeron, A., Son, H., Krishnan, R., El-Sayes, N., et al. (2018). Multi-modal potentiation of oncolytic virotherapy by Vanadium compounds. *Mol. Ther.* 26, 56–69. doi: 10.1016/j.ymthe.2017.10.014

Shah, H. S., Joshi, S. A., Haider, A., Kortz, U., Ur-Rehman, N., and Iqbal, J. (2015). Synthesis of chitosan-coated polyoxometalate nanoparticles against cancer and its metastasis. *RSC Adv.* 5, 93234–93242. doi: 10.1039/C5RA18489D

Smith, D. M., Pickering, R. M., and Lewith, G. T. (2008). A systematic review of vanadium oral supplements for glycaemic control in type 2 diabetes mellitus. *Qjm-an Inter. J. Med.* 101, 351–358. doi: 10.1093/qjmed/hcn003

Sun, T. D., Cui, W., Yan, M., Qin, G., Guo, W., Gu, H. X., et al. (2016). Target delivery of a novel Antitumor Organoplatinum(IV)-substituted Polyoxometalate Complex for Safer and more effective colorectal cancer therapy *in vivo*. *Adv. Mater.* 28, 7397–7404. doi: 10.1002/adma.201601778

Thompson, K. H., Lichter, J., Lebel, C., Scaife, M. C., Mcneill, J. H., and Orvig, C. (2009). Vanadium treatment of type 2 diabetes: a view to the future. *J. Inorg. Biochem.* 103, 554–558. doi: 10.1016/j.jinorgbio.2008.12.003

Thompson, K. H., and Orvig, C. (2006). Vanadium in diabetes: 100 years from Phase 0 to Phase, I. *J. Inorg. Biochem.* 100, 1925–1935. doi: 10.1016/j.jinorgbio.2006.08.016

Trevino, S., Sánchez-Lara, E., Sarmiento-Ortega, V. E., Sánchez-Lombardo, I., Flores-Hernández, J. A., Pérez-Benítez, A., et al. (2015). Hypoglycemic, lipid- lowering and metabolic regulation activities of metforminium decavanadate (H2Metf)3 [V10O28]·8H2O using hypercaloric-induced carbohydrate and lipid deregulation in Wistar rats as biological model. *J. Inor. Biochem.* 147, 85–92. doi: 10.1016/j.jinorgbio.2015.04.002

Turian, G. (1951). Action plasmogene du fer chez les Mycobacteries. Le bacille de la fleole, indicateur biologique du fer. 34,917-920. *Helv. Chim. Acta* 34, 917–920. doi: 10.1002/hlca.19510340325

Turner, T. L., Nguyen, V. H., Mclauchlan, C. C., Dymon, Z., Dorsey, B. M., Hooker, J. D., et al. (2012). Inhibitory effects of decavanadate on several enzymes and Leishmania tarentolae *in vitro*. *J. Inorg. Biochem.* 108, 96–104. doi: 10.1016/j.jinorgbio.2011.09.009

Upadhyay, A., Fontes, F., Gonzalez-Juarrero, M., McNeil, M. R., Crans, D. C., Jackson, M., et al. (2015). MenI, a novel menaquinone reductase in *Mycobacterium tuberculosis* is required for survival in macrophages. *ACS Central Sci.* 2015, 1, 292–302. doi: 10.1021/acscentsci.5b00212

Vilas Boas, L. V., and Costa Pessoa, J. (1987). "Vanadium," in *Comprehensive Coordination Chemistry. The Synthesis, Reactions, Properties & Applications of Coordination Compounds*, eds G. Wilkinson, Sir, R. D. Gillard, and J. A. Mccleverty (New York, NY: Pergamon Press), 453–583.

Wang, L., Zhou, B. B., and Liu, J. R. (2013). Anticancer Polyoxometalates. *Prog. Chem.* 25, 1131–1141.

Weinstein, S., Jahn, W., Glotz, C., Schlünzen, F., Levin, I., Janell, D., et al. and Yonath, A. (1999). Metal compounds as tools for the construction and the interpretation of medium-resolution maps of ribosomal particles. *J. Struct. Biol.* 127, 141–151. doi: 10.1006/jsbi.1999.4135

Willsky, G. R., Chi, L.-H., Godzala, M. III, Kostyniak, P. J., Smee, J. J., Trujillo, A. M., et al. (2011). Anti-diabetic effects of a series of vanadium dipicolinate complexes in rats with streptozotocin-induced diabetes. *Coord. Chem. Rev.* 255, 2258–2269. doi: 10.1016/j.ccr.2011.06.015

Willsky, G. R., Goldfine, A. B., Kostyniak, P. J., Mcneill, J. H., Yang, L. Q., Khan, H. R., et al. (2001). Effect of vanadium(IV) compounds in the treatment of diabetes: *in vivo* and *in vitro* studies with vanadyl sulfate and bis(maltolato)oxovandium(IV). *J. Inorg. Biochem.* 85, 33–42. doi: 10.1016/S0162-0134(00)00226-9

Willsky, G. R., Halvorsen, K., Godzala, M. E., Iii, C.hi, L.-H., Most, M. J., Kaszynski, P., et al. (2013). Coordination chemistry may explain pharmacokinetics and clinical response of vanadyl sulfate in type 2 diabetic patients. *Metallomics* 5, 1491–1502. doi: 10.1039/c3mt00162h

Willsky, G. R., Leung, J. O., Offermann, P. V. Jr., Plotnick, E. K., and Dosch, S. F. (1985). Isolation and characterization of vanadate- resistant mutants of Saccharomyces cerevisiae. *J. Bacteriol.* 164, 611–617.

Willsky, G. R., Preischel, D. A., and Mccabe, B. C. (1984a). Vanadium metabolism in S-Cerevisiae. *Biophys. J.* 45, A76–A76.

Willsky, G. R., White, D. A., and Mccabe, B. C. (1984b). Metabolism of added Ortho-Vanadate to Vanadyl and High- molecular-weight Vanadates by Saccharomyces-Cerevisiae. *J. Biol. Chem.* 259, 3273–3281.

Winkler, P. A., Huang, Y., Sun, W., Du, J., and and, L.ü, W. (2017). Electron cryo-microscopy structure of a human TRPM4 channel. *Nature* 552, 200–204. doi: 10.1038/nature24674

Yamada, H., Yamaguchi, M., Igarashi, Y., Chikamatsu, K., Aono, A., Murase, Y., ... & Mitarai, S. (2018). *Mycolicibacterium smegmatis*, basonym Mycobacterium smegmatis, expresses morphological phenotypes much more similar to *Escherichia coli* than *Mycobacterium tuberculosis* in quantitative structome analysis and CryoTEM examination. *Front Microbiol*, *9*, 1992. doi:10.3389/fmicb.2018.01992

Zhai, F. Y., Wang, X. H., Li, D. L., Zhang, H., Li, R., and Song, L. S. (2009). Synthesis and biological evaluation of decavanadate Na(4)Co(H(2)O)(6)V(10)O(28) center dot 18H(2)O. *Biomed. Pharmacother.* 63, 51–55. doi: 10.1016/j.biopha.2008. 01.006

Zhang, Y., Yang, X. D., Wang, K., and Crans, D. C. (2006), The permeability and cytotoxicity of insulin-mimetic vanadium (III,IV,V)-dipicolinate complexes, *J. Inorg. Biochem.* 100, 80–87. doi: 10.1016/j.jinorgbio.2005.10.006

Zhou, Z. H., Zhang, H., Jiang, Y. Q., Lin, D. H., Wan, H. L., and Tsai, K. R. (1999). Complexation between vanadium(V) and citrate: spectroscopic and structural characterization of a

dinuclear vanadium(V) complex. *Transit. Metal Chem.* 24, 605–609. doi: 10.1023/A:1006947218366

Zizic, M., Miladinovic, Z., Stanic, M., Hadzibrahimovic, M., Zivic, M., and Zakrzewska, J. (2016). V-51 NMR investigation of cell-associated vanadate species in Phycomyces blakesleeanus mycelium. *Res. Microbiol.* 167, 521–528. doi: 10.1016/j.resmic.2016.04.012

Zizic, M., Zivic, M., Spasojevic, I., Bogdanovic Pristov, J., Stanic, M., Cvetic-Antic, T., et al. (2013). The interactions of vanadium with Phycomyces blakesleeanus mycelium: enzymatic reduction, transport and metabolic effects. *Res. Microbiol.* 164, 61–69. doi: 10.1016/j.resmic.2012. 08.007

Zwolak, I. (2014). Vanadium carcinogenic, immunotoxic and neurotoxic effects: a review of *in vitro* studies. *Toxicol. Mech. Method.* 24, 1–12. doi: 10.3109/15376516.2013.843110

Chapter 2: Pt^{IV}- or Mo^{VI}-Substituted Decavanadates Inhibit the Growth of *Mycobacterium smegmatis*

2.1. Introduction

The applications of polyoxometalates (POMs) have increased in the medical field because of the continuing reports of POMs, including polyoxovanadates (POVs), with promising biological effects, despite the challenges with low biocompatibility and compound accessibility (Bijelic et al., 2018; Bijelic et al., 2019; Colovic et al., 2020; Crans et al., 2019; Pessoa et al., 2015; Rhule et al., 1998). The presence of vanadium in different clusters leads to an increased antiproliferative activity compared to that of polyoxomolybdates and polyoxotungstates (Bijelic et al., 2015; Levina and Lay, 2017; Liu et al., 2005; Pisano et al., 2019). POVs with antidiabetic, antibacterial and anticancer agents have been reported and their activity has been attributed to their effects on different enzymes. The enzyme and proteins include actin (Ramos et al., 2010), kinases (Pluskey et al., 1997), and ATPases (Fraqueza et al., 2012), as well as hormone-like responses associated with the activation of a high-affinity receptor of the Fc region of the immunoglobin E (IgE), an antibody also known as FcεRI, is important in signal transduction (Al-Qatati et al., 2013) and the indirect activation of a G protein-coupled receptor (Althumairy et al., 2020a). In the recent study, novel Lindquist-type hexavanadate hybrids covalently linked to a β-alanine ethyl ester and L-alanine were designed and synthesized as a first step for site-specific delivery of a POM (Hu et al., 2019). Two polyanions were derived from the carboxyl-derivative of Lindqvist-type hexavanadate parent, $[Bu_4N]_2[V_6O_{13}\text{-}\{(OCH_2)_3CCH_2OOCCH_2CH_2\text{-}COOH\}_2]$ (Hu et al., 2019). These novel polyanions were found to be effective against carcinoma cell lines, and their activities were higher

than that of the commercial drug 5-fluorouracil (5-FU) (Hu et al., 2019). Similarly, a POV nanocage consisting of $\{V_5O_9Cl\}$ molecular building blocks and the organic triazine-benzoic acid linker was found to have antitumor properties (Zheng et al., 2019). These results show the biomedical potential of such compounds and suggest that the desirable effects of POVs are of interest. Therefore, the fundamental knowledge about the properties of vanadium-containing-oxo-clusters, particularly their effects on biological responses, is essential.

Decavanadate ($[V_{10}O_{28}]^{6-}$, abbreviated V_{10}) is an isopolyoxometalate that has been found to exhibit a range of biological activities including the interactions with Na^+, K^+, and Ca^{2+}-ATPases (Cantley et al., 1977), inhibition of protein phosphatases, as well as crystallization with various enzymes including a protein tyrosine phosphatase (PTP), DNA polymerases and nucleases (Aureliano and Crans, 2009; Lee et al., 2015; McLauchlan et al., 2015; Pope and Muller, 1991; Sarafianos et al., 1996; Tonks, 2006). In addition to its ability to normalize elevated blood glucose levels in streptozotocin (STZ)-induced diabetic rats, decavanadate exhibits its effects in various biological systems including signal transduction activation of FcεRI (Althumairy et al., 2020a; Althumairy et al., 2020b). The effects of decametalates on bacteria remain less explored than their anticancer and antidiabetic effects (Fukuda and Yamase, 1997). Recently, decavanadate was found to inhibit the growth of *M. tb* and *M. smeg*, and was also found to be much more potent than the monovanadate (V_1), a known phosphatase inhibitor (**Figure 2.1**) (Samart et al., 2018). In the following work, we examine the effects of two known substituted polyoxovanadates, monomolybdononavanadate ($[V_9MoO_{28}]^{5-}$, abbreviated V_9Mo) and monoplatino(IV)-nonavanadate ($[H_2PtV_9O_{28}]^{5-}$, abbreviated V_9Pt), on the growth of *M. smeg*. These POVs have structures very similar to the V_{10}; however, replacing individual vanadium atoms by Pt^{IV} and Mo^{VI} results in a different chemical composition, such as a slightly lower symmetry and, most

importantly, a lower charge by one unit, compared to the parent V_{10} (**Figure 2.1**) (Aureliano and Crans, 2009; Sanchez-Lombardo et al., 2016; Lee et al., 2008).

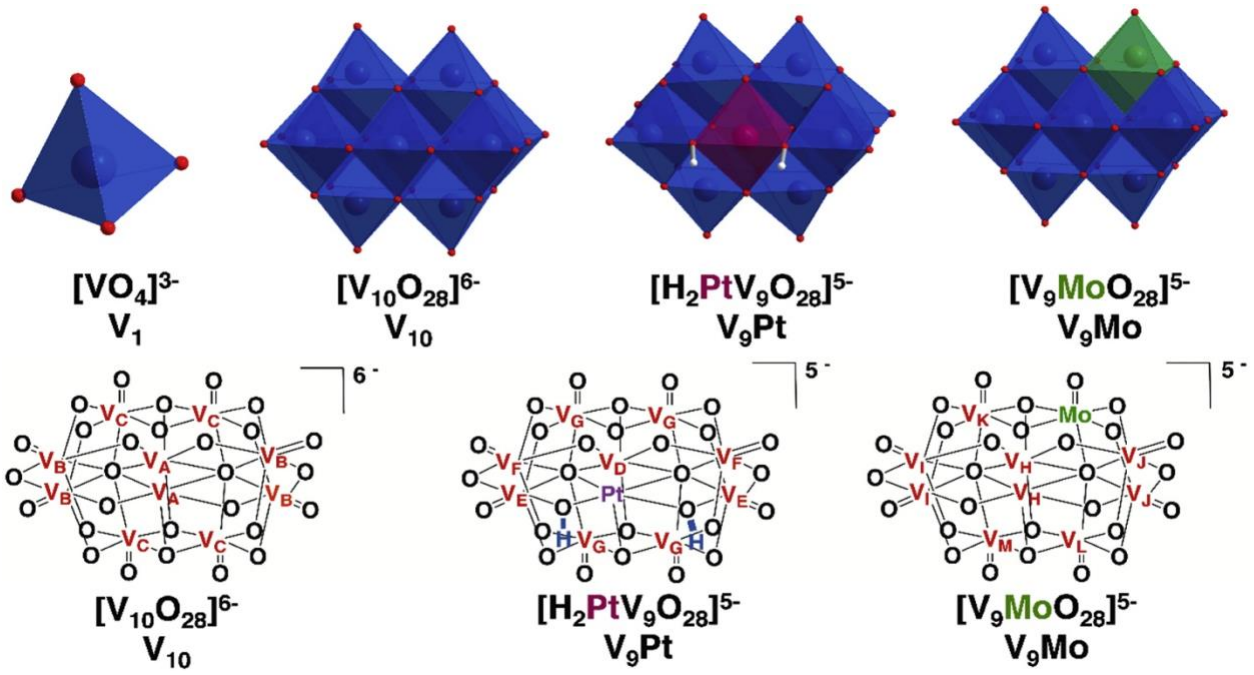

Figure 2.1. Structures and polyhedral representations of $[VO_4]^{2-}$ (V_1), $[V_{10}O_{28}]^{6-}$ (V_{10}), $[H_2PtV_9O_{28}]^{5-}$ (V_9Pt) and $[Mo^{VI}V_9O_{28}]^{5-}$ (V_9Mo) illustrating the differences between the simple vanadate ion and the polyanions investigated in this work at pH 7.4. For illustrative purposes, Pt is depicted in maroon, Mo in green, V atoms in red, and O atoms in black. The V atoms in the structures and in the ^{51}V NMR spectra below are labeled as V_A - V_C in V_{10}, V_D – V_G in V_9Pt and V_H - V_M in V_9Mo.

V_{10} is a compact polyanion that consists of ten octahedrally coordinated vanadium(V) atoms, eight of which contain one terminal oxo ligand and five shared oxygens in their octahedra, and two of which are located in the interior with six bridging oxygens in their octahedra (**Figure 2.1**) (Aureliano and Crans, 2009; Crans et al., 1994; Crans et al., 2017). Its structure has the dimensions of 5.8 Å × 7.8 Å × 8.4 Å with an overall net charge of minus 6 at pH 7.4 (Crans et al., 1994). In the V_9Pt cluster, one of the two internal vanadium atoms is replaced by a platinum(IV) atom (**Figure 2.1**). Unlike V_{10}, the V_9Pt ion has a minus 5 charge due to the replacement of one central addenda site by a Pt^{IV} ion. The dimensions of V_9Pt are similar to those of the decavanadate

(5.5 Å × 7.7 Å × 8.5 Å), calculated from the XRD data (Lee et al., 2008)). The crystal structure of the protonated salt shows that the complex has a C_{2v} point group symmetry, and the two protons on the polyanion are located on oxygens bridging Pt and V. These protons are important for the formation of a dimer assembly, $[H_4(Pt^{IV}V_9O_{28})_2]^{10-}$, through four interanion O-H···O hydrogen bonds (Lee et al., 2008). These hydrogen bonds between two V_9Pt ions persist even after dissolving the polyanion salt in water, as shown by broad ^{51}V NMR lines, but upon heating they are broken, resulting in discrete V_9Pt ions. In the V_9Mo cluster, one of the external vanadium atoms is replaced by molybdenum (Irma Sanchez-Lombardo et al., 2016). Single-crystal X-ray analysis of the analogous $[(CH_3)_4N]_4[H_2MoV_9O_{28}]CI\cdot 6H_2O]$ polyanion has shown a random distribution of molybdenum and vanadium atoms over four "capping" metal atom positions (Strukan et al., 1997). Since the structure is not available in the Cambridge Crystal Structure Database, we assumed that the dimensions of the POM are very similar because of the similarity in the Mo—O and V—O bond lengths. Due to their different composition, the spectroscopic properties of the structurally related V_9Pt, V_9Mo and V_{10} are different, as well as their solubilities and stabilities in biological medium.

The biological effects of V_{10} have been explored in many types of microorganisms, including *M. tb* and *M. smeg*, in previous studies which are summarized in **Table 2.1**. However, these studies focus on the effects of V_{10} and not the substituted V_{10}'s. Such studies investigate the inherent effects of the decavanadate structure, since substituted V_{10}'s are structurally similar to the parent V_{10} but have slightly different properties. The inhibition of V_{10} in mycobacteria was significantly more potent than other oxovanadates and hence further investigations of the nature of this inhibition were made in this bacterium. *M. tb* and *M. smeg* have a very thick, waxy membrane compared to that of Gram-negative microorganisms, which is known to be very

hydrophobic and impenetrable by many compounds (Chiaradia et al., 2017 and Li et al., 2023). which makes the development of anti-tuberculosis drugs very challenging (Chan et al., 2016; Lopes et al., 2020; Plutin et al., 2016; Williams et al., 2014). Two phosphatases have been identified in the genome of the *M. tb,* and both are believed to be secreted and, thus, found outside the cell (Dutta et al., 2016; Grundner et al., 2005; Zhou et al., 2010).

Previous studies have shown that the *M. tb and M. smeg* extrude a component which attributes to the rapid hydrolysis of the decavanadate in the growth medium (Samart et al., 2018). We suggest that this component effectively reduces the stability of V_{10} after its interaction with growth medium, nevertheless, the biological activity of the decavanadate is stronger than that of the monovanadate (V_1) (Samart et al., 2018). Accompanying speciation studies in the cell culture media allow us to calculate adjusted EC_{50} values for the POVs present in solution at the beginning of the study. The adjusted EC_{50} values represent the minimum effect these compounds exert and this is important in the event of the compounds' decomposition under given conditions.

Table 2.1. Previous studies of various decavanadates (V_{10}) in other microorganisms.

Solid decavanadates tested	**Microorganism**[a, b]	**Ref**
$(tert\text{-}BuNH_3)_6[V_{10}O_{28}]$	Bacteria – *Streptococcus pneumoniae*[b]	(Fukuda and Yamase, 1997)
$(C_6H_{14}N_5O)_4[H_2V_{10}O_{28}]\cdot 9H_2O$ $(C_6H_{14}N_5O)_6[V_{10}O_{28}]\cdot 4H_2O$ *$C_6H_{14}N_6O$ = Moroxydine or ABOB[c, d]	Bacteria – *Staphylococcus aureus*,[b] *Staphylococcus epidermis*,[b] MRSA (methicillin-resistant *Staphylococcus aureus*),[b] MRSE (Methicillin-resistant *Staphylococcus epidermis*)[b]	(Liu et al., 2004)
$Chitosan–Ca_3V_{10}O_{28}$	Bacteria –*Eschercihia coli,*[a] *Staphylococcus aureus*[b]	(Chen et al., 2006)
$V_{10}O_{28}^{6-}$ [e]	Virus – *Chlorella* virus	(Bougie and Bisaillon, 2006)

Solid decavanadates tested	Microorganism[a, b]	Ref
$(NH_4)_6[V_{10}O_{28}]\cdot 6H_2O$	Protozoa – *Leishmania tarentolae*	(Turner et al., 2012)
$[H_2V_{10}O_{28}][4\text{-picH}]_4\cdot 2H_2O$ *4-pic = 4-picoline	Bacteria – *Pseudomonas aeruginosa* [a], *Bacillus cirroflagellosus* [b], Fungi – *Aspergillus niger*, *Penicillium notatum*	(Shahid et al., 2014)
$[4\text{-}(CH_3O)C_6H_4CH_2NH_3]_6V_{10}O_{28}\cdot 2H_2O$	Bacteria – *Enterococcus faecium* [b]	(Toumi et al., 2015)
$V_{10}O_{28}^{6-}$ [e]	Protozoa – *Leishmania tarentolae*	(Dorsey et al., 2018)
$Zn_3(FLC)_6V_{10}O_{28}\cdot 10H_2O$ *FLC = fluconazole	Fungi – *Candida albicans*, *Candida glabrata*, *Candida krusei*, *Candida parapsilosis*, *Cryptococcus tropicalis*	(Guo et al., 2018)
$Na_6V_{10}O_{28}$	Mycobacteria– *Mycobacterium smegmatis*, *Mycobacterium tuberculosis*	(Samart et al., 2018)
$(3\text{-Hpca})4[H_2V_{10}O_{28}]\cdot 2H_2O\cdot 2(3\text{-pca})$ *3-pca = 3-pyridinecarboxamide $(4\text{-Hpca})_4[H_2V_{10}O_{28}]\cdot 2(4\text{-pca})$ *4-pca = 4-pyridinecarboxamide	Protozoa– *Giardia intestinalis* Bacteria – *Escherichia coli* [a]	(Missina et al., 2018)
$(NH_4)_4(HMTA—H)_2V_{10}O_{28}\cdot 4H_2O$ *HMTA = hexamethylenetetramine	Bacteria- *Escherichia coli,*[a] *Salmonella typhimurium,*[a] *Enterococcus feacium,*[b] *Streptocoque* B (*Streptococcus agalactiae*)[b] Fungi – *Candida albicans*	(Jammazi et al., 2019)
$(NH_4)_6V_{10}O_{28}$	Bacteria – *Escherichia coli* [a]	(Marques-da-Silva et al., 2019)

[a] Gram-negative bacterium. [b] Gram-positive bacterium. [c] $C_6H_{14}N_6O$ = Moroxydine.

[d] $C_6H_{14}N_6O$ = ABOB. [e] no cation was indicated in the study.

We hypothesize that the replacement of one vanadium by another metal, such as Mo and Pt, impacts properties of the V_9X polyanions and causing different biological responses than

observed with V_{10}. To test our hypothesis, we examined the effects of these monosubstituted isostructural V_{10}s in *M. smeg* and their stability in media in order to demonstrate that the effects are not simply caused by the polyanion's stability. Hence our studies were accompanied by the detailed spectroscopic investigation of the species formed in the growth medium and a calculation of the EC_{50} value of the growth inhibitor of *M. smeg* based on the observation of the species at the beginning of the experiment in the growth medium determining a maximum EC_{50} for all the decametalates.

2.2. Materials and Methods

2.2.1. General Materials

Sodium metavanadate ($NaVO_3$) and sodium molybdate (Na_2MoO_4) were purchased from Sigma Aldrich and used as received. Monoplatinononavanadate ($[H_2PtV_9O_{28}]^{5-}$, abbreviated V_9Pt) was synthesized following the reported procedure for preparation of the sodium salt ($Na_5[H_2PtV_9O_{28}]\cdot 21H_2O$) (Lee et al., 2008). The pH throughout this study was adjusted by using solutions of HCl and NaOH mixed in doubly deionized water (DDI) water, resulting in final concentrations of 6 M HCl, 0.1 M HCl and 0.1 M NaOH, respectively. All materials and solutions used in the cell culture were purchased and used as received. The Difco™ Middlebrook 7H9 Broth medium (BD Biosciences, final pH = 6.6 ± 0.2 (Ref no. 271310)) was autoclaved before use. Oleic acid (Sigma Aldrich), albumin (VWR), dextrose (Sigma Aldrich), and Tyloxapol (Chem-Impex Int'l Inc) were used as received for the biological assays. The bacterial stock was grown and incubated by shaking in 50 mL polypropylene conical tubes (30 × 115 mm) for 24 h at 37 °C before the addition to a 96 well microplate.

2.2.2. General Methods

All NMR spectra were recorded at an ambient temperature using a Bruker NMR spectrometer at 105.2 MHz for ^{51}V and 400.13 MHz for ^{1}H. The ^{51}V NMR spectra were recorded in DDI water, 7H9 medium, supernatant, and heated supernatant at several time-points (0, 1, 5 and 24 h) to determine changes in speciation of V_9Mo and V_9Pt during a 24 h interval. The parameters used for the ^{51}V NMR studies were as follows: 4096 scans in the f1 domain, O1P = −500 ppm, SW = 990 ppm, 0.01 s relaxation delay, 45° pulse angle, 16 µs pulse; the locking was off, and the shimming was skipped. The ^{51}V NMR spectra were reported relatively to a neat $VOCl_3$ solution at 0 ppm and referenced against an external reference of an aqueous $NaVO_4$ solution at pH 12 (two signals at −535.7 ppm and − 560.4 ppm) (Althumairy et al., 2020a). The data was processed using MestreNova NMR processing software (version 14.0.1).

2.2.3. Preparation of the monomolybdononavanadate solution

Monomolybdononavanadate ($[V_9MoO_{28}]^{5-}$, abbreviated V_9Mo) solution was freshly prepared by using a modified procedure from the literature (Irma Sanchez-Lombardo et al., 2016): sodium metavanadate (0.5501 g, 4.500 mmol) and sodium molybdate (0.1216 g, 0.5000 mmol) were dissolved in 15.0 mL of DDI water, resulting in a 5:1 vanadium to molybdenum molar ratio. The solution was boiled at 95 °C for 7 min to ensure the dissolution of sodium metavanadate. The solution pH was adjusted from 6.00 to 5.00 by a dropwise addition of 6 M HCl, resulting in a clear bright orange solution, and the final volume was adjusted to 25.0 mL with DDI water. The final stock solution (100.0 mM total vanadium) was characterized by ^{51}V NMR to determine the relative concentrations of V_9 and V_{10}.

2.2.4. Preparation of the stock solutions for speciation studies

A 2.0 mM stock solution of V_9Pt was prepared by dissolving solid $Na_5[H_2PtV_9O_{28}]\cdot 21H_2O$ (0.0140 g, 0.0100 mmol) in 5.0 mL DDI water. A 2.0 mM stock solution of V_9Mo was prepared by using appropriate volumes of a 100 mM V_9Mo stock solution and DDI water; the pH was adjusted to 5.00 by a dropwise addition of 0.1 M HCl and 0.1 M NaOH if necessary. 1.0 mM control solutions of V_9Mo and V_9Pt were prepared by mixing 1000 μL of a 2.0 mM stock solution with 1000 μL of DDI H_2O. 1.0 mM solutions of V_9Mo and V_9Pt in 7H9 medium, supernatant, and heated supernatant were prepared using the same method. The pH of all solutions was measured at several time-points (0, 1, 5 and 24 h) to determine changes in speciation during a 24 h interval.

2.2.5. Cell culture studies

M. smeg was grown in the Middlebrook 7H9 medium (Ref no. 271310; Difco) supplemented with 10% OAD (oleic acid, albumin, dextrose), 0.2% (*v*/v) glycerol, and 10% Tyloxapol. Bacteria were incubated by shaking at 37 °C and left to grow overnight to mid-logarithmic growth phase to an optical density of 0.6–0.7 at 600 nm (OD_{600}).

2.2.6. Preparation of stock solutions of the vanadium compounds and inhibitory cell culture studies

The 4.0 mM solutions were prepared in DDI H_2O. The stock solutions of the vanadates were added to the Middlebrook 7H9 medium in 96 microplate wells and diluted to the final concentration of 1.0 mM. The final concentrations in a 96 well microplate were run in 10 serial 2-fold dilutions and ranged from 1.0 to 0.002 mM. The growth inhibitory effects of the vanadium complexes were determined by measuring the lowest concentration of complexes that inhibited the bacterial growth by 50% (EC_{50}) by using a Bio-Rad Benchmark Reader to check the cell viability at OD_{600} in 96 microplate wells. The data was collected in triplicate and shown with error

bars that represent standard deviations. Experiments were repeated and similar patterns were confirmed, and, in the case of $V_{10,}$ the results are similar to those reported in the literature.

2.2.7. Spectroscopic speciation studies

The 2.0 mM aqueous stock solutions of vanadium compounds, V_9Pt and V_9Mo, were diluted to the final concentration of 1.0 mM in 2 mL aliquots to measure the speciation and hence the stability of the substituted decavanadates in water, in 7H9 medium (pH 6.58), non-heated 7H9 medium supernatant, and heated 7H9 medium supernatant at different time points (0, 1, 5 and 24 h) using ^{51}V NMR analysis. The pH of a V_9Mo aqueous solution was adjusted to 5.06 by the dropwise addition of 0.1 M HCl and 0.1 M NaOH. The ^{51}V NMR signals were integrated, and the amounts of species were measured in 1.0 mM solutions which was in the middle range of the concentrations studied in the culture growth. The results of all spectroscopic studies were compared to those of the control samples. The calculations determining the amounts of both the V_9Pt and V_9Mo complexes are provided below and summarized in the corresponding table in the Results section. The NMR data is shown and summarized in the Results and Appendix II sections.

The studies in the media in which the *M. smeg* had grown are referred to as the studies in media supernatant and were done prior to and after heating of the supernatant. The supernatant fraction came from the culture in which *M. smeg* was grown after shaking for 24 h at 37 °C. The culture was centrifuged at 2000 ×*g* for 20 min in a Beckman centrifuge model GS-6R. The cell pellet was removed, and the supernatant was collected and filtered to remove any remaining cells. The filtered supernatant was then divided into two fractions, the first fraction (non-heated supernatant) was added to the polyoxometalates. The second fraction was heated for 35–45 min at 80 °C (heated supernatant) to decompose most proteins that may have been secreted during the

bacteria growth. The heated supernatant was centrifuged and filtered to remove any residual proteins prior to addition of the POVs.

2.2.8. Calculation of the V_9Pt concentration

The ^{51}V NMR analysis in aqueous solution shows three signals for V_9Pt at δ (ppm) -371.0 (V_D), −450.9 ($V_{E/F}$) and − 475.0 (V_G), and some formation of the hydrolysis products was observed in the form of V_1(−558.5 ppm) and V_4 (−571.1 ppm). The percentage of the intact V_9Pt was calculated from the integration of the signals in the 1.0 mM spectrum collected at $t = 0$, determining the contribution of V_1 (3.9%) and V_4 (0.2%) (**Table A2.S1, Figures. A2.S1-A2.S2**).

$$\%\mathbf{V_9Pt} = (V_D + V_{E/F} + V_G)) \times 100\% = (0.102+0.676+0.191) \times 100\% = \mathbf{96.9}\%$$

2.2.9. Calculation of the V_9Mo concentration

The V_9Mo aqueous solution contains both V_9Mo and V_{10} complexes, and their concentrations are calculated below. The calculation also had to be adjusted for the presence of V_1 (27.8%), as it tends to form in solutions of lower concentrations. The peak assignment of the V_9Mo complex is provided in Fig. S7.

$$\%\mathbf{V10} = [(1/2 \times (V_H + V_I + V_J)) \times 0.722] \times 100\%$$
$$= [(1/2 \times (0.160 + 0.141 + 0.235)) \times 0.722] \times 100\% = \mathbf{19.3}\%$$
$$\%\mathbf{V9Mo} = 100\% - \%V_{10} - \%V_1 = 100\% - 19.3\% - 27.8\% = \mathbf{52.9}\%$$

2.2.10. Calculation of the V_{10} concentration

The V_{10} aqueous solution also formed some hydrolysis projects when added to the media. The peak assignment of the V_{10} complex is −422, −499 and − 519 ppm as shown in **Figure. A2.S11**.

2.3. Results

2.3.1. Biological studies: Growth inhibition of *M. smeg* mc^2 155 by substituted decavanadates

The inhibition of the *M. smeg* growth by the two substituted decavanadates, V_9Mo and V_9Pt, was evaluated in the 7H9 culture medium by measuring the EC_{50} values. The growth curves of *M. smeg* treated with different oxometalate concentrations (expressed in terms of the optical density at 600 nm, OD_{600}) are shown in Appendix II (**Figures.A2. S14-A2.S16**), and a histogram in **Figure 2.2** compares the effects of V_9Mo and V_9Pt with V_{10}. The growth effect of V_{10} was measured previously (Samart et al., 2018), and was remeasured using the same dilution factors as the ones for V_9Mo and V_9Pt. The growth data in **Figure 2.2** was normalized to the growth OD at zero concentration of oxometalate. The order of the efficacy is monovanadate (V_1) – lowest effect (data not shown), followed by V_9Mo, V_9Pt and V_{10}. V_{10} and V_9Pt show comparable inhibitory effects and are 4-fold more potent than V_9Mo, while, V_9Mo is 12-fold more potent than V_1. The EC_{50} values calculated for two heteropolyoxometalates are shown in **Table 2.2** and compared to those of the V_{10} and V_1 reported previously (Samart et al., 2018). In **Table 2.2**, we also list the adjusted EC_{50} values for two oxometalates, considering detailed speciation described in the section below.

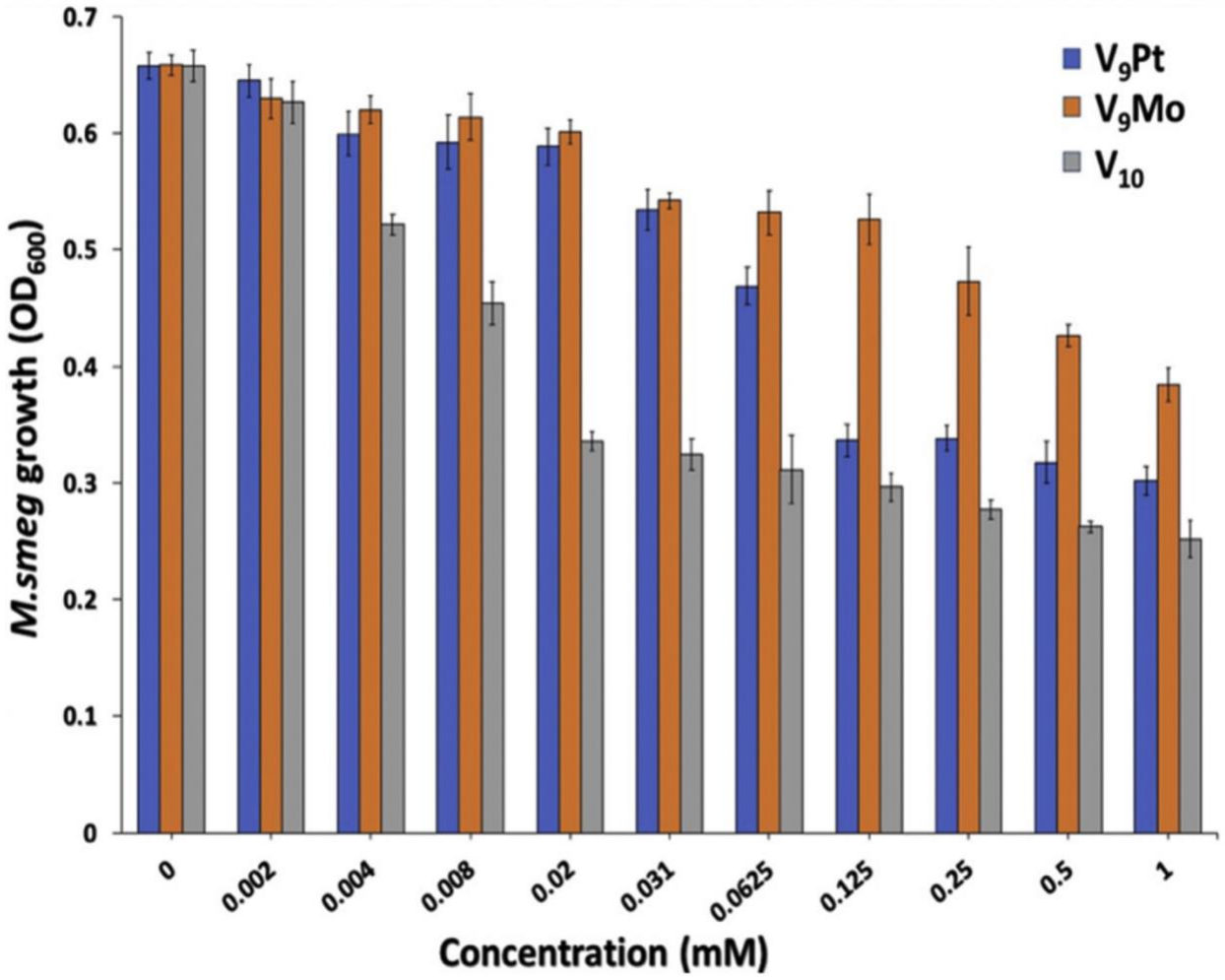

Figure. 2.2. Histogram showing the growth of *M. smeg* treated with V_9Pt (blue), V_9Pt (orange), and V_{10} (grey) respectively, with concentrations varying from 0.002 to 1.00 mM in 96 wells plate. Plates were incubated for 24 h at 37°C. Error bars shown are standard deviations determined in one growth study with triplicate readings.

Table 2.2. The growth inhibitory concentration of **V_9Pt, V_9Mo, V_{10} and V_1** on *M. smeg* growth indicated as EC50 values.

Complex	EC_{50}(mM)	St. Error	EC_{50} per V- atom/ mM	St. Error	Ref
V_9Pt[a]	0.0061	±0.0010	0.055	±0.009	This work
V_9Pt[b,adj]	0.0048	±0.0008	0.043	±0.007	This work
V_9Mo[a]	0.048	±0.026	0.43	±0.23	This work

Complex	EC_{50}(mM)	St. Error	EC_{50} per V- atom/ mM	St. Error	Ref
$V_9Mo^{b,adj}$	0.015	±0.008	0.14	±0.07	This work
V_{10}	0.0037	±0.0004	0.037	±0.004	(Samart *et. al* 2018)
$V_{10}^{b,adj}$	0.0036	±0.0004	0.036	±0.004	(Samart *et. al* 2018) and this work
V_1	0.19	±0.07	0.19	±0.07	(Samart *et. al* 2018)

[a] The concentrations of V_{10}, V_9Pt and V_9Mo added to the solutions are given.

[b] The concentrations of these compounds change in the cell culture medium as described below. The EC_{50} values were then recalculated based on ^{51}V NMR studies done at 1 mM samples at t = 0.

[adj] adjusted

2.3.2. Speciation chemistry of substituted decavanadates: V_9Pt

The speciation chemistry of V_9Pt was examined by carrying out ^{51}V NMR studies in an aqueous solution, 7H9 medium (pH 6.58), supernatant, and heated supernatant over a 24 h period. The ^{51}V NMR spectra were compared to that of a 1.0 mM V_9Pt aqueous solution (**Figures. A2.S3-A2.S5**) under the same conditions. The ^{51}V NMR spectra in the 7H9 medium are presented in the manuscript, and the remaining spectra are included in the Appendix II. The Pt atom breaks the symmetry of the polyoxoanion, resulting in four different types of vanadium atoms, two of which overlap, generating a total of three signals for the V_9Pt (V_D, −371.0, $V_{E/F}$ –450.9, and V_G − 475.0 ppm). In comparison to the V_{10} spectra, the signals are slightly shifted and differ in the relative intensities from 2:4:4 in V_{10} to 1:6:2 in V_9Pt (refer to **Figures. A2.S1** and **A2.S2**) (Lee et al., 2008). All spectra contain small amounts of V_1 and V_4 indicated by their weak signals. No

significant changes were observed in the intensity of the signals of V_1 and V_4 over the course of the experiments.

The results of the spectroscopic studies of a 2.0 mM V_9Pt stock solution diluted to a final concentration of 1.0 mM in the 7H9 medium are shown in **Figure 2.3**. The results demonstrate that the V_9Pt polyanion remains intact with only small amounts (<5%) of vanadium oligomers and complexes forming in solution after 24 h. The spectrum collected at 0 h showed three signals of the V_9Pt, V_1 with a contribution of the vanadium-phosphate species ($HVPO_7^{3-}$, V_1 + PV), V_2, V_4 and vanadium citrate complexes (V_2cit^{2-}), a biogenic metal chelator present in the medium (Gorzsas et al., 2004; Kaliva et al., 2002). The percentage of each species measured at various time points remains almost unaltered even after 24 h (see **Table 2.3**). In the supernatant samples, in addition to the signals presented in the 7H9 medium, a new weak signal assigned to the $Vcit^-$ anion was observed. The amount of V_9Pt decreased from 96% in aqueous solution to 79% in the culture medium and approximately 74% in the supernatant. Similar chemistry was observed when the supernatant was heated (**Figure A2.S5 and Table A2.S1**).

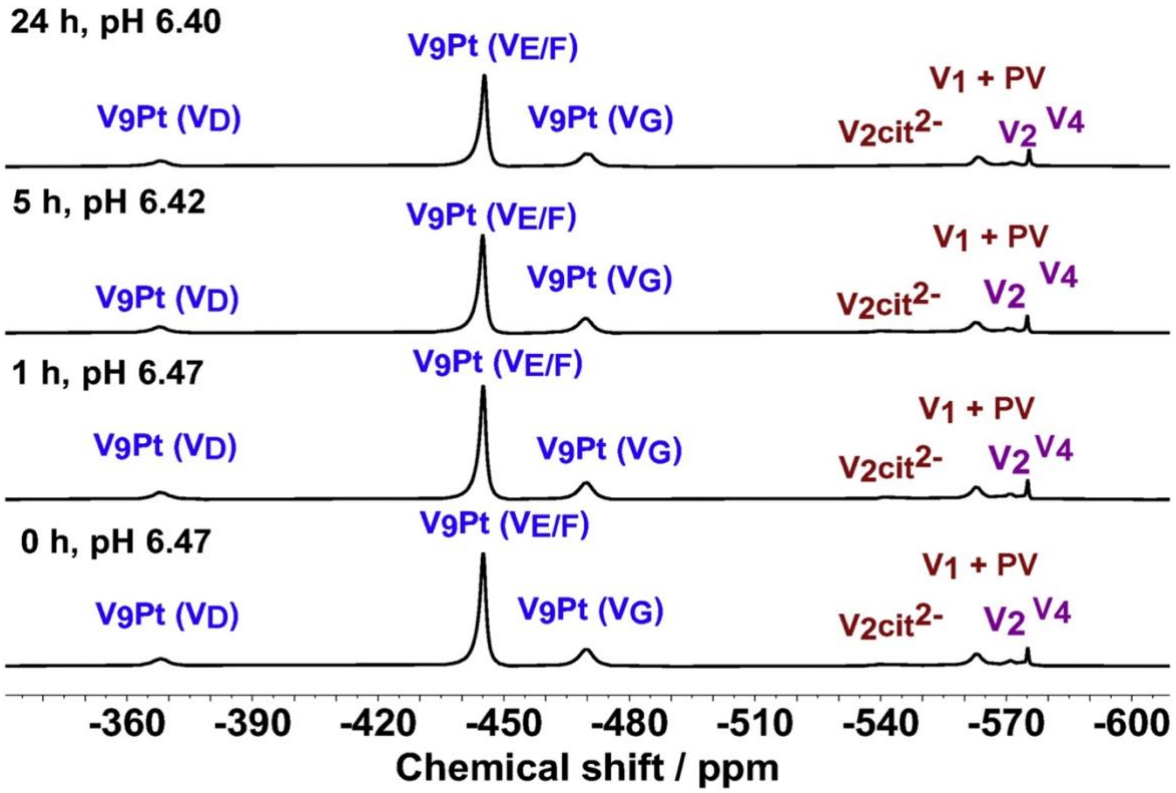

Figure 2.3. ^{51}V NMR spectra of V_9Pt in the 7H9 medium as a function of time. The signals are assigned to the polyoxoanion V_9Pt as follows: (−379 (V_D), −445 ($V_{E/F}$) and − 470 (V_G)), the combined V_1 + PV signal (−573) (Andersson et al., 2005), V_2 (−571) (Crans et al., 2006), V_4 (−575) (Crans et al., 2006), and V_2cit^{2-} (−541, −547) (Gorzsas et al., 2004), where cit = citrate. The spectra recorded for a 1.0 mM aqueous solution of V_9Pt was recorded as a control and shown in Figure A2.S2. The V_9Pt peaks are identical to those reported in the literature (Lee et al., 2008).

Table 2.3. A summary of the species observed in the V_9Pt and V_9Mo in 1.0 mM solutions in 7H9 growth medium at t = 0 h.

^{51}V NMR Peak	Species	Integration/ fraction of total V(V)	Concentration in V-atoms, mM	Concentration in V_9X Molecules, mM
		V_9Pt in the 7H9 medium		
V_G	V_9Pt	0.100	0.100	
V_D	V_9Pt	0.710	0.710	0.789
V_E	V_9Pt	0.194	0.194	

^{51}V NMR Peak	Species	Integration/ fraction of total V(V)	Concentration in V-atoms, mM	Concentration in V_9X Molecules, mM
V_2cit^{2-}	V_2cit^{2-}	0.055	0.055	0.043
V_1 + PV	V_1 + PV	0.126	0.126	0.099
V_2	V_2	0.043	0.043	0.033
V_4	V_4	0.044	0.044	0.034
		V_9Mo in the 7H9 medium		
V_H	V_9Mo + V_{10}	0.133	0.133	0.015
V_I	V_9Mo + V_{10}	0.115	0.115	0.013
V_J	V_9Mo + V_{10}	0.089	0.089	0.010
V_K	V_9Mo	0.060	0.060	0.007
V_L	V_9Mo	0.073	0.073	0.008
V_M	V_9Mo	0.018	0.018	0.002
V_1 + PV	V_1 + PV	0.491	0.491	0.055
V_2	V_2	0.037	0.037	0.004
V_4	V_4	0	0	0
V_2cit^{2-}	V_2cit^{2-}	0.044	0.044	0.005

As shown in **Figure 2.3 and Table 2.3**, 21.1% of V_9Pt is hydrolyzed in the medium, making it necessary to adjust the EC50 value. Therefore, the adjusted EC50 value can be calculated as 78.9% of the value listed in **Table 2.2**. The actual EC50 value in **Table 2.2** is listed as the "adjusted EC50 value in the medium", and the calculation is provided below.

$$EC50\ (V9Pt_{adj}) = 0.0061\ mM\ x\ 0.789 = 0.0048\ mM \quad (0.048\ mM\ per\ V\ atom)$$

2.3.3. Speciation chemistry of substituted decavanadates: V_9Mo

The speciation chemistry of the V_9Mo complex was studied by carrying out spectroscopic studies in an aqueous solution, 7H9 medium (pH 6.58), supernatant and heated supernatant over 24 h where the aqueous solutions of V_9Mo were used as controls. The spectra related to the aqueous speciation data are shown in **Figures. A2.S6, A2.S7, and 2.4**.

In the aqueous solution, the peaks assigned V_H – V_M correspond to the V_9Mo peaks which are identical to the peaks of the 100.0 mM V_9Mo stock solution (**Figures. A2.S6 and A2.S7**). The peaks labeled V_H – V_J contain 65.2% (or 0.652 mM) of a V_9Mo oligomer and 34.8% (or 0.348 mM) of V_{10} (**Figure. A2.S7**). The intensity of V_H-V_K and V_M signals stayed consistent throughout the experiment with the exception of V_L. The concentration of V_L increased over time and was almost equal to the concentration of V_M after 24 h (0.07 mM and 0.08 mM, respectively). The isomeric shifts in **Figure. 2.4a** and b (δ (ppm) = −423, −438*, −494, −503, −513, −515, −523 ppm) are identical to those reported previously as the fully deprotonated form of V_9Mo, $[MoV_9O_{28}]^{5-}$ (pKa 2.77). We attribute these spectral differences to changes in isomer content of V_9Mo which is consistent with the literature (Howarth et al., 1989).

Since the growth studies are carried out at pH 6–6.5, the stability study with V_9Mo is also done in this pH range (pH 6.2–6.3). The pH of the V_9Mo stock solution was adjusted to 6.3, and the stability study was carried out and data is shown in **Figure. 2.4b**. These spectra show that increasing the pH from 5 to 6 results in the formation of only 18% of V_1 which is maintained over 24 h. Considering the higher stability of V_9Mo at slightly lower pH values, a decreasing amount of V_1 is, therefore, attributed to the increasing amount of V_{10} (Howarth et al., 1989).

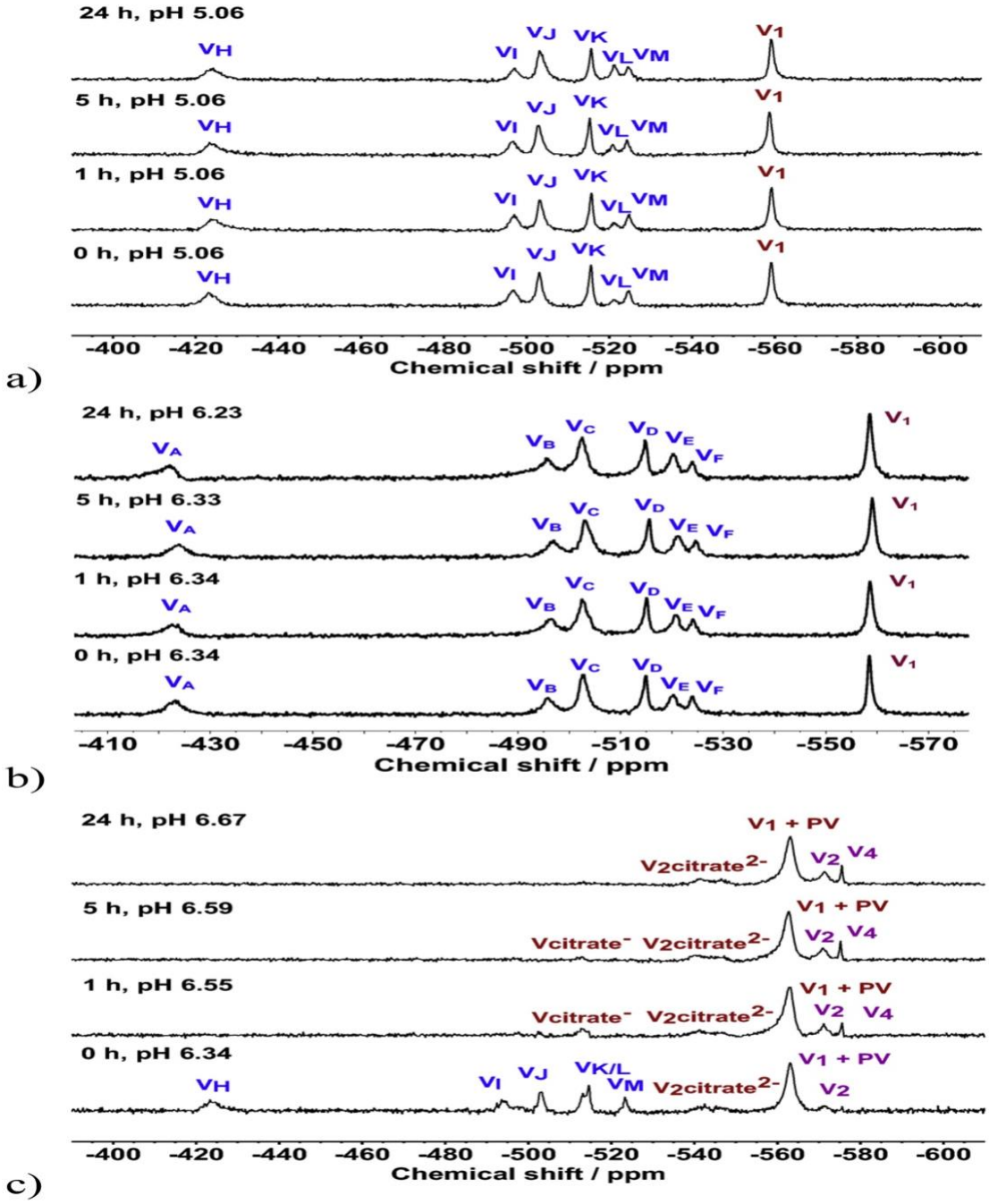

Figure 2.4. Speciation studies of V_9Mo carried out by ^{51}V NMR in a function of time in **a)** 1.0 mM aqueous stock solution at pH 5.06, **b)** 1.0 mM aqueous solution at pH 6.2–6.3, and **c)** the 1.0 mM 7H9 growth medium. The identified vanadium(V) species δ (ppm) in 7H9 medium (near neutral pH) were for V_9Mo (V_H, V_I, V_J, V_K, V_L and V_M = −423 ppm, −494 ppm, −503 ppm, −513 ppm, −515 ppm and − 523 ppm), the combined V_1 + PV (−563) (Andersson et al., 2005), V_2 (−570) (Crans et al., 2006), V_4 (−575) (Crans et al., 2006), $Vcit^-$ (−514) and V_2cit^{2-}(−543) (Gorzsas et al., 2004) and at **b)** 1.0 mM aqueous solution of V_9Mo (at pH near 5). The V_9Mo peaks are identical to those reported in the literature (Howarth et al., 1989).

The results of the speciation studies of V_9Mo in 7H9 medium (pH 6.58), supernatant and heated supernatant are shown in **Figure 2.4** and **A2.S8-A2.S10** where all results are compared to a 1.0 mM aqueous V_9Mo solution at pH = 5.06 (**Figure 2.4a**). From a 100.0 mM stock solution the sample was prepared by dilution of stock to a final concentration of 1.0 mM. The ^{51}V NMR experiments for the aqueous control were performed without any adjustment of the pH. The pH measured in the freshly prepared solution was 5.06 which remained the same throughout the experiment **Figure 2.4b** demonstrates that the V_9Mo polyanion remained intact over 24 h. However, vanadate monomer formed in the solution, and its concentration remained around 0.278 mM, or 27.8% for the duration of the study. Speciation of V_9Mo was evaluated in the 7H9 medium (pH 6.58) over 24 h and is shown in **Figure 2.4b**. The pH has decreased upon the addition of V_9Mo, resulting in the pH of 6.34 at $t = 0$ h. **Figure 2.4b** demonstrates that part of V_9Mo hydrolyzes into the vanadium oligomers, V_1 + PV, V_2 and V_4 within 1 h which is evident by the disappearance of peaks V_H-V_J and V_M. This speciation profile is consistent with the literature, as V_9Mo is less stable at pH >6 (Howarth et al., 1989).

The concentrations of V_1 + PV (where PV corresponds to the vanadium phosphate complex formed in solution), V_2 and V_4 increase after 24 h of incubation. After 1 h, vanadium(V) citrate complexes started to form at −544 ppm, corresponding to the V_2cit^{2-} complex, and at −517 ppm, corresponding to the $Vcit^{-}$ complex (Gorzsas et al., 2004; Kaliva et al., 2002). A broad peak at −544 ppm may represent the presence of several vanadium(V) citrate isomers, the concentrations of which increase after 24 h. The observed decrease in the stability of V_9Mo could be explained by the increasing pH and/or its interactions with the components in the 7H9 medium, indicated by the formation of the citrate and PV complexes.

The V_9Mo complex immediately falls apart in the non-heated supernatant (**Figure. A2.S9**), resulting in the formation of several vanadium oligomers (V_1 + PV and V_2) and vanadium(V) citrate complexes: V_2cit^{2-} (a broad peak at −544 ppm) and $Vcit^{-}$(−517 ppm). The concentration of V_1 + PV decreases from 0.96 mM to 0.77 mM and the concentrations of V_2 and vanadium(V) citrates increase as a function of time after 24 h. A lack of the stability of V_9Mo in the supernatant can be also explained by an increasing pH and its interactions with the supernatant leading to the formation of vanadium(V) citrate complexes. However, V_9Mo appears to be more stable in the heated supernatant (**Figure. A2.S10**) because the complex does not form vanadium oligomers as quickly at 0 h, and significant amounts of V_9Mo are present after 1 h. At t = 0 h, V_1 + PV, V_2, and the citrate complexes start forming, and the tetramer (V_4) forms after 1 h. The trace amounts of the V_9Mo complex are present in the heated supernatant for 5 h, evident by the presence of the overlapping V_K and V_L peaks in the spectra, and the complex eventually falls apart after 24 h.

The ^{51}V NMR data was used to calculate the amounts of different vanadium species present at given experimental conditions. Using the integration values from the spectra, the fractions of all vanadium species were found and then used to calculate the amounts of all vanadium species at different time points (t = 0, 1, 5 and 24 h). A sample calculation is provided in the experimental section for a 1.0 mM V_9Mo control solution at 0 h. The results of these calculations are summarized in **Table 2.3** which represents the changes in concentrations of different species over the course of 24 h.

As shown in **Figure 2.4c**, 68.0% of V_9Mo is hydrolyzed in the medium, making it necessary to adjust its EC_{50} value. Therefore, the adjusted EC_{50} value can be calculated as 32.0% of the value listed in **Table 2.2**. The actual EC_{50} value in **Table 2.2** is listed as the "adjusted EC_{50} value in the medium", and the calculation is provided below.

$\%\mathbf{V9Mo} = [(1/2*(V_H + V_I + V_J)) + V_K + V_L + V_M]*100\%$

$= [(1/2*(0.133 + 0.115 + 0.089)) + 0.060 + 0.073 + 0.018]*100\% = \mathbf{32.0}\%$

$\mathbf{EC_{50}}$ (**V9Mo**,*adj*) = 0.048mM*0.320 = **0.0154mM** (**0.0154mMperV− atom**)

The adjusted EC_{50} values of V_9Mo and V_9Pt clusters were also added to **Table 2.2** to account for the presence of other vanadium oligomers in aqueous solutions. The EC_{50}value of V_9Pt (0.055 mM) is lower than the EC_{50} value of V_9Mo (0.43 mM) by a factor of 8 in terms of concentration, confirming that V_9Pt has shown more potent inhibitory effects on the bacterial growth (**Figure 2.2**). The data in **Table 2.2** shows that V_{10} is a more potent bacterial growth inhibitor than V_9Mo and V_9Pt V_9Mo with the EC_{50}value of 0.0069 mM. A previous study has shown that the inhibitory activity (the EC_{50}values) of V_{10} and V_1 were 0.0037 mM (0.037 mM in terms of V atoms) and 0.19 mM, respectively (Samart et al., 2018). The biological data was supported by the ^{51}V NMR speciation data under the conditions needed for cell growth, providing more insights about the inhibitory activity of the clusters and their speciation chemistry.

2.3.4. Speciation chemistry of decavanadates: V_{10}

The speciation chemistry of the V_{10} complex was reported previously but some of these experiments are reported here for comparison at 1.0 mM. Spectroscopic studies in an aqueous solution, 7H9 medium, supernatant and heated supernatant over 24 h were reported previously (Samart et al., 2018). Here we show the studies in the 7H9 media at 1.0 mM and in aqueous solution at pH 6–6.5 which was used as a control (**Figure. A2.S11**). The spectra in 7H9 media are shown in **Figures. A2.S12 and A2.S13**. We note that the hydrolysis of the V_{10} increases dramatically when *M. smeg*. is added to the growth media as reported previously, **Figure. A2.S13**.

2.4. Discussion

The biological effects of large POMs are well-known, and in this work, we are investigating the subtle differences in properties caused by the transition metal ion substitution in the structure of a large anion. We recently reported dramatic differences between V_{10} and V_1 on the growth inhibition of *M. smeg.,* as V_{10} is 50-fold more potent than V_1 (Samart et al., 2018). Exploring the inhibitory effects of monosubstituted decavanadates would allow to determine the properties of V_{10} that lead to those effects. Both V_9Pt and V_9Mo are structurally similar to V_{10}; in one cluster, the interior vanadium is replaced by the Pt ion, and in another cluster the surface vanadium is replaced by the Mo ion. Both POVs have a minus 5 charge which is different from the minus 6 charge of V_{10}.

In this work, we investigate the growth inhibitory effects of the two substituted decavanadates, V_9Pt and V_9Mo, on *M. smeg* mc^2 *155*. Our results have demonstrated that V_{10} and V_9Pt show comparable inhibitory effects and are 4 times more potent than V_9Mo, while, V_9Mo is 12 times more potent than V_1. The weaker inhibitory effects by V_9Mo compared to the V_9Pt can be explained by its lack of stability in the growth medium although the V_{10} which also hydrolyzes in cell culture media is slightly more potent than V_9Pt. The similarities in the size and structure of all POVs are responsible for the observed growth inhibition that is greater than that of the vanadate monomer and other simple oxovanadates. One major difference between the V_{10} and the V_9Pt and V_9Mo is the difference in overall charge. In the following section we analyze their speciation chemistries in order to assure that we attribute the growth effects to the particular properties of monosubstituted V_{10}'s.

The inhibitory activity of V_9Pt and V_9Mo was evaluated by calculating the EC_{50} values. The EC_{50} values were initially calculated in terms of the concentration of molecules and V atoms

added to the growth media, and then compared to the corresponding values of V_{10} and V_1 (**Table 2.2**). These EC50 calculations rely on the assumption that only one species is present in the V9Mo and V_9Pt samples and no decomposition takes place. Since these clusters are unstable in the growth medium, speciation analysis must be carried out to properly attribute the observed growth effects of the POVs. Since V_9Pt and V_9Mo have different stabilities with the former being very stable, and the latter hydrolyzing pretty rapidly after addition to the media, the data at 0 h was used to adjust the EC_{50} calculations for consistency. That is these values represent the maximum EC_{50} in this system and the initial growth response when the compounds are added to the growth medium.

Particularly in the case of the V_9Mo the compound is decomposing over time. As described in the manuscript, such analysis required time-dependent studies in the presence and absence of cells which led us to calculate the EC_{50} values reflecting the amounts of POVs present during the growth studies. This study compared stabilities of the POVs at 25 °C and since the growth studies were done at 37 °C, the decomposition is likely to have been even faster. Previous studies in aqueous solution show that decomposition of V_{10} follows first-order kinetics in a temperature-dependent manner with the rate of V_{10} hydrolysis being 6 times faster as the temperature is raised (Ramos et al., 2009). Another study with coordination complexes has shown that changes in vanadium oligomerization take place as the temperature changes (Crans et al., 1995). It follows that the changes in coordination complexes as the temperature change are less than that observed in V_{10}. The adjusted values shown in **Table 2.1** take into account the changes in V_{10} concentration upon addition to media, and these values represent the initial effects of the POVs.

The spectroscopic studies of the V_9Pt and V_9Mo complexes were carried out under four different conditions (aqueous solution, 7H9 medium, heated, and non-heated supernatant) to illustrate both chemical and biological transformations that affect the stabilities of V_{10} and its

monosubstituted derivatives. The 7H9 growth medium has nucleophilic components that hydrolyze polyoxovanadates over time, making the clusters decompose faster than under any other conditions. The speciation studies were also carried out in heated and non-heated supernatant. This was done because we found for V_{10}, that the *M. smeg* extruded a material that hydrolyzed V_{10}, therefore speciation studies needed to be carried out under conditions in the presence and absence of extruded components. The speciation data of both V_9Pt and V_9Mo complexes confirms that there is a difference in the species observed under different conditions which were measured and confirmed by ^{51}V NMR (**Figures 2.3, 2.4, A2.S5-A2S10**). The ^{51}V NMR data in the 7H9 medium is presented in the manuscript, since it was used to calculate the EC_{50} values, and the remaining data is presented in the Appendix II.

The ^{51}V NMR data has shown that the stabilities of both V_9Mo and V_9Pt are time dependent. The V_9Pt cluster remains intact for extended periods of time with <10% of the complex falling apart within 24 h. Specifically, the 1.0 mM V_9Pt control remained intact with the small quantities of V_1 and V_4 present in the solution. The 1.0 mM V_9Mo control at pH 5.06 remained intact, with a gradual increase in the concentration one of the peaks over time (V_E) the signal intensity of which is proportional to the isomer content. (**Table 2.2, Figure. A2.S8**). The results in the 7H9 medium for V_9Mo show immediate formation of oligomers (V_1 + PV and V_2), and $Vcit^-$ complexes after the sample preparation. V_9Mo falls apart within one hour, resulting in the increasing concentrations of vanadium oligomers and the $Vcit^-$ complex (**Figure 2.4**) (Gorzsas et al., 2004). The concentrations of all species increase over 24 h, except that $Vcit^-$ eventually converts into the V_2cit^{2-} complex between 5 and 24 h. Contrary to these results, the V_9Pt complex stays intact in 7H9 medium with the increasing amounts of V_1 + PV, V_2, and V_2cit^{2-} complexes also form over time (**Figure. 2.3**).

The V_9Mo falls apart in the non-heated supernatant at 0 h, resulting in the immediate formation of large quantities of V_1 + PV (95.9% of the total vanadium) and a small amount of V_2 (**Figure. A2.S9**). The amounts of the citrate complexes, $Vcit^-$ and V_2cit^{2-}, increase over 24 h. The concentrations of all species, except for the V_1 + PV, increase as a function of time and an increasing pH. The V_9Pt complex stays mostly intact in the supernatant, with the formation of V_1 + PV, V_2, V_4, $Vcit^-$, and V_2cit^{2-} also being observed (**Figure. A2.S4**). The V_9Mo complex is considerably more stable in the heated supernatant which is evident by the presence of the V_D and V_F peaks at 1 h and the V_D peak at 5 h (**Figure. A2.S10**). The complex eventually falls apart after 24 h, resulting in an increased isomer content. The V_9Pt exhibits a similar trend as seen under other conditions (**Figure. A2.S5**). The analysis shows that a 1.0 mM V_9Mo solution in the 7H9 medium at 0 h has only 32.0% of V_9Mo per sample in contrast to a 1.0 mM V_9Pt solution that has 78.9% of V_9Pt. The higher stability of the V9Pt cluster results in the adjusted EC_{50} value to be similar to the EC_{50} based on the amount of cluster added to the solution. The lack of stability of the V_9Mo cluster results in a significant difference between the adjusted and original EC_{50} values (**Figure 2.2, Table 2.2**). The EC_{50} values of $V_{10}$from the previous study were compared to those of V_9Pt and V_9Mo, indicating its most potent inhibitory effects. This pattern holds once the values are adjusted for the hydrolysis upon addition to the 7H9 media.

The changes in speciation chemistry were also confirmed by color observations over 24 h. The color changes of V_9Mo and V_9Pt were monitored in the aqueous solution, 7H9 medium, supernatant, and heated supernatant at different time points to confirm NMR data and the stability of the compounds. The colorimetric data is shown in Appendix II (**Figure. A2.S17**). The colors of the V_9Mo and V_9Pt solutions are pale yellow and orange, respectively, in all samples at 0 h. The V_9Mo samples have shown slight color changes in 7H9 medium, supernatant, and heated

supernatant as the time increased which is consistent with the NMR data, indicating the decomposition of V_9Mo. The V_9Pt samples do not change color over 24 h, confirming the stability of V_9Pt which is consistent with the NMR data.

The biological activity of POVs and their derivatives have been reported in different systems, such as tuberculosis, cancer and diabetic cells, and animals (Bijelic et al., 2018; Bijelic et al., 2019; Postal et al., 2016; Sanchez-Lara et al., 2018). Many studies have been investigating the activity of decavanadate and other polyoxometalates as antidiabetic and anticancer agents (Aureliano, 2011; Pessoa et al., 2015; Rhule et al., 1998). Incorporation of different transition metal ions can drastically change the biological activity of POMs which was documented in the nickel(II)-containing POV, $K_7[NiV_{13}O_{38}]$, showing antiproliferative activity against human tumor (KB) cells (Liu et al., 2005). A recent study has shown that decavanadate is a growth inhibitor of two mycobacterial species, and their activity was significantly higher than that of a known phosphatase inhibitor V_1 (Samart et al., 2018). The ability of a series of platinum(II) coordination complexes to act as anti-tuberculosis agents was also reported (Leite et al., 2013; Plutin et al., 2016). However, no studies were published using molybdenum compounds for anti-tuberculosis applications. This work demonstrated that the growth inhibitory effects of V_9Pt and V_9Mo, on *M. smeg mc2 155*, despite the similar structural arrangement to V_{10}, are significantly different. Although the higher stability of V_9Pt over V_9Mo may explain the greater effect of V_9Pt, the fact that V_{10} is less stable and more effective than V_9Pt, stability cannot be the only factor important for growth inhibitions.

In summary, the results have shown that the all vanadium-containing oxometalate is more potent than the corresponding Pt-substituted POV even though V_{10} hydrolyzes slowly in the media and more rapidly in the media upon addition of *M. smeg*. Similarly, a vanadium coordination

complex has recently been reported to be more potent than cisplatin in brain tumor cells (Levina et al., 2020). The results presented here may suggest that different charges and other types of solution chemistry, including redox, are important factors contributing to the fine-tuning of the observed growth inhibition. Future studies must be carried out to deduce the mechanism of action of these POVs, and that other POVs must be evaluated under similar conditions to answer the questions raised by this study.

2.5. Conclusion

The following study investigated the inhibitory effects of two V_{10} derivatives, V_9Pt and V_9Mo, on the growth of *M. smeg*. Our results have shown that V_{10} is the most potent inhibitor, yet the V_9Pt cluster appears to be most stable under the growth conditions which was confirmed by the spectroscopic studies. The V_9Mo complex is the least potent inhibitor out of the three polyoxovanadates which may be in part be due to its lack of stability under the growth conditions. Although V_{10} was found to be relatively stable in media, the additions of the *M. smeg*. facilitated hydrolysis of the anion.

The speciation analysis included ^{51}V NMR studies confirming at least partial hydrolyses of the anions in 7H9 medium, non-heated and heated supernatant and formation of some vanadium-oxo oligomers, vanadium citrate and vanadophosphate polyanions. Our study demonstrated that the substitution of one V^V ion in V_{10} by a Pt^{IV} or a Mo^{VI} ion results in isostructural derivatives which also inhibit the growth of *M. smeg*., with the platinum (IV)-derivative PtV_9 exhibiting a slightly lower activity, but a higher solution stability than the parent V_{10} and the V_9Mo anions.

2.6. References

Al-Qatati, A., Fontes, F. L., Barisas, B. G., Zhang, D., Roess, D. A., and Crans, D. C. (2013). Raft Localization of Type I Fcε Receptor and Degranulation of RBL-2H3 Cells Exposed to Decavanadate, a Structural Model for V_2O_5. *Dalton Trans.* 42, 11912. doi: 10.1039/c3dt50398d.

Althumairy, D., Postal, K., Barisas, B. G., Nunes, G. G., Roess, D. A., and Crans, D. C. (2020a). Polyoxometalates function as indirect activators of a G protein-coupled receptor. *Metallomics* 12, 1044–1061. doi: 10.1039/d0mt00044b.

Althumairy, D., Zhang, X., Baez, N., Barisas, G., Roess, D. A., Bousfield, G. R., et al. (2020b). Glycoprotein G-protein Coupled Receptors in Disease: Luteinizing Hormone Receptors and Follicle Stimulating Hormone Receptors. *Diseases* 8, 35. doi: 10.3390/diseases8030035.

Andersson, I., Gorzsás, A., Kerezsi, C., Tóth, I., and Pettersson, L. (2005). Speciation in the aqueous H+/H2VO4–/H2O2/phosphate system. *Dalton Trans.*, 3658. doi: 10.1039/b508273k.

Aureliano, M. (2011). Recent Perspectives into Biochemistry of Decavanadate. *WJBC* 2, 215. doi: 10.4331/wjbc.v2.i10.215.

Aureliano, M., and Crans, D. C. (2009). Decavanadate ($V_{10}O_{28}^{6-}$) and Oxovanadates: Oxometalates with Many Biological Aactivities. *Journal of Inorganic Biochemistry* 103, 536–546. doi: 10.1016/j.jinorgbio.2008.11.010.

Bijelic, A., Aureliano, M., and Rompel, A. (2018). The antibacterial Activity of Polyoxometalates: Structures, Antibiotic Effects and Future Perspectives. *Chem. Commun.* 54, 1153–1169. doi: 10.1039/C7CC07549A.

Bijelic, A., Aureliano, M., and Rompel, A. (2019). Polyoxometalates as Potential Next-Generation Metallodrugs in the Combat Against Cancer. *Angew. Chem. Int. Ed.* 58, 2980–2999. doi: 10.1002/anie.201803868.

Bijelic, A., Molitor, C., Mauracher, S. G., Al-Oweini, R., Kortz, U., and Rompel, A. (2015). Hen Egg-White Lysozyme Crystallisation: Protein Stacking and Structure Stability Enhanced by a Tellurium(VI)-Centred Polyoxotungstate. *ChemBioChem* 16, 233–241. doi: 10.1002/cbic.201402597.

Bougie, I., and Bisaillon, M. (2006). Inhibition of a metal-dependent viral RNA triphosphatase by decavanadate. *Biochemical Journal* 398, 557–567. doi: 10.1042/BJ20060198.

Cantley, L. C., Josephson, L., Warner, R., Yanagisawa, M., Lechene, C., and Guidotti, G. (1977). Vanadate is a Ppotent (Na,K)-ATPase Inhibitor Found in ATP Derived from Muscle. *Journal of Biological Chemistry* 252, 7421–7423. doi: 10.1016/S0021-9258(17)40978-1.

Chan, H., Pearson, C. S., Green, C. M., Li, Z., Zhang, J., Belfort, G., et al. (2016). Exploring Intein Inhibition by Platinum Compounds as an Antimicrobial Strategy. *Journal of Biological Chemistry* 291, 22661–22670. doi: 10.1074/jbc.M116.747824.

Chen, S., Wu, G., Long, D., and Liu, Y. (2006). Preparation, Characterization and Antibacterial Activity of Chitosan–$Ca_3V_{10}O_{28}$ Complex Membrane. *Carbohydrate Polymers* 64, 92–97. doi: 10.1016/j.carbpol.2005.10.024.

Chiaradia, L., Lefebvre, C., Parra, J., Marcoux, J., Burlet-Schiltz, O., Etienne, G., ... & Daffé, M. (2017). Dissecting the mycobacterial cell envelope and defining the composition of the native mycomembrane. Sci. Rep, 7(1), 1-12. doi:10.1038/s41598-017-12718-4.

Čolović, M. B., Lacković, M., Lalatović, J., Mougharbel, A. S., Kortz, U., and Krstić, D. Z. (2020). Polyoxometalates in Biomedicine: Update and Overview. *CMC* 27, 362–379. doi: 10.2174/0929867326666190827153532.

Crans, D. C., Baruah, B., and Levinger, N. E. (2006). Oxovanadates: a novel probe for studying lipid–water interfaces. *Biomedicine & Pharmacotherapy* 60, 174–181. doi: 10.1016/j.biopha.2006.02.006.

Crans, D. C., Holst, H., Keramidas, A. D., and Rehder, D. (1995). A Slow Exchanging Vanadium(V) Peptide Complex: Vanadium(V)-Glycine-Tyrosine. *Inorg. Chem.* 34, 2524–2534. doi: 10.1021/ic00114a009.

Crans, D. C., Mahroof-Tahir, M., Anderson, O. P., and Miller, M. M. (1994). X-ray Structure of $(NH_4)_6$(Gly-Gly)$_2V_{10}O_{28}$.cntdot.$4H_2O$: Model Studies for Polyoxometalate-Protein Interactions. *Inorg. Chem.* 33, 5586–5590. doi: 10.1021/ic00102a036.

Crans, D. C., Peters, B. J., Wu, X., and McLauchlan, C. C. (2017). Does anion-cation organization in Na+-containing X-ray crystal structures relate to solution interactions in inhomogeneous nanoscale environments: Sodium-decavanadate in solid state materials, minerals, and microemulsions. *Coordination Chemistry Reviews* 344, 115–130. doi: 10.1016/j.ccr.2017.03.016.

Crans, D. C., Sánchez-Lombardo, I., and McLauchlan, C. C. (2019). Exploring Wells-Dawson Clusters Associated with the Small Ribosomal Subunit. *Front. Chem.* 7, 462. doi: 10.3389/fchem.2019.00462.

Dorsey, B. M., McLauchlan, C. C., and Jones, M. A. (2018). Evidence That Speciation of Oxovanadium Complexes Does Not Solely Account for Inhibition of Leishmania Acid Phosphatases. *Front. Chem.* 6, 109. doi: 10.3389/fchem.2018.00109.

Dutta, N. K., He, R., Pinn, M. L., He, Y., Burrows, F., Zhang, Z.-Y., et al. (2016). Mycobacterial Protein Tyrosine Phosphatases A and B Inhibitors Augment the Bactericidal Activity of the Standard Anti-tuberculosis Regimen. *ACS Infect. Dis.* 2, 231–239. doi: 10.1021/acsinfecdis.5b00133.

Fraqueza, G., Ohlin, C. A., Casey, W. H., and Aureliano, M. (2012). Sarcoplasmic Reticulum Calcium ATPase Interactions with Decaniobate, Decavanadate, Vanadate, Tungstate and Molybdate. *Journal of Inorganic Biochemistry* 107, 82–89. doi: 10.1016/j.jinorgbio.2011.10.010.

Fukuda, N., and Yamase, T. (1997). In Vitro Antibacterial Activity of Vanadate and Vanadyl Compounds against Streptococcus pneumoniae. *Biological & Pharmaceutical Bulletin* 20, 927–930. doi: 10.1248/bpb.20.927.

Gorzsás, A., Getty, K., Andersson, I., and Pettersson, L. (2004). Speciation in the Aqueous $H+/H_2VO^{4-}/H_2O_2$/citrate System of Biomedical Interest. *Dalton Trans.*, 2873. doi: 10.1039/b409429h.

Grundner, C., Ng, H.-L., and Alber, T. (2005). Mycobacterium tuberculosis Protein Tyrosine Phosphatase PtpB Structure Reveals a Diverged Fold and a Buried Active Site. *Structure* 13, 1625–1634. doi: 10.1016/j.str.2005.07.017.

Guo, S., Yang, W., Zhao, M., Tian, R., Zhang, B., and Qi, Y. (2018). In Vitro Anticandidal Activity and Mechanism of a Polyoxovanadate Functionalized by Zn-Fluconazole Complexes. *Molecules* 23, 1122. doi: 10.3390/molecules23051122.

Howarth, O. W., Pettersson, L., and Andersson, I. (1989). Monomolybdononavanadate and cis- and trans-dimolybdo-octavanadate. *J. Chem. Soc., Dalton Trans.*, 1915. doi: 10.1039/dt9890001915.

Hu, X., Wang, H., Huang, B., Li, N., Hu, K., Wu, B., et al. (2019). A New Scheme for Rational Design and Synthesis of Polyoxovanadate Hhybrids with High Antitumor Activities. *Journal of Inorganic Biochemistry* 193, 130–132. doi: 10.1016/j.jinorgbio.2019.01.013.

Jammazi, D., Ratel-Ramond, N., Rzaigui, M., and Akriche, S. (2019). Trapped Mixed [(water)4–(ammonium)4]4+ Octamer in a 3D-binodal (4,8)-Connected Decavanadate core with hexamethylenetetramine: Synthesis, structure, photophysical and antimicrobial properties. *Polyhedron* 168, 146–154. doi: 10.1016/j.poly.2019.04.042.

Kaliva, M., Kyriakakis, E., and Salifoglou, A. (2002). Reactivity Investigation of Dinuclear Vanadium (IV,V)−Citrate Complexes in Aqueous Solutions. A Closer Look into Aqueous Vanadium−Citrate Interconversions. *Inorg. Chem.* 41, 7015–7023. doi: 10.1021/ic020323r.

Lee, S.-Y., Fiene, A., Li, W., Hanck, T., Brylev, K. A., Fedorov, V. E., et al. (2015).

Polyoxometalates—Potent and Selective Ecto-nucleotidase Inhibitors. *Biochemical Pharmacology* 93, 171–181. doi: 10.1016/j.bcp.2014.11.002.

Lee, U., Joo, H.-C., Park, K.-M., Mal, S. S., Kortz, U., Keita, B., et al. (2008). Facile Incorporation of Platinum (IV) into Polyoxometalate Frameworks: Preparation of [H2PtIVV9O28]5− and Characterization by195Pt NMR Spectroscopy. *Angew. Chem. Int. Ed.* 47, 793–796. doi: 10.1002/anie.200703082.

Leite, G. G. S., Baeza, L. C., Batista, A. A., Barbosa, M. I. F., Pavan, F. R., Leite, C. Q. F., et al. (2013). Genes Differentially Expressed by Mycobacterium tuberculosis after Exposure to Ruthenium Phosphinic Compound and Isoniazid. *Int J of Micr Res* 5, 357–362. doi: 10.9735/0975-5276.5.1.357-362.

Levina, A., and Lay, P. A. (2017). Stabilities and Biological Activities of Vanadium Drugs: What is the Nature of the Active Species? *Chem. Asian J.* 12, 1692–1699. doi: 10.1002/asia.201700463.

Levina, A., Pires Vieira, A., Wijetunga, A., Kaur, R., Koehn, J. T., Crans, D. C., et al. (2020). A Short-Lived but Highly Cytotoxic Vanadium(V) Complex as a Potential Drug Lead for Brain Cancer Treatment by Intratumoral Injections. *Angew. Chem. Int. Ed.* 59, 15834–15838. doi: 10.1002/anie.202005458.

Li, Y., Acharya, A., Yang, L., Liu, J., Tajkhorshid, E., Zgurskaya, H. I., ... & Gumbart, J. C. (2023). Insights into substrate transport and water permeation in the mycobacterial transporter MmpL3. *Biophys. J.* 122, 1–11. doi: 10.1016/j.bpj.2023.03.018

Liu, X.S., Zahi, H.J., Peng, Li, D.H., Dai, Z.M., Wang, E.B., Hu, N.H., Jia, H.Q. (2004). Self-assembly Synthesis, Structure Characterization and Antibacterial Activity of Complexes (ABOB）4[$H_2V_{10}O_{28}$]·9H_2O and（ABOB6[$V_{10}O_{28}$]·4H_2O（ABOB=Moroxydine. *Chem. J. Chinese Universities* 25.

Liu, Y., Tian, S., Liu, S., and Wang, E. (2005). In Vitro Inhibitory Effect of Polyoxometalates on Human Ttumor Cells. *Transition Met Chem* 30, 113–117. doi: 10.1007/s11243-004-3825-1.

Lopes, L. G. F., Carvalho, E. M., and Sousa, E. H. S. (2020). A Bioinorganic Chemistry Perspective on the Roles of Metals as Drugs and Targets Against *Mycobacterium tuberculosis* – a journey of opportunities. *Dalton Trans.* 49, 15988–16003. doi: 10.1039/D0DT01365J.

Marques-da-Silva, D., Fraqueza, G., Lagoa, R., Vannathan, A. A., Mal, S. S., and Aureliano, M. (2019). Polyoxovanadate Inhibition of *Escherichia coli* Growth Shows a Reverse Correlation with Ca^{2+} -ATPase Inhibition. *New J. Chem.* 43, 17577–17587. doi: 10.1039/C9NJ01208G.

McLauchlan, C. C., Peters, B. J., Willsky, G. R., and Crans, D. C. (2015). Vanadium–phosphatase

Complexes: Phosphatase Inhibitors Favor the Trigonal Bipyramidal Transition State Geometries. *Coordination Chemistry Reviews* 301–302, 163–199. doi: 10.1016/j.ccr.2014.12.012.

Missina, J. M., Gavinho, B., Postal, K., Santana, F. S., Valdameri, G., de Souza, E. M., et al. (2018). Effects of Decavanadate Salts with Organic and Inorganic Cations on *Escherichia coli*, *Giardia intestinalis*, and Vero Cells. *Inorg. Chem.* 57, 11930–11941. doi: 10.1021/acs.inorgchem.8b01298.

Pessoa, J. C., Etcheverry, S., and Gambino, D. (2015). Vanadium Compounds in Medicine. *Coordination Chemistry Reviews* 301–302, 24–48. doi: 10.1016/j.ccr.2014.12.002.

Pisano, M., Arru, C., Serra, M., Galleri, G., Sanna, D., Garribba, E., et al. (2019). Antiproliferative Activity of Vanadium Compounds: Effects on the Major Malignant Melanoma Molecular Ppathways. *Metallomics* 11, 1687–1699. doi: 10.1039/c9mt00174c.

Pluskey, S., Mahroof-Tahir, M., Crans, D. C., and Lawrence, D. S. (1997). Vanadium Oxoanions and cAMP-Dependent Protein Kinase: an Anti-Substrate Inhibitor. *Biochemical Journal* 321, 333–339. doi: 10.1042/bj3210333.

Plutín, A. M., Alvarez, A., Mocelo, R., Ramos, R., Castellano, E. E., da Silva, M. M., et al. (2016). Anti- Mycobacterium tuberculosis Activity of Platinum(II)/ N , N -disubstituted- N ′-acyl thiourea Complexes. *Inorganic Chemistry Communications* 63, 74–80. doi: 10.1016/j.inoche.2015.11.020.

Pope, M. T., and Müller, A. (1991). Polyoxometalate Chemistry: An Old Field with New Dimensions in Several Disciplines. *Angew. Chem. Int. Ed. Engl.* 30, 34–48. doi: 10.1002/anie.199100341.

Postal, K., Maluf, D. F., Valdameri, G., Rüdiger, A. L., Hughes, D. L., de Sá, E. L., et al. (2016). Chemoprotective Activity of Mixed Valence Polyoxovanadates Against Diethylsulphate in *E. coli* Cultures: Insights from Solution Speciation Studies. *RSC Adv.* 6, 114955–114968. doi: 10.1039/C6RA15826A.

Ramos, S., Duarte, R. O., Moura, J. J. G., and Aureliano, M. (2009). Decavanadate Interactions with Actin: Cysteine Oxidation and Vanadyl Formation. *Dalton Trans.*, 7985. doi: 10.1039/b906255f.

Ramos, S., Moura, J. J. G., and Aureliano, M. (2010). Actin as a Potential Target for Decavanadate. *Journal of Inorganic Biochemistry* 104, 1234–1239. doi: 10.1016/j.jinorgbio.2010.08.001.

Rhule, J. T., Hill, C. L., Judd, D. A., and Schinazi, R. F. (1998). Polyoxometalates in Medicine. *Chem. Rev.* 98, 327–358. doi: 10.1021/cr960396q.

S X, L., J H, Z., J, P., H D, L., M Z, D., B E, W., et al. (2004). Self-assembly Synthesis,Structure

Characterization and Antibacterial Activity of Complexes （ABOB）4[H2V10O28]·9H2O and （ABOB）6[V10O28]·4H2O（ABOB=Moroxydine. *Chem. J. Chinese Universities* 25.

Samart, N., Arhouma, Z., Kumar, S., Murakami, H. A., Crick, D. C., and Crans, D. C. (2018). Decavanadate Inhibits Mycobacterial Growth More Potently Than Other Oxovanadates. *Front. Chem.* 6, 519. doi: 10.3389/fchem.2018.00519.

Sánchez-Lara, E., Treviño, S., Sánchez-Gaytán, B. L., Sánchez-Mora, E., Eugenia Castro, M., Meléndez-Bustamante, F. J., Mendez-Rojas, M.A., Gonzalez-Vergara, E. (2018). Decavanadate Salts of Cytosine and Metformin: A Combined Experimental-Theoretical Study of Potential Metallodrugs Against Diabetes and Cancer. *Front. Chem.* 6, 402. doi: 10.3389/fchem.2018.00402.

Sánchez-Lombardo, I., Baruah, B., Alvarez, S., Werst, K. R., Segaline, N. A., Levinger, N. E., Crans, D. C.. (2016). Size and Shape Trump Charge in Interactions of Oxovanadates with Self-Assembled Interfaces: Application of Continuous Shape Measure Analysis to the Decavanadate Anion. *New J. Chem.* 40, 962–975. doi: 10.1039/C5NJ01788B.

Sarafianos, S. G., Kortz, U., Pope, M. T., and Modak, M. J. (1996). Mechanism of Polyoxometalate-mediated Inactivation of DNA Polymerases: An Analysis with HIV-1 Rreverse Transcriptase Indicates Specificity for the DNA-binding Cleft. *Biochemical Journal* 319, 619–626. doi: 10.1042/bj3190619.

Shahid, M., Sharma, P. K., Anjuli, Chibber, S., and Siddiqi, Z. A. (2014). Isolation of a Decavanadate Cluster $[H_2V_{10}O_{28}][4\text{-picH}]_4\cdot 2H_2O$ (4-pic = 4-picoline): Crystal Structure, Electrochemical Characterization, Genotoxic and Antimicrobial Studies. *J Clust Sci* 25, 1435–1447. doi: 10.1007/s10876-014-0721-5.

Strukan, N., Cindric´, M., and Kamenar, B. (1997). Synthesis and Structure of $[(CH_3)4N]_4[H_2MoV_9O_{28}]Cl\cdot 6H_2O$. *Polyhedron* 16, 629–634. doi: 10.1016/0277-5387(96)00316-6.

Tonks, N. K. (2006). Protein Tyrosine Phosphatases: From Genes, to Function, to Disease. *Nat Rev Mol Cell Biol* 7, 833–846. doi: 10.1038/nrm2039.

Toumi, S., Ratel-Ramond, N., and Akriche, S. (2015). Decavanadate Cage-like Cluster Templated by Organic Counter Cation: Synthesis, Characterization and Its Antimicrobial Effect Against Gram Positive E. Feacium. *J Clust Sci* 26, 1821–1831. doi: 10.1007/s10876-015-0881-y.

Turner, T. L., Nguyen, V. H., McLauchlan, C. C., Dymon, Z., Dorsey, B. M., Hooker, J. D., et al. (2012). Inhibitory Effects of Decavanadate on Several Enzymes and Leishmania tarentolae In Vitro. *Journal of Inorganic Biochemistry* 108, 96–104. doi: 10.1016/j.jinorgbio.2011.09.009.

Williams, M., Mizrahi, V., and Kana, B. D. (2014). Molybdenum Cofactor: A Key Component of *Mycobacterium tuberculosis* Pathogenesis? *Critical Reviews in Microbiology* 40, 18–29. doi: 10.3109/1040841X.2012.749211.

Zheng, Y., Gan, H., Zhao, Y., Li, W., Wu, Y., Yan, X., et al. (2019). Self-Assembly and Antitumor Activity of a Polyoxovanadate-Based Coordination Nanocage. *Chem. Eur. J.* 25, 15326–15332. doi: 10.1002/chem.201903333.

Zhou, B., He, Y., Zhang, X., Xu, J., Luo, Y., Wang, Y., et al. (2010). Targeting Mycobacterium Pprotein Tyrosine Phosphatase B for Antituberculosis Agents. *Proc. Natl. Acad. Sci. U.S.A.* 107, 4573–4578. doi: 10.1073/pnas.0909133107.

Chapter 3: Exploring growth of *Mycobacterium smegmatis* treated with anticarcinogenic vanadium-compounds

3.1. Introduction

The power of metal complexes as anticancer agents, the best examples being Pt-based compounds such as cisplatin, carboplatin and oxaliplatin, has been demonstrated in clinical settings over several decades (Cirri et al., 2021; Dasari and Tchounwou, 2014; Dilruba and Kalayda, 2016; Graf and Lippard, 2012; Jin et al., 2021; Johnstone et al., 2013; Xu et al., 2021; Rottenberg et al., 2021; Zhou et al., 2020). In addition to Pt-based compounds, a number of other metal-based compounds have been reported to have anticancer properties including Ru-containing anticancer compounds (Thota et al., 2018), Cu-containing anticancer compounds (Manov et al., 2022), vanadium-containing compounds (Crans et al., 2018; Selman et al., 2018) and other transition metal-based compounds (Crans and Kostenkova, 2020; Shahbazi et al., 2020; Fernandes et al., 2020; Bauer et al., 2019; Needham et al., 2021; Frei et al., 2020; Imberti and Sadler, 2020). Although the compounds that make it to the clinic are highly effective, patients treated with anticancer agents are very susceptible to bacterial infections (Manov et al., 2022; Eyvazi et al., 2020; Pulcini et al., 2021; Ross et al., 2022; Rossi et al., 2021).

Microbial infections can be very serious; some have been reported to modulate host cell transformation and hence promote the production of carcinogenic metabolites participating in inflammation responses, to disrupt cell metabolism, and to modify genomic or epigenetic characteristics (Eyvazi et al., 2020; Pulcini et al., 2021; Ross et al., 2022; Rossi et al., 2021). Reducing the potential problems prompting patient evaluation and intravenous administration of broad spectrum antibiotics is critically important and may represent a practice difference for the

patient (Eyvazi et al., 2020; Pulcini et al., 2021; Ross et al., 2022; Rossi et al., 2021). Thus, information on the effects of anticarcinogenic compounds on various bacterial strains are of general interest.

When evaluating effects of metal complexes on bacterial cells, it is, however, important to consider that these compounds are coordination complexes and many of these compounds do not remain intact during study due to their inherent hydrolytic instability in complex biological media (Doucette et al., 2016; Esteban-Fernandez et al., 2010; Levina et al., 2017; Nunes et al., 2021; Wexselblatt et al., 2013). In addition, the effects of the metal complex versus its ligand can be important, particularly in cases where the ligand has potent effects on the cells being studied (Nunes et al., 2021; Loizou et al., 2021; Creaven et al., 2010; Correia et al., 2014) Here we use a recently identified anticancer compound, a Schiff base vanadium-based catecholate complex (oxidovanadium(IV) complexed to N-(salicylideneaminato)-N'-(2-hydroxyethyl)ethane-1,2-diamine 3,5-di-tert-butylcatecholato ligand)) (Crans et al., 2019; Levina et al., 2020) which was found to be significantly more potent than cisplatin in several cancer lines including glioma multiforme, an aggressive brain cancer (T98g), lung cancer cells (A549), and pancreas cancer cells (PANC-1) [34]. Because this vanadium compound is uniquely more stable than generally observed for Schiff base V(V) catecholato complexes, this class of compounds has been proposed for targeted injections directly into tumors (Levina et al., 2020).

In this study, we also investigate several related vanadium complexes (V-complexes) containing known, non-innocent catecholato ligands to determine whether there are identifiable relationships between effects of the metal complex on bacterial growth and complex stability in bacterial growth media. For those complexes that do not remain intact, biological effects of the resulting products including the non-innocent ligand is of considerable interest.

Table 3.1 shows a summary of studies in which the V-complex, the ligand and free metal ion were evaluated in different bacteria, fungi, or pathogens (Correia et al., 2014; Maurya et al., 2010; Rosu et al., 2012; Machado et al., 2015; He et al., 2018; Missina et al., 2018). Although vanadate was reported to inhibit growth of *M. smeg* some time ago (Costello and Hedgecock, 1959), we have recently demonstrated that cell growth of *M. smeg* is much more sensitive to the large compact decavanadate anion (V_{10}-anion) than the smaller vanadate monomer (V_1 anion) (Samart et al., 2018). Furthermore, replacing one of the V-atoms in the V_{10} cluster to form a monosubstituted polyoxidovanadate affects growth inhibition with the order being V_{10} > V_9Pt > V_9Mo (Kostenkova et al., 2021). The sensitivity of *M. smeg* to monosubstituted polyanions further motivated studies here examining cell growth effects for a number of related intact and hydrolyzed coordination complexes with non-innocent ligands in this representational bacterial system.

Table 3.1. Previous studies of the effect of various V-complexes in other microorganisms.

Vanadium Complexes	Microorganism (a, b, c)	Inhibitory activity	Results	Reference
- **$M_2[CH_2\{V^VO_2(sal\text{-}bhz)\}_2]\cdot 2H_2O$** - **$M_2[CH_2\{V^VO_2(sal\text{-}fah)\}_2]\cdot 2H_2O$** **M = K^+ or Cs^+ for sal-bhz** (5,5'-methylbis (salicylaldehyde) and benzoylhydrazide**);** **M = K^+ for sal-fah** (5,5'-methylbis(salicylaldehyde) and 2-furoylhydrazide)	- **Protozoa:** *Entamoeba histolytica*	IC_{50} values between 0.36 µM and 2.32 µM	Complexes had potent antibacterial activity compared to hydrazone ligand.	(Maurya et al., 2010)
-$[VO(L)_2(H_2O)]SO_4$ **-L = 1-phenyl-2,3-dimethyl-4-(1*H*-indole-3-carboxaldehyde)-3-pyrazolin-5-one (HL).**	**- Bacteria:** *Staphylococcus aureus*[a], *Klebsielle pneumoniae*[b], *Legionella monocytogenes*[b], *Escherichia coli*, *Pseudomonas aeruginosa*[b], and *Salmonella typhimurium*[b]	IC_{50} values between 16 and 64 µg/mL	Complexes had potent antibacterial activity compared to Schiff base ligand	(Rosu et al., 2012)

	- Fungi: *Candida albicans* and *Asperg illus flavus*			
- **Complexes with 8-hydroxyquinoline (8HQ)**	**- Bacteria:** *Mycobacterium tuberculosis*	IC_{50} values between 2.9 µM and 42.23 µM	Complexes had less potent activity compared to 8-hydroxyquinolin e (8HQ) ligand	(Correia et al., 2014)
- **V(IV)O(Salophen)** - **$[VO(C_{20}H_{16}N_4O_2)]\cdot H_2O$**	**-Parasite:** *Leishmania amazonensis*	IC_{50} values of 3.51µM and 6.65 µM	Complexes had more potent activity compared to H_2Salophen ligand	(Machado et al., 2015)
- **Complexes with chlorido-substituted hydrazone ligands ([VOL(OEt)(EtOH)]**	**- Bacteria:** *Bacillus subtilis*[a], *Staphylococcus aureus, Escherichia coli, and Pseudomonas fluorescens*[b] - **Fungi:** *Candida albicans* and *Aspergillus niger*	MICs values at 1.2 µg/mL and >150 µg/mL	Complexes have stronger activities compared to the free chloride hydrazones	(He et al., 2018)
- **$(3Hpca)_4[H_2V_{10}O_{28}]\cdot 2H_2O\cdot 2(3\text{-pca})$; (complex I)** - **$(4\text{-Hpca})_4[H_2V_{10}O_{28}]\cdot 2(4\text{-pca})$; (complex II)**	**- Bacteria:** *Escherichia coli*	GI_{50} values at 0.47 and 0.67 mmol L^{-1}	Cation increases toxicity	(Missina et al., 2018)
- **Complexes formed with 1,10-phenanthroline or 4,7-dimethyl-1,10-phenanthroline ligands**	- **Cancer cells**[c]**:** Ovarian, cisplatin sensitive A2780, breast MCF7 and prostate PC3		Complexes have variable potency comparable with effects of free phenanthroline ligand and duration of treatment	(Nunes et al., 2021)
- **Complexes with Vitamin E-hydroxylamino-Triazine Ligands**	- **Cancer cells:** Human Cal33 cells, Hela cells, embryonic mouse fibroblasts (NIH/3T3)		Complexes are less toxic than free ligands for all three cell lines	(Loizou et al., 2021)

[a] Gram-positive bacteria; [b] Gram-negative bacteria; [c] Cancer cell lines (A2780, MCF7 and PC3).

The structure of the classes of coordination complexes where both complex and ligand have previously been investigated in bacteria are listed in **Figure 3.1** (Nunes et al., 2021; Correia et al.,

2014; Maurya et al., 2010; Rosu et al., 2012; Machado et al., 2015; He et al., 2018). The compounds reported include complexes with hydrazones (Maurya et al., 2010), Schiff bases (Rosu et al., 2012), quinolones (Correia et al., 2014) and related studies with phenanthrolines (Nunes et al., 2021) and Vitamin E-hydroxylamino-Triazine ligands (Loizou et al., 2021). Several phenanthroline complexes have been studied extensively in cancer cells (**Table 3.1**); because the ligand has been shown to have variable effects depending on time of treatment, it serves as an excellent comparison for these studies carried out in bacteria (Nunes et al., 2021). Previous studies demonstrate that compounds are sensitive to the oxidation state of the metal ion and the ligand as well as the nature of the coordination complexes. It is, however, important to note that both the biological and chemical systems investigated made direct comparisons difficult (Mosquillo et al., 2020).

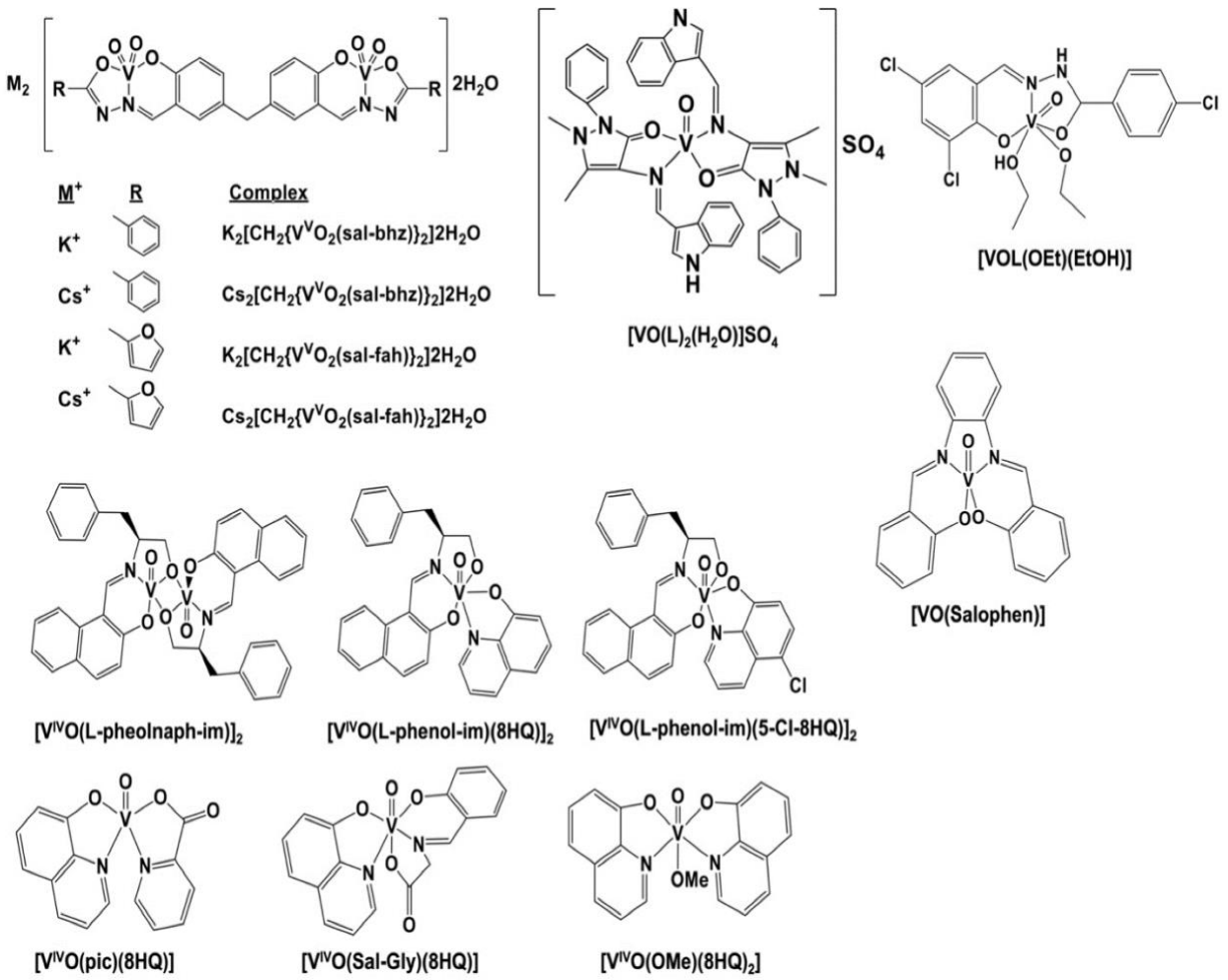

Figure 3.1. The structure of the classes of coordination complexes where activity of both the complex and ligand was investigated in bacteria (Correia et al., 2014; Maurya et al., 2010; Rosu et al., 2012; Machado et al., 2015; He et al., 2018).

Generally, complexes formed by hydrazones and Schiff bases were found to be more potent than their ligands (Maurya et al., 2010; Rosu et al., 2012) while compounds formed from quinolones were less potent than their respective ligands (Correia et al., 2014). Recently, we identified an non-toxic Schiff base oxidovanadium(V) complex (N-(salicylideneaminato)-N'-(2-hydroxyethyl)ethane-1,2-diamine) containing a hydrophobic and sterically-hindered catecholate ligand (3,5-di-tert-butylcatecholato ligand) which is effective against several cancer cell types including glioma multiforme, an aggressive brain cancer (T98g), lung cancer cells (A549),

pancreas cancer cells (PANC-1), cultured human bone cancer cells, breast cancer (MDA-MB-231) and human foreskin fibroblasts, (HFF-1) (Crans et al., 2019; Levina et al., 2020; Griffin et al., 2019; Lima et al., 2021). Several catecholate ligands have been reported to be toxic (Chen et al., 2022; Lambert de Malezieu et al., 2021; Schweigert et al., 2001) and, as a result, either more or less potent than their parent vanadium complexes (Correia et al., 2014; Crans et al., 2019). In contrast, to the parent catecholate, the sterically hindered catechol 3,5-di-tert-butylcatechol in a complex has been reported to be less toxic in female Swiss mice (Lima et al., 2021). To obtain more information on the effects of intact complexes versus ligand, we selected a group of complexes with varying stability that contained a ligand such as a catechol with the potential to inhibit *M. smeg* growth.

3.2. Materials and Methods

3.2.1. Materials

3.2.1.1. Cell culture materials.

The Middlebrook 7H9 Broth medium (Ref. no. 271310; Difco™)) was obtained from BD Biosciences and autoclaved before use. The medium was supplemented with oleic acid (0.6% v/v; Sigma Aldrich), 5 mg mL^{-1} albumin (VWR), 2 mg mL^{-1} dextrose (Sigma Aldrich), and 10% Tyloxapol (Chem-Impex Int'l Inc). *M. smeg* has been maintained in our laboratory for some time as has been reported previously (Kumar et al., 2020).

3.2.1.2. Chemicals for synthesis and spectroscopic studies.

Catechol ligands were purchased from Sigma-Aldrich. Dimethyl sulfoxide (DMSO, 99.9%) was purchased from Sigma-Aldrich and deuterium oxide (D_2O, 99.9%) was purchased from Cambridge Isotope Laboratories. Reagents were used as received without further purification.

Eight Schiff base vanadium catecholato coordination complexes were selected and prepared using procedures described initially by the Pecoraro group and described previously by our group (Cornman et al., 1992; Chatterjee et al., 2011; Goncharova-Zapata et al., 2013). DMSO was used for solubilizing the compounds for NMR spectroscopic studies and cell culture studies. Infrared spectra were obtained using a Bruker Tensor II FT-IR spectrometer in attenuated total reflectance mode with a 4 cm^{-1} resolution.

3.2.2. Methods

3.2.2.1. Cell culture and growth conditions.

M. smeg was cultured in Middlebrook 7H9 medium (Ref no. 271310; Difco) supplemented with 10% OAD (oleic acid, albumin, dextrose), 0.2% (v/v) glycerol, and 10% Tyloxapol and incubated with shaking for 24h at 37°C. *M. Smeg* was grown to a mid-logarithmic growth phase assessed via spectrophotometry and occurred at an optical density of 0.6 at 600nm (OD_{600}). In some experiments where *M. Smeg* was treated with vanadium complexes, **t**he cell culture supernatant was collected for ^{51}V NMR studies.

3.2.2.2. Minimum inhibitory concentration (MIC) measurements.

The inhibitory activity of the tested compounds was determined by measuring the lowest concentration that caused bacterial growth inhibition of 50% (IC_{50}). *M. Smeg* was grown to mid-log phase of 0.6-0.8 at OD_{600}. The final concentrations of the compounds used in these studies were obtained using serial dilutions to final concentration range of 2mM to 0.0039mM and placed with *M. smeg* in 7H9 media into a 96 well plate. Plates were incubated for 24h at 37°C. A Bio-Rad Benchmark Reader was used to check the cell viability at OD_{600} at appropriate times. IC_{50} was determined to check the lowest concentration of complexes that was inhibited the bacterial growth by 50%.

3.2.2.3. Statistical analysis.

For each treatment, data were represented as the mean and standard deviation of the IC_{50} from triplicate measurements. The IC_{50} was calculated using GraFit 5 data analysis software (Ver.5.0.13).

3.2.3. Chemistry

3.2.3.1. Synthesis of Schiff base vanadium catecholato coordination complexes.

The complexes were prepared from $[V(O)_2(Hshed)]$ through a condensation reaction as described by the Pecoraro group (Cornman et al., 1992) and our group (Chatterjee et al., 2011; Goncharova-Zapata et al., 2013). See **Figure 3.2** for the structures of the compounds and their abbreviations. After preparation of the $[VO_2(Hshed)]$ precursor (Cornman et al., 1992; Chatterjee et al., 2011; Goncharova-Zapata et al., 2013) the catechol was added to generate the complexes used in this study. [VO(Hshed)(cat)] (Cornman et al., 1992; Chatterjee et al., 2011; Goncharova-Zapata et al., 2013); [VO(Hshed)(dtb)], (Cornman et al., 1992; Chatterjee et al., 2011; Goncharova-Zapata et al., 2013); $[VO(Hshed)(4NO_2)]$ (Cornman et al., 1992; Chatterjee et al., 2011; Goncharova-Zapata et al., 2013); [VO(Hshed)(tbc)] (Cornman et al., 1992; Chatterjee et al., 2011; Goncharova-Zapata et al., 2013); and three new complexes [VO(Hshed)(CN)]); [VO(Hshed)(3OMet)] and [VO(Hshed)(Coum)]).

3.2.3.2. Synthesis of [VO(Hshed)(CN)]).

To a 250 mL round bottom Schlenk flask acetone (100 mL) was added which was then degassed with argon. $[VO_2(Hshed)]$ (0.290g, 1.00 mmol) was added to the degassed acetone followed by 3,4-dihydroxybenzonitrile (0.135g, 1.00 mmol). A deep purple solution resulted after approximately 20 seconds. The solution was stirred overnight under argon. The reaction mixture was vacuum filtered and then concentrated to dryness under reduced pressure at room temperature.

The purple residue was dissolved in a minimal amount of acetone and then *n*-hexane (100 mL) was added. The solution was allowed to stand in a -20 °C freezer overnight. The dark microcrystalline precipitate was vacuum filtered, washed with cold n-hexane (< 0 °C, 2 x 25 mL), and dried under vacuum for 3 days to yield 0.341 g (0.838 mmol, 84%) purple solid. ^{51}V NMR (in CD_3CN): -138 ppm, -113 ppm (minor isomer). ^{1}H NMR (400 MHz, CD_3CN): δ 8.74 (s, 1H), 7.64-7.62 (dd, 1 H), 7.59-7.54 (dt, 1H), 7.17-7.13 (m, 1H), 7.00-6.96 (dt, 1H), 6.91-6.88 (m, 1H) 6.83-6.80 (d, 1H), 4.23-4.18 (dd, 1H), 4.10-4.03 (dt, 1H), 3.79-3.72 (m, 1H), 3.69-3.63 (m, 1H), 3.59-3.49 (m, 2H), 3.39-3.31 (m, 1H), 3.04-2.90 (m, 2H), 2.81-2.78 (t, 1H). IR (ATR, 4 cm^{-1}): 3049 (O-H), 2218 (C≡N), 1712 (Aromatic), 953 (V=O). UV-vis peaks (in DMSO): 280 nm and 305 nm.

3.2.3.3. Synthesis of [VO(Hshed)(3OMet)]

To a 250 mL round bottom Schlenk flask, acetone (100 mL) was added which was then degassed with argon. [VO_2(Hshed)] (0.290g, 1.00 mmol) was added to the degassed acetone followed by 3-methoxy catechol (0.140g, 1.00 mmol). A deep purple solution resulted after approximately 20 seconds. The solution was stirred overnight under argon. The reaction mixture was vacuum filtered and then concentrated to dryness under reduced pressure at room temperature. The purple residue was dissolved in a minimal amount of acetone and then *n*-hexane (100 mL) was added. The solution was allowed to stand in a -20 °C freezer overnight. The dark microcrystalline precipitate was vacuum filtered, washed with cold n-hexane (< 0 °C, 2 x 25 mL), and dried under vacuum for 3 days to yield 0.280 g (0.680 mmol, 68%) purple solid. ^{51}V NMR in CD_3CN: 288 ppm. ^{1}H NMR (400 MHz, CD_3CN): δ 8.63 (s, 1H), 7.51-7.48 (t, 1H), 6.87-6.83 (t, 1H), 6.76-6.66 (m, 2 H), 6.34-6.32 (d, 1H), 6.07-6.05 (d, 1H), 5.99-5.97 (d, 1H), 3.90-3.87 (m, 3H), 3.84-3.76 (m, 2H), 3.66-3.61 (m, 2H), 3.49-3.39 (m, 1H), 3.38-3.31 (m, 1H), 2.99-2.91 (m,

1H), 2.84-2.81 (t, 1H). IR (ATR, 4 cm^{-1}): 1636 (Aromatic), 1304, 1267, 1108 (C-O), 954 (V=O). UV-vis peaks (in DMSO): 280 nm, 335 nm, 390 nm, and 565 nm.

3.2.3.4. Synthesis of [VO(Hshed)(Coum)].

The following reaction was carried out under argon atmosphere, typically using Schlenk line to set up the reaction followed by argon balloon during the reaction. The **H_2**Coum (0.196 g, 1.10 mmol, recrystallized from benzene) and solid VO_2(Hshed) (0.290 g, 1.0 mmol) were added to a 100 mL round bottom Schlenk flask followed by absolute ethanol (50 mL). The conversion of the yellow VO_2(Hshed) to the purple/black VO(Hshed)(Coum) occurred over 4 h (colors changed from light yellow to brown to dark purple). However, the mixture was allowed to stir covered overnight under argon after which time the dark purple reaction mixture was cooled in a dry ice/acetone bath for 1 min and then was vacuum filtered, leaving a purple black solid on the filter paper. The solid was washed twice with cold absolute ethanol (<0 °C, 25 mL) and then dried under vacuum for 3 days to yield 0.339 g (0.753 mmol, 75% yield) purple/black solid. The filtrate was concentrated, suspended in cold EtOH and filtered but yielded no additional product. ^{51}V NMR in CD_3CN: -46 ppm, -10 ppm (minor isomer). ^{1}H NMR (400 MHz, CD_3CN): δ 8.71 (s, 1H), 7.69-7.67 (d, 1H), 7.61-7.58 (dd, 1H), 7.56-7.51 (dt, 1H), 6.96-6.92 (dt, 1H), 6.80-6.77 (d, 1H), 6.65 (s, 1H), 6.24 (s, 1H), 5.98-5.95 (s, 1H), 4.49-4.44 (m, 1H), 4.23-4.17 (dd, 1H), 4.10-4.02 (dt, 1H), 3.82-3.74 (m, 1H), 3.70-3.63 (m, 1H), 3.60-3.48 (m, 2H), 3.39-3.31 (m, 1H), 3.04-2.91 (m, 1H), 2.81-2.78 (t, 1H). IR (ATR, 4 cm^{-1}): 1719 (C=O), 1636 (Aromatic), 1289, 1151 (C-O), 955 (V=O). Calc for $C_{20}H_{19}N_2O_7V$: C, 53.19; H, 4.07; N, 6.06. Found: C, 53.34; H, 4.25; N, 6.22. UV-vis peaks (in DMSO): 280 nm, 360 nm, and 520 nm.

3.2.3.5. Preparation of stock solution for NMR spectroscopic studies.

A 20.0mM stock solution of the respective V-complex was prepared in DMSO by dissolving 0.0580g, 0.0764g, 0.0989g, and 0.0825g of $[V(O)_2(Hshed)]$, [VO(Hshed)(cat)], [VO(Hshed)(dtb)], or [VO(Hshed)(3OMet)], respectively, in 10ml DMSO. The solution of each V-complex was diluted to form a solution with highest final concentration of 10.0mM in 50:50 DMSO:H_2O or 50:50 DMSO:7H9 media.

3.2.3.6. Preparation of stock solutions for cell culture experiments.

A 20 mM stock solution of the respective V-complex and its free ligands was prepared in DMSO and diluted with 7H9 media to a concentration of 2.0 mM for biological studies.

3.2.4. UV-Visible spectra.

Absorbance spectra of V-complexes were measured at 0, 1, 5, and 24 h using a UV-visible spectrophotometer (BioTek Synergy™ HTX Multi-Mode Microplate Reader) in the 200 nm to 800 nm wavelength range. Samples were prepared in H_2O, 7H9 media or the supernatant fraction obtained from *M. smeg* cell culture.

3.2.5. Nuclear Magnetic Resonance (NMR) measurements.

^{51}V NMR using a Bruker 400MHz spectrometer was used to observe species present at different time points in DMSO-H_2O samples and DMSO-7H9 media. Studies of the bacterial supernatant from *M. smeg* culture were attempted as well. Speciation of V-complexes were measured through the integration of the vanadium peaks in the NMR spectra. The stability of the V-complexes and precursor complex $[V(O)_2(Hshed)]$ was also checked using ^{51}V NMR spectroscopy.

3.2.6. Analysis of species in stock solutions and media as a function of time.

The species present were analyzed based on spectroscopic data in aqueous-DMSO solutions and in growth media solutions before and after *M. smeg* growth as described above. The 20.0 mM stock solutions of V-complexes were prepared in DMSO and diluted to the final concentration of 10.0 mM in DI H_2O (50:50, DMSO:H_2O) or to the final concentration of 10.0 mM in 7H9 medium (50:50, DMSO:7H9). Samples were incubated at 37°C during the stability studies. The V-complexes in double distilled H_2O and in 7H9 medium (pH 6.65 prior to adding the DMSO solution) were measured at different time points (0, 1, 5 and 24 h) using UV-vis spectroscopy and ^{51}V NMR spectroscopy. The UV-vis spectra were recorded using DMSO:H_2O (50:50) as a reference and for fresh media and for supernatant previously obtained from *M. smeg* culture. For studies using cell culture supernatant, at each time point (0, 1, 5 and 24 h), a 1 mL aliquot of supernatant was collected from the 5 mL sample for ^{51}V NMR analysis. The 7H9 media samples measured as a function of time are shown in **Figure 4** and others are shown in Appendix III. The NMR spectra were analyzed by integrating the ^{51}V NMR spectra and assuming that all the V-compounds were present as V(V) species. The species present in the spectra were calculated based on the mole fraction of the observed signals and the known concentration of V-complexes added to the solutions.

3.3. Results

3.3.1. Compound design.

We first investigated the effects of a series of Schiff base vanadium(V) catecholato compounds related to the oxidovanadium(V) complex (N-(salicylideneaminato)-N'-(2-hydroxyethyl)ethane-1,2-diamine) complex which exhibits potent anticancer properties (Crans et al., 2019; Levina et al., 2020; Griffin et al., 2019) and is shown in **Figure 3.2**. The varying effects

of these compounds on *M. smeg* growth of each vanadium complexes was compared to the effects of its free ligands (see Appendix III; **Figure A3.S1**). The complexes selected for investigation contained non-innocent ligands or formed complexes with different electronic properties. We selected the known V-scaffold [VO_2(Hshed)], the most potent anti-cancer agent **[**VO(Hshed)(dtb)], and control compounds with different electronic properties the parent [VO(Hshed)(cat)], and two compounds with electronic withdrawing ligands [VO(Hshed)(tbc)] and [VO(Hshed)(4NO_2)].

In addition, ^{51}V NMR was used to designed three new complexes in acetonitrile (CD_3CN), the hydrophobic [VO(Hshed)(Coum)], and a complex with an electron withdrawing ligand –CN, [VO(Hshed)(CN)], and a complex with an electron donating ligand OMet, [VO(Hshed)(3OMet)] (**Figures A3.S2-A3.S4**). In selecting this series of compounds, we expected varying degrees of complex stability in H_2O and in 7H9 media. The stability and speciation of the complexes was investigated by using NMR and UV-vis spectroscopy.

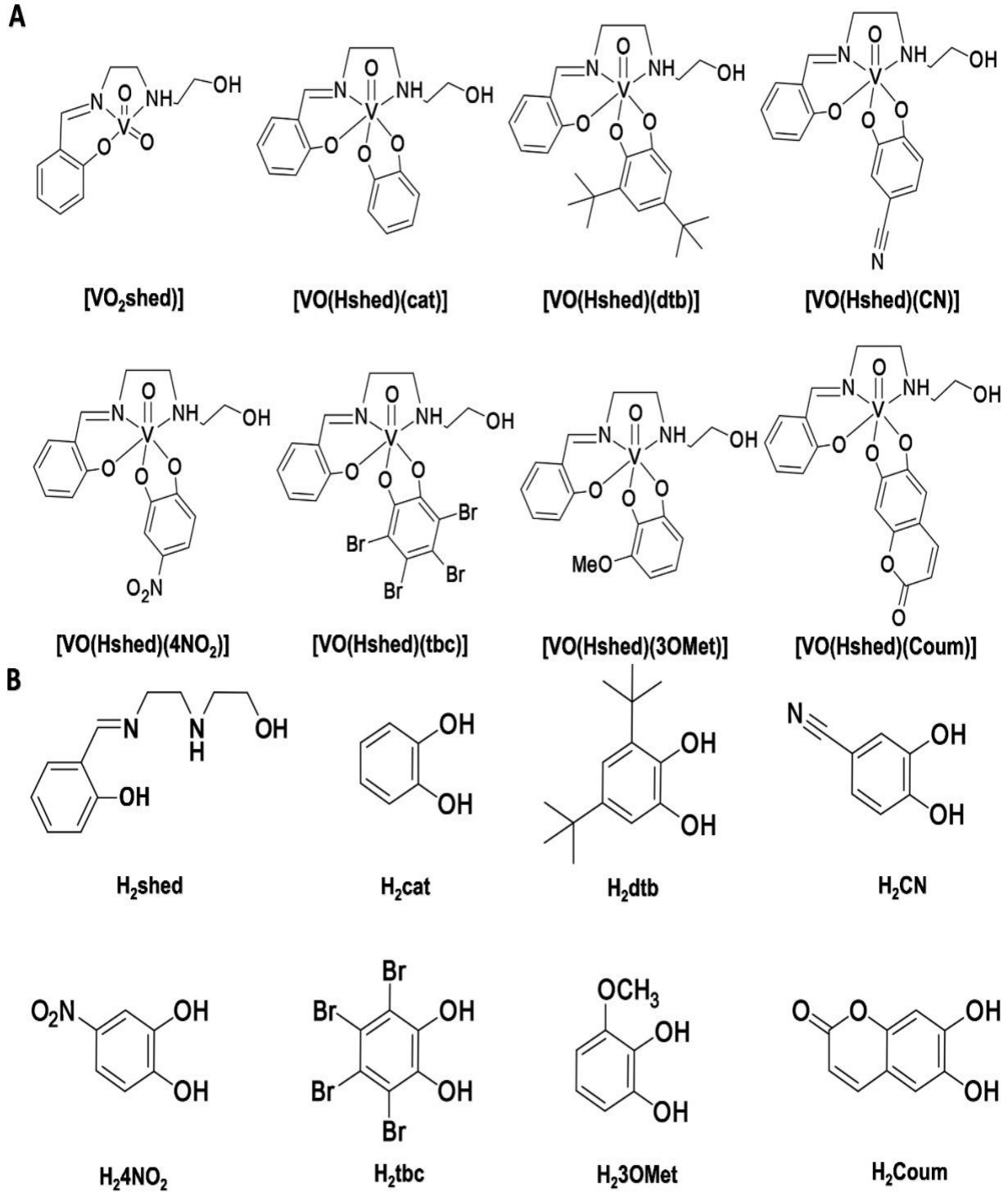

Figure 3.2. The schematic formulas for the **(A)** vanadium complexes and **(B)** free ligands.

3.3.2. Growth Inhibition of Vanadium Complexes and Free Ligands Determined using the Minimum Inhibitory Concentration (MIC)

The biological activity of V-complexes and free ligands was investigated in terms of their respective antibacterial effects on the growth of *M. smeg* by measuring IC_{50} values. The growth inhibition data of *M. smeg* treated with three different V-complexes and free catechol ligands are shown in **Figure 3.3** including (a) **[**VO(Hshed)(dtb)] and H_2dtb, b) [VO(Hshed)(tbc)] and H_2tbc, and c) [VO(Hshed)(cat)] and H_2cat. The IC_{50} values and the growth inhibition curves for the effects of the additional V-complexes, their free catechol, and the Schiff base V-Hshed scaffold on the bacterial growth are shown in Appendix III (**Figure A3.S1**). It was necessary to use DMSO to dissolve hydrophobic compounds into solution for preparation of stock solutions. For studies with *M. smeg*, the stock solution was diluted with cell medium to prepare a solution containing 10% DMSO which was then diluted via serial dilution to lower V-complex concentrations containing less DMSO. To clarify the role of DMSO in cell studies, cell growth inhibition up to 20% DMSO was evaluated and was significant. The effects of DMSO alone on the growth of *M. smeg* is shown in **Figure A3.S5**. When cells were treated with 10% DMSO alone, the highest DMSO concentration used in our studies of V-compound effects on *M. smeg* growth, growth inhibition was reduced to values that were still significant but markedly lower than seen for 20% DMSO. For compounds that were present in serially diluted medium and contained less than 10% DMSO, there were insignificant effects of DMSO on *M. smeg* growth indicating that the IC_{50} values for all the complexes and catechols tested were due to compound effects and not to the presence of DMSO (**Table 3.2**).

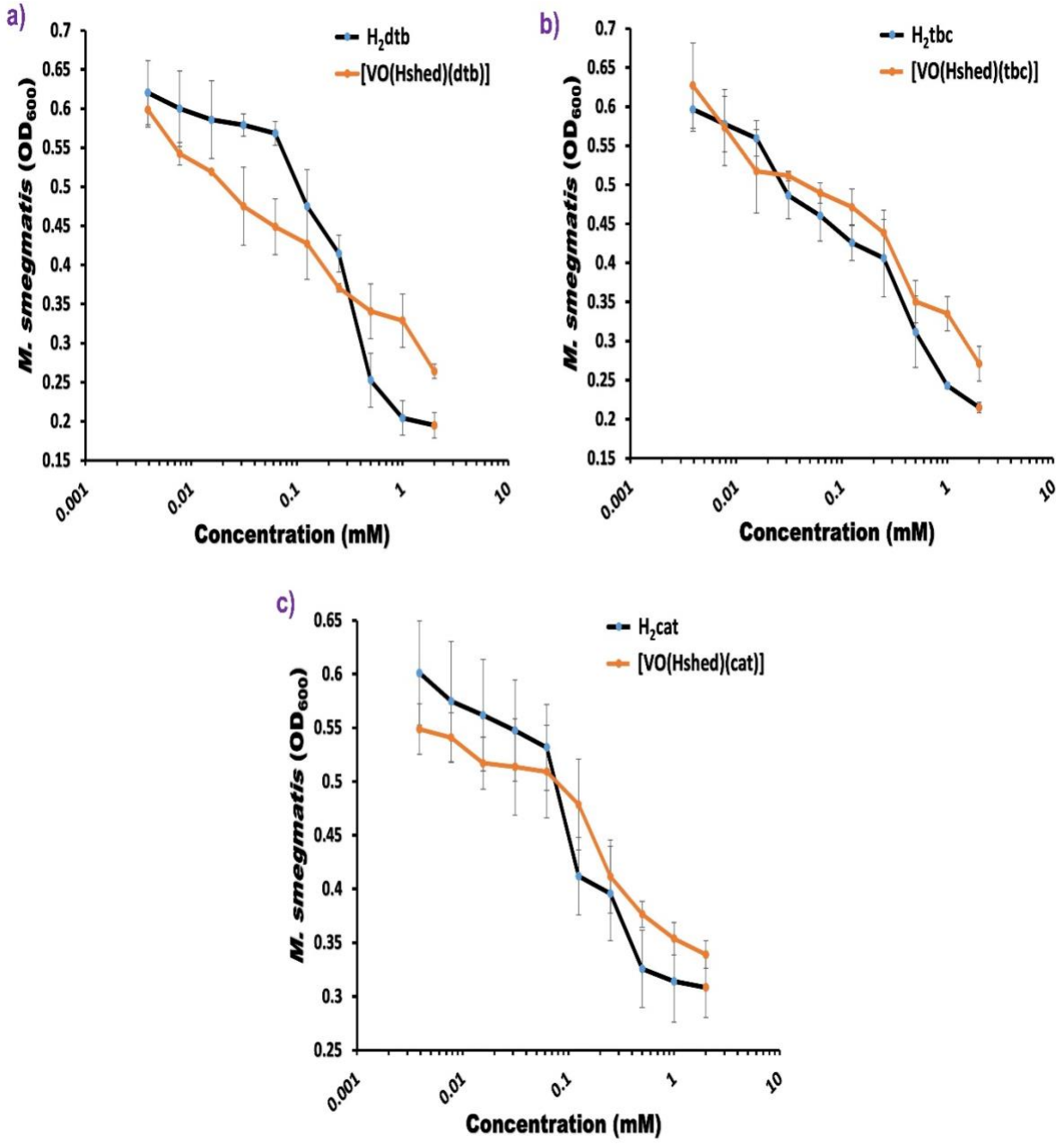

Figure 3.3. The growth curve of *M. smeg* treated with **(a)** [VO(Hshed)(dtb)] and H_2dtb, **(b)** [VO(Hshed)(tbc)] and H_2tbc, and **(c)** [VO(Hshed)(cat)] and H_2cat. The compounds were added to the culture medium (as described in methods) at the concentrations ranging from 0.004 to 2.00 mM. Plates were incubated for 24 h at 37 °C. The viable cell in the culture was assessed spectrophotometrically at 600 nm and IC_{50} was determined based on a 4-parameter IC_{50} equation. The error bars of the standard deviation for triplicate measurements are shown.

Table 3.2. Antibacterial activity (IC_{50}) of the Schiff base V-Hshed scaffold and free catechols against

Tested compounds	IC_{50} (μM)	The effect of complexes compared to the free catechol
[VO(Hshed)(dtb)]	119±0.09	2x more potent in terms of concentration
H_2dtb	241±0.07	
[VO(Hshed)(Coum)]	370±0.13	1.4x more potent in terms of concentration
H_2Coum	506±0.28	
[VO(Hshed)(4NO_2)]	472±0.02	1.3x more potent in terms of concentration
$H_2$4NO_2	610±0.05	
[VO(Hshed)(tbc)]	449±0.22	Same effect in terms of concentration
H_2tbc	416±0.19	
[VO(Hshed)(cat)]	518±0.29	5x less potent in terms of concentration
H_2cat	109±0.05	
[VO(Hshed)(3OMet)]	555±0.23	2x less potent in terms of concentration
$H_2$3OMet	262±0.15	
[VO(Hshed)(CN)]	608±0.07	1.4x less potent in terms of concentration
H_2CN	447±0.04	
[V($O)_2$(Hshed)]	516±0.31	Schiff base V-complex scaffold

The IC_{50} values of V-complexes and their free ligands are shown in **Table 3.2**. Although all the V-complexes and their free ligands were comparatively weak growth inhibitors of *M. smeg,* differences in growth inhibition where observed between the V-complex and its free ligand. The IC_{50} of [VO(Hshed)(dtb)], [VO(Hshed)(Coum)], and [VO(Hshed)($4NO_2$)] indicated that these compounds were more potent in inhibiting bacterial growth with IC_{50} of 119µM, 370µM, and 472µM, respectively. In complexes, their ligands showed 2-, 1.4-, and 1.3-fold more growth inhibition than did the free ligands. [VO(Hshed)(cat)], [VO(Hshed)(3OMet)], and [VO(Hshed)(CN)] showed less inhibitory activity against the bacterial growth with IC_{50} of 518µM, 555µM, and 608µM, respectively, when compared with their free ligands. Finally, the IC_{50} of [VO(Hshed)(tbc)] had a similar activity, an IC_{50} of 449µM, when compared with its free ligand with an IC_{50} of 416µM.

3.3.3. Solution chemistry and stability of vanadium catechol complexes in reference solutions and in growth media as monitored by UV-vis spectroscopy

To further investigate whether the observed effects of compounds or their ligands on *M.smeg* growth in cell culture were related to complex stability, spectroscopic studies were undertaken. We examine the V-compounds in three different solutions. 1) Simple H_2O-DMSO containing no other additives. 2) 7H9-DMSO media with nutrients for *M. smeg* growth but without other additives and 3) 7H9-media in which *M. smeg* had grown and the media contains bovine serum albumin (BSA), oleic acid and dextrose and from which cells had then been removed ("referred to as "supernatant"). UV-vis studies and subsequent NMR spectroscopic studies would show which compounds remained intact and for how long. The stability of the V-compounds was not expected to be the same in these three solutions nor was the response of each compound to these conditions likely to be the same.

First, the V-catechol complexes with different ligands were analyzed using UV-vis spectroscopy to explore the speciation and the stability of these complexes in both in H_2O:DMSO and in 7H9:DMSO at 37 °C. 7H9 medium was used in *M. smeg* growth studies which made its effects on compound speciation and stability of particular interest. The samples were initially dissolved in DMSO due to the low solubility of the compounds and their weak growth inhibition. Hence, the stabilities of the compounds described differ here from studies of compound stability reported in cancer cell lines studies where the compound concentration and temperature were lower and there was less DMSO present in the original stock solution (Crans et al., 2019). To conserve space, the spectra of the complexes shown in **Figure 3.4** were recorded in 7H9:DMSO at 37 °C while the UV-vis spectra of complexes in H_2O:DMSO and in supernatant: DMSO are presented in Appendix III (**Figures A3.S6 and A2.S7**). Because of the dilution of the original compound stock solution to 0.250 mM V-compound with H_2O or 7H9 media, the DMSO content decreased from 50% in the stock solution to about 6% for the UV-vis studies.

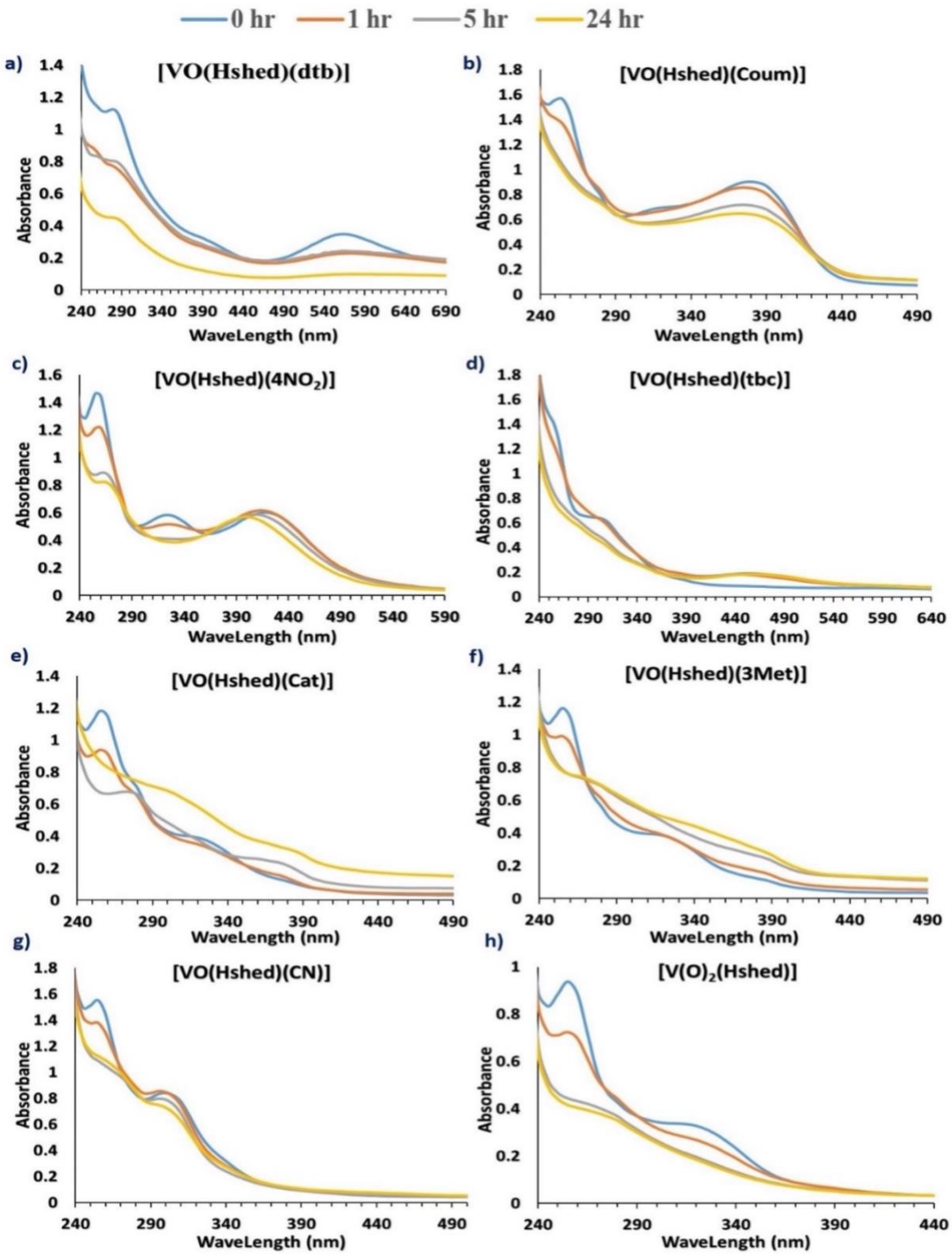

Figure 3.4. UV-vis spectra for all of the complexes at 0.250 mM in 7H9:DMSO as a function of time (0 h,1 h, 5 h, 24 h).

UV-vis spectroscopy can be used to show time-dependent changes in complex structure and hence complex stability. The spectra of complex and of free ligands at time zero (t=0) in H_2O:DMSO and in 7H9:DMSO were recorded as reference for the spectra in 7H9:DMSO and are shown in Appendix III (**Figure A3.S8**) as well as summarized in **Table 3.3**.

For comparison, the stability of the Schiff base oxido-vanadium(V) complex scaffold, [VO_2(Hshed)], which provided the basic framework for all the complexes in this series, was also evaluated. The main absorption peaks were observed at wavelengths at 255 nm and 325 nm in aqueous solution and were similarly observed in 7H9 media. The addition of catechol ligands, as expected, added additional signals to the complexes with shifts that depended on the electronic properties of the catechol.

The UV-vis spectra of [VO(Hshed)(dtb)] exhibited two absorption bands at 280nm (sh) and 565nm (m) in water and two major signals at 280 and 565nm in 7H9:DMSO. Both the signal for free H_2dtb catechol ligand at 280 nm (**Figure 3.4 and Figure A3.S6**) and the signal at 565 nm decreased at the 1 h time point and were gone at the 5 h timepoint. This indicated that the compound was present initially in 7H9 media but, as shown in **Figure 3.4**, began to hydrolyze. However, there are some differences in the spectra. For [VO(Hshed)(4NO_2)], [VO(Hshed)(tbc)] and [VO(Hshed)(CN)], there is a signal around 300-330 nm suggesting some isomer formation for these V-compounds. The data at the zero-time point has been summarized for all the complexes (nm, absorbance, and extinction coefficient) and is listed in **Table 3.3**.

Table 3.3. UV-vis parameters observed from the Schiff base V-catecholate-complexes and free catecholate ligands in the mixed solutions (50:50 H2O: DMSO) and 50:50 7H9:DMSO at t = 0 h at 0.250 mM at 37 °C.

Complex	**Complex (H_2O/DMSO) absorbance (nm)/ ε ($x10^3$ M^{-1})**	**Complex (7H9/DMSO) absorbance (nm)/ ε ($x10^3$ M^{-1})**
[VO(Hshed)(dtb)]	(280, 1.161, 4.6); (565, 0.396,1.6)	(280, 1.123,4.5); (565, 0.347,1.4)
[VO(Hshed)(Coum)]	(255, 1.344, 5.3); (275, 0.727, 2.9); (370, 0.870, 3.5)	(255, 1.562, 6.2); (280, 0.836, 3.3); (325, 0.678, 2.7); (380, 0.901, 3.6)
[VO(Hshed)(4NO_2)]	(255, 1.299, 5.2); (325, 0.533, 2.1); (405, 0.552, 2.2)	(260, 1.445, 5.8); (325, 0.583, 2.3); (420, 0.568, 2.3)
[VO(Hshed)(tbc)]	(255, 0.854, 3.4); (310, 0.284, 1.1)	(305, 0.613, 2.5)
[VO(Hshed)(cat)]	(255, 0.951, 3.8); (280, 0.579, 2.3); (375, 0.117, 0.47)	(255, 1.183, 4.7); (280, 0.743, 3.0); (325, 0.349, 1.4); (380, 0.138, 0.55)
[VO(Hshed)(3OMet)]	(255, 0.831, 3.3); (280, 0.408, 1.6)	(255, 1.162, 4.6); (325, 0.441, 1.8); (385, 0.156, 0.62)
([VO(Hshed)(CN)]	(255, 1.473, 5.9); (300, 0.666, 2.7)	(255, 1.55, 6.2); (300, 0.789, 3.2)
[V($O)_2$(Hshed)]	(255, 0.682, 2.7); (325, 0.200, 0.80)	(255, 0.937, 3.7); (325, 0.312, 1.2)
[H_2dtb] ligand	(280, 0.218, 0.90)	(280, 0.513, 2.1)
[H_2Coum] ligand	(255, 0.371, 1.5); (300, 0.524, 2.1); (345, 0.972, 3.9)	(295, 0.639, 2.6); (350, 0.939, 3.8)

[$H_2$4NO_2] ligand	(310, 0.652, 2.6); (350, 0.784, 3.1)	(265, 0.726, 2.9); (320, 0.575, 2.3); (430, 0.767, 3.1)
[H_2tbc] ligand	(275, 0.241,0. 1.0); (300, 0.203,0.81)	(255, 0.941, 3.8); (300, 0.574, 2.3)
[H_2cat] ligand	(275, 0.364, 1.5)	(275, 0.642, 2.6)
[$H_2$3OMet] ligand	(270, 0.137, 0.50)	(270, 0.417, 1.7)
[H_2CN] ligand	(250, 1.172, 4.7): (290, 0.453, 1.8)	(250, 1.293, 5.2); (290, 0.792, 3.2)

The UV-vis spectra of [VO(Hshed)Coum] had main absorption peaks at wavelengths of 255nm (m), 280nm (sh) and 385nm (m) in aqueous solution and, in 7H9 media, an extra peak of 325nm (sh). This additional peak in 7H9 media indicated the formation of an additional species. The decrease of the two major species as a function of time suggested that this complex is present in solution for some time before hydrolyzing. [VO(Hshed)(4NO_2) exhibited three major signals at 255, 325 and 405 nm. During the first hour the signal at 255 and 325 nm decreased whereas the signal at 405 nm remained at the same intensity with a small change in the location of its maximum.

The spectra for the other complexes examined indicated that the complexes remained intact briefly in 7H9 media (**Figure 2.4**) or H_2O:DMSO (**Figure A3.S6**). However, between 1 h and 5 h some remained intact for the first hour of the experiment when present at 6% DMSO concentrations and higher temperature which showed enhanced stabilities compared to previous studies (Correia et al., 2014; Crans et al., 2019; Levina et al., 2020). In addition, when compounds were examined in 7H9 media, a 280 nm peak appeared that was due to formation of free catechol.

Previously, *M. smeg* was found to excrete a material that was able to catalyze the hydrolysis of V_{10} (Samart et al., 2018). For this reason, we also examined the effects of the V-compounds in the supernatant of the 7H9 media in which *M. smeg* had grown. Analogous experiments were conducted in this study to determine if there is a difference from the results for media alone listed in **Table 3.4**. In this series 0.250 mM V compounds were added to the supernatant obtained from 7H9 media after *M. smeg* growth. Data showing the stability of compounds after incubation in supernatant are shown in Appendix III (**Figure A3.S7**). These data show that there was no significant change in speciation in supernatant obtained after *M. smeg* culture when compared to data obtained using fresh media as shown in **Figure 3.4**. However, the signal at 280 nm now indicates the presence of protein, primarily in the form of bovine serum albumin (Chaturvedi et al., 2015) although some formation of free catechol cannot be ruled out since this also yield an absorbance at 280 nm.

Table 3.4. Species observed in Schiff base vanadium catecholate-complexes in the mixture solution (50:50 H2O: DMSO) and 50:50 7H9:DMSO growth medium at t = 0 h.

Complex	**Complex δ (DMSO) or δ (H_2O/DMSO) ppm / mM / %**	**Complex δ (7H9 media) ppm / mM / %**	**[VO_2-(Hshed)] at δ / [mM] / %**	**V_1 at δ ppm / [mM] / %**	**V_4 at δ ppm / [mM] / %**
[VO(Hshed)(dtb)] / (H_2O/DMSO)	387, 353(m) / 0.43, 7.36 / 4.3, 73.6	--	--	-541 / 2.11 / 21.1	-557 / 0.10 /1.0
[VO(Hshed)(dtb)] / (7H9 media)	--	394, 359 (m) / 0.42, 5.45 / 4.2, 54.5	--	-544 / 4.14 / 41.4	--
[VO(Hshed)(Coum)] / (H_2O/DMSO)	-103 / 1.2 / 12	-	-524 / 1.5 / 15	-544 / 7.4 / 74	
[VO(Hshed)(Coum)] / (7H9 media)	-	-	-	-544 / 10 / 100	-
[VO(Hshed)(cat)] / (H_2O/DMSO)	206, 196 (m) / 0.73,2.47 / 7.3, 24.7	--	-524 / 1.79 / 17.9	-543 / 5.02/ 50.2	--

[VO(Hshed)(cat)] / (7H9 media)	--	205, 193 (m) / 0.32, 1.83 / 3.2,18.3	-526 / 2.10/ 21.0	-544 / 5.74 /57.4	--
[VO(Hshed)(3OMet)] / (H_2O/DMSO)	265, 254(m) / 1.47, 4.63 / 14.7, 46.3		-520 / 0.23 /2.3	-540 / 3.56 / 35.6	-560 / 0.11 / 1.1
[VO(Hshed)(3OMet)] / (7H9 media)	--	265, 253(m) / 0.78, 3.15 / 7.8, 31.5	--	-541 / 6.06 / 60.6	--
[$V(O)_2$(Hshed)] / (H_2O/DMSO)	--	--	-524 / 0.0	-543 /8.78 / 87.8	-558/1.22 / 12.2
[$V(O)_2$(Hshed)] / (7H9 media)	--	--	-526 / 0.0	-541 /9.94 /99.4	-565/0.11 / 1.1
[VO(Hshed)(tbc)] / (H_2O/DMSO)	-470, -480 / 2.0, 0.5 / 20, 5	-	-	-544 / 7.4 / 74	
[VO(Hshed)(tbc)] / (7H9 media)	-	-	-524 / 0.05 / 0.5	-544 / 9.8 / 98	-570 / 0.15 / 1.5
[VO(Hshed)(CN)] / (H_2O/DMSO)	-460 / 0.1 / 1	-	-524 / 3.3 / 33	-544 / 6.6 / 66	
[VO(Hshed)(CN)] / (7H9 media)		-480 / 0.05 / 0.5	-	-544 / 9.95 / 99.5	-
[VO(Hshed)(4NO_2)] / (H_2O/DMSO)	-460 / 0.1 / 1	-	-524 / 2.5 / 25	-544 / 6.6 / 66	-
[VO(Hshed)(4NO_2)] / (7H9 media)	-	-	-	-544 / 10 / 100	-

3.3.4. Solution chemistry and stability of vanadium catechol complexes in reference solution and in cell growth media

The stability of vanadium complexes was also investigated at different times using ^{51}V NMR spectroscopy in DMSO:H2O, DMSO:7H9 medium, and supernatants obtained following *M. smeg* culture. The representative ^{51}V NMR spectra of 10 mM [VO(Hshed)(dtb)], [VO(Hshed)(cat)], and [$V(O)_2$(Hshed)] in the mixture solution of H_2O, DMSO (50:50, H_2O:DMSO) and in 7H9 (50:50, H_2O:media) are shown in **Figures. 3.5, 3.6 and 3.7**, respectively. The NMR spectra of 10 mM [VO(Hshed)(dtb)], [VO(Hshed)(cat)], and [$V(O)_2$(Hshed)] in the mixture with supernatants are

shown in Appendix III (**Figures A3.S9, A3.S10, and A3.S11**) respectively. The remaining data for the additional complexes are listed in **Table 3.4**.

The ^{51}V NMR spectra were obtained using 10 mM of [VO(Hshed)(dtb)] in 50:50 H_2O:DMSO. Subsequently, spectra were recorded to determine how much complex remained intact at different time points when the complex was in 50:50 H_2O:DMSO or in 50:50 7H9:DMSO media (**Figure 3.5**).

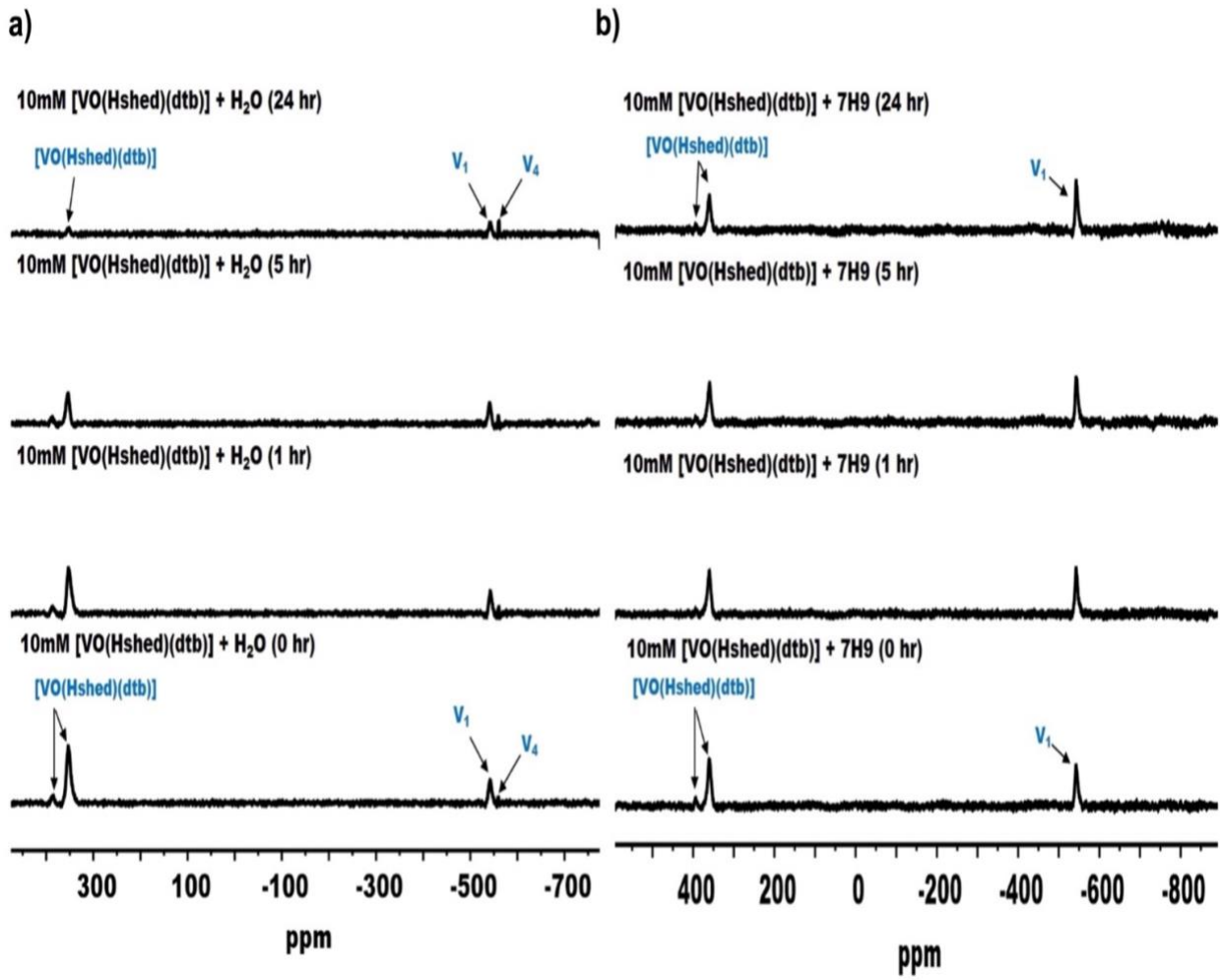

Figure 3.5. The ^{51}V NMR spectra of 10mM [VO(Hshed)(dtb)] at 0, 1, 5, and 24 h time points in a) 50:50 H_2O:DMSO and in b) 50:50 7H9 growth medium:DMSO.

The spectra of [VO(Hshed)(dtb)] at time=0 (t=0) showed two peak signals assigned to [VO(Hshed)(dtb)] at δ = 387 and 353 ppm, in addition to the presence of the other two signals

assigned to vanadate monomer (HVO_4^{2-}), V_1 at δ = -541 ppm and tetrameter, vanadate tetramer ($V_4O_{12}^{4-}$) V_4 at δ = -557 ppm. The percentage of each species measured at the initial time point is summarized in **Table 3.4**.

Over a 24 h time period, the [VO(Hshed)(dtb)] complex decreased as a function of time with an increase in V_1, and V_4, (**Figure 3.5a**) was monitored by ^{51}V NMR spectroscopy. The spectrum recorded at the initial time (t= 0 h) showed two complex signals at δ (ppm) = 394 and 359 (m), in addition to one signal attributed to V_1 at δ = -544 ppm. The ^{51}V NMR spectra of [VO(Hshed)(dtb)] in 7H9 was also carried out as a function of time and only small changes were observed in the spectra from 0 h. and the complex is stable under the conditions used in the cell growth assay in 7H9 medium (**Figure 3.5b**). The observation of the [VO(Hshed)(dtb)] complex in the growth assay is consistent with at least some of the observed growth effects that can be attributed to the intact [VO(Hshed)(dtb)] complex.

Monitoring the [VO(Hshed)(cat)] complex in H_2O over a 24 h time period showed a decrease of the complex as a function of time and an increase in monomer, V_1 and vanadate tetramer, V_4 (**Figure 3.6a**). The spectrum recorded at the initial time (t= 0 h) showed two complex signals at δ (ppm) = 196 and 206 (m) in addition to two signals attributed to [VO_2(Hshed)] at δ = -524 ppm and V_1 at δ = -544 ppm. Similarly, the ^{51}V NMR spectra of [VO(Hshed)(cat)] in 7H9 were carried out as a function of time and the complex was found to slowly hydrolyze in 7H9 medium (**Figure 3.6b**) to form [VO_2(Hshed)] and V_1. These spectra showed that [VO(Hshed)(cat)] complex existed in the 7H9 growth medium, suggesting that some of the observed growth inhibition can be attributed to the intact [VO(Hshed)(cat)] complex.

Studies were carried out with the other complexes and these results are summarized in **Table 3.4**. For [VO(Hshed)(Coum)] complex, significant amount of intact complex and the

[VO_2(Hshed)] was observed in H_2O: DMSO solution in addition to V_1 hydrolysis product. However, the complex was hydrolyzed in 7H9 media before the ^{51}V NMR spectrum was recorded. For the [VO(Hshed)($4NO_2$)] complex, a trace level of complex and an intermediate species are observed in addition to a 1:5 ratio of [VO_2(Hshed)] scaffold and V_1 hydrolysis product in H_2O: DMSO. However, all complexes were hydrolyzed in 7H9 media:DMSO before the ^{51}V NMR spectrum was recorded.

For the [VO(Hshed)(CN)] a 1:3 ratio of [VO_2(Hshed)] scaffold and V_1 hydrolysis product were observed in H_2O: DMSO. However, all complexes were hydrolyzed in 7H9 media:DMSO solution before the ^{51}V NMR spectrum was recorded. For the [VO(Hshed)(tbc)] complex the spectra were very noisy and only trace level of signals observed in addition to the major peak for V_1. Since this compound was investigated at the same concentrations as the other complexes, the noisy spectrum is presumably reflecting that this compound not only hydrolyze but undergo redox chemistry at the 37° C temperature in both H_2O: DMSO and the 7H9 medium:DMSO solutions. Combined these results show that some of these compounds are more stable than reported previously at lower temperatures and DMSO concentrations, but that several of the compounds remain unstable in 7H9 growth medium:DMSO and only hydrolyzed compounds are observed by the time the ^{51}V NMR spectra were recorded.

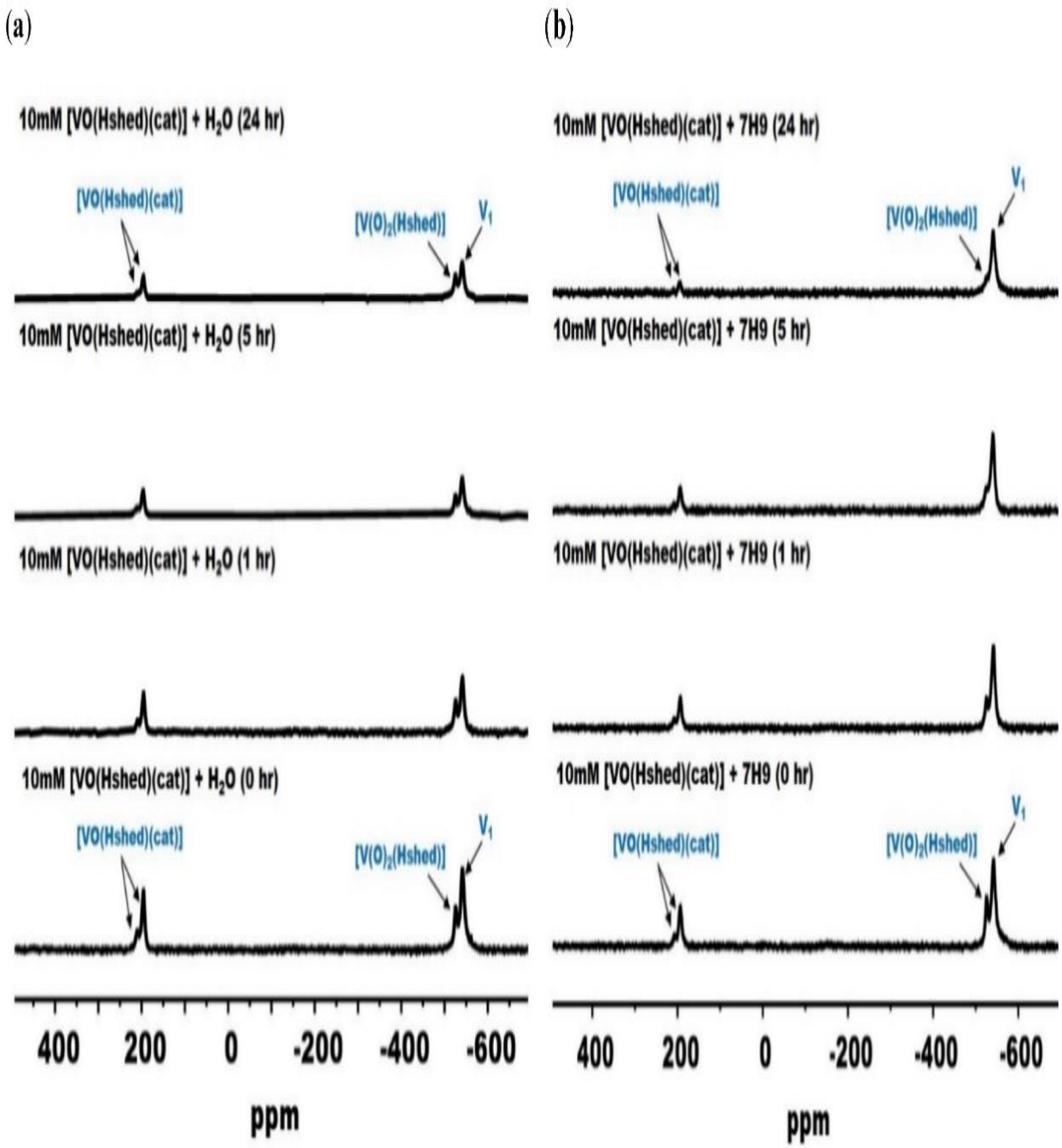

Figure 3.6. The ^{51}V NMR spectra of 10 mM [VO(Hshed)(cat)] at 0, 1, 5, and 24 h time points in **a)** 50:50 H_2O:DMSO and in **b)** 50:50 7H9 growth medium:DMSO.

In **Figure 3.7**, the NMR spectra are shown for the [VO(Hshed)] scaffold over a 24 h time period. These results indicate that the scaffold complex was unstable and immediately hydrolyzed to form V_1 within 1 h in either H_2O:DMSO or in 7H9:DMSO.

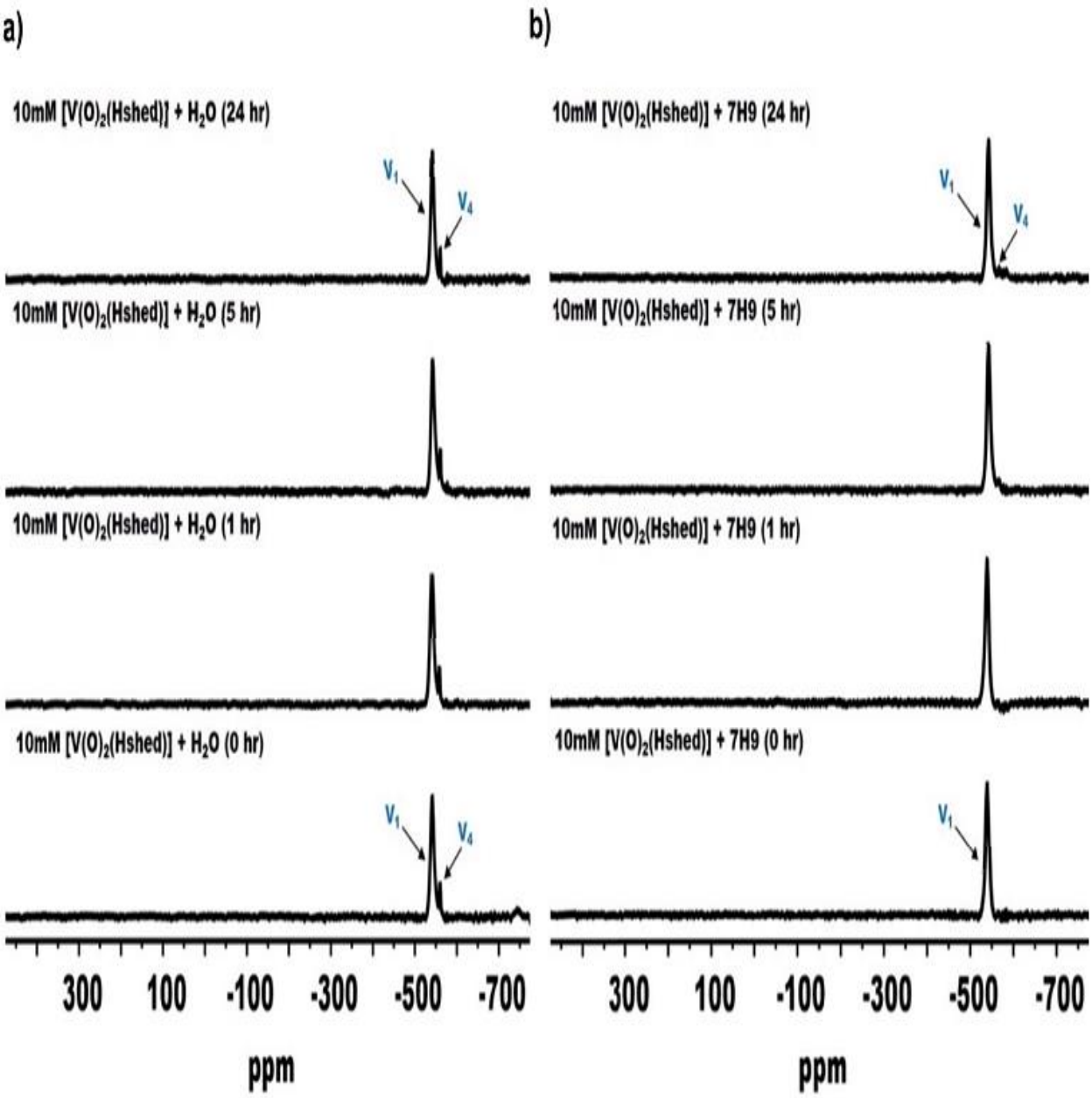

Figure 3.7. The ^{51}V NMR spectra of 10mM $[V(O)_2(Hshed)]$ at 0, 1, 5, and 24 h time points in a) H2O:DMSO (50:50) and in b) 7H9 growth medium:DMSO (50:50).

Select studies were carried out with the [VO(Hshed)(3OMet)] complex and the [VO(Hshed)(CN)] complex. Both hydrolyzed rapidly with little intact complex left in solution by the time the spectra were run. This information is summarized in **Table 3.4**. These data show higher stability than reported previously in pure aqueous solution or in media used to grow cancer cells (Correia et al., 2014; Crans et al., 2019; Levina et al., 2020).

3.4. Discussion

The results shown in **Table 3.2** demonstrate that complexes with reported anticancer activity have limited growth effects on the *M. smeg.* However, as shown in **Table 3.2**, some complexes are more biologically active than their catecholate ligand while, for other complexes, the free catecholates are more potent growth inhibitors of *M. smeg*. Therefore, we were successful in demonstrating that within a class of compounds, biological activity can be based on subtle variations in the ligand coordinated to the vanadium. As described in the Introduction, most of the reported investigations have focused on compounds where the observed V-complex is more potent than the free ligand (He et al., 2018; Machado et al., 2015; Maurya et al., 2010; Rosu et al., 2012) or metal ions (Missina et al., 2018). However, the quinolones and phenanthroline complexes deviate from these general observations because the free ligand is the most effective bioactive component of the complex (Correia et al., 2014; Nunes et al., 2021; Ribeiro et al., 2021). It should be noted, however, that most of these V-quinolone complexes are difficult to evaluate because the complexes are hydrophobic and, because of their hydrophobicity, their biological activities were not evaluated under the same conditions used in aqueous assays. A careful analysis has been reported for the effects of a range of different vanadium-complexes with phenanthroline ligands in different cancer cell lines (Nunes et al., 2021) and summarized in **Table 3.1**. These studies show that bioprocessing occurs after administration of these complexes and that their hydrolysis products are important for complex activity. Importantly, time-dependent responses were also observed (Nunes et al., 2021) over 72 h and low concentration the ligand were found to be more effective than the complex (Le et al., 2017).

Speciation is particularly important when the ligand is, by itself, a potent agent. It is also important that interactions with cellular components (Levina et al., 2017) including proteins be

considered (Aureliano et al., 2022; Pessoa et al., 2021). Such interactions can affect delivery and uptake of both the ligand and the complex and, because of time dependent effects, potentially produce more potent species with longer incubations (Nunes et al., 2021). These studies also underscore the importance of complex bioprocessing and the need for studies exploring effects of speciation studies as well as investigation of effects of both ligands and complexes by metabolites as well as a range of proteins. Hence, we were interested in evaluating a system in which speciation and the biological effects could be determined for both complex and free ligand.

In this study, we characterized the effects of the Schiff base V-complex scaffold as well as the catecholate ligand examined in *M. smeg* growth assays. Limited effects of the Schiff base V-complex scaffold were observed while the catecholate ligand showed more varied growth inhibitory activity as has been reported previously (Crans et al., 2019; Levina et al., 2020). Due to the limited water solubility of these complexes, the speciation studies were done in the presence of higher concentrations of DMSO which was required to solubilize the compound for addition to the cell culture at the high concentrations needed in this study. Because the DMSO concentration was higher than those reported previously in speciation studies (Crans et al., 2019; Levina et al., 2020), the complexes were more stable than reported previously except for the [VO(Hshed)(tbc)] complex that seems to be redox active when dissolved. Temperature may also contribute to compound stability; accompanying speciation studies done here used the same temperature from cell studies whereas previous studies were done at ambient temperature. These subtle differences in conditions may explain changes in the observed stabilities of the compounds (Crans et al., 2019; Levina et al., 2020) and are reminder of the importance of investigating the activity of the ligands used in the complexes under consideration under conditions similar to corresponding biological studies.

The growth effects of the complexes was according to the following order: [VO(Hshed)(dtb)] > [VO(Hshed)(Coum)] > [VO(Hshed)(tbc)] > [VO(Hshed)(4NO_2)] > [VO(Hshed)(cat)] =[$V(O)_2$(Hshed)] > [VO(Hshed)(3OMet)] > [VO(Hshed)(CN)]. We anticipate that the ligand potency as a growth inhibitor is important to the overall properties of the complex as a growth inhibitor and thus determined the order of the ligand potencies. The order is H_2cat > H_2dtb > $H_2$3OMet > H_2tbc > H_2CN > H_2Coum > $H_2$4NO_2. Surprisingly, we find that H_2cat is the most growth inhibiting catechol followed by H_2dtb and $H_2$3OMet. When examining the effects of the Schiff base V-complexes, only the [VO(Hshed)(dtb)] complex was found to be a potent growth inhibitor while [VO(Hshed)(cat)] and [VO(Hshed)(3OMet)] were among the least potent complexes. This result suggests that the potency of the ligand is not one of the factors that is critical for effects by V-complexes. Hence not only was the effect of the free catechol overcome by complex formation, but different properties were found to be important to the biological effects of these Schiff base V-complexes. It is possible that the electronic properties of the catechols are important. However, the anticipated electronic effects of substituents were $H_2$3OMet > H_2dtb > H_2cat > H_2tbc > H_2CN > $H_2$4NO_2 while the effects of the H_2Coum ligand were less predictable. Electronic effects alone cannot explain the observed effects, although they may be contributing, at least in part, to the overall activity of the complex. We have investigated the electronic effects of the complexes elsewhere but in general found that the complexes that readily undergo redox chemistry are not very stable (Haase et al., 2023). These studies confirm the expectation that the electronic effects on the catechol ligand is not the sole factor explaining the effects of the Schiff base V-complexes or showing a pattern explaining the properties of these complexes.

As we recently reported that complex hydrophobicity (Crans et al., 2019) and the stability of the Schiff base V-complex may be important to complex activity (Crans et al., 2019; Levina et al.,

2020). Hence it is critical to know whether the complex remains intact when assessing its observed activities in growth effects. In the present work we chose a system in which the activities of the complexes, although weak, were compared and differences could be identified. The two most stable and hydrophobic complexes were the VO(Hshed)(dtb)] and VO(Hshed)(Coum)] complexes and these complexes were also found to be the most effective inhibitors of *M. smeg* growth. This result suggests that stability and hydrophobicity of the complexes should be important factors when predicting compound effects on cell growth.

Perhaps the most surprising result in this series of work here is the fact that the H_2cat ligand is the catechol exhibit the highest growth inhibitory activity. Both the H_2dtb ligand and the H_2Coum ligand are hydrophobic and hence are readily taken up by cells. The H_2dtb ligand is the most sterically hindered catechol. Sterics are likely to be important for complex formation because the H_2dtb ligand protects the V-atom from hydrolysis as suggested by the complexes greater stability. From these results, we conclude that both hydrophobicity and steric hindrance are important factors for observed growth inhibition effects on *M. smeg* but that the catecholato ligand toxicity is not necessarily related to this growth effect particularly if the complex is, at least in part, stable as was observed under the conditions of these studies.

3.5. Conclusions

The growth effects of an anticancerous non-toxic Schiff base oxidovanadium(V) complex coordinated to 3,5-di-tert-butylcatecholato was assessed for comparison to the growth effects a series of subtly different non-toxic compounds using *M. smeg*. We specifically chose to examine 1) the growth effects of Schiff's base oxidovanadium complexes coordinated to a catechol and 2) the growth effects of the complexes' respective free catecholates for comparison and to determine 3) when the metal coordination complex is more potent than ligand alone. Schiff base

oxidovanadium catecholate compounds are coordination complexes and many of these compounds undergo hydrolysis. To obtain more information on the effects of intact complexes versus ligand we selected a class of complexes with varying stability that contained a ligand with the potential to inhibit growth of *M. smeg.* We then investigated both the species present under biological conditions and the effects of the intact complex and the hydrolyzed complex as well as the free ligand. The order of growth effects of ligands differed from that of the complexes and complex stability. This did not appear to be critical for growth inhibition because the most inhibitory catechol ligands were not found to form comparably inhibitory complexes.

Considering speciation of the V-complex in cell growth medium, we concluded that both hydrophobicity and steric hindrance were important factors for the observed growth inhibition of *M. smeg* as well as the anticancer properties of the various V-complexes.

3.6. References

Aureliano, M., Gumerova, N. I., Sciortino, G., Garribba, E., McLauchlan, C. C., Rompel, A., & Crans, D. C. (2022). Polyoxidovanadates' interactions with proteins: An overview. *Coordination Chemistry Reviews*, *454*, 214344. https://doi.org/10.1016/j.ccr.2021.214344

Bauer, E. B., Haase, A. A., Reich, R. M., Crans, D. C., & Kühn, F. E. (2019). Organometallic and coordination rhenium compounds and their potential in cancer therapy. *Coordination Chemistry Reviews*, *393*, 79–117. https://doi.org/10.1016/j.ccr.2019.04.014

Chatterjee, P. B., Goncharov-Zapata, O., Quinn, L. L., Hou, G., Hamaed, H., Schurko, R. W., Polenova, T., & Crans, D. C. (2011). Characterization of noninnocent metal complexes using solid-state NMR spectroscopy: O-dioxolene vanadium complexes. *Inorganic Chemistry*, *50*(20), Article 20. https://doi.org/10.1021/ic200046k

Chaturvedi, S. K., Ahmad, E., Khan, J. M., Alam, P., Ishtikhar, M., & Khan, R. H. (2015). Elucidating the interaction of limonene with bovine serum albumin: A multi-technique approach. *Molecular BioSystems*, *11*(1), Article 1. https://doi.org/10.1039/C4MB00548A

Chen, X., Hu, X., Lu, Q., Yang, Y., Linghu, S., & Zhang, X. (2022). Study on the differences in sludge toxicity and microbial community structure caused by catechol, resorcinol and hydroquinone with metagenomic analysis. *Journal of Environmental Management*, *302*, 114027. https://doi.org/10.1016/j.jenvman.2021.114027

Cirri, D., Bartoli, F., Pratesi, A., Baglini, E., Barresi, E., & Marzo, T. (2021). Strategies for the Improvement of Metal-Based Chemotherapeutic Treatments. *Biomedicines*, *9*(5), Article 5. https://doi.org/10.3390/biomedicines9050504

Cornman, C. R., Colpas, G. J., Hoeschele, J. D., Kampf, J., & Pecoraro, V. L. (1992). Implications for the spectroscopic assignment of vanadium biomolecules: Structural and spectroscopic characterization of monooxovanadium(V) complexes containing catecholate and hydroximate based noninnocent ligands. *Journal of the American Chemical Society*, *114*(25), Article 25. https://doi.org/10.1021/ja00051a026

Correia, I., Adão, P., Roy, S., Wahba, M., Matos, C., Maurya, M. R., Marques, F., Pavan, F. R., Leite, C. Q. F., Avecilla, F., & Costa Pessoa, J. (2014). Hydroxyquinoline derived vanadium(IV and V) and copper(II) complexes as potential anti-tuberculosis and anti-tumor agents. *Journal of Inorganic Biochemistry*, *141*, 83–93. https://doi.org/10.1016/j.jinorgbio.2014.07.019

Costello, R. L., & Hedgecock, L. W. (1959). Effect of Metavanadate Ion on the Growth in Vitro of Mycobacterium tuberculosis. *Journal of Bacteriology*, *77*(6), Article 6. https://doi.org/10.1128/jb.77.6.794-799.1959

Crans, D. C., Koehn, J. T., Petry, S. M., Glover, C. M., Wijetunga, A., Kaur, R., Levina, A., & Lay, P. A. (2019). Hydrophobicity may enhance membrane affinity and anti-cancer effects of Schiff base vanadium(V) catecholate complexes. *Dalton Transactions*, *48*(19), Article

19. https://doi.org/10.1039/C9DT00601J

Crans, D. C., & Kostenkova, K. (2020). Open questions on the biological roles of first-row transition metals. *Communications Chemistry*, *3*(1), Article 1. https://doi.org/10.1038/s42004-020-00341-w

Crans, D. C., Yang, L., Haase, A., & Yang, X. (2018). Health benefits of vanadium and its potential as an anticancer agent. In A. Sigel, H. Sigel, E. Freisinger, & R. K. O. Sigel (Eds.), *Metallo-Drugs: Development and Action of Anticancer Agents* (pp. 251–280). https://doi.org/10.1515/9783110470734-009

Creaven, B. S., Duff, B., Egan, D. A., Kavanagh, K., Rosair, G., Thangella, V. R., & Walsh, M. (2010). Anticancer and antifungal activity of copper(II) complexes of quinolin-2(1H)-one-derived Schiff bases. *Inorganica Chimica Acta*, *363*(14), Article 14. https://doi.org/10.1016/j.ica.2010.08.009

Dasari, S., & Bernard Tchounwou, P. (2014). Cisplatin in cancer therapy: Molecular mechanisms of action. *European Journal of Pharmacology*, *740*, 364–378. https://doi.org/10.1016/j.ejphar.2014.07.025

Dilruba, S., & Kalayda, G. V. (2016). Platinum-based drugs: Past, present and future. *Cancer Chemotherapy and Pharmacology*, *77*(6), Article 6. https://doi.org/10.1007/s00280-016-2976-z

Doucette, K. A., Hassell, K. N., & Crans, D. C. (2016). Selective speciation improves efficacy and lowers toxicity of platinum anticancer and vanadium antidiabetic drugs. *Journal of Inorganic Biochemistry*, *165*, 56–70. https://doi.org/10.1016/j.jinorgbio.2016.09.013

Esteban-Fernández, D., Moreno-Gordaliza, E., Cañas, B., Antonia Palacios, M., & Milagros Gómez-Gómez, M. (2010). Analytical methodologies for metallomics studies of antitumor Pt-containing drugs. *Metallomics*, *2*(1), Article 1. https://doi.org/10.1039/B911438F

Eyvazi, S., Vostakolaei, M. A., Dilmaghani, A., Borumandi, O., Hejazi, M. S., Kahroba, H., & Tarhriz, V. (2020). The oncogenic roles of bacterial infections in development of cancer. *Microbial Pathogenesis*, *141*, 104019. https://doi.org/10.1016/j.micpath.2020.104019

Fernandes, N., Rodrigues, C. F., Moreira, A. F., & Correia, I. J. (2020). Overview of the application of inorganic nanomaterials in cancer photothermal therapy. *Biomaterials Science*, *8*(11), Article 11. https://doi.org/10.1039/D0BM00222D

Frei, A., Zuegg, J., Elliott, A. G., Baker, M., Braese, S., Brown, C., Chen, F., Dowson, C. G., Dujardin, G., Jung, N., King, A. P., Mansour, A. M., Massi, M., Moat, J., Mohamed, H. A., Renfrew, A. K., Rutledge, P. J., Sadler, P. J., Todd, M. H., … Blaskovich, M. A. T. (2020). Metal complexes as a promising source for new antibiotics. *Chemical Science*, *11*(17), Article 17. https://doi.org/10.1039/D0SC90075C

Goncharova-Zapata, O., Chatterjee, P. B., Hou, G., Quinn, L. L., Li, M., Yehl, J., Crans, D. C., & Polenova, T. (2013). Effect of ancillary ligand on electronic structure as probed by 51V solid-state NMR spectroscopy for vanadium–o-dioxolene complexes. *CrystEngComm*, *15*(43), Article 43. https://doi.org/10.1039/c3ce41322e

Graf, N., & Lippard, S. J. (2012). Redox activation of metal-based prodrugs as a strategy for drug delivery. *Advanced Drug Delivery Reviews*, *64*(11), Article 11. https://doi.org/10.1016/j.addr.2012.01.007

Griffin, E., Levina, A., & Lay, P. A. (2019). Vanadium(V) tris-3,5-di-tert-butylcatecholato complex: Links between speciation and anti-proliferative activity in human pancreatic cancer cells. *Journal of Inorganic Biochemistry*, *201*, 110815. https://doi.org/10.1016/j.jinorgbio.2019.110815

Haase, A. A., Murakami, H. A., Koehn, J. T., Hagan, J., Beuning, C. N., Levina, A., Lay, P. A., & Crans, D. C. (2023). Exploring Electronic Properties of New Non-Innocent Vanadium(V) Compounds. *In Progress*.

He, L.-Y., Qiu, X.-Y., Cheng, J.-Y., Liu, S.-J., & Wu, S.-M. (2018). Synthesis, characterization and crystal structures of vanadium(V) complexes derived from halido-substituted tridentate hydrazone compounds with antimicrobial activity. *Polyhedron*, *156*, 105–110. https://doi.org/10.1016/j.poly.2018.09.017

Imberti, C., & Sadler, P. J. (2020). 150 years of the periodic table: New medicines and diagnostic agents. In *Advances in Inorganic Chemistry* (Vol. 75, pp. 3–56). Elsevier. https://doi.org/10.1016/bs.adioch.2019.11.001

Jin, S., Guo, Y., Guo, Z., & Wang, X. (2021). Monofunctional Platinum(II) Anticancer Agents. *Pharmaceuticals*, *14*(2), Article 2. https://doi.org/10.3390/ph14020133

Johnstone, T. C., Wilson, J. J., & Lippard, S. J. (2013). Monofunctional and Higher-Valent Platinum Anticancer Agents. *Inorganic Chemistry*, *52*(21), Article 21. https://doi.org/10.1021/ic400538c

Kostenkova, K., Arhouma, Z., Postal, K., Rajan, A., Kortz, U., Nunes, G. G., Crick, D. C., & Crans, D. C. (2021). PtIV- or MoVI-substituted decavanadates inhibit the growth of Mycobacterium smegmatis. *Journal of Inorganic Biochemistry*, *217*, 111356. https://doi.org/10.1016/j.jinorgbio.2021.111356

Kumar, S., Koehn, J. T., Gonzalez-Juarrero, M., Crans, D. C., & Crick, D. C. (2020). Mycobacterium tuberculosis Survival in J774A.1 Cells Is Dependent on MenJ Moonlighting Activity, Not Its Enzymatic Activity. *ACS Infectious Diseases*, *6*(10), Article 10. https://doi.org/10.1021/acsinfecdis.0c00312

Lambert de Malezieu, M., Courtel, P., Sleno, L., Abasq, M.-L., & Ramassamy, C. (2021). Synergistic properties of bioavailable phenolic compounds from olive oil: Electron transfer and neuroprotective properties. *Nutritional Neuroscience*, *24*(9), Article 9. https://doi.org/10.1080/1028415X.2019.1666480

Le, M., Rathje, O., Levina, A., & Lay, P. A. (2017). High cytotoxicity of vanadium(IV) complexes with 1,10-phenanthroline and related ligands is due to decomposition in cell culture medium. *JBIC Journal of Biological Inorganic Chemistry*, *22*(5), Article 5. https://doi.org/10.1007/s00775-017-1453-4

Levina, A., Crans, D. C., & Lay, P. A. (2017). Speciation of metal drugs, supplements and toxins in media and bodily fluids controls in vitro activities. *Coordination Chemistry Reviews*, *352*, 473–498. https://doi.org/10.1016/j.ccr.2017.01.002

Levina, A., Pires Vieira, A., Wijetunga, A., Kaur, R., Koehn, J. T., Crans, D. C., & Lay, P. A. (2020). A Short-Lived but Highly Cytotoxic Vanadium(V) Complex as a Potential Drug Lead for Brain Cancer Treatment by Intratumoral Injections. *Angewandte Chemie International Edition*, *59*(37), Article 37. https://doi.org/10.1002/anie.202005458

Lima, L. M. A., Murakami, H., Gaebler, D. J., Silva, W. E., Belian, M. F., Lira, E. C., & Crans, D. C. (2021). Acute Toxicity Evaluation of Non-Innocent Oxidovanadium(V) Schiff Base Complex. *Inorganics*, *9*(6), Article 6. https://doi.org/10.3390/inorganics9060042

Loizou, M., Hadjiadamou, I., Drouza, C., Keramidas, A. D., Simos, Y. V., & Peschos, D. (2021). Vanadium(V) Complexes with Siderophore Vitamin E-Hydroxylamino-Triazine Ligands. *Inorganics*, *9*(10), Article 10. https://doi.org/10.3390/inorganics9100073

Machado, P. de A., Mota, V. Z., Cavalli, A. C. de L., de Carvalho, G. S. G., Da Silva, A. D., Gameiro, J., Cuin, A., & Coimbra, E. S. (2015). High selective antileishmanial activity of vanadium complex with stilbene derivative. *Acta Tropica*, *148*, 120–127. https://doi.org/10.1016/j.actatropica.2015.04.018

Manov, H.; Staneva, D.; Vasileva-Tonkova, E.; Alexandrova, R.; Stoyanova, R.; Kukeva, R.; Stoyanov, S.; Grabchev, I. (2022). A New Cu(II) Complex of PAMAM Dendrimer Modified with 1,8-Naphthalimide: Antibacterial and Anticancer Activity. *Biointerface Res. Appl. Chem. 12*, 5534–5547. doi: 10.33263/BRIAC124.55345547.

Maurya, M. R., Khan, A. A., Azam, A., Ranjan, S., Mondal, N., Kumar, A., Avecilla, F., & Pessoa, J. C. (2010). Vanadium complexes having [(VO)-O-IV](2+) and [(VO2)-O-V](+) cores with binucleating dibasic tetradentate ligands: Synthesis, characterization, catalytic and antiamoebic activities. *Dalton Trans.*, *39*(5), Article 5. https://doi.org/10.1039/B915752B

Missina, J. M., Gavinho, B., Postal, K., Santana, F. S., Valdameri, G., de Souza, E. M., Hughes, D. L., Ramirez, M. I., Soares, J. F., & Nunes, G. G. (2018). Effects of Decavanadate Salts with Organic and Inorganic Cations on Escherichia coli, Giardia intestinalis, and Vero Cells. *Inorganic Chemistry*, *57*(19), Article 19. https://doi.org/10.1021/acs.inorgchem.8b01298

Mosquillo, M. F., Smircich, P., Lima, A., Gehrke, S. A., Scalese, G., Machado, I., Gambino, D., Garat, B., & Pérez-Díaz, L. (2020). High Throughput Approaches to Unravel the Mechanism of Action of a New Vanadium-Based Compound against *Trypanosoma cruzi*. *Bioinorganic Chemistry and Applications*, *2020*, 1–10. https://doi.org/10.1155/2020/1634270

Needham, R. J., Prokes, I., Habtemariam, A., Romero-Canelón, I., Clarkson, G. J., & Sadler, P. J. (2021). NMR studies of group 8 metallodrugs: Os-187-enriched organo-osmium half-sandwich anticancer complex. *Dalton Transactions*, *50*(37), Article 37. https://doi.org/10.1039/D1DT02213J

Nunes, P., Correia, I., Cavaco, I., Marques, F., Pinheiro, T., Avecilla, F., & Pessoa, J. C. (2021). Therapeutic potential of vanadium complexes with 1,10-phenanthroline ligands, quo vadis? Fate of complexes in cell media and cancer cells. *Journal of Inorganic Biochemistry*, *217*, 111350. https://doi.org/10.1016/j.jinorgbio.2020.111350

Pessoa, J. C., Santos, M. F. A., Correia, I., Sanna, D., Sciortino, G., & Garribba, E. (2021). Binding of vanadium ions and complexes to proteins and enzymes in aqueous solution. *Coordination Chemistry Reviews*, *449*, 214192. https://doi.org/10.1016/j.ccr.2021.214192

Pulcini, C. D., Lentz, S., Saladino, R. A., Bounds, R., Herrington, R., Michaels, M. G., & Maurer, S. H. (2021). Emergency management of fever and neutropenia in children with cancer: A review. *The American Journal of Emergency Medicine*, 50, 693–698. https://doi.org/10.1016/j.ajem.2021.09.055

Ribeiro, N., Bulut, I., Cevatemre, B., Teixeira, C., Yildizhan, Y., André, V., ... & Correia, I. (2021). Cu (II) and V (IV) O complexes with tri-or tetradentate ligands based on (2-hydroxybenzyl)-L-alanines reveal promising anticancer therapeutic potential. *Dalton Transactions*, *50*(1), 157-169. https://doi.org/10.1039/D0DT03331F

Ross, J. A., Komoda, K., Pal, S., Dickter, J., Salgia, R., & Dadwal, S. (2022). Infectious complications of immune checkpoint inhibitors in solid organ malignancies. *Cancer Medicine*, *11*(1), Article 1. https://doi.org/10.1002/cam4.4393

Rossi, J.-F., Lu, Z. Y., Massart, C., & Levon, K. (2021). Dynamic Immune/Inflammation Precision Medicine: The Good and the Bad Inflammation in Infection and Cancer. *Frontiers in Immunology*, *12*, 595722. https://doi.org/10.3389/fimmu.2021.595722

Rosu, T., Pahontu, E., Ilies, D.-C., Georgescu, R., Mocanu, M., Leabu, M., Shova, S., & Gulea, A. (2012). Synthesis and characterization of some new complexes of Cu(II), Ni(II) and V(IV) with Schiff base derived from indole-3-carboxaldehyde. Biological activity on prokaryotes and eukaryotes. *European Journal of Medicinal Chemistry*, *53*, 380–389. https://doi.org/10.1016/j.ejmech.2012.03.046

Rottenberg, S., Disler, C., & Perego, P. (2021). The rediscovery of platinum-based cancer therapy. *Nature Reviews Cancer*, *21*(1), Article 1. https://doi.org/10.1038/s41568-020-00308-y

Samart, N., Arhouma, Z., Kumar, S., Murakami, H. A., Crick, D. C., & Crans, D. C. (2018). Decavanadate Inhibits Mycobacterial Growth More Potently Than Other Oxovanadates. *Frontiers in Chemistry*, *6*, 519. https://doi.org/10.3389/fchem.2018.00519

Schweigert, N., Zehnder, A. J. B., & Eggen, R. I. L. (2001). Chemical properties of catechols and their molecular modes of toxic action in cells, from microorganisms to mammals. Minireview. *Environmental Microbiology*, *3*(2), Article 2. https://doi.org/10.1046/j.1462-2920.2001.00176.x

Selman, M., Rousso, C., Bergeron, A., Son, H. H., Krishnan, R., El-Sayes, N. A., Varette, O., Chen, A., Le Boeuf, F., Tzelepis, F., Bell, J. C., Crans, D. C., & Diallo, J.-S. (2018). Multi-modal Potentiation of Oncolytic Virotherapy by Vanadium Compounds. *Molecular Therapy*, *26*(1), Article 1. https://doi.org/10.1016/j.ymthe.2017.10.014

Shahbazi, M.-A., Faghfouri, L., Ferreira, M. P. A., Figueiredo, P., Maleki, H., Sefat, F., Hirvonen, J., & Santos, H. A. (2020). The versatile biomedical applications of bismuth-based nanoparticles and composites: Therapeutic, diagnostic, biosensing, and regenerative properties. *Chemical Society Reviews*, *49*(4), Article 4. https://doi.org/10.1039/C9CS00283A

Thota, S., Rodrigues, D. A., Crans, D. C., & Barreiro, E. J. (2018). Ru(II) Compounds: Next-Generation Anticancer Metallotherapeutics? *Journal of Medicinal Chemistry*, *61*(14), Article 14. https://doi.org/10.1021/acs.jmedchem.7b01689

Wexselblatt, E., Yavin, E., & Gibson, D. (2013). Platinum(IV) Prodrugs with Haloacetato Ligands in the Axial Positions can Undergo Hydrolysis under Biologically Relevant Conditions. *Angewandte Chemie International Edition*, *52*(23), Article 23. https://doi.org/10.1002/anie.201300640

Xu, Z., Wang, Z., Deng, Z., and Zhu, G. (2021). Recent advances in the synthesis, stability, and activation of platinum(IV) anticancer prodrugs. *Coordination Chemistry Reviews* 442, 213991. doi: 10.1016/j.ccr.2021.213991.

Zhou, J., Kang, Y., Chen, L., Wang, H., Liu, J., Zeng, S., & Yu, L. (2020). The Drug-Resistance Mechanisms of Five Platinum-Based Antitumor Agents. *Frontiers in Pharmacology*, *11*, 343. https://doi.org/10.3389/fphar.2020.00343

Chapter 4: Speciation studies and growth inhibition of *Mycolicibacteria* by mixed valence polyoxometalates: phosphotetradecavanadate and chloropentadecavanadate

4.1. Introduction

Polyoxovanadates (POVs) are a class of polyoxometalates (POMs) that contains vanadium and have shown a number of beneficial biological activities such as antitumor activity (Bijelic et al., 2019; Cartuyvels et al., 2008; Zhou et al., 2013), antiviral (Francese et al., 2019; Fukuda et al., 1991; Yamase, 2013), anti-HIV (Inouye et al., 1992; Judd et al., 2001; Witvrouw et al., 2000), antiparasitic (Missina et al., 2018; Saha et al., 1991; Turner et al., 2012),[10-12] antidiabetic (Ilyas et al., 2014; Pereira et al., 2009; Trevino et al., 2016), and antibacterial effects (Ayass et al., 2016; Bijelic et al., 2018; Gumerova et al., 2018; Kostenkova et al., 2021; Missina et al., 2018). Despite the numerous reports, in most cases the active form of the POV or POM materials has not been identified since the materials often interconvert and decompose under physiological conditions (Cartuyvels et al., 2008). Considering that desirable biological activities have recently been discovered, it is important to investigate the details of the interactions of these complex molecules with membranes, proteins, and other biological systems (Costa Pessoa et al., 2015; Fraqueza et al., 2019; Fraqueza et al., 2012; Luong et al., 2016; Roess et al., 2008; Vanhaecht et al., 2012). POVs can exist in a number of geometries, with the vanadium atoms assuming oxidation state (IV), (V) or mixed-valence (Hayashi, 2011). The most studied POV, decavanadate, $[V_{10}O_{28}]^{6-}$ (abbreviated V_{10}), has shown not only versatility in its chemistry (Crans et al., 2017; Sanchez-Lara et al., 2018) but also with regard to its biological effects (Aureliano, 2011; Missina et al., 2018; Samart et al., 2018). Although V_{10} can readily reduce, the chemistry of mixed valence POM is much more

versatile and is believed to involved reactive oxygen species (ROS) and exert novel reactivities (Turner et al., 2012). In the following work, we will explore the growth effects of two mixed-valence polyoxovanadates (MV-POV) and combining biological studies with speciation analysis in the cell culture media will determine the species present when the biological effects are observed. These studies will provide information on the activity of fundamental POV-structure and the interplay between structural recognition and redox chemistry.

Biological activities of V_{10} include interaction with a number of different classes of proteins (Crans et al., 1990). Ribonuclease A is inhibited by V_{10} and has been reported to be a mixed type inhibitor for bovine calf intestine alkaline phosphatase (Messmore and Raines, 2000; Turner et al., 2012). V_{10} is a non-competitive inhibitor of cyclic AMP-dependent protein kinase with respect to ATP and a competitive inhibitor to the substrate kemptide (Pluskey et al., 1997). The enzyme inhibition, in this case, is through the interaction of V_{10} with the peptide substrate and not the protein. These studies demonstrate the affinity of V_{10} for a peptide sequence (Leu-Arg-Arg-Ala-Ser-Leu-Gly) (Pluskey et al., 1997; Tiago et al., 2007). V_{10} has induced the crystallization of SR Ca^{2+}-ATPase dimers (Dux and Martonosi, 1983; Maurer and Fleischer, 1984) and was found bound to the *Francisella tularensis* Acid Phosphatase A (AcpA) enzyme in its X-ray structure, documenting the formation of V_{10} since monomeric vanadate (V_1) was added to the medium (Felts et al., 2006). The ectonucleotidase NTPDase1 binds V_{10} but a homolog crystal (Zebisch et al., 2012). Finally, a crystal structure of activated receptor tyrosine kinase in complex with substrates and V_{10} (Bae et al., 2009) and a Cryo-EM structure of human TRPM4 channel in complex with Ca^{2+} and V_{10} were reported (Winkler et al., 2017).

The effect of several POMs on the growth of microorganisms has been reported although these studies are more difficult to interpret because speciation studies were not investigated (Bijelic

et al., 2018 and Bijelic et al., 2019). Early studies show that the combination of chitosan (a hydrophilic biopolymer derived from chitin by a deacetylation process) and $Ca_3V_{10}O_{28}$ inhibits the growth of *Staphylococcus aureus* and *Escherichia coli* (Chen et al., 2006), and the observed effects were attributed to the combined chitosan antimicrobial activity and the V_{10} inhibition of ion pump (Chen et al., 2006). V_{10} increases the intracellular superoxide levels of *Leishmania tarentolae* promastigote leading to a 50% viability inhibition of the protozoa (Turner et al., 2012), also inhibiting the *L. tarentolae* secreted acid phosphatase activity (Dorsey et al., 2018). The antibacterial activity of different POMs showed that $[NaP_5W_{30}O_{110}]^{14-}$, $[P_{2cyto}W_{18}O_{62}]^{6-}$, and $[H_3P_2W_{15}V_3O_{62}]^{6-}$ exhibited a strong inhibitory activity against the growth of *M. catarrhalis*, with the highest activity demonstrated by Preyssler-type structures (Gumerova et al., 2018). V_{10} inhibited the growth of S*treptococcus pneumonia* (Fukuda and Yamase, 1997), *Bacillus cirroflagellosus* and two fungi species, *Aspergillus niger,* and *Penicillium notatum* (Shahid et al., 2014). Furthermore, V_{10} with counter ions of nicotinamide and isonicotinamide inhibited *Escherichia coli* growth and *Giardia intestinalis* adhesion (Missina et al., 2018). The counterions facilitate the cellular uptake of the V_{10} species compared to the corresponding Na^+ salt (Missina et al., 2018). Similarly, the growth of V_1 and V_{10} on two strains of *M.tb* and *M. smeg* was investigated, and the speciation studies accompanying the biological assays investigated the species observed in the growth media (Samart et al., 2018). Consequently, we demonstrated that V_{10} was a greater growth inhibitor by a factor of more than 100 of two strains of mycobacteria than the mononuclear phosphatase inhibitor, V_1 (Samart et al., 2018). In our previous study, we investigated the inhibitory effects of two V_{10} derivatives, V_9Pt and V_9Mo, on the growth of *M. smeg* (Kostenkova et al., 2021). The results showed that the substitution of one V^V ion in V_{10} by a Pt^{IV} or a Mo^{VI} ion results in isostructural derivatives which also inhibit the growth of *M. smeg* (Kostenkova et al.,

2021). We demonstrated that V_{10} is the most potent inhibitor and the V_9Pt cluster appears to be most stable under the growth conditions which was confirmed by the spectroscopic studies (Kostenkova et al., 2021).

MV-POV is a group of POVs with particularly rich chemistry (Gumerova and Rompel, 2018; Monakhov et al., 2015). Their structural versatility is due to vanadium's ability to adopt two different coordination geometries: VO_4 tetrahedral and VO_5 square-pyramidal (Hayashi, 2011). The simplest vanadates ($H_2VO_4^-$ and HVO_4^{2-}, **Figure 4.1a**) combine to form species that can contain from 1 to more than 10 vanadium atoms depending on concentration, pH and ionic strength of the media (Hayashi, 2011 and Miras et al., 2014). V_{10} is an isopolyoxometalate is constituted from 10 VO_6 units, forming a dense and compact structure, **Figure 4.1b** (Monakhov et al., 2015). MV-POV, however, generally are heteropolyoxoanions, commonly encapsulating anions and forming structures analogous to the Keggin structure (heteropoly acids) (Hayashi, 2011). In this subclass, the VO_5 units are condensed with the base of the pyramidal units directed towards the center of the cluster in pseudo-spherical geometries interacting electrostatically with the encapsulated anion (Hayashi, 2011). Two members of the MV-POV class are presented in **Figure 4.1c** and **Figure 4.1d**.

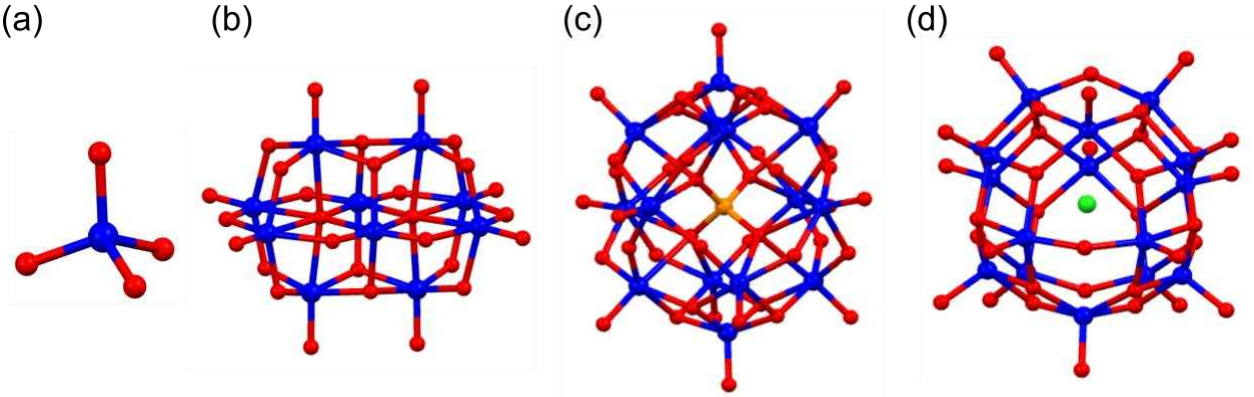

Figure. 4.1. Ball and stick representation of the anions metavanadate (V_1), decavanadate (V_{10}), phosphotetradecavanadate (V_{14}) and chloropentadecavanadate (V_{15}). The hydrogen atoms and counterions were omitted for clarity but the formulas of the oxovanadates and their abbreviations are listed in the figure. Vanadium atoms are shown in blue, oxygen in red, phosphate in orange and chloride in green.

The $K(NH_4)_4H_6V_{14}O_{38}(PO_4)]\cdot 11H_2O$ (V_{14}) is a mixed-valence Keggin-type POV containing 12 V^V atoms and 2 V^{IV} atoms with an encapsulated phosphate anion and have been prepared with K^+ and NH_4^+ counterions (Postal et al., 2016). The $[(CH_3)_4N]_6[V_{15}O_{36}(Cl)]$ (V_{15}) contains 7 V^V and 8 V^{IV} atoms with an encapsulated chloride anion and prepaired with 6 $(CH_3)_4N^+$ cations (Nunes et al., 2012). In *E. coli* cultures, the V_{15} anion was found to have chemoprotective activity against the diethyl sulfate, increasing the cell viability up to 40%. In contrast, V_{14} enhanced the deleterious action of the alkylating agent (Postal et al., 2016). The difference in the biological responses was attributed to their structure, charge, and stability in solution (Nunes et al., 2012; Postal et al., 2016). In the following, we will carry out biological studies with MV-POVs (V_{14} and V_{15}, **Figure 4.1**) linked to speciation studies to determine what species exist when the *Mycobacterium* growth is inhibited. Using the combined spectroscopic signature for vanadium(V) and vanadium(IV) we can follow the vanadium species in these two most common oxidation states for biological systems.

4.2. Material and Methods

4.2.1. Materials

All solutions, flasks, and materials employed in the biological assays, including the Middlebrook 7H9 medium, were autoclave-sterilized. The $K(NH_4)_4[H_6V_{14}O_{38}(PO_4)]\cdot 11H_2O$ (V_{14}) and $[(CH_3)_4N]_6[V_{15}O_{36}(Cl)]$ (V_{15}) were prepared according to literature procedures and solutions were prepared using ultrapure water (Milli-Q, 18.2 MΩ cm resistivity at 25 °C) (Nunes et al., 2012; Postal et al., 2016). Deuterium oxide (D_2O, 99.9%) was purchased from Cambridge Isotope

Laboratories, Inc. The Difco™ Middlebrook 7H9 Broth (BD), oleic acid (Sigma Aldrich), Tyloxapol (Chem-Impex Int'l Inc), albumin (VWR Chemicals) and dextrose (Sigma Aldrich) and all reagents were used as received from the supplier.

4.2.2. Cell culture and growth conditions.

M. smeg were grown in Middlebrook 7H9 medium (Ref. no. 271310; Difco). The medium was prepared based on the manufacturer's instructions with 0.200% (v/v) glycerol. *M smeg* were grown in 7H9 medium supplemented with 10% of OAD (0.6% v/v Oleic acid, 5 mg mL^{-1} Albumin, and 2 mg mL^{-1} Dextrose), and 10% of Tyloxapol (Singh and Reyrat, 2009).

4.2.3. Bacterial Strain and Growth Measurements

The cultures were incubated with shaking for 24 h at 37 °C and left to grow to mid-logarithmic growth phase to an optical density of 0.600 (OD_{600}). This wavelength was selected to prevent the interference of the culture media and compound solution typical absorption bands (Postal et al., 2016). Stock solutions were added to the 7H9 medium in a 96 well plate and diluted in serial 3-fold dilution for a final concentration range between 2.00 to 0.000100 mmol L^{-1}. The half-maximal inhibitory concentration (IC_{50}) was calculated using the GraFit data analysis software.

4.2.4. Preparation of the Heated and Non-Heated Supernatant for Spectroscopic Studies

The preparation of the supernatant fraction for the spectroscopic studies was made by the incubation of *M. smeg* cells with shaking in 50 mL polypropylene conical tubes (30x115 mm) for 24 h at 37 °C. After this period, the culture was centrifugated at 2000×g for 15 min in a Beckman centrifuge model GS-6R and filtrated by using a sterile syringe filter 0.2 µm supor to remove any remaining cells.

The supernatant was collected, and one portion was heated for 45 min at 80 °C to denature and precipitate the proteins. The heated supernatant was centrifugated at 2000×g for 15 min in a Beckman centrifuge model GS-6R, decanted and filtrated to remove the precipitated proteins.

4.2.5. Nuclear Magnetic Resonance (NMR) Measurements

Vanadium-51 nuclear magnetic resonance (^{51}V NMR) measurements were recorded on a Bruker spectrometer at 78.9 MHz for ^{51}V and 400.13 MHz for ^{1}H, using 4096 scans for the ^{51}V NMR analysis and a window from -53 to -1043 ppm. The chemical shifts of vanadium(V) species were referenced against an external reference of Na_3VO_4 (100 mmol L^{-1}, pH 12.8, signals at −535 (V_1) and −559 ppm (V_2)) (Samart et al., 2018). The samples were freshly prepared, and spectra were recorded at time points 0, 1, 5, and 24 h with the samples incubated at 37 °C. The proportion of each vanadium(V) species in the media was determined using the integration of the vanadium peaks in the spectrum as recorded previously. The pH of the solutions was measured immediately prior the recording of the NMR spectra.

4.2.6. Preparation of V_{14} and V_{15} Stock Solutions for Spectroscopy Studies

The aqueous stock solution of each POV was freshly prepared with double distilled water in a concentration of 4.00 mmol L^{-1}, with a pH of 4.60 to V_{14} and 4.70 to V_{15}. The suspension was heated and stirred to dissolve the solid, the solution was cooled to room temperature. The 0.200 and 1.00 mmol L^{-1} solutions were prepared after diluting the stock solution with water, 7H9 media or supernatant.

4.2.7. Preparation of Citrate and Phosphate solutions with V_{15} for Spiked ^{51}V NMR Studies

The citric acid and potassium dihydrogen phosphate (KH_2PO_4) 10.0 mmol L^{-1} stock solutions were prepared in D_2O heated until complete dissolution. The ^{51}V NMR spiked samples

were prepared by adding 0.500 mL of the citric acid or KH_2PO_4 stock solution to 0.500 mL of 4.00 mmol L^{-1} of the V_{15} solution.

4.3. Results

4.3.1. Growth effects of V_{14}, V_{15} on *M. smeg*

The effects of V_{14} and V_{15} on the growth of *M. smeg* cultures were determined in 7H9 media, by monitoring the absorbance at 600 nm and using 3-fold serial dilutions of the POVs concentration beginning at 2.00 mmol L^{-1} and ending at 0.000100 mmol L^{-1}. The growth inhibition for the treatment with V_{15} was found to be more potent than the effects of V_{14} and the data is presented in **Figure 4.2**. **Table 4.1** summarizes the observed IC_{50} values compared to the corresponding values for V_1 and V_{10} in terms of the POV and vanadium atom concentrations. V_1 shows a limited growth effect (190 µmol L^{-1}) on the inhibition of *M. smeg* cultures, whereas V_{10} inhibited the cultures-growth with a 3.70 µmol L^{-1} affinity, reported previously (Samart et al., 2018). V_{15} was more effective in inhibiting growth than V_{10} by a factor of 2 in terms of concentration, while V_{14} showed to be 8 times less effective. These studies confirm the greater effect of POVs compared to V_1. These observations reflect a combined response to all the species in the cell culture growth medium; however, considering that the effect depends on speciation, the other oxovanadates in the growth media must be considered. Since the nature of the species forming in solutions of MV-POV was not previously determined, speciation studies in the media are crucial to understanding the effects of these compounds on *M. smeg*.

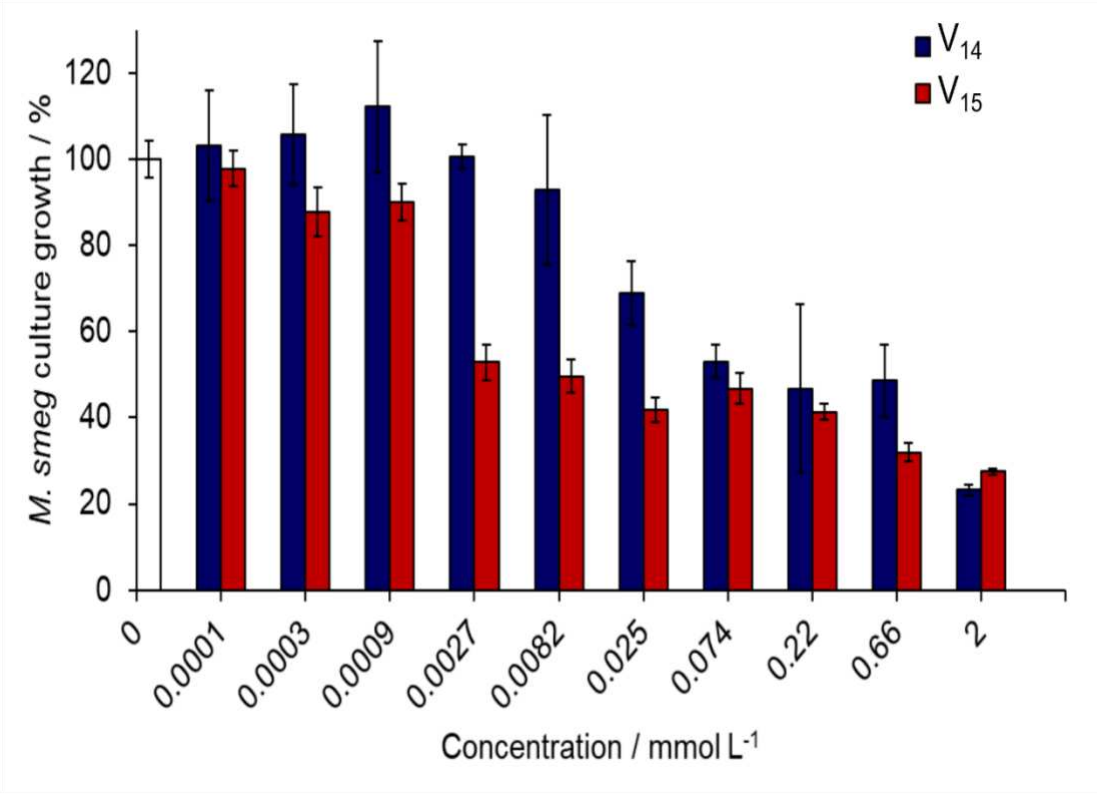

Figure. 4.2. Histogram showing the Cell culture growth for *M. smeg* treated with $K(NH_4)_4[H_6PV_{14}O_{42}]\cdot 11H_2O$ (**V14**, blue) and $[(CH_3)_4N]_6[V_{15}O_{36}Cl]$ (V_{15}, red), respectively, with concentrations varying from 0.000100 to 2.00 mmol L^{-1} in both treatments. All experiments were performed in biological triplicate and the error bars indicate the standard deviation from the mean values.

Table 4.1. The IC_{50} values for V_{14}, V_{15}, V_{10}, and V_1 treated *M. smeg*.

	IC_{50} µmol L^{-1}	Stand. Error	IC_{50} per V-atom/ µmol L^{-1}	Stand. Error	Ref
V_{14}	29.0	±13	406	±182	(This work)
V_{15}	1.90	±0.90	28.5	±13.0	(This work)
V_{10}	3.70	±0.40	37.0	±4.00	(Samart et al., 2018)
V_1	190	±71.0	190	±71.0	(Samart et al., 2018)

4.3.2. Stability and speciation on V_{14} and V_{15} in solution

4.3.2.1. Speciation studies in aqueous solution as a function of time

POVs are known to exhibit complex solution chemistry, depending on the solution conditions and parameters such as concentration, pH, time, and temperature. ^{51}V NMR studies of

V14 and **V15** were recorded at 0.200 and 1.00 mmol L^{-1} to determine the speciation chemistry in solution by monitoring two different concentration ranges in the growth studies

For **V14**, ^{51}V NMR studies were done both at 0.20 and 1.00 mmol L^{-1}, presenting similar spectra with the presence of the oxidized V^{V}_{14} and V_1 signals in addition to the two signals attributed to V_{10} at $\delta = -513$ and -519 ppm (**Figure 4.3**). After 24h, the 1.00 mmol L^{-1} of **V14** showed that the intensity of the V_{10} signals have increase and the minor third V_{10} signal was also observed in the spectrum at –423 ppm (**Figure 4.3b**).

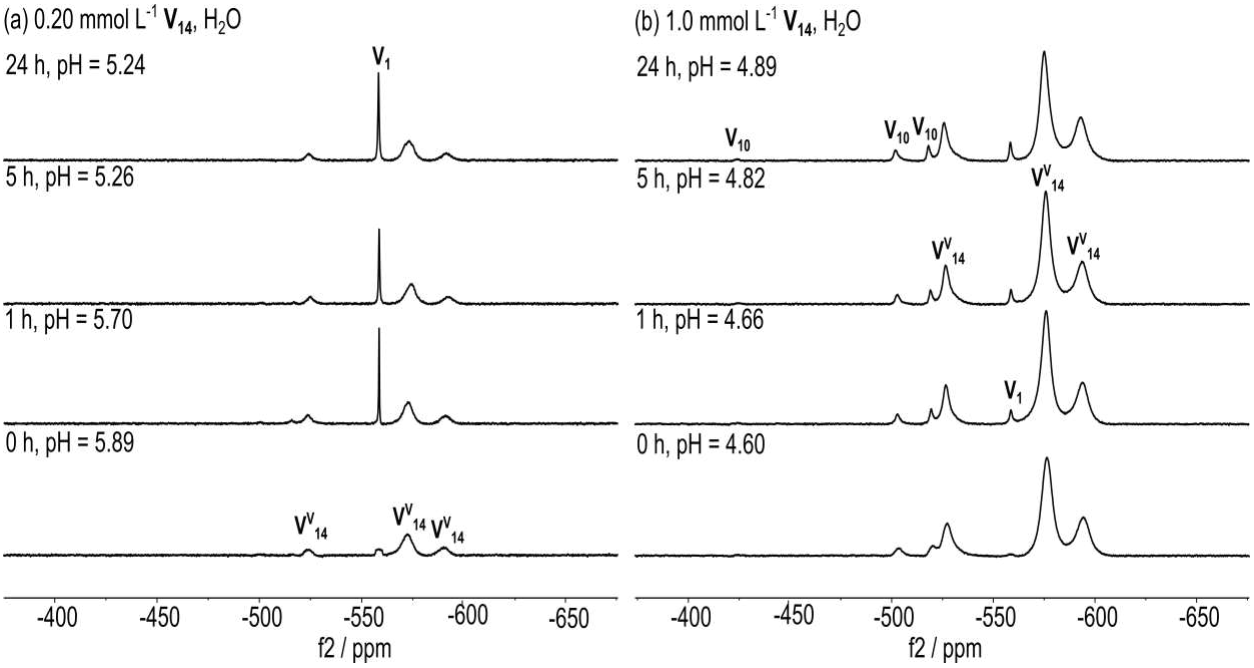

Figure 4.3. ^{51}V NMR spectra of V_{14} in aqueous solution at 0, 1, 5 and 24 h time points. Data for two concentrations are shown in (a) 0.20 and (b) 1.0 mmol L^{-1}. The observed species were: V_1 ($H_2VO_4^-$), V^{V}_{14} ($H_4V_{14}O_{42}P^{5-}$) and V_{10} ($HV_{10}O_{28}^{5-}$).

The aqueous solution ^{51}V NMR spectra for V_{15} in both 0.200 and 1.00 mmol L^{-1} (**Figure 4.4**) showed signals assigned to V_1 and V_2 at −557 and −571 ppm, respectively. It is important to note that even at the higher concentration of **V15** (1.00 mmol L^{-1}), the V_1 was the only species observed at the beginning of the incubation until 24 h when the low-intensity signals assigned to V_2 and V_{10} appeared.

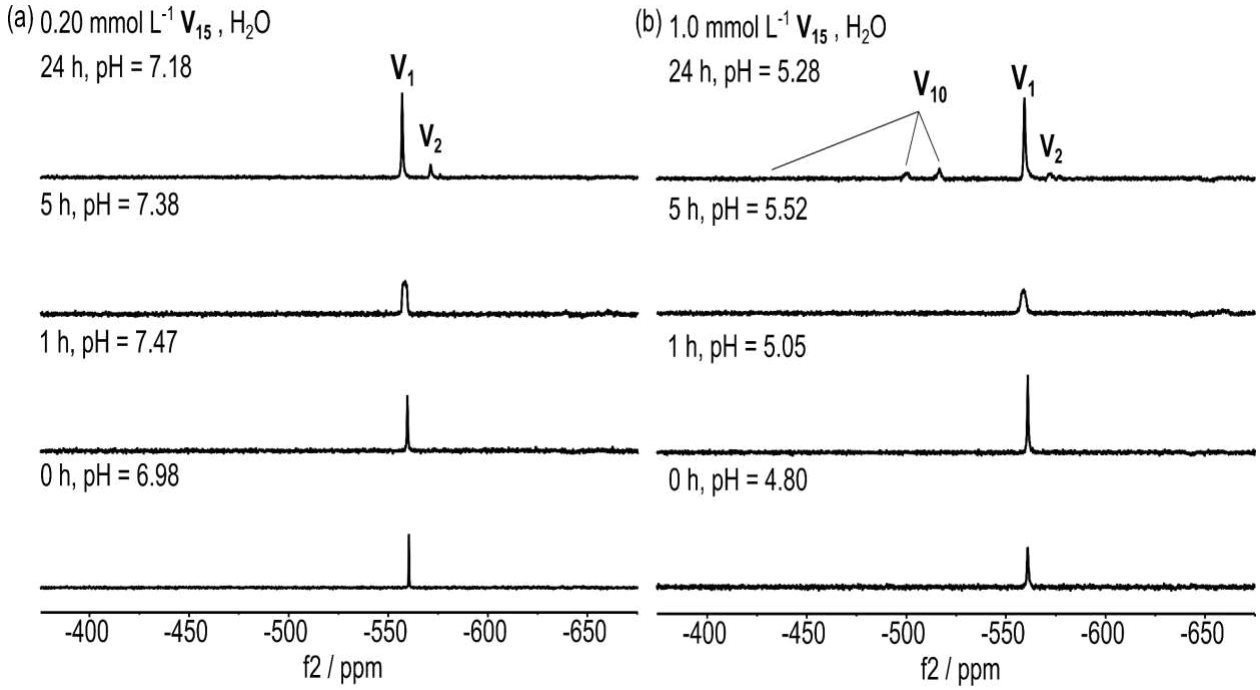

Figure 4.4. ^{51}V NMR spectra of V_{15} using water as media at 0, 1, 5 and 24 h time points. Data for two concentrations are shown in (a) 0.20 and (b) 1.0 mmol L^{-1}. The observed species were: V_1 ($H_2VO_4^-$), V_2 ($H_2V_2O_7^{2-}$) and V_{10} ($HV_{10}O_{28}^{5-}$).

The preliminary results show that the two MV-POV species follow different decomposition patterns in aqueous solution. The **V_{14}** undergoes hydrolysis and oxidation faster than **V_{15}** generating both oligomeric and POMs in solution. In contrast, **V_{15}** is present mainly in its pseudo-spherical aggregated form, with the formation of simple oligomeric species, V_1 and V_2 and V10 at 24 h. These results are supported by the minor changes in solution pH and color changes which accompanied the spectral changes. Specifically, the green aqueous solution of **V_{14}** changes to yellow over the course of the 24-hour experiment, while the aqueous green solution of **V_{15}** remained green over the evaluation time. Importantly, the aqueous solution analysis indicated that under the conditions of the cell culture studies, concentrations from 20.0 to 1.00 µmol L^{-1}, the formation of V_{10} would not be observed in the MV-POV stock solutions prepared. Therefore, the growth effects presented in this work would likely be a result of the presence of MV-POVs and not V_{10}. In the following studies, biological studies of bacterial growth inhibition were

complemented by spectroscopic studies to characterize the speciation and determine which complexes were intact under biological conditions.

4.3.2.2. Speciation studies in 7H9 media as a function of time

Studies had to be carried out to determine the species responsible for the inhibitory effect and stability of **V14** and **V15** anions under conditions of cell growth of the *M. smeg*. The 7H9 media contains several components, such as citrate and phosphate, that can form complexes with vanadate and other aqueous vanadium(V) under the growth conditions; therefore, the solution was analyzed by ^{51}V NMR (Samart et al., 2018). Vanadium(IV), in addition to metavanadate and decavanadate, can also form complexes with citrate and phosphate under the *M. smeg* growth conditions.

The ^{51}V NMR spectrum of **V14** shows additional vanadium(V) species than those observed in aqueous solution (**Figure 4.5**), attributed to the interaction between the MV-POV with some components of the culture media. First, however, the appearance of the vanadium(V) oligomers are observed and attributed to V_1, V_2 and $V_4O_{12}^{4-}$ (V_4) signals at both 0.200 and 1.00 mmol L^{-1}. At the 1.00 mmol L^{-1} solution, signals at –583 ppm were ascribed to $V_5O_{15}^{5-}$ (V_5) and signal at –497 and –514 ppm to V_{10}, documenting the fact that a higher concentration of vanadium(V) is forming in the solution from **V14** decomposition.

After 1 h, the appearance of signals at −541 and −547 ppm was attributed to the interaction of the POV with citrate (cit) and the formation of a 2 V:1 cit anionic complex V_2cit^{3-}, previously detected in the tertiary aqueous solution $H^+/H_2VO_4^-$/citrate (Gorzsas et al., 2004 and Samart et al., 2018). In addition, a new low-intensity signal at −518 ppm was observed and assigned to be a $Vcit^-$ species (Gorzsas et al., 2004), formed by the interaction of the MV-POV with citrate in the media. The spectrum at 0.200 mmol L^{-1} of **V14**, at the initial time, shows a signal at −566 ppm

attributed to the rapidly exchanging V_1 and the vanadium complex with phosphate (VP = $HVPO_7^{3-}$) (Andersson et al., 2005) causing the broadening and shifting the V_1 signal (Samart et al., 2018).

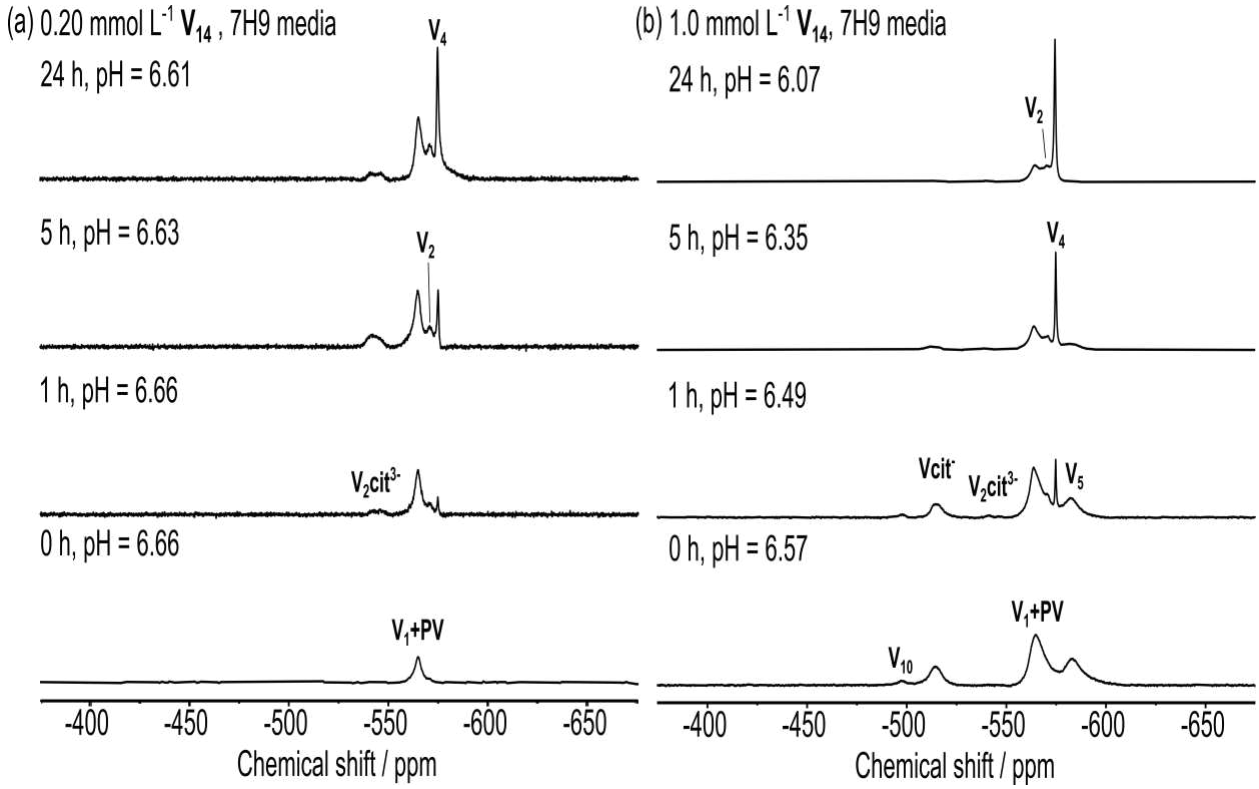

Figure. 4.5. ^{51}V NMR spectra of **V_{14}** in 7H9 media at 0, 1, 5 and 24 h time points. Data for two concentrations are shown in (a) 0.200 mmol L^{-1} and (b) 1.00 mmol L^{-1}. The vanadium(V) species observed were: V_1 ($H_2VO_4^-$), V_2 ($H_2V_2O_7^{2-}$), V_4 ($V_4O_{12}^{4-}$), PV ($HVPO_7^{3-}$), V_{10} ($HV_{10}O_{28}^{5-}$) and vanadium-citrate complexes ($Vcit^-$ and V_2cit^{3-}).

For V_{15}, the spectra at 0.200 and 1.00 mmol L^{-1} were also different from those observed in aqueous solution (**Figure 4.6**). Initially, only signals attributed to V_1 and PV were observed. After 5 h, V_2 and V_4 species were observed with chemical shifts at $\delta = -572$ and -575 ppm for V_{15}. Interestingly, the low concentrations of free V^V were not sufficient to form detectable amounts of V_{10} and vanadium-citrate complexes ($Vcit^-$ and V_2cit^{3-}) by NMR.

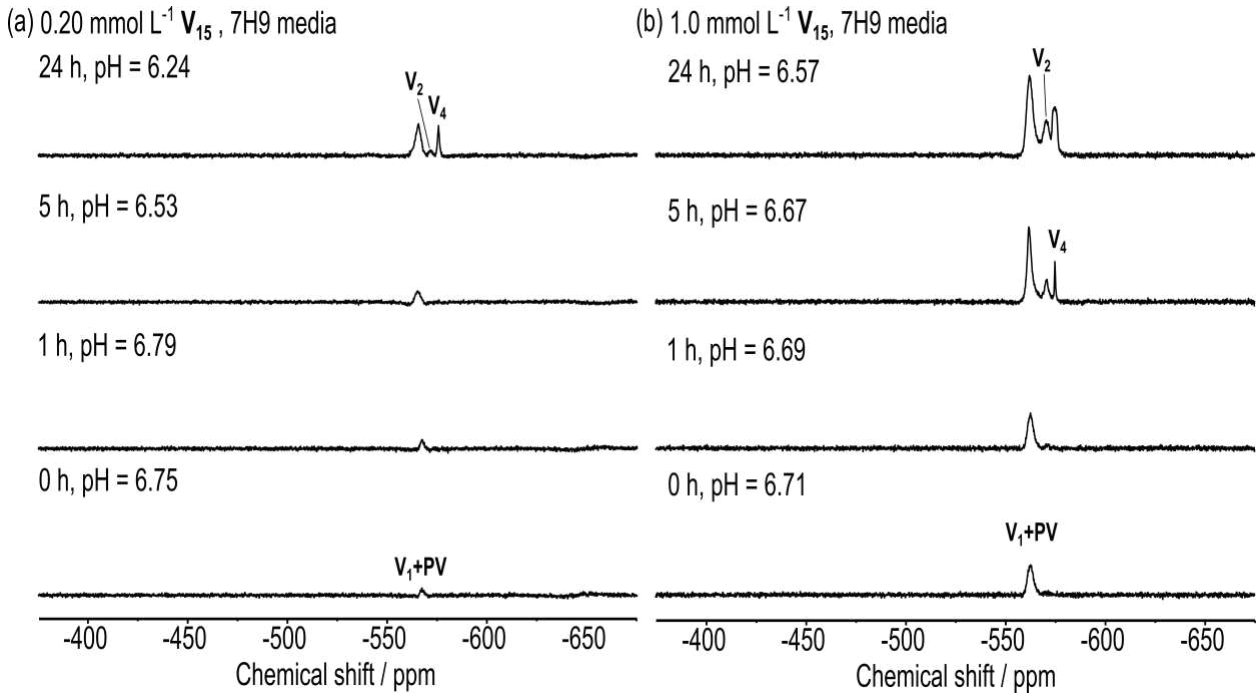

Figure. 4.6. ^{51}V NMR spectra of **V15** in 7H9 media at 0, 1, 5 and 24 h time points. Data are shown for (a) 0.200 mmol L^{-1} and (b) 1.00 mmol L^{-1}. The vanadium(V) species observed were: V_1 ($H_2VO_4^-$), PV ($HVPO_7^{3-}$), V_2 ($H_2V_2O_7^{2-}$) and V_4 ($V_4O_{12}^{4-}$).

4.3.2.3. Speciation in heated and non-heated supernatant after growth of *M. smeg*

Spectroscopic studies in the *M. smeg* supernatant had been performed to evaluate if the MV-POVs produce different species in the presence of media that may contain protein-based excretion products from the mycobacteria (Samart et al., 2018). Since speciation might change depending on the amount of protein in the media (Bijelic and Rompel, 2018), we evaluated two supernatant conditions, the heated supernatant where proteins were denaturated (called heated supernatant), and non-heated supernatant that contains potential excreted material (called non-heated supernatant).

The ^{51}V NMR spectra recorded at 0.200 and 1.00 mmol L^{-1} for V_{14} in the non-heated (**Figure 4.7**) and heated supernatant (**Figure 4.8**) showed different speciation. For the 0.200 mmol L^{-1} solutions, both conditions presented the V_1+PV species signal at −564 ppm. While, the non-

heated supernatant shows signals attributed to the V_2cit^-, V_2, and V_4 species after 1 h of analysis, indicating that even at lower concentrations, the hydrolyzed V_{14} species leads to different species that might interact with the media (**Figure 4.7**).

The ^{51}V NMR spectra for 1.00 mmol L^{-1} V_{14} in non-heated supernatant solution showed species with signals at $\delta = -564$, -583, -498 and -514 ppm assigned to V_1, PV, V_5, and V_{10}, respectively. The signals of V_1, PV, V_2cit^{3-}, V_4, and $Vcit^-$ were detected after 1 h and were maintained during the experiment at 24 h with a variation in their intensity, demonstrating increased hydrolysis of V_{14} after 24 h (**Figure 4.7**).

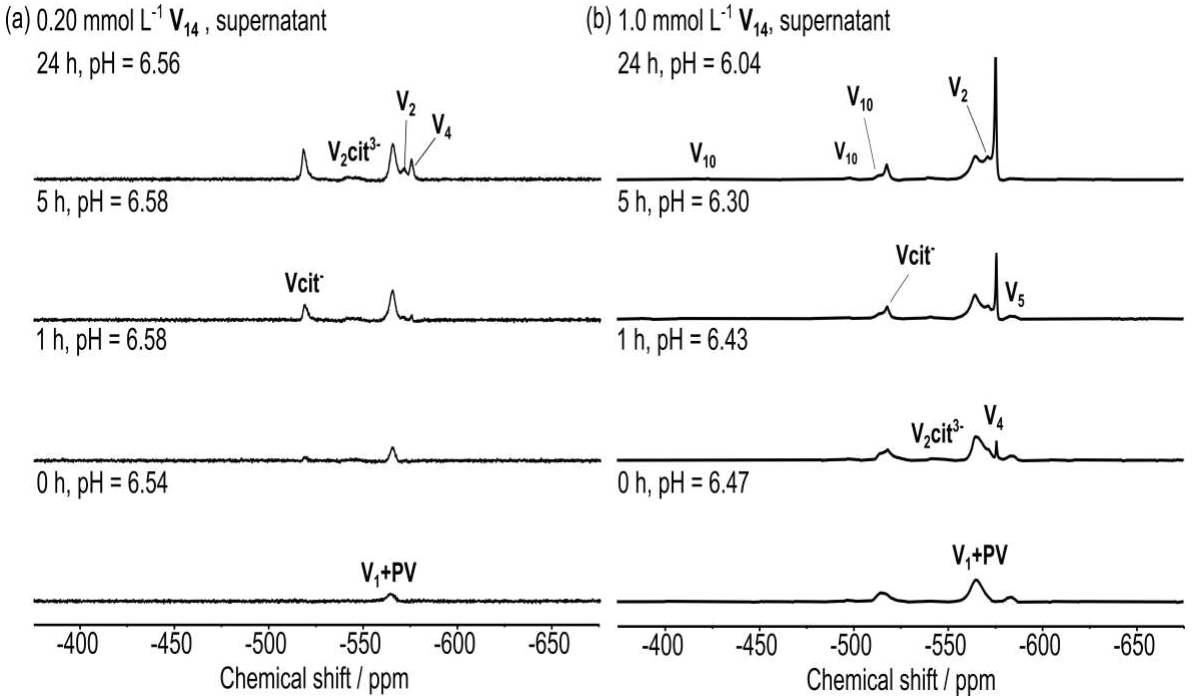

Figure. 4.7. ^{51}V NMR spectra of V_{14} in the non-heated supernatant after *M. smeg* growth as media at 0, 1, 5 and 24 h time points. Data for two concentrations are shown in (a) 0.200 and (b) 1.00 mmol L^{-1}. The vanadium(V) species observed were: V_1 ($H_2VO_4^-$), V_2 ($H_2V_2O_7^{2-}$), V_4 ($V_4O_{12}^{4-}$), V_5 ($V_5O_{15}^{5-}$), $VCit^-$, V_2Cit^{3-}, PV ($HVPO_7^{3-}$), and V_{10} ($HV_{10}O_{28}^{5-}$).

The ^{51}V NMR spectra of 0.200 mmol L^{-1} V_{14} in heated supernatant solution showed the formation of $Vcit^-$ and V_2cit^{3-} complexes only at the 24 h point (**Figure 4.8**). From the ^{51}V NMR spectra of 1.00 mmol L^{-1} V_{14} in the heated supernatant, the species observed in the heated

supernatant were the same as the non-heated supernatant after the 5 h incubation. The heated supernatant, containing less protein, showed less decomposition, suggesting that the proteins in the media may be involved in the decomposition of the MV-POV (**Figure 4.8**).

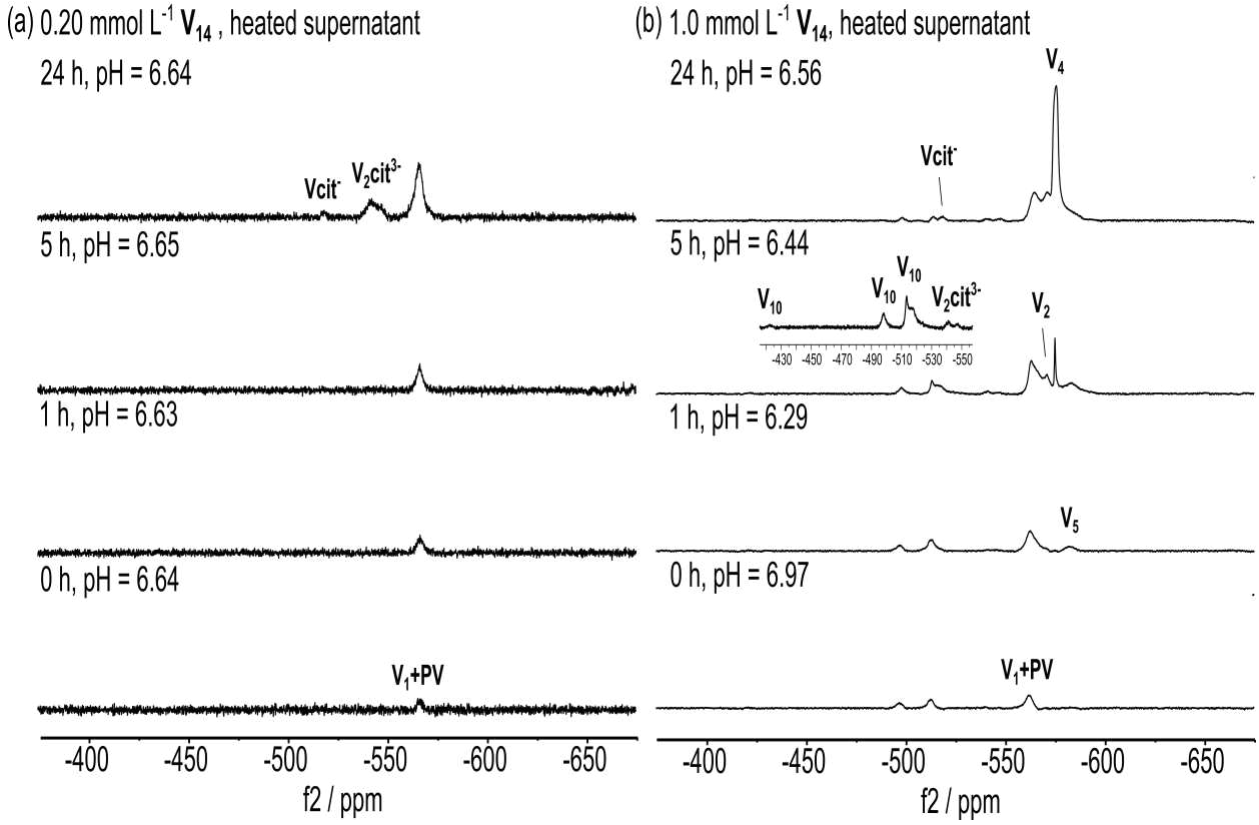

Figure. 4.8. ^{51}V NMR spectra of V_{14} in heated supernatant at 0, 1, 5 and 24 h time points. Data for two concentrations are shown in (a) 0.200 mmol L^{-1} and (b) 1.00 mmol L^{-1}.

The ^{51}V NMR spectra of the protein-containing supernatant obtained for V_{15} showed no difference in the species formed at 0.200 and 1.00 mmol L^{-1} initially, with one signal forming at −566 ppm attributed to V_1 (**Figure. 4.9**). In the spectrum recorded after 5 h incubation, for the sample 0.200 mmol L^{-1}, the species presented in the equilibrium changes, and the signals shift their position in the spectrum, indicating the formation of the V_1+PV species and the $Vcit^{-}$, with a low-intensity signal at −518 ppm. At this point, in the 1.00 mmol L^{-1} solution, two signals at −571 (V_2) and −576 ppm (V_4) appeared, indicating the further hydrolysis of the MV-POV. Interestingly,

the V_{15} solution in the supernatant does not show the formation of the vanadium(V) complex with citrate, V_2cit^{3-} at 1 h, as seen previously for V_{14} and V_{10} (Samart et al., 2018).

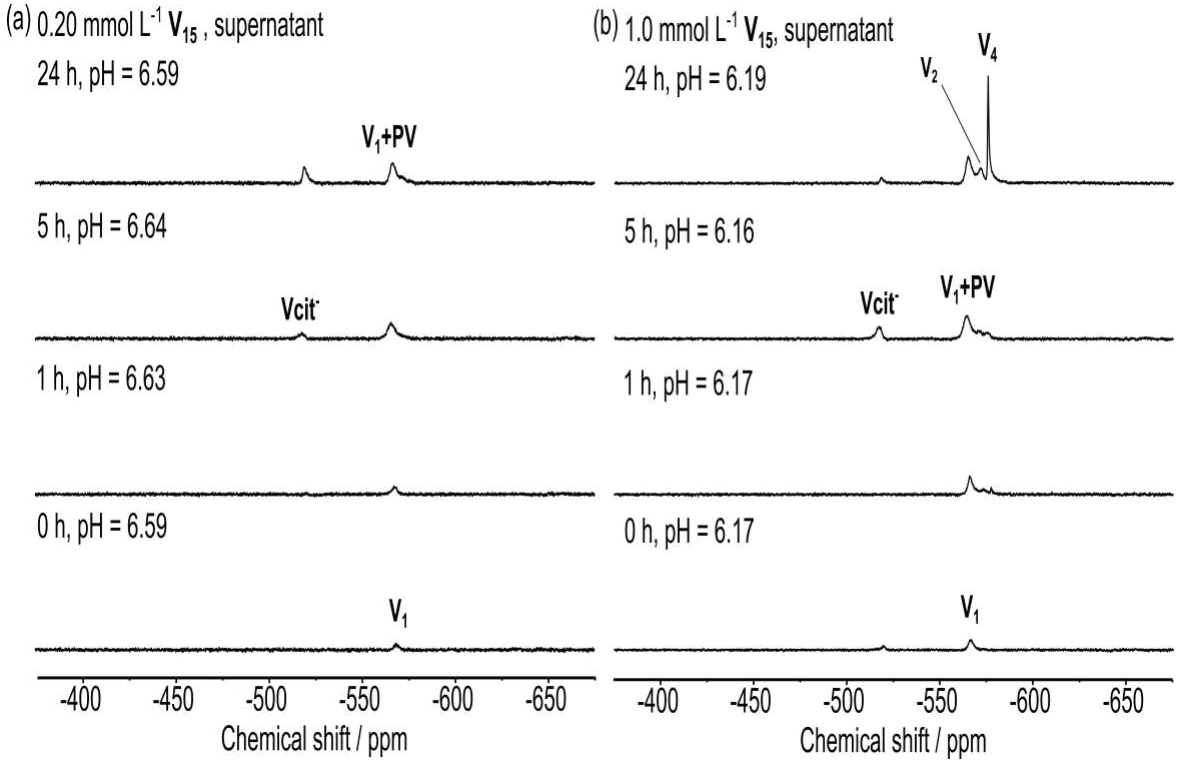

Figure. 4.9. ^{51}V NMR spectra of V_{15} in the supernatant after *M. smeg* growth as media at 0, 1, 5 and 24 h time points. Data for two concentrations are shown in (a) 0.200 and (b) 1.00 mmol L^{-1}. The vanadium(V) species observed were: V_1 ($H_2VO_4^-$), V_2 ($H_2V_2O_7^{2-}$), V_4 ($V_4O_{12}^{4-}$), PV ($HVPO_7^{3-}$) and $Vcit^-$.

For the V_{15} heated supernatant at 0.200 and 1.00 mmol L^{-1}, the species showed a lower intensity of the $Vcit^-$ signal at 5 h of 0.200 mmol L^{-1}, while the low intensity of the $Vcit^-$ in the heated supernatant of 1.00 mmol L^{-1} was observed at 24 h suggests that proteins play a role in the formation of this complex (**Figure 4.10**).

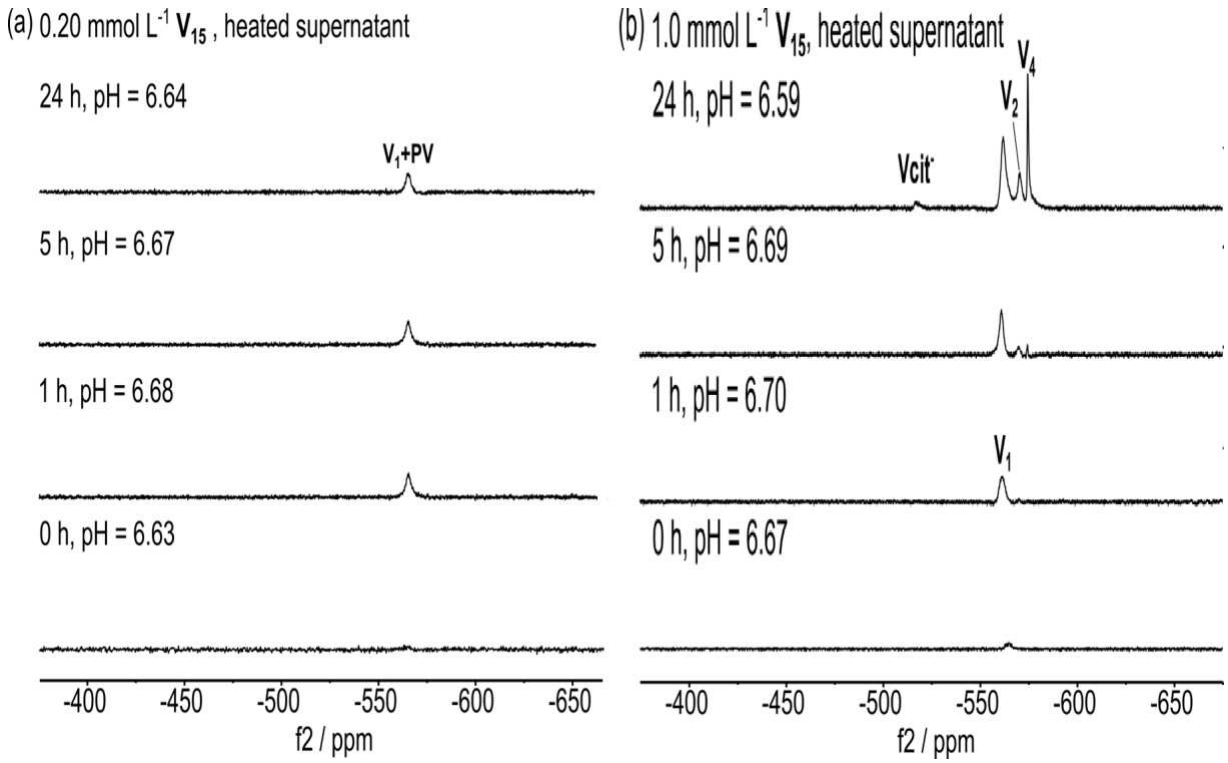

Figure 4.10. ^{51}V NMR spectra of V_{15} in heated supernatant at 0, 1, 5 and 24 h time points. Data for two concentrations are shown in (a) 0.20 mmol L^{-1} and (b) 1.0 mmol L^{-1}.

4.3.2.4. Summary of the observed chemical species of V_{14} and V_{15} in aqueous solution, 7H9 media, non-heated and heated supernatant.

The summary of the chemistry observed for V_{14} using ^{51}V NMR spectroscopy are shown in **Figure 4.11**. V_{14} did exist in aqueous solution as mixed-valence and fully oxidized oxometallate cluster, however, the presence of media and proteins led to a decomposition of the V_{14} structure and none was observed at the end of the growth study. Since the lifetime of this MV-POV was longer than 24 h in aqueous solution the decomposition reflects reaction with the media. In media, V_{14} in its polynuclear form was present during part of the experiment and by the 24 h time point, it was decomposed. As a result, the observed inhibition measured was not just that of V_{14} but the combined inhibitory effect of V_{14} and all its decomposition products. Even though V_{14} was decomposed by the end of the 24-hour experiment, the observed inhibition was nearly as potent as

V_{10}. This suggests that the real activity of V_{14} if it had remained intact in solution, could be much greater than that observed.

Aqueous solution

$$V_{14} \longrightarrow \text{MV-POV } (V_{14}) + V^{V}_{14} + V_1 + V_{10} + V^{IV}$$

7H9 media

$$V_{14} \longrightarrow \text{MV-POV } (V_{14}) + PV + V_2 + V_4 + V_5 + V_2cit^{3-} + Vcit^{-} + V^{IV}$$

Supernatant

$$V_{14} \longrightarrow \text{MV-POV } (V_{14}) + PV + V_2 + V_4 + V_5 + V_{10} + V_2cit^{3-} + Vcit^{-} + V^{IV}$$

Heated supernatant

$$V_{14} \longrightarrow \text{MV-POV } (V_{14}) + PV + V_2 + V_4 + V_5 + V_{10} + V_2cit^{3-} + Vcit^{-} + V^{IV}$$

Figure. 4.11. Summary of the observed chemical species of V_{14} solution in aqueous solution, 7H9 media, non-heated and heated supernatant at 1.00 mmol L^{-1}.

The observed decomposition of the V_{15} was summarized and shown in **Figure 4.12**. V_{15} is an MV-POV and thus contains 7 V^{V} and 8 V^{IV} atoms, and as for that, it does not show an observable NMR spectrum once the free electrons of the V^{IV} atoms are delocalized. Importantly, the absence or the low intensity of any vanadium species signal at the spectrum indicates that the MV-POV structure remains mostly intact.

Aqueous solution

$$V_{15} \longrightarrow \text{MV-POV } (V_{15}) + V_1 + V_{10} + V^{IV}$$

7H9 media

$$V_{15} \longrightarrow \text{MV-POV } (V_{15}) + PV + V_2 + V_4 + V^{IV}$$

Supernatant

$$V_{15} \longrightarrow \text{MV-POV } (V_{15}) + PV + V_2 + V_4 + Vcit^{-} + V^{IV}$$

Heated supernatant

$$V_{15} \longrightarrow \text{MV-POV } (V_{15}) + PV + V_2 + V_4 + Vcit^{-} + V^{IV}$$

Figure. 4.12. Summary of the observed chemical species of V_{15} solution in aqueous solution, 7H9 media, non-heated and heated supernatant at 1.00 mmol L^{-1}.

4.4. Discussion

Biological effects of several POMs and a few MV-POMs have been reported, mostly evaluated in cell culture and mammalian systems (Bijelic et al., 2019; Leon et al., 2014; Zhou et al., 2013), due to their potential application in medicine. The two investigated MV-POVs (V_{14} and V_{15}) were found to be better inhibitors of the *M. smeg* growth than the phosphatase inhibitor V_1. This observation confirms the reported inhibitory growth effect of V_{10} on *M. smeg* and suggests that the activity of the POVs may be more general than only V_{10} (Kostenkova et al., 2021 and Samart et al., 2018). The inhibitory growth effect observed for V_{15}, was 15 times more potent than V_{14} and 100 times stronger than V_1. The growth effects of V_{14} on *M. smeg* culture were 8 times less effective to those observed for V_{10}, while in contrast, V_{15} was 2-fold more potent than V_{10}.

V_{10} is thermodynamically favorable and likely to take place upon hydrolysis in the growth media. Therefore, it was important to determine what species of V_{14} and V_{15} were formed during the growth to evaluate the effects of each oxometallate and to determine if V_{10} would contribute in part to the observed inhibition.

The ^{51}V NMR spectroscopic results presented here show different behavior depending on the media and time of incubation. The hydrolysis and oxidation of V_{14} induce the formation of a more complex equilibria mixture in water and growth media than V_{15} solutions. Both V_{14} and V_{15} form similar vanadium(V) species (V_1, V_2, V_4, and V_{10}), and complexes with media components (PV, V-complex, Vcit), all of which were different than those observed in the aqueous solution, **(Figure 4.11 and 4.12)**. The formation of these species can be attributed to the hydrolysis of the polyoxoanion as previously reported (Kostenkova et al., 2021; Nunes et al., 2012; Samart et al., 2018). Although, the formation of the complexes between media and POV (PV, V-complex, Vcit) does not appear to potently inhibit the mycobacteria growth since they were all observed in the

previous study of V_1 inhibitory effect and this only resulted in a modest inhibition of growth of *M. smeg* (Samart et al., 2018).

Although limited information is available on the biological effects of V_{14} and V_{15}, we previously reported studies with *E. coli* (Hamilton et al., 2006; Nunes et al., 2012; Postal et al., 2016). The studies investigated the chemoprotective properties of V_{14} and V_{15}, in which, V_{15} protected the growth of *E. coli* cultures treated with an alkylating agent, diethyl sulfate. Metal oxo compounds have been previously reported to protect cells against DNA damage (Luong et al., 2016). Where, V_{15} was able to effectively deactivate the alkylating agent in comparison V_{14}, oligomers, and V_{10} that were much less effective in protecting the *E. coli* against the alkylating agent (Hamilton et al., 2006; Nunes et al., 2012; Postal et al., 2016).

The interactions between POMs and proteins are of interest in several other contexts including specific protein labeling, applications of POMs for treatment of various diseases (Rhule et al., 1998; Shigeta et al., 1995; Stroobants et al., 2013) and stabilizing interactions are a useful tool for crystallographers with challenging systems (Bashan and Yonath, 2008; Bijelic and Rompel, 2015; Bijelic and Rompel, 2017). For example, reorganization of the peptide structure for the Tyrosinase proteinase (Mauracher et al., 2014) shows that stabilizing interactions are important and might consist of a general phenomenon (Bijelic and Rompel, 2015 and Bijelic and Rompel, 2017). The fact is that several POMs are included in the currently commercially available kits for life-scientists to assist protein crystallization to suggest that these compounds are already used routinely. V_{10} was reported to induce an allergenic response on the Type I Fcε receptor on the membranes of 2 H3-RBL cells (Al-Qatati et al., 2013 and Roess et al., 2008). This effect was observed even though direct contact of the V_{10} with the membrane or the protein kinase receptor is not observed (Samart et al., 2020).

4.5. Conclusion

In this work, we demonstrate that MV-POVs can be even more potent inhibitors of growth of *M. smeg* than V_{10} and simple oxovanadates. The detailed speciation studies in aqueous, 7H9 media, growth media supernatant and protein-free growth media supernatant characterized the chemistry of V_{14} and V_{15} and allowed assignment of the inhibitory species to be a larger POV and not smaller decomposition products. The MV-POV is at least 10-200-fold more potent than the simple monomeric vanadate. The study of the effects of these oxometallates on the *M. smeg* combined with spectroscopic studies allows for the identification of the two members of MV-POVs compounds as active growth inhibitors. The inhibitory mechanism of growth in the presence of MV-POVs, could involve several factors. One possibility is that the bacteria release a non-protein material, which interacts with the MV-POVs, leading to growth inhibition. This interaction might disrupt essential cellular processes or interfere with bacterial metabolism. Furthermore, hydrolytic and oxidative conversions of the MV-POVs may play a role in the growth inhibition process. However, further research should focus on understanding the mode of action of MV-POVs in biological systems.

4.6. References

Al-Qatati, A., Fontes, F. L., Barisas, B. G., Zhang, D., Roess, D. A., and Crans, D. C. (2013). Raft localization of Type I Fcε receptor and degranulation of RBL-2H3 cells exposed to decavanadate, a structural model for V2O5. *Dalton Trans.* 42, 11912. doi: 10.1039/c3dt50398d.

Andersson, I., Gorzsás, A., Kerezsi, C., Tóth, I., and Pettersson, L. (2005). Speciation in the aqueous H+/H2VO4–/H2O2/phosphate system. *Dalton Trans.*, 3658. doi: 10.1039/b508273k.

Arhouma, Z., Murakami, H. A., Koehn, J. T., Li, X., Roess, D. A., Crick, D. C., et al. (2022). Exploring Growth of Mycobacterium smegmatis Treated with Anticarcinogenic Vanadium Compounds. *Inorganics* 10, 50. doi: 10.3390/inorganics10040050.

Aureliano, M. (2011). Recent perspectives into biochemistry of decavanadate. *World J Biol Chem* 2, 215–225. doi: 10.4331/wjbc.v2.i10.215.

Ayass, W. W., Fodor, T., Lin, Z., Smith, R. M., Xing, X., Abdallah, K., et al. (2016). Synthesis, Structure, and Antibacterial Activity of a Thallium(III)-Containing Polyoxometalate, $[Tl_2\{B\text{-}\beta\text{-}SiW_8O_{30}(OH)\}_2]^{12-}$. *Inorg. Chem.* 55, 10118–10121. doi: 10.1021/acs.inorgchem.6b01921.

Bae, J. H., Lew, E. D., Yuzawa, S., Tomé, F., Lax, I., and Schlessinger, J. (2009). The selectivity of receptor tyrosine kinase signaling is controlled by a secondary SH2 domain binding site. *Cell* 138, 514–524. doi: 10.1016/j.cell.2009.05.028.

Bashan, A., and Yonath, A. (2008). The linkage between ribosomal crystallography, metal ions, heteropolytungstates and functional flexibility. *J Mol Struct* 890, 289–294. doi: 10.1016/j.molstruc.2008.03.043.

Bijelic, A., Aureliano, M., and Rompel, A. (2018). The antibacterial activity of polyoxometalates: structures, antibiotic effects and future perspectives. *Chem. Commun.* 54, 1153–1169. doi: 10.1039/C7CC07549A.

Bijelic, A., Aureliano, M., and Rompel, A. (2019). Polyoxometalates as Potential Next-Generation Metallodrugs in the Combat Against Cancer. *Angew. Chem. Int. Ed.* 58, 2980–2999. doi: 10.1002/anie.201803868.

Bijelic, A., and Rompel, A. (2015). The use of polyoxometalates in protein crystallography – An attempt to widen a well-known bottleneck. *Coordination Chemistry Reviews* 299, 22–38. doi: 10.1016/j.ccr.2015.03.018.

Bijelic, A., and Rompel, A. (2017). Ten Good Reasons for the Use of the Tellurium-Centered Anderson–Evans Polyoxotungstate in Protein Crystallography. *Acc. Chem. Res.* 50, 1441–1448. doi: 10.1021/acs.accounts.7b00109.

Cartuyvels, E., Van Hecke, K., Van Meervelt, L., Görller-Walrand, C., and Parac-Vogt, T. N. (2008). Structural characterization and reactivity of γ-octamolybdate functionalized by proline. *Journal of Inorganic Biochemistry* 102, 1589–1598. doi: 10.1016/j.jinorgbio.2008.02.005.

Chen, S., Wu, G., Long, D., and Liu, Y. (2006). Preparation, characterization and antibacterial activity of chitosan–Ca3V10O28 complex membrane. *Carbohydrate Polymers* 64, 92–97. doi: 10.1016/j.carbpol.2005.10.024.

Costa Pessoa, J., Garribba, E., Santos, M. F. A., and Santos-Silva, T. (2015). Vanadium and proteins: Uptake, transport, structure, activity and function. *Coordination Chemistry Reviews* 301–302, 49–86. doi: 10.1016/j.ccr.2015.03.016.

Crans, D. C., Peters, B. J., Wu, X., and McLauchlan, C. C. (2017). Does anion-cation organization in Na+-containing X-ray crystal structures relate to solution interactions in inhomogeneous nanoscale environments: Sodium-decavanadate in solid state materials, minerals, and microemulsions. *Coordination Chemistry Reviews* 344, 115–130. doi: 10.1016/j.ccr.2017.03.016.

Crans, D. C., Willging, E. M., and Butler, S. R. (1990). Vanadate tetramer as the inhibiting species in enzyme reactions in vitro and in vivo. *J. Am. Chem. Soc.* 112, 427–432. doi: 10.1021/ja00157a063.

Dorsey, B. M., McLauchlan, C. C., and Jones, M. A. (2018). Evidence That Speciation of Oxovanadium Complexes Does Not Solely Account for Inhibition of Leishmania Acid Phosphatases. *Front. Chem.* 6, 109. doi: 10.3389/fchem.2018.00109.

Dux, L., and Martonosi, A. (1983). Two-dimensional arrays of proteins in sarcoplasmic reticulum and purified Ca2+-ATPase vesicles treated with vanadate. *J Biol Chem* 258, 2599–2603.

Felts, R. L., Reilly, T. J., and Tanner, J. J. (2006). Structure of Francisella tularensis AcpA: prototype of a unique superfamily of acid phosphatases and phospholipases C. *J Biol Chem* 281, 30289–30298. doi: 10.1074/jbc.M606391200.

Francese, R., Civra, A., Rittà, M., Donalisio, M., Argenziano, M., Cavalli, R., et al. (2019). Anti-zika virus activity of polyoxometalates. *Antiviral Research* 163, 29–33. doi: 10.1016/j.antiviral.2019.01.005.

Fraqueza, G., Batista de Carvalho, L. A. E., Marques, M. P. M., Maia, L., Ohlin, C. A., Casey, W. H., et al. (2012). Decavanadate, decaniobate, tungstate and molybdate interactions with sarcoplasmic reticulum Ca2+-ATPase: quercetin prevents cysteine oxidation by vanadate but does not reverse ATPase inhibition. *Dalton Trans.* 41, 12749. doi: 10.1039/c2dt31688a.

Fraqueza, G., Fuentes, J., Krivosudský, L., Dutta, S., Mal, S. S., Roller, A., et al. (2019). Inhibition of Na+/K+- and Ca2+-ATPase activities by phosphotetradecavanadate. *Journal of Inorganic Biochemistry* 197, 110700. doi: 10.1016/j.jinorgbio.2019.110700.

Fukuda, N., and Yamase, T. (1997). In vitro antibacterial activity of vanadate and vanadyl compounds against Streptococcus pneumoniae. *Biol Pharm Bull* 20, 927–930. doi: 10.1248/bpb.20.927.

Fukuma, M., Seto, Y., and Yamase, T. (1991). In vitro antiviral activity of polyoxotungstate (PM-19) and other polyoxometalates against herpes simplex virus. *Antiviral Research* 16, 327–339. doi: 10.1016/0166-3542(91)90047-U.

Gorzsás, A., Getty, K., Andersson, I., and Pettersson, L. (2004). Speciation in the aqueous H+/H2VO4–/H2O2/citrate system of biomedical interest. *Dalton Trans.*, 2873. doi: 10.1039/b409429h.

Gumerova, N. I., Al-Sayed, E., Krivosudský, L., Čipčić-Paljetak, H., Verbanac, D., and Rompel, A. (2018). Antibacterial Activity of Polyoxometalates Against Moraxella catarrhalis. *Front. Chem.* 6, 336. doi: 10.3389/fchem.2018.00336.

Gumerova, N. I., and Rompel, A. (2018). Synthesis, structures and applications of electron-rich polyoxometalates. *Nat Rev Chem* 2, 0112. doi: 10.1038/s41570-018-0112.

Hamilton, E. E., Fanwick, P. E., and Wilker, J. J. (2006). Alkylation of Inorganic Oxo Compounds and Insights on Preventing DNA Damage. *J. Am. Chem. Soc.* 128, 3388–3395. doi: 10.1021/ja056568v.

Hayashi, Y. (2011). Hetero and lacunary polyoxovanadate chemistry: Synthesis, reactivity and structural aspects. *Coordination Chemistry Reviews* 255, 2270–2280. doi: 10.1016/j.ccr.2011.02.013.

Ilyas, Z., Shah, H. S., Al-Oweini, R., Kortz, U., and Iqbal, J. (2014). Antidiabetic potential of polyoxotungstates: in vitro and in vivo studies. *Metallomics* 6, 1521–1526. doi: 10.1039/c4mt00106k.

Inouye, Y., Tokutake, Y., Kunihara, J., Yoshida, T., Yamase, T., Nakata, A., et al. (1992). Suppressive Effect of Polyoxometalates on the Cytopathogenicity of Human Immunodeficiency Virus Type 1 (HIV-1) in Vitro and Their Inhibitory Activity against HIV-1 Reverse Transcriptase. *Chem. Pharm. Bull.* 40, 805–807. doi: 10.1248/cpb.40.805.

Judd, D. A., Nettles, J. H., Nevins, N., Snyder, J. P., Liotta, D. C., Tang, J., et al. (2001). Polyoxometalate HIV-1 Protease Inhibitors. A New Mode of Protease Inhibition. *J. Am. Chem. Soc.* 123, 886–897. doi: 10.1021/ja001809e.

Kostenkova, K., Arhouma, Z., Postal, K., Rajan, A., Kortz, U., Nunes, G. G., et al. (2021). PtIV- or MoVI-substituted decavanadates inhibit the growth of Mycobacterium smegmatis. *J Inorg Biochem* 217, 111356. doi: 10.1016/j.jinorgbio.2021.111356.

León, I. E., Porro, V., Astrada, S., Egusquiza, M. G., Cabello, C. I., Bollati-Fogolin, M., et al. (2014). Polyoxometalates as antitumor agents: Bioactivity of a new polyoxometalate with copper on a human osteosarcoma model. *Chemico-Biological Interactions* 222, 87–96. doi: 10.1016/j.cbi.2014.10.012.

Luong, T. K. N., Mihaylov, T. T., Absillis, G., Shestakova, P., Pierloot, K., and Parac-Vogt, T. N. (2016). Phosphate Ester Bond Hydrolysis Promoted by Lanthanide-Substituted Keggin-type Polyoxometalates Studied by a Combined Experimental and Density Functional Theory Approach. *Inorg. Chem.* 55, 9898–9911. doi: 10.1021/acs.inorgchem.6b01802.

Mauracher, S. G., Molitor, C., Al-Oweini, R., Kortz, U., and Rompel, A. (2014). Latent and active abPPO4 mushroom tyrosinase cocrystallized with hexatungstotellurate(VI) in a single crystal. *Acta Crystallogr D Biol Crystallogr* 70, 2301–2315. doi: 10.1107/S1399004714013777.

Maurer, A., and Fleischer, S. (1984). Decavanadate is responsible for vanadate-induced two-dimensional crystals in sarcoplasmic reticulum. *J Bioenerg Biomembr* 16, 491–505. doi: 10.1007/BF00743241.

Messmore, J. M., and Raines, R. T. (2000). Decavanadate Inhibits Catalysis by Ribonuclease A. *Archives of Biochemistry and Biophysics* 381, 25–30. doi: 10.1006/abbi.2000.1951.

Miras, H. N., Vilà-Nadal, L., and Cronin, L. (2014). Polyoxometalate based open-frameworks (POM-OFs). *Chem. Soc. Rev.* 43, 5679–5699. doi: 10.1039/C4CS00097H.

Missina, J. M., Gavinho, B., Postal, K., Santana, F. S., Valdameri, G., de Souza, E. M., et al. (2018). Effects of Decavanadate Salts with Organic and Inorganic Cations on *Escherichia coli* , *Giardia intestinalis* , and Vero Cells. *Inorg. Chem.* 57, 11930–11941. doi: 10.1021/acs.inorgchem.8b01298.

Monakhov, K. Yu., Bensch, W., and Kögerler, P. (2015). Semimetal-functionalised polyoxovanadates. *Chem. Soc. Rev.* 44, 8443–8483. doi: 10.1039/C5CS00531K.

Nunes, G. G., Bonatto, A. C., de Albuquerque, C. G., Barison, A., Ribeiro, R. R., Back, D. F., et al. (2012). Synthesis, characterization and chemoprotective activity of polyoxovanadates against DNA alkylation. *Journal of Inorganic Biochemistry* 108, 36–46. doi: 10.1016/j.jinorgbio.2011.11.019.

Pereira, M. J., Carvalho, E., Eriksson, J. W., Crans, D. C., and Aureliano, M. (2009). Effects of decavanadate and insulin enhancing vanadium compounds on glucose uptake in isolated rat adipocytes. *Journal of Inorganic Biochemistry* 103, 1687–1692. doi: 10.1016/j.jinorgbio.2009.09.015.

Pluskey, S., Mahroof-Tahir, M., Crans, D. C., and Lawrence, D. S. (1997). Vanadium oxoanions and cAMP-dependent protein kinase: an anti-substrate inhibitor. *Biochem J* 321 (Pt 2), 333–339. doi: 10.1042/bj3210333.

Postal, K., Maluf, D. F., Valdameri, G., Rüdiger, A. L., Hughes, D. L., de Sá, E. L., et al. (2016). Chemoprotective activity of mixed valence polyoxovanadates against diethylsulphate in E. coli cultures: insights from solution speciation studies. *RSC Adv.* 6, 114955–114968. doi: 10.1039/C6RA15826A.

Rhule, J. T., Hill, C. L., Judd, D. A., and Schinazi, R. F. (1998). Polyoxometalates in Medicine. *Chem. Rev.* 98, 327–358. doi: 10.1021/cr960396q.

Roess, D. A., Smith, S. M. L., Winter, P., Zhou, J., Dou, P., Baruah, B., et al. (2008). Effects of Vanadium-Containing Compounds on Membrane Lipids and on Microdomains Used in Receptor-Mediated Signaling. *Chemistry & Biodiversity* 5, 1558–1570. doi: 10.1002/cbdv.200890144.

Saha, A. K., Crans, D. C., Pope, M. T., Simone, C. M., and Glew, R. H. (1991). Inhibition of human seminal fluid and Leishmania donovani phosphatases by molybdate heteropolyanions. *Journal of Biological Chemistry* 266, 3511–3517. doi: 10.1016/S0021-9258(19)67825-7.

Samart, N., Althumairy, D., Zhang, D., Roess, D. A., and Crans, D. C. (2020). Initiation of a novel mode of membrane signaling: Vanadium facilitated signal transduction. *Coordination Chemistry Reviews* 416, 213286. doi: 10.1016/j.ccr.2020.213286.

Samart, N., Arhouma, Z., Kumar, S., Murakami, H. A., Crick, D. C., and Crans, D. C. (2018). Decavanadate Inhibits Mycobacterial Growth More Potently Than Other Oxovanadates. *Front. Chem.* 6, 519. doi: 10.3389/fchem.2018.00519.

Sánchez-Lara, E., Treviño, S., Sánchez-Gaytán, B. L., Sánchez-Mora, E., Eugenia Castro, M., Meléndez-Bustamante, F. J., et al. (2018). Decavanadate Salts of Cytosine and Metformin: A Combined Experimental-Theoretical Study of Potential Metallodrugs Against Diabetes and Cancer. *Front. Chem.* 6, 402. doi: 10.3389/fchem.2018.00402.

Shahid, M., Sharma, P. K., Anjuli, Chibber, S., and Siddiqi, Z. A. (2014). Isolation of a Decavanadate Cluster $[H_2V_{10}O_{28}][4\text{-picH}]4\cdot 2H_2O$ (4-pic = 4-picoline): Crystal Structure, Electrochemical Characterization, Genotoxic and Antimicrobial Studies. *J Clust Sci* 25, 1435–1447. doi: 10.1007/s10876-014-0721-5.

Shigeta, S., Mori, S., Watanabe, J., Baba, M., Khenkin, A. M., Hill, C. L., et al. (1995). *In vitro* Antimyxovirus and Anti-Human Immunodeficiency Virus Activities of Polyoxometalates. *Antivir Chem Chemother* 6, 114–122. doi: 10.1177/095632029500600206.

Singh, A. K., and Reyrat, J. (2009). Laboratory Maintenance of *Mycobacterium smegmatis*. *Current Protocols in Microbiology* 14. doi: 10.1002/9780471729259.mc10c01s14.

Stroobants, K., Moelants, E., Ly, H. G. T., Proost, P., Bartik, K., and Parac-Vogt, T. N. (2013). Polyoxometalates as a Novel Class of Artificial Proteases: Selective Hydrolysis of Lysozyme under Physiological pH and Temperature Promoted by a Cerium(IV) Keggin-Type Polyoxometalate. *Chem. Eur. J.* 19, 2848–2858. doi: 10.1002/chem.201203020.

Tiago, T., Martel, P., Gutiérrez-Merino, C., and Aureliano, M. (2007). Binding modes of decavanadate to myosin and inhibition of the actomyosin ATPase activity. *Biochimica et Biophysica Acta (BBA) - Proteins and Proteomics* 1774, 474–480. doi: 10.1016/j.bbapap.2007.02.004.

Treviño, S., Velázquez-Vázquez, D., Sánchez-Lara, E., Diaz-Fonseca, A., Flores-Hernandez, J. Á., Pérez-Benítez, A., et al. (2016). Metforminium Decavanadate as a Potential Metallopharmaceutical Drug for the Treatment of Diabetes Mellitus. *Oxid Med Cell Longev* 2016, 6058705. doi: 10.1155/2016/6058705.

Turner, T. L., Nguyen, V. H., McLauchlan, C. C., Dymon, Z., Dorsey, B. M., Hooker, J. D., et al. (2012). Inhibitory effects of decavanadate on several enzymes and Leishmania tarentolae In Vitro. *Journal of Inorganic Biochemistry* 108, 96–104. doi: 10.1016/j.jinorgbio.2011.09.009.

Vanhaecht, S., Absillis, G., and Parac-Vogt, T. N. (2012). Hydrolysis of DNA model substrates catalyzed by metal-substituted Wells–Dawson polyoxometalates. *Dalton Trans.* 41, 10028. doi: 10.1039/c2dt30588g.

Winkler, P. A., Huang, Y., Sun, W., Du, J., and Lü, W. (2017). Electron cryo-microscopy structure of a human TRPM4 channel. *Nature* 552, 200–204. doi: 10.1038/nature24674.

Witvrouw, M., Weigold, H., Pannecouque, C., Schols, D., De Clercq, E., and Holan, G. (2000). Potent Anti-HIV (Type 1 and Type 2) Activity of Polyoxometalates: Structure−Activity Relationship and Mechanism of Action. *J. Med. Chem.* 43, 778–783. doi: 10.1021/jm980263s.

Yamase, T. In Biomedical Inorganic Polymers: Bioactivity and Applications of Natural and Synthetic Polymeric Inorganic Molecules; Müller, W. E. G., Wang, X., Schröder, H. C., Ed.; Springer Berlin Heidelberg: Berlin, Heidelberg, 2013; pp 65-116.

Zebisch, M., Krauss, M., Schäfer, P., and Sträter, N. (2012). Crystallographic evidence for a domain motion in rat nucleoside triphosphate diphosphohydrolase (NTPDase) 1. *J Mol Biol* 415, 288–306. doi: 10.1016/j.jmb.2011.10.050.

Zhou, Z., Zhang, D., Yang, L., Ma, P., Si, Y., Kortz, U., et al. (2013). Nona-copper(ii)-containing 18-tungsto-8-arsenate(iii) exhibits antitumor activity. *Chem. Commun.* 49, 5189. doi: 10.1039/c3cc41628c.

SUMMARY

ANTIBACTERIAL GROWTH EFFECTS AND SPECIATION OF SEVERAL VANADIUM SALTS AND COMPLEXES

In my dissertation work, I explored the properties of various types of vanadium compounds, such as vanadium salts, oxometalates and coordination complexes, to investigate their effects on bacterial growth. While vanadium in oxidation state +5 (V^V) is known to function as a phosphatase inhibitor and has a range of physiological activities, its potential as an antibacterial agent and its impact on bacterial growth have not been extensively studied.

The work presented in Chapters 1 and 2 of this dissertation is the first investigation of the effects of decavanadate (V_{10}) and monosubstituted decavanadates (V_9X) where X is Pt^{IV} or Mo^{VI}. The results of these studies revealed that V_{10} and the two monosubstituted decavanadates (V_9Pt and V_9Mo) exhibited greater potency in inhibiting the growth of mycobacteria than V_1. These findings demonstrated that when one V^V ion in V_{10} is substituted by a Pt^{IV} or Mo^{VI} ion, isostructural derivatives are formed. These derivatives were found to inhibit the growth of *M. smeg* with slight variations in their activities and less effectiveness than V_{10}. It is evident that the growth inhibition of *M. smeg* by V_9Pt and V_9Mo is primarily caused by the structure of decavanadate rather than the changes in charges or redox properties resulting from the substitution of a V^V ion by a Pt^{IV} or Mo^{VI} ion in the decametalate. This suggests that the inherent characteristics of decavanadate play a significant role in its inhibitory effects on bacterial growth.

The study regarding the activity of two pseudospherical mixed-valence polyoxovanadates (V_{14} and V_{15}) on the growth of *M. smeg*. (Chapter 4) represented the first study to test the antibacterial activity of these compounds. The results were significantly different than previous

studies reported in *E. coli.* These MV-POVs contain both vanadium in oxidation state +4 (V^{IV}) and vanadium in oxidation state +5 (V^{V}) within their structures, exhibiting intriguing redox properties and serving as models for studying redox chemistry in complex systems. However, their effects on cell growth are complex due to their instability under biological conditions. Both V_{14} and V_{15} are more potent inhibitors of *M. smeg*. growth compared to monomeric vanadate (V_1). However, there were notable differences in their inhibitory activities. V_{14} exhibited a weaker growth inhibitory effect on *M. smeg.* compared to V_{10}, while V_{15} showed more potency effective than V_{10} in inhibiting bacterial growth. These findings support that the inhibitory effect of V_{10} on *M. smeg*. is not exclusive to that particular oxometalate structure and that the inhibitory growth effects of vanadium compounds on *M. smeg*. can vary depending on their specific structures and redox properties.

The work presented in Chapter 3 investigated two phenomena, such as the effects of anticarcinogenic metal compounds on bacteria and, secondly, address the question of whether the activity is related to the effects of intact complex or from ligand. These studies examined the antibacterial effects of a series of anticarcinogenic vanadium compounds to determine if these compounds potentially inhibited bacterial growth. Our studies showed that their effects on bacteria were much less than those observed on cancer cells. Thus, the compounds showed selectivity against cancer cells. This study is indeed the first extensive study that evaluated the growth effects of a coordination complex (a Schiff base oxidovanadium complex) coordinated to a catecholate ligand and compared the effects of complexes with the effects of the corresponding free ligands under biological conditions. Evaluating the effects of a series of vanadium coordination anticancer complexes that exhibit the effects on the growth of a representative bacterium can shed light on the different effects of complexes versus free ligand. By comparing the growth effects of these

complexes with the effects of the free catecholates, it becomes possible to assess whether the complexation of the metal ion enhances or diminishes the growth inhibition activity. The results obtained from Schiff base V-catecholate complexes indicate that the properties of a catecholate ligand itself, such as toxicity, hydrophobicity (tendency to repel water) and steric bulk (molecular shape and bulkiness) play a role in their antibacterial activity. Our findings indicated that the observed antibacterial growth activity of the complexes is not solely related to their stability but also is sensitive to the specific structure and reactivity of the catechol ligands. Hence small changes in ligand structure can change the effect of the complex. Such subtle effects can be used when developing compounds with biological activities and particularly in continued efforts of developing the anticancer properties of these Schiff base vanadium(V) catecholate complexes.

Appendix I: Decavanadate Inhibits Mycobacterial Growth More Potently Than Other Oxovanadates

This appendix consists of the supplemental materials for data contained in Chapter 1. The data in this section includes relevant material that reinforces and support the main points of the results in Chapter I.

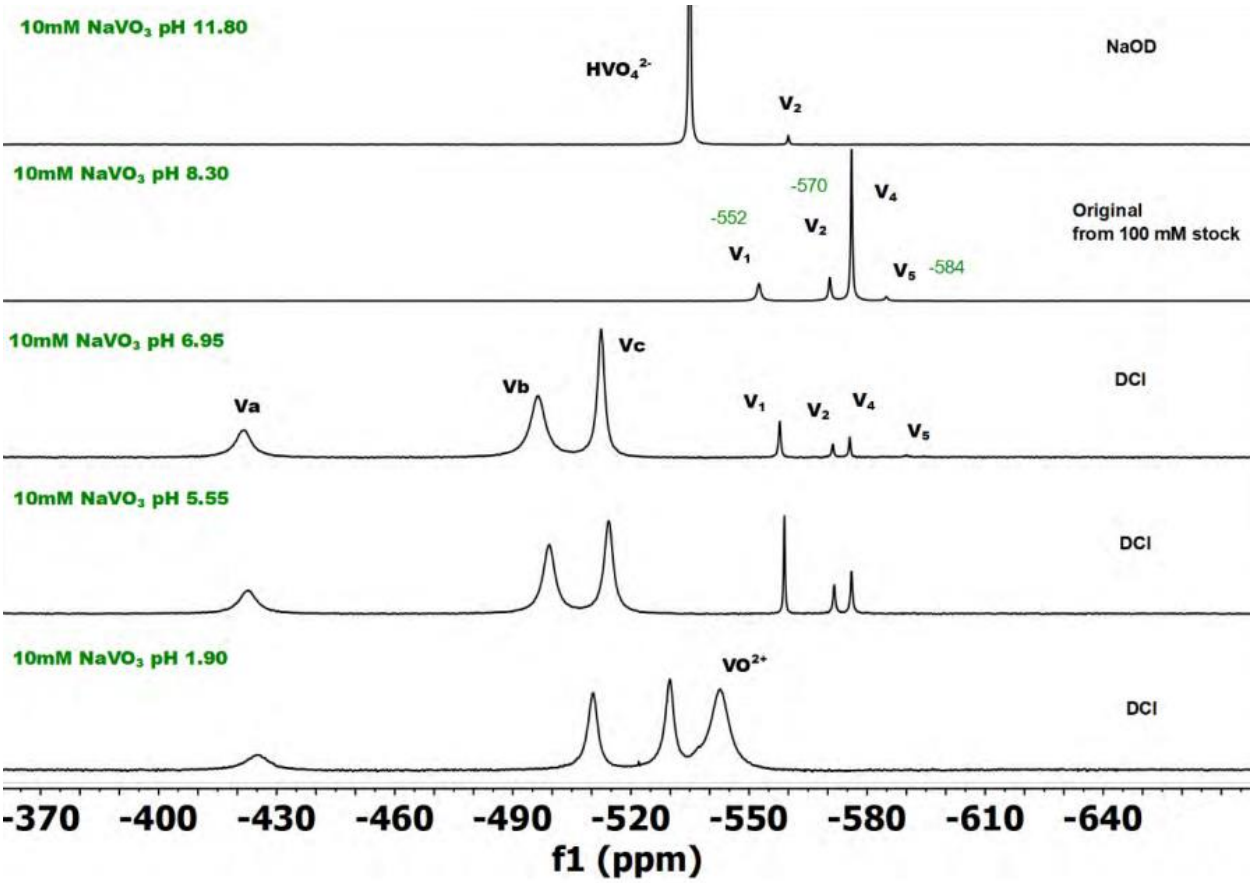

Figure A1.S1. The 10 mM sodium metavanadate (NaVO3) at varying pH values adjust by using 6 M DCl and 6 M NaOD solution. The original solution of NaVO3 colorless at pH 8.30 spectra show signal monomer (V1), dimer (V2), tetramer (V4) and pentamer (V5). In acid pH 5.55-6.95 get decavanadate form (V10) (The decavanadate have 3 difference V atom as Va, Vb and Vc signal show -420 to -530 ppm) and at low pH NaVO3 change charge lose proton transfer. NaVO3 in basic pH 11.80 adjust by NaOD show signal 2 peaks assignment monomer vanadate form HVO4 2- at -535 ppm and dimer form at -559 ppm.

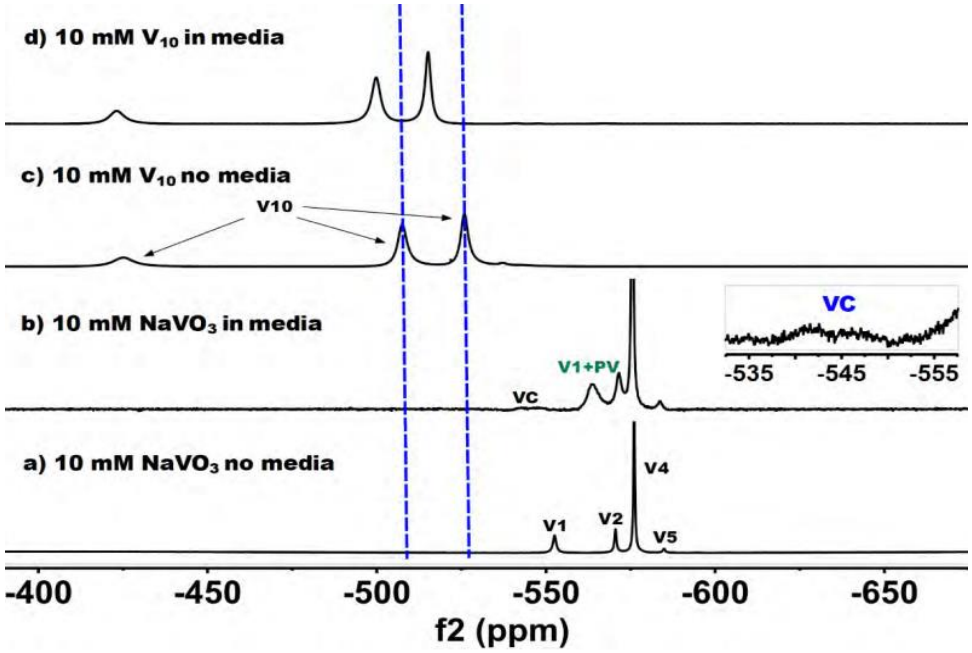

Figure A1.S2. Spectra of a) NaVO3 in aqueous solution (no media), b) NaVO3 in media and c) V10 in aqueous solution (no media) and d) V10 in media. Key for signals in the case of the VCit complex two different broad peaks at -537 and -550 ppm are shown. In the case of PV the rapid exchange between V1 and PV lead to only one signal at -559 ppm including both these compounds.

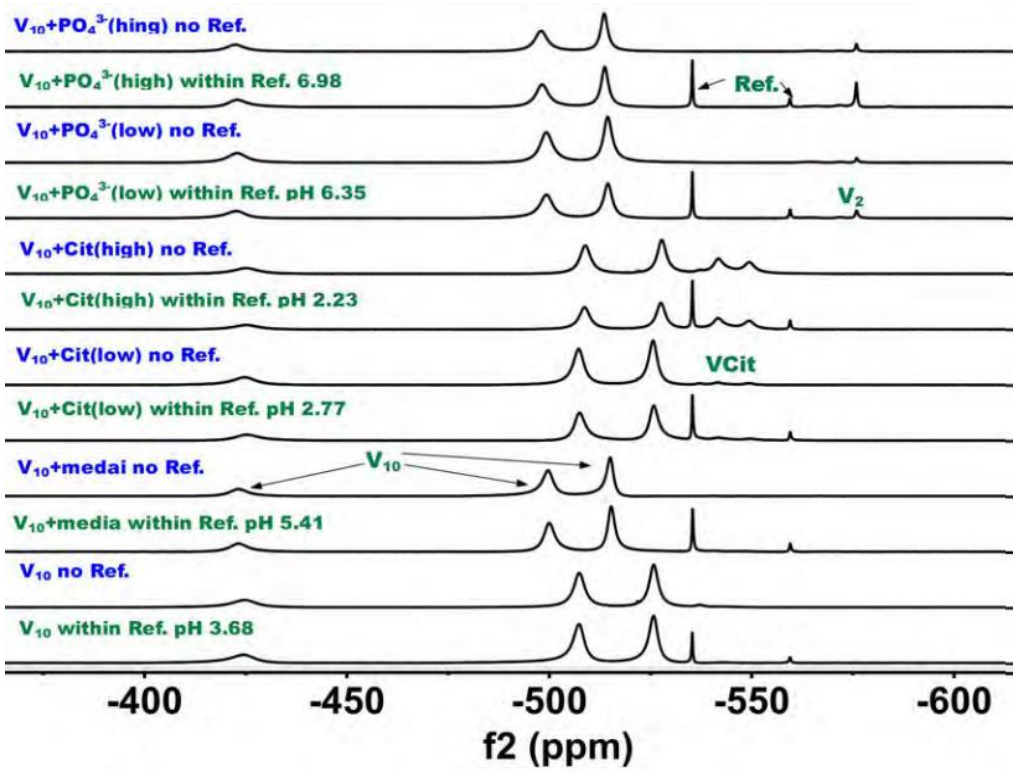

Figure A1.S3. Spectra of V10 at various conditions including different pH values in the presence and absence of media and reference.

1) 0 hr

pH		
	10mM	3.3mM
V_1	7.42	7.39
V_{10}	7.30	7.33

2) 1 hr

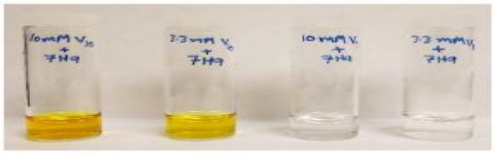

pH		
	10mM	3.3mM
V_1	7.04	7.01
V_{10}	6.78	6.88

3) 5 hrs

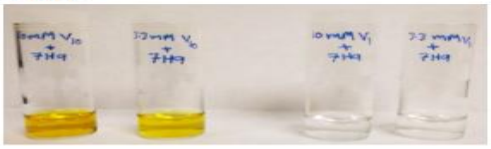

pH		
	10mM	3.3mM
V_1	7.10	7.05
V_{10}	6.63	6.82

4) 24 hrs

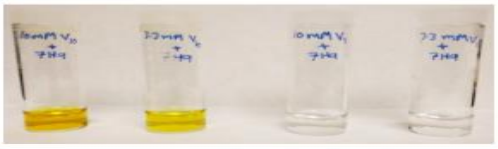

pH		
	10mM	3.3mM
V_1	7.02	6.97
V_{10}	6.47	6.50

Figure A1.S4. V_1 & V_{10} added to 7H9 medium (in the absence of bacteria) at different time points (both 3.3 and 10 mM V_1 (colorless right) and V_{10} (yellow/oranges); pH was measured and shown in table. No green color is developing in either samples – indicating no redox in samples.

1) 0 hr

pH		
	10mM	3.3mM
V_1	7.32	7.30
V_{10}	7.24	7.27

2) 1 hr

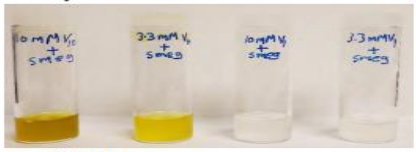

pH		
	10mM	3.3mM
V_1	6.89	6.84
V_{10}	6.40	6.66

3) 5 hrs

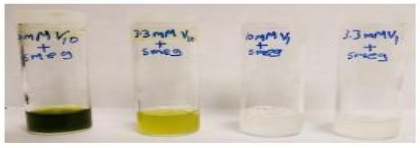

pH		
	10mM	3.3mM
V_1	6.83	6.78
V_{10}	6.43	6.41

4) 24 hrs

pH		
	10mM	3.3mM
V_1	6.54	6.58
V_{10}	6.22	6.20

Figure A1.S5. V_1 & V_{10} added to 7H9 medium with *M. smeg* at different time points (both 3.3 and 10 mM V_1 (colorless right) and V_{10} (yellow/oranges); pH was measured and shown in table. Green color is developing after 5 hours of incubations in the samples containing V10 consistent with redox.

1) 0 hr

pH		
	10mM	3.3mM
V_1	6.86	6.82
V_{10}	6.75	6.79

2) 1 hr

pH		
	10mM	3.3mM
V_1	6.85	6.80
V_{10}	6.37	6.63

3) 5 hrs

pH		
	10mM	3.3mM
V_1	6.88	6.83
V_{10}	6.17	6.26

4) 24 hrs

pH		
	10mM	3.3mM
V_1	6.67	6.57

Figure A1.S6. V_1 & V_{10} added to supernatant at different time points (both 3.3 and 10 mM V_1 (colorless right) and V_{10} (yellow/oranges); pH was measured and shown in table.

Time incubated	V_{10} or V_1 - 7H9 media				V_{10} or V_1 – *M. smeg* in 7H9 media				V_{10} or V_1 – supernatant after *M. smeg* growth (cells removed)			
V-treatment	V_{10} (mM)		V_1 (mM)		V_{10} (mM)		V_1 (mM)		V_{10} (mM)		V_1 (mM)	
V-species concentration	10.0 mM	3.3 mM	10.0 mM	3.3 mM	10.0 mM	3.3 mM	10.0 mM	3.3 mM	10.0 mM	3.3 mM	10.0 mM	3.3 mM
0	7.30	7.33	7.42	7.39	7.24	7.27	7.32	7.30	6.75	6.79	6.86	6.82
1	6.78	6.88	7.04	7.01	6.40	6.66	6.89	6.84	6.37	6.63	6.85	6.80
5	6.63	6.82	7.10	7.05	6.43	6.41	6.83	6.78	6.17	6.26	6.88	6.83
24	6.47	6.50	7.02	6.97	6.22	6.20	6.54	6.58	6.07	6.12	6.67	6.57

Table A1.S1. The pH values measured in 7H9 media, *M. Smeg* cultures and supernatant after incubation with V samples.

Appendix II: Pt^{IV}- or Mo^{VI}-substituted decavanadates inhibit the growth of *Mycobacterium smegmatis*

This appendix is a part of the supplemental materials for data showed in Chapter 2. The data in this section provides important relevant materials that reinforces and support the main points of the results in Chapter 2.

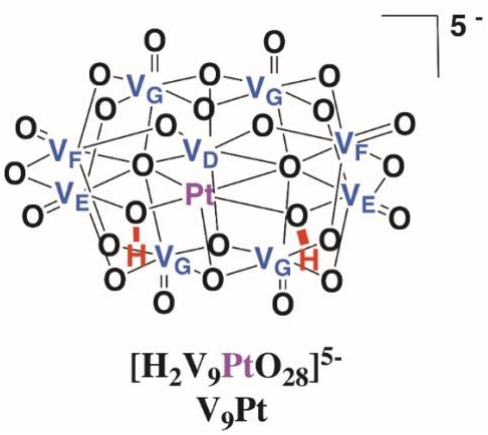

Figure A2. S1. A structure of the V_9Pt complex with the correct assignment of the peaks in the ^{51}V NMR.

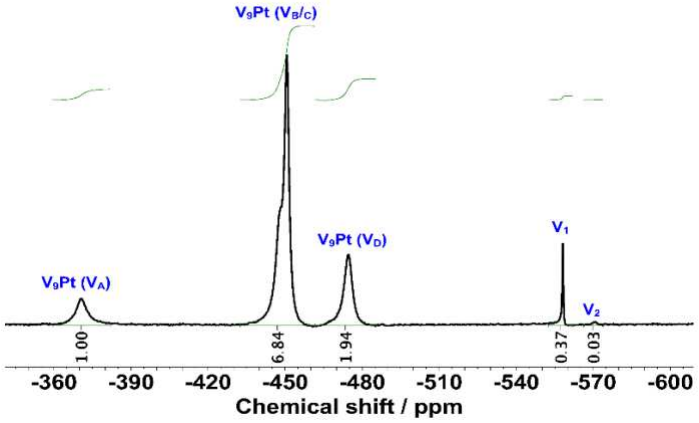

Figure A2.S2. ^{51}V NMR spectrum of 1.0 mM aqueous solution of $Na_5[H_2PtV_9O_{28}]\cdot 21H_2O$, pH 5.6, used as the control for speciation studies. The insert presents the structure of the $[H_2PtV_9O_{28}]^{5-}$ (V_9Pt) anion present in solution with the assignments for the non-equivalents vanadium(V) atoms $V_D - V_G$. Signals at δ –558 and –571 ppm refers to V_1 and V_2.

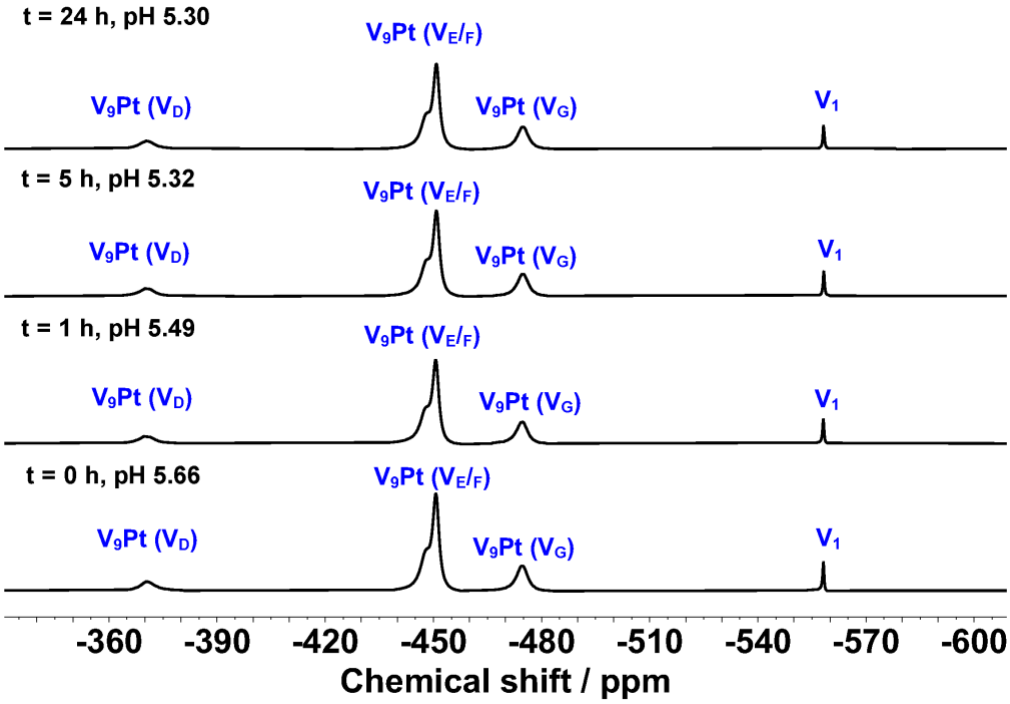

Figure A2.S3. ^{51}V NMR spectra showing the speciation data of the 1.0 mM V_9Pt aqueous control solution over 24 h studied by.

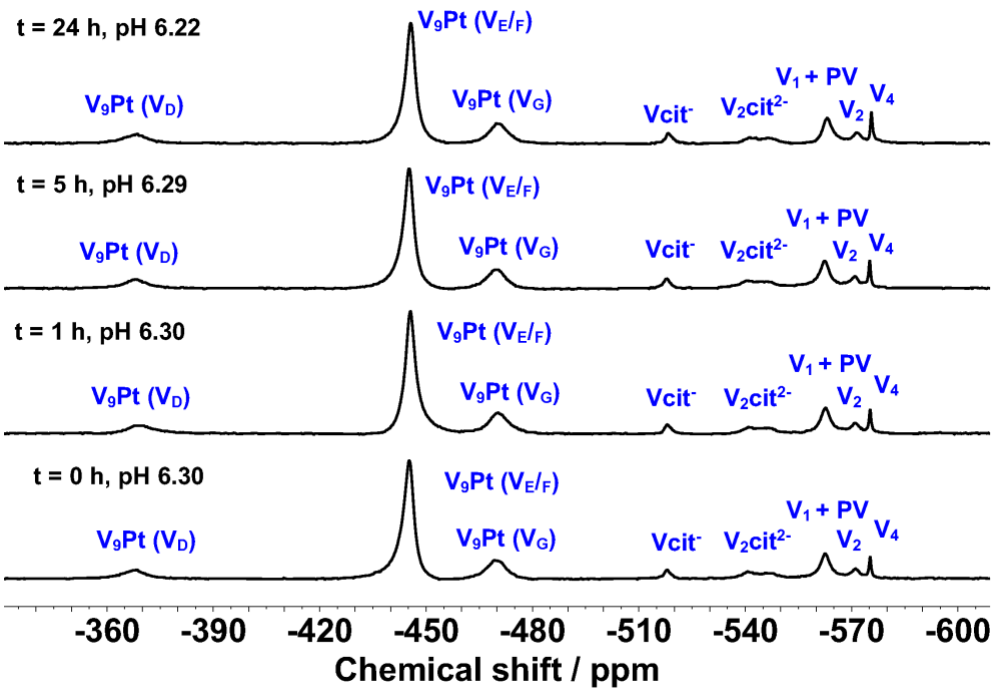

Figure A2.S4. ^{51}V NMR spectra showing the speciation data of the V$_9$Pt complex in the non-heated supernatant (1.0 mM solution) over 24 h.

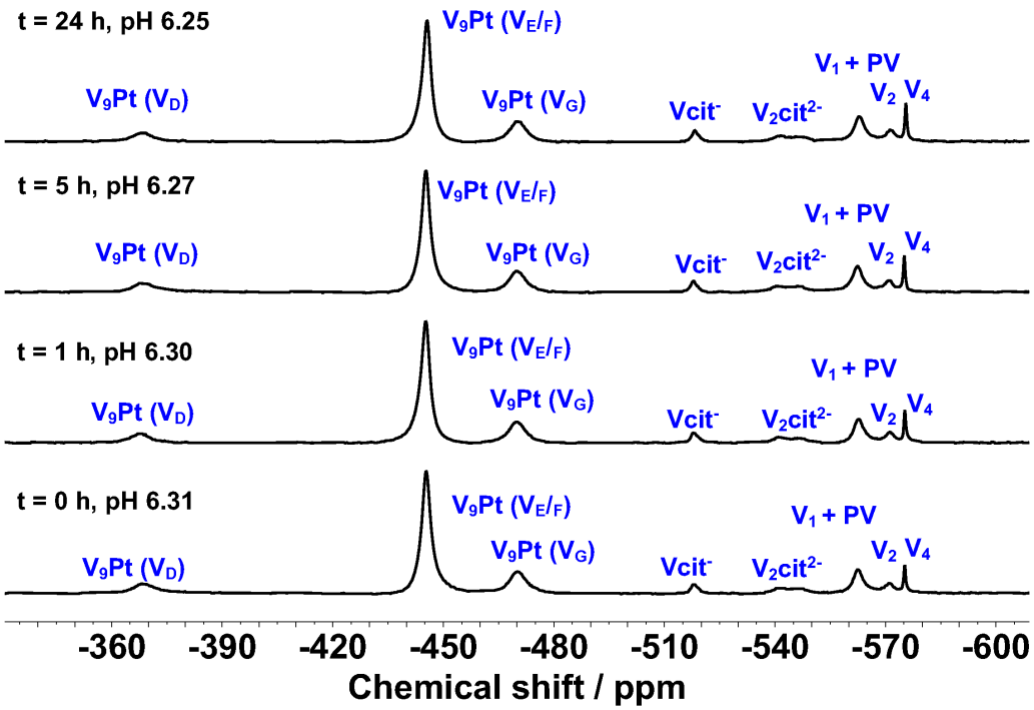

Figure A2.S5. ^{51}V NMR spectra showing the speciation data of the V$_9$Pt complex in the heated supernatant (1.0 mM solution) over 24 h.

Table A2.S1. A summary of the speciation data of the V_9Pt complex collected at t = 0 h and t = 24 h in a 1.0 mM aqueous control solution, 1.0 mM solutions in the 7H9 medium, non-heated, and heated supernatant

Experimental Condition	Species Monitored	t = 0 hours, %	t = 24 hours, %
V_9Pt Aqueous Solution	V_9Pt	96.9	96.1
	V_1	3.8	3.4
	V_4	0.2	0.4
V_9Pt in 7H9 Medium	V_9Pt	78.9	80.7
	V_1 + PV	10.1	9.0
	V_2	3.6	3.5
	V_4	3.2	4.4
	V_2cit^{2-}	4.3	2.5
V_9Pt in supernatant	V_9Pt	73.9	75.3
	V_1 + PV	10.7	9.7
	V_2	3.5	3.7
	V_4	2.9	4.4
	$Vcit^{-}$	2.2	2.2
	V_2cit^{2-}	6.7	4.6
V_9Pt in heated supernatant	V_9Pt	75.2	70.6
	V_1 + PV	10.0	11.6
	V_2	3.8	4.2
	V_4	4.0	5.0
	$Vcit^{-}$	2.0	2.5
	V_2cit^{2-}	4.9	6.1

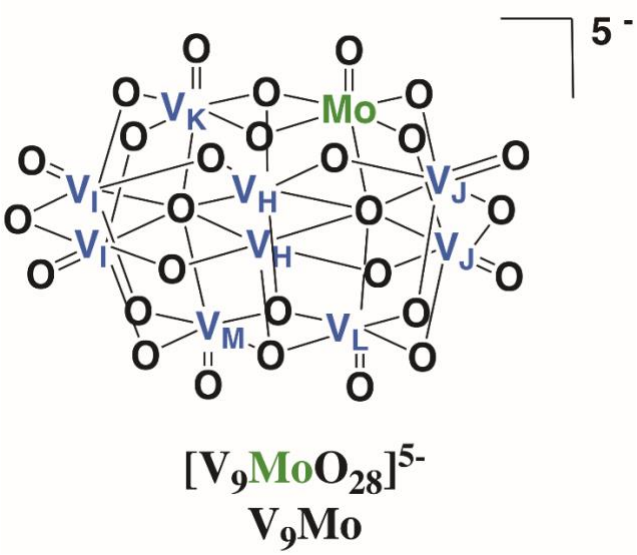

Figure A2.S6. A structure of the V_9Mo complex with the correct assignment of the peaks in the ^{51}V NMR.

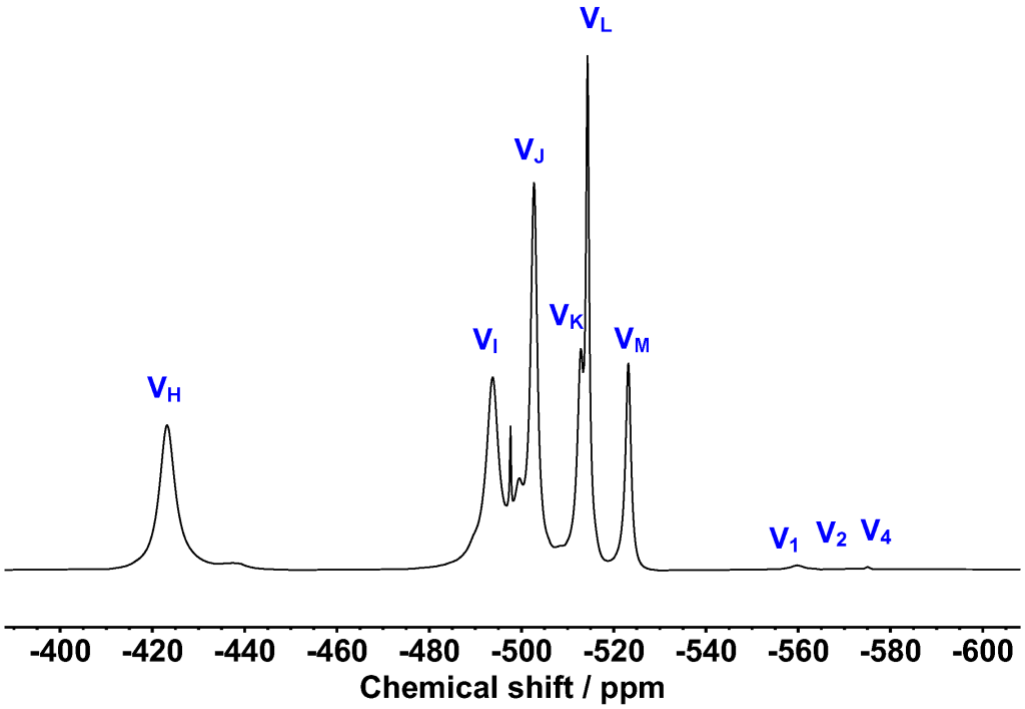

Figure A2.S7. ^{51}V NMR spectrum of a 100 mM V_9Mo aqueous stock solution prepared for the speciation and biological studies, pH = 5.06, as described in the Experimental Section. The insert presents the structure of the $[V_9MoO_{28}]^{5-}$ (V_9Mo) anion and the assignments for the non-equivalents vanadium(V) atoms V_H – V_M. Signals at δ –558, –570 and –574 ppm were attributed to V_1, V_2 and V_4.

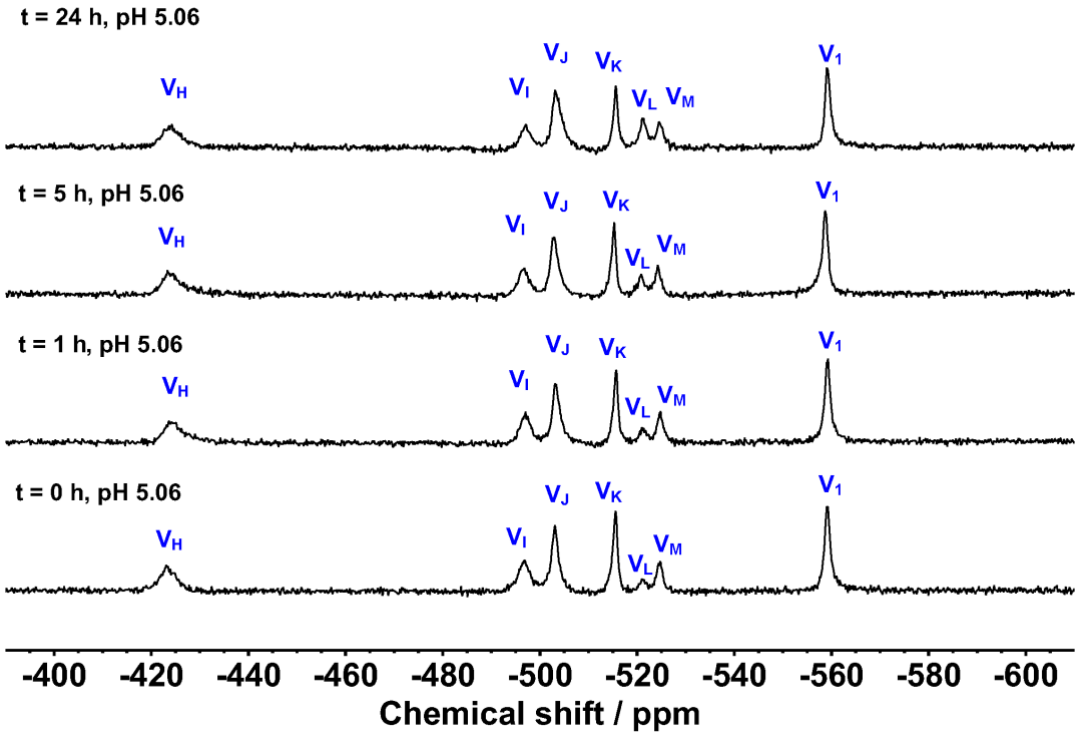

Figure A2.S8. ^{51}V NMR spectra showing the speciation data of the 1.0 mM V_9Mo aqueous control solution over 24 h.

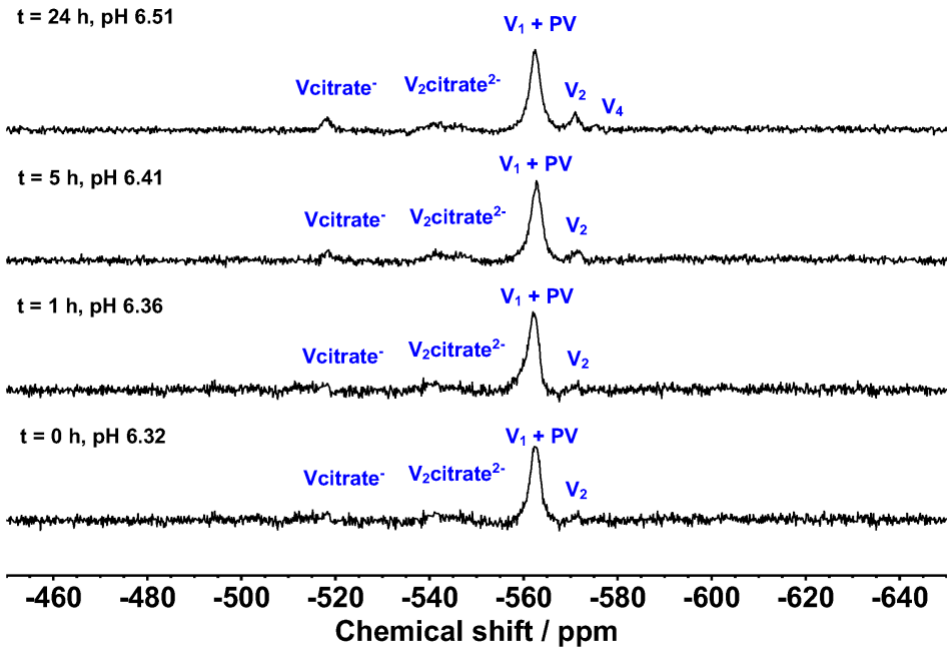

Figure A2.S9. ^{51}V NMR spectra showing the speciation data of the V_9Mo complex in the non-heated (1.0 mM solution) over 24 h.

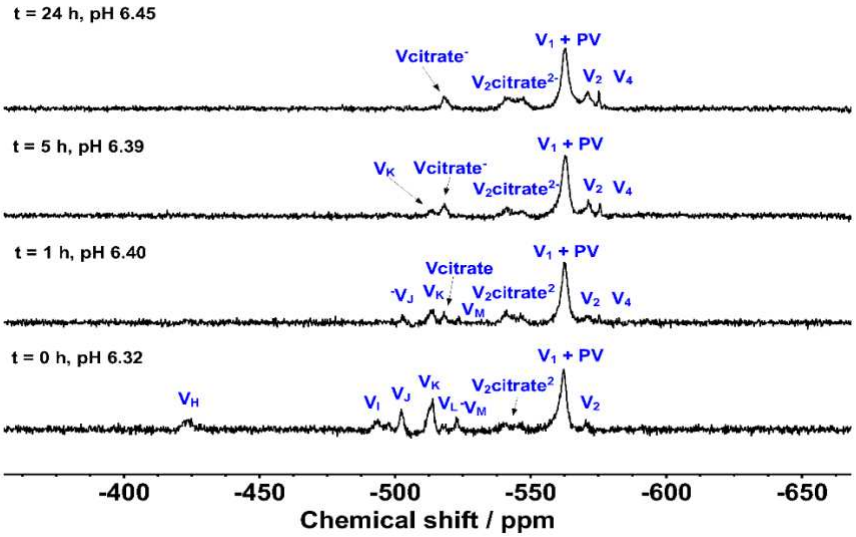

Figure A2.S10. ^{51}V NMR spectra showing the speciation data of the V_9Mo complex in the heated supernatant (1.0 mM solution) over 24 h.

Table A2.S2. A summary of the speciation data of the V_9Mo complex collected at t = 0 h and t = 24 h in a 1.0 mM aqueous control solution, 1.0 mM solutions in the 7H9 medium, non-heated and heated supernatant.

Experimental Condition	Species Monitored	t = 0 hours, %	t = 24 hours, %
V_9Mo Aqueous Solution (pH 5.06)	V_9Mo	42.5	48.5
	V_{10}	28.3	23.0
	V_1	29.2	28.5
V_9Mo Aqueous Solution (pH 6.34)	V_9Mo	57.2%	55.7%
	V_{10}	24.1%	25.1%
	V_1	18.7%	19.2%
V_9Mo in 7H9 Medium	V_9Mo	15.4	0
	V_{10}	35.5	0
	V_1 + PV	49.1	67.6
	V_2	3.7	16.0
	V_4	0	6.3
	$Vcit^{-}$	0	0
	V_2cit^{2-}	4.4	11.0
V_9Mo in non-heated supernatant	V_1 + PV	95.9	77.0
	V_2	0.4	13.3
	$Vcit^{-}$	0.8	6.2
	V_2cit^{2-}	8.9	6.2
V_9Mo in heated supernatant	V_9Mo	12.4	0
	V_{10}	25.8	0
	V_1 + PV	53.8	55.3
	V_2	2.3	13.0
	V_4	0	4.6
	$Vcit^{-}$	0	7.8
	V_2cit^{2-}	5.7	20.8

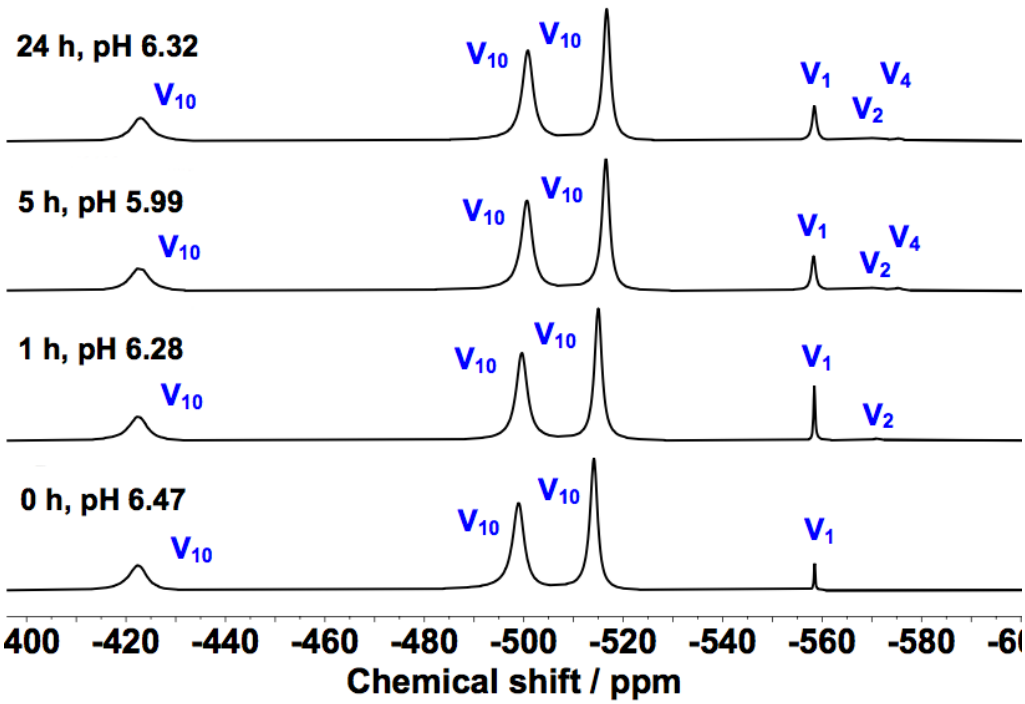

Figure A2.S11. ^{51}V NMR spectra showing the speciation data of the $Na_6V_{10}O_{28}$ aqueous control at pH 6 (1.0 mM solution) over 24 h.

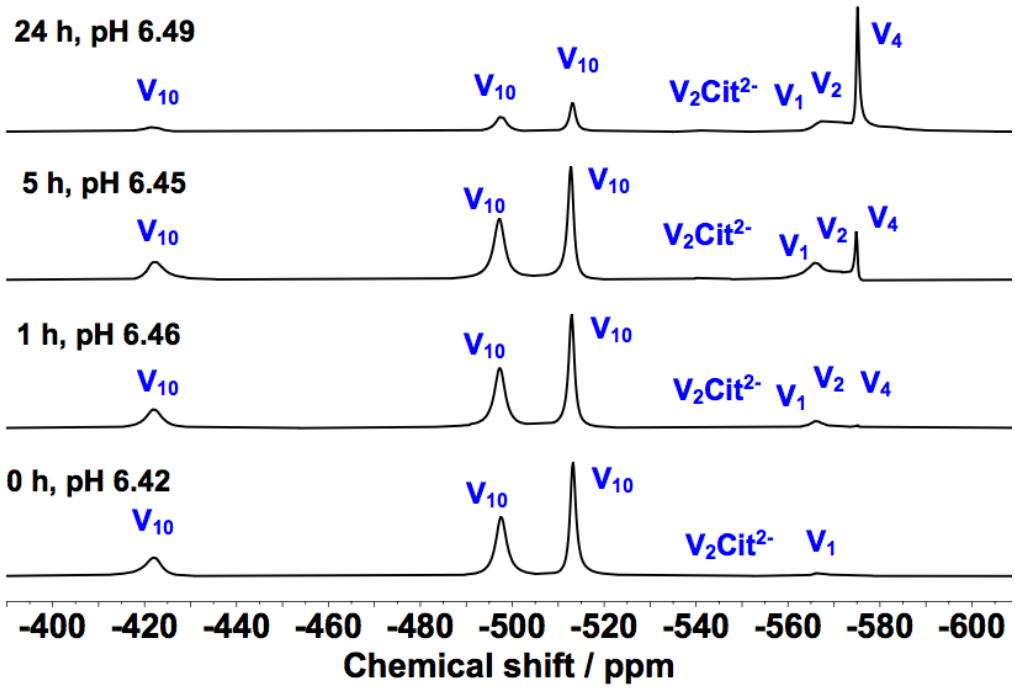

Figure A2.S12A. ^{51}V NMR spectra showing the speciation data of the $Na_6V_{10}O_{28}$complex in the 7H9 media (1.0 mM solution) over 24 h. The V_1 peak is a composite of V_1 + PV (–563 ppm).

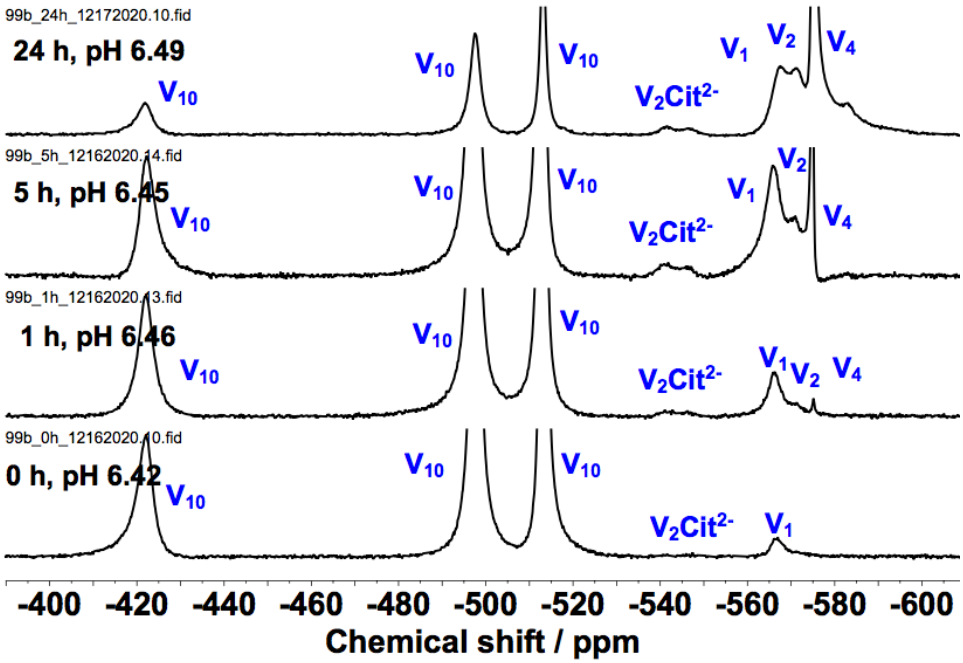

Figure A2.S12B. ^{51}V NMR spectra showing the speciation data of the $Na_6V_{10}O_{28}$ complex in the 7H9 media (1.0 mM solution) over 24 h. The V_1 peak is a composite of V_1 + PV (–563 ppm). The spectrum was enlarged for better representation of the hydrolysis products.

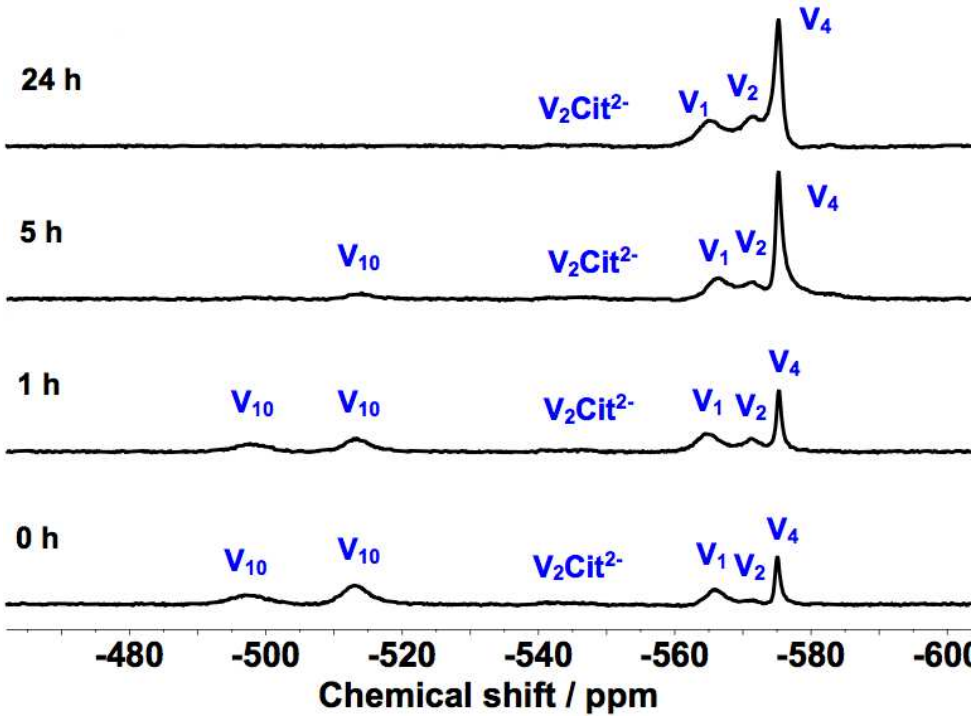

Figure A2.S13. ^{51}V NMR spectra showing the speciation data of the $Na_6V_{10}O_{28}$ complex in the 7H9 media (1.1 mM solution) upon addition of *M. smeg* cells over 24 h. The V_1 peak is a composite of V_1 + PV (–563 ppm). (Samart *et. al* 2018)

Table A2.S3. A summary of the speciation data of the $Na_6V_{10}O_{28}$ complex (shown in Figs. S11-S12) collected at t = 0 h and t = 24 h in a 1.0 mM aqueous control solution and 1.0 mM solutions in the 7H9 medium.

Experimental Condition	Species Monitored	t = 0 hours, %	t = 24 hours, %
$Na_6V_{10}O_{28}$ in aqueous solution	V_{10}	98.4	91.5
	V_1	1.6	5.9
	V_2	0	1.8
	V_4	0	0.7
$Na_6V_{10}O_{28}$ in 7H9 Medium	V_{10}	97.8	34.4
	V_1 + PV	2.2	10.0
	V_2	0	9.0
	V_4	0	38.1
	V_5	0	7.9
	V_2cit^{2-}	0	1.4

II. Biological Data

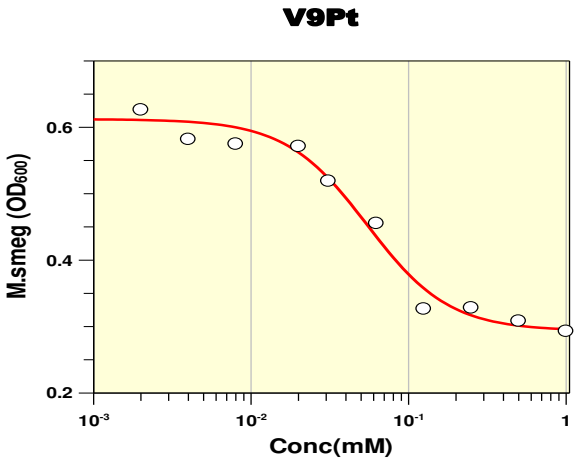

Parameter	Value	Std. Error
Y Range	0.3186	0.0258
IC 50	0.0546	0.0091
Slope factor	1.6702	0.3873
Background	0.2937	0.0192

Figure A2.S14. The cell growth curve is shown for treatment of V_9Pt, with concentration varying from 0.002 to 1.00 mM.

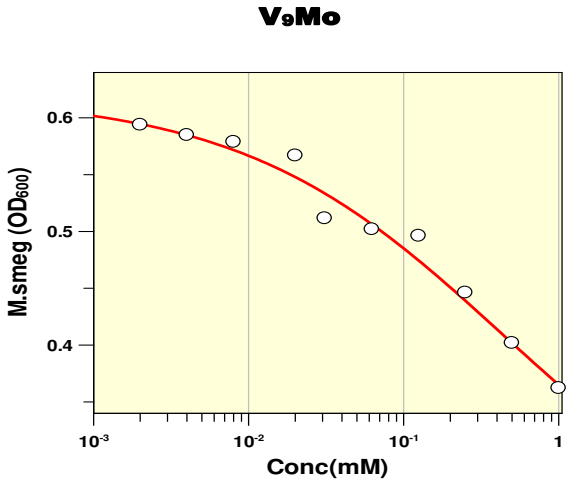

Parameter	Value	Std. Error
Y Range	0.4191	0.0840
IC 50	0.4316	0.2370
Slope factor	0.5152	0.1170
Background	0.2002	0.0794

Figure A2.S15. The cell growth curve is shown for treatment of V_9Mo, with concentration varying from 0.002 to 1.00 mM.

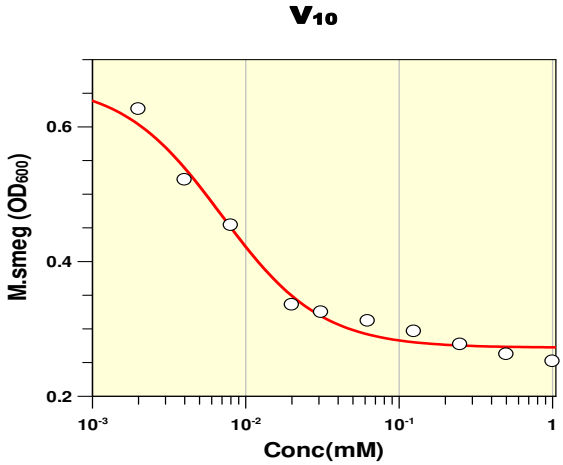

Parameter	Value	Std. Error
Y Range	0.3940	0.0211
IC 50	0.0069	0.0009
Slope factor	1.3391	0.1831
Background	0.2722	0.0098

Figure A2.S16. The cell growth curve is shown for treatment of V_{10}, with concentration varying from 0.002 to 1.00 mM.

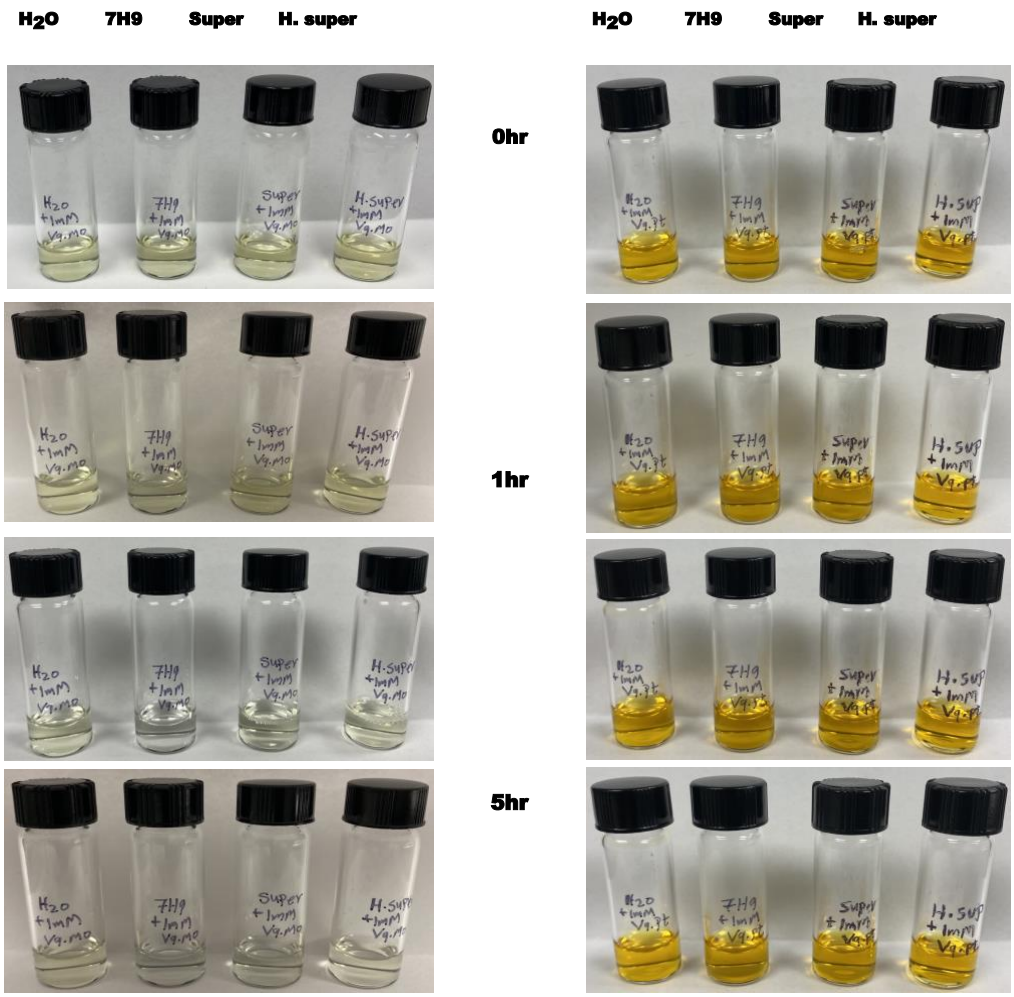

Figure A2.S17. Color changes of a) V_9Mo and b) V_9Pt in aqueous solution, 7H9 medium, supernatant, and heated supernatant at different time points.

Appendix III: Exploring Growth of *Mycobacterium smegmatis* Treated with Anticarcinogenic Vanadium Compounds

This appendix includes the following information that supported the data presented in Chapter 3. These information were used to compare the different effects of the vanadium catechols against bacterial growth and to compare the stability and speciation of these complexes in aqueous solution, 7H9 medium, and supernatant.

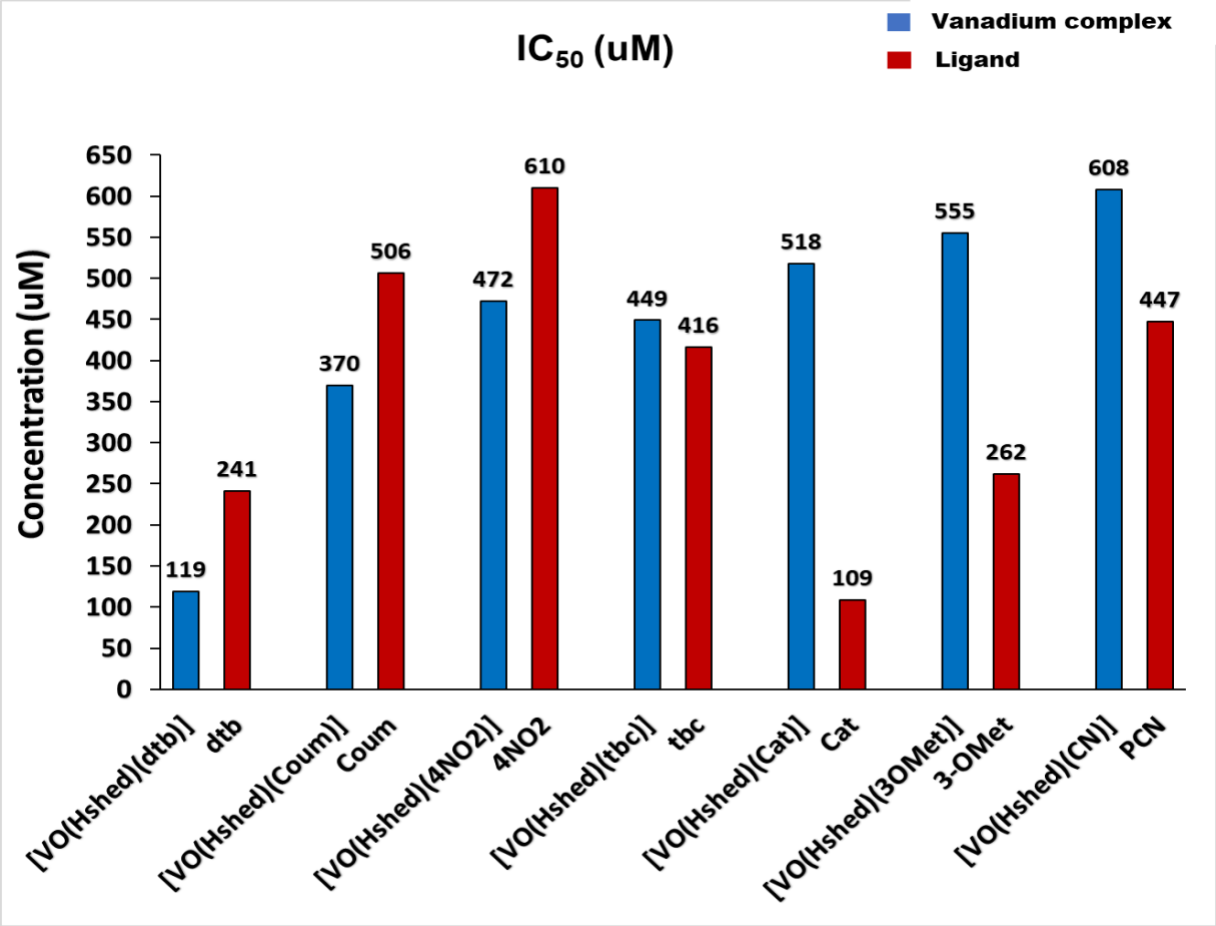

Figure A3.S1. The histograms of the IC50 values for the effects of the V-complexes and their free ligands on the bacterial growth.

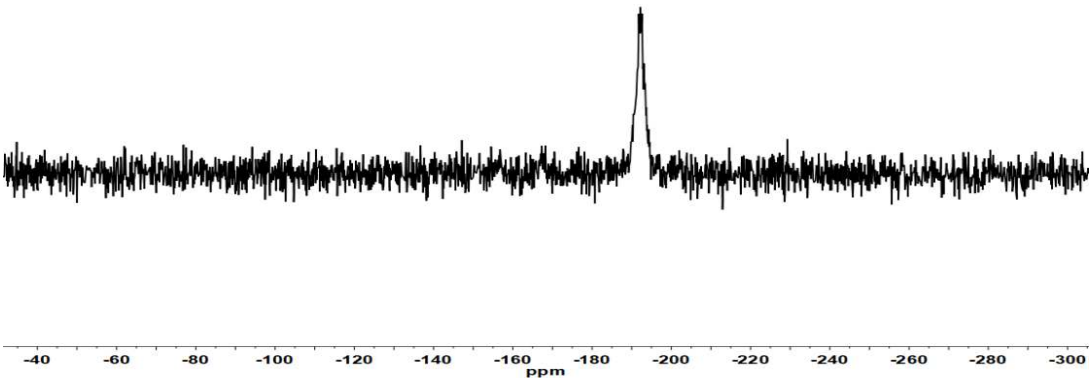

Figure A3.S2. The ^{51}V NMR spectrum of [VO(Hshed)(Coum)] in CD_3CN.

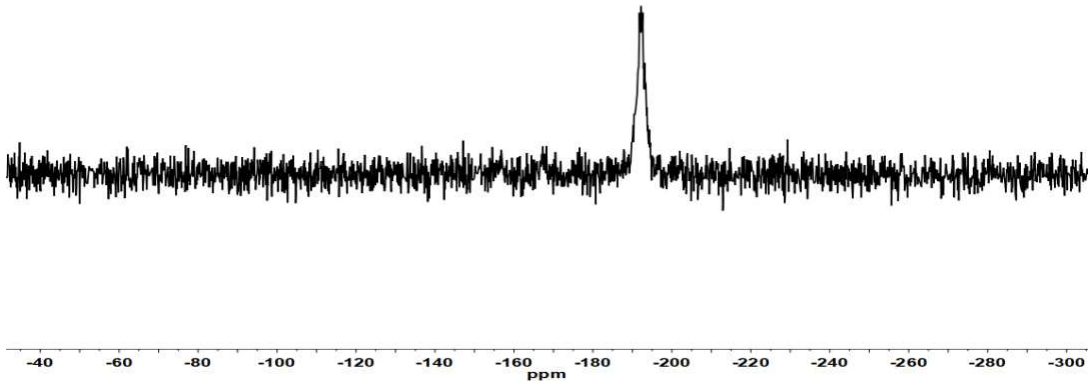

Figure A3.S3. The ^{51}V NMR spectrum of [VO(Hshed)(CN)] in CD_3CN.

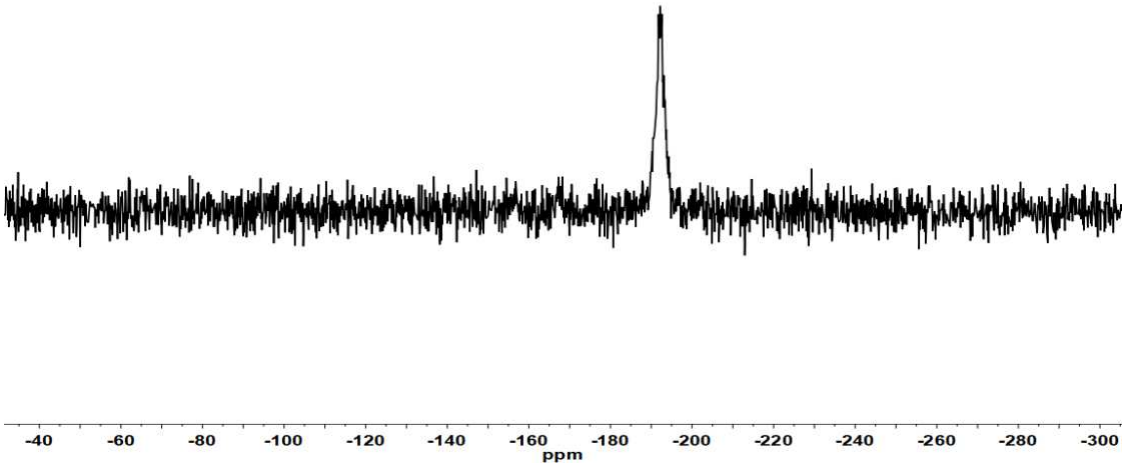

Figure A3.S4. The ^{51}V NMR spectrum of [VO(Hshed)(3OMet)] in CD_3CN.

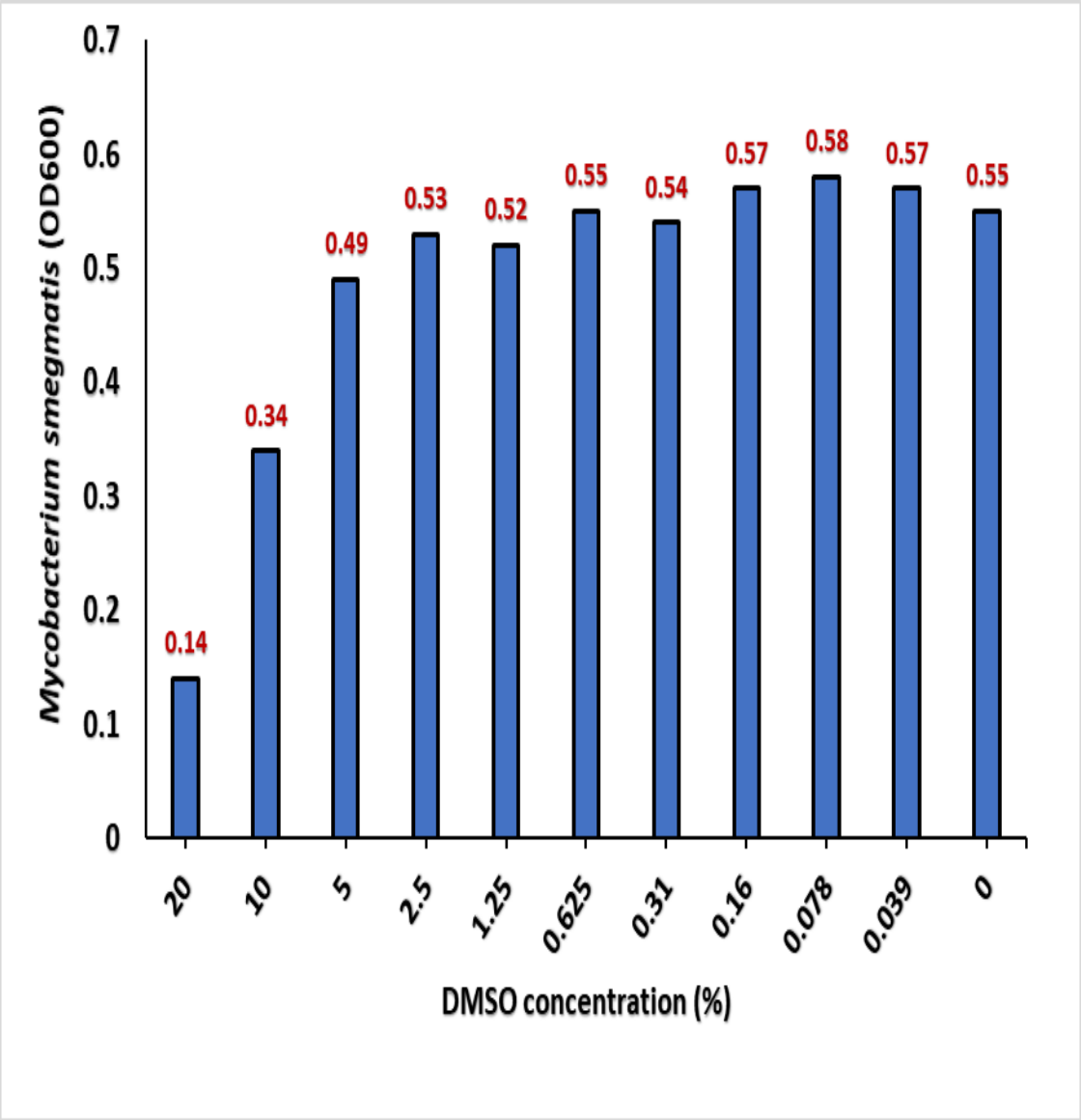

Figure A3.S5. The growth of *M. smeg* in the presence of DMSO.

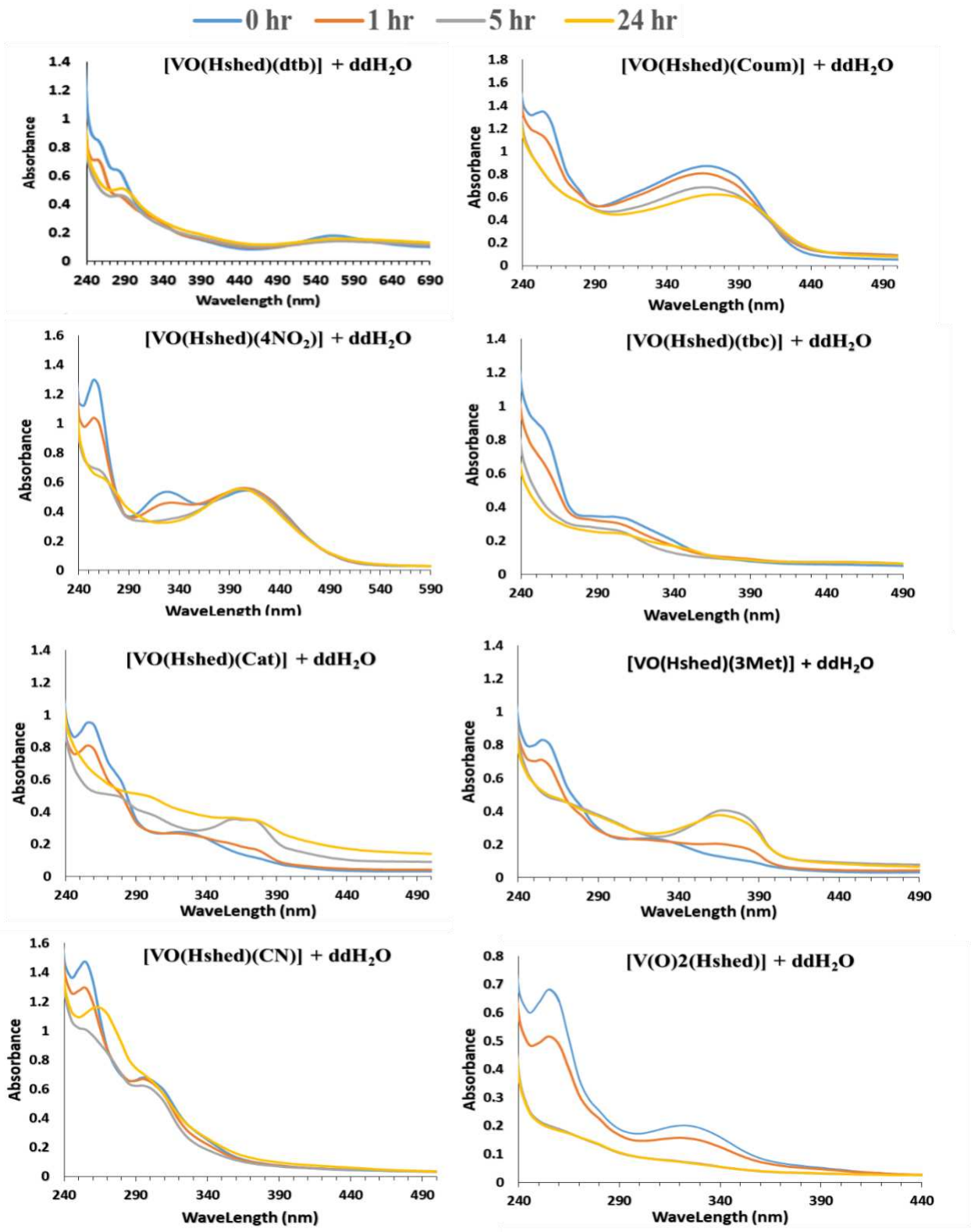

Figure A3.S6. The UV-vis spectra are recorded of all the complexes at 0.250 mM in ddH_2O as a function of time (0 ,1, 5, 24 h).

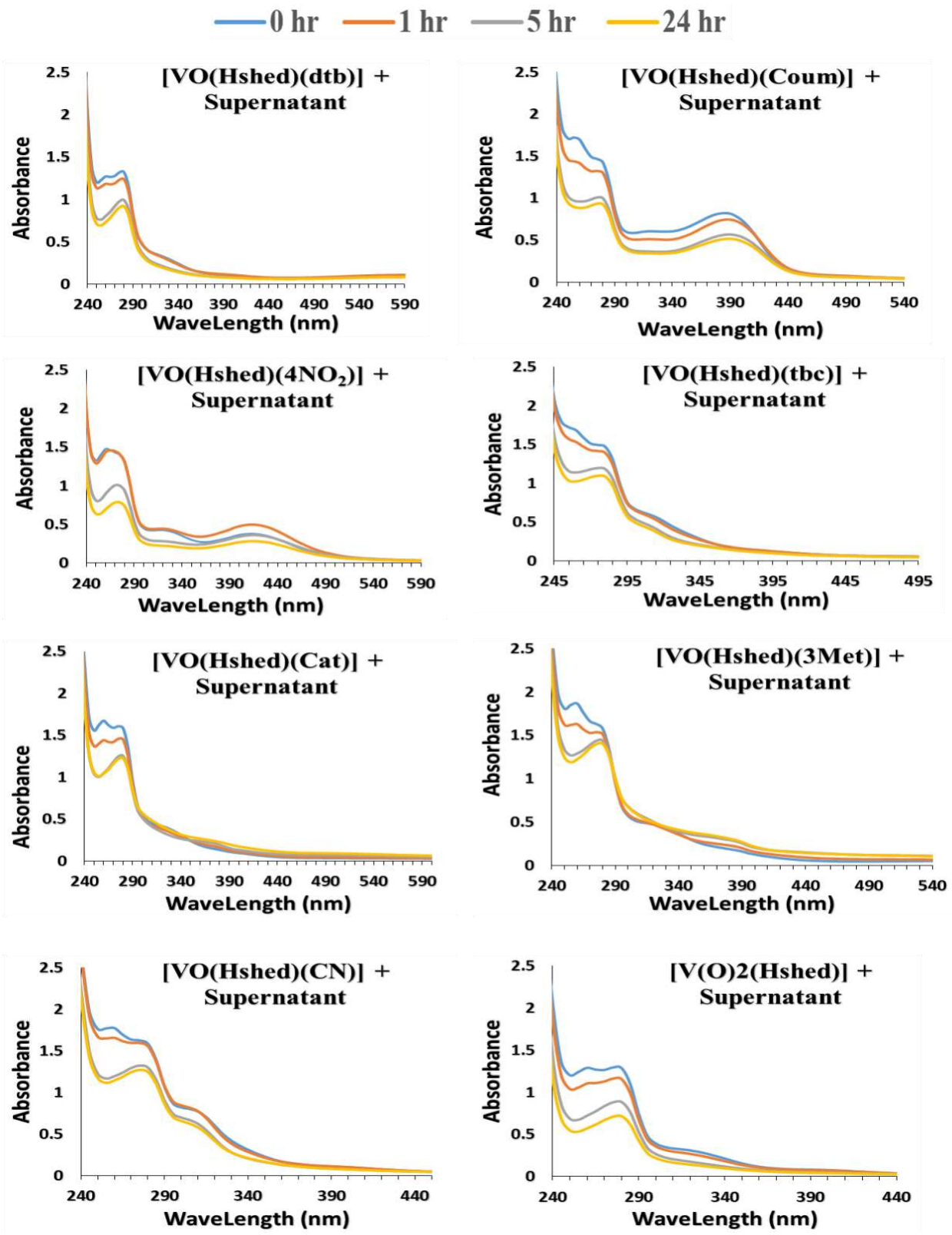

Figure A3.S7. The UV-vis spectra are recorded of all the complexes at 0.250 mM in supernatant fraction as a function of time (0,1, 5, 24 h).

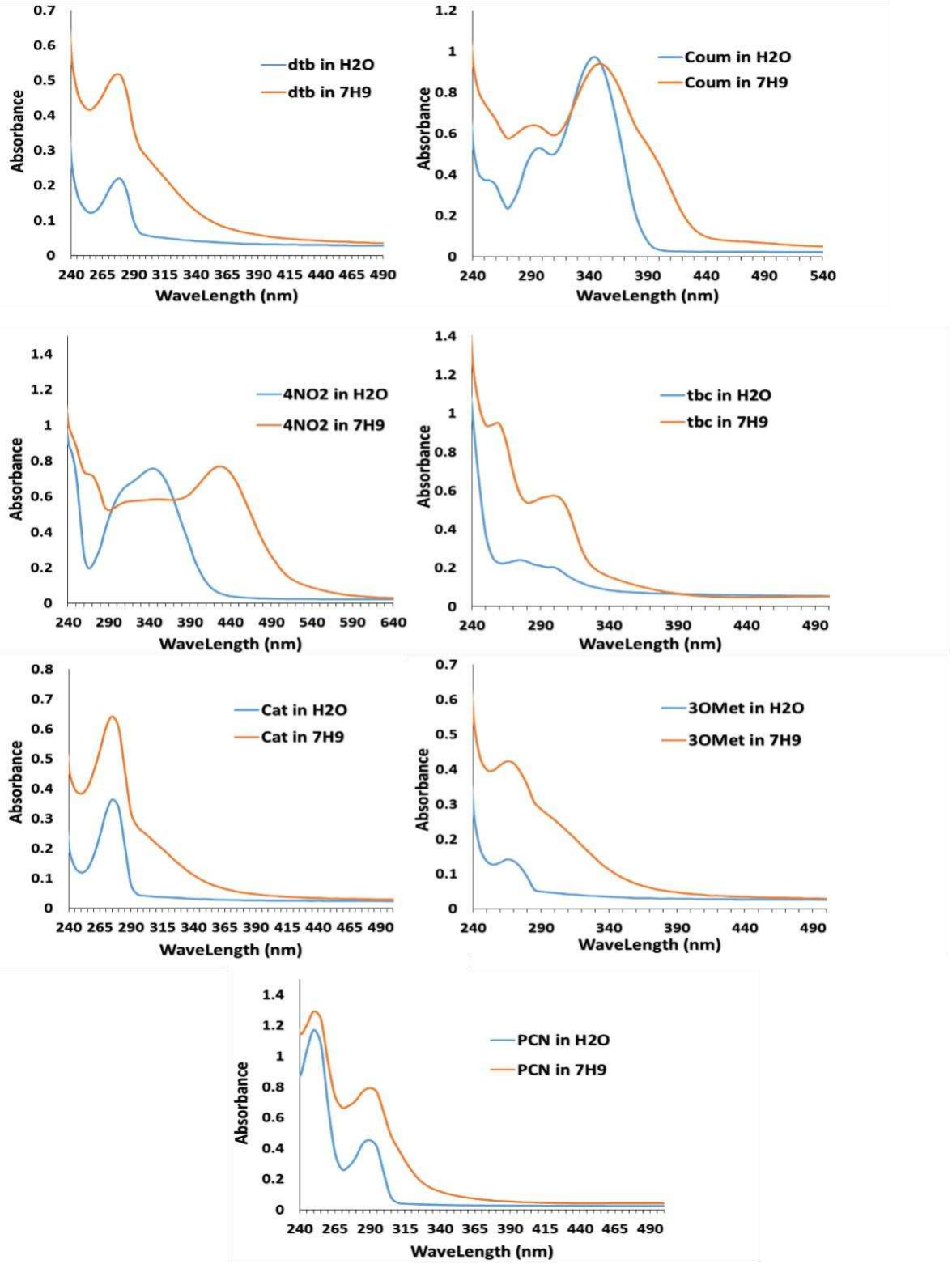

Figure A3.S8. The UV-vis spectra are recorded of all the free ligands at 0.250 mM in ddH_2O and 7H9 medium at time zero (0 h).

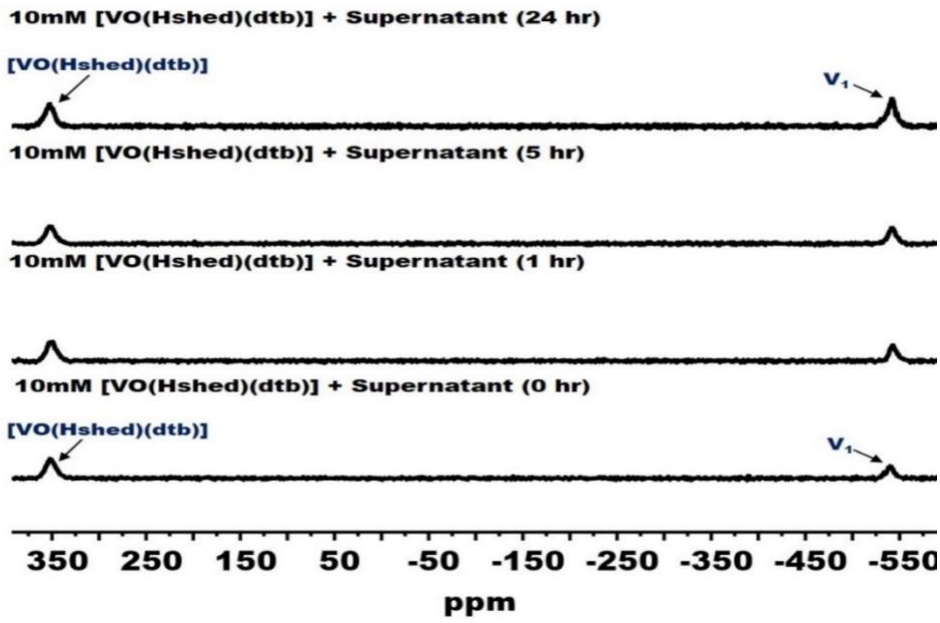

Figure A3.S9. The ^{51}V NMR spectra of 10mM [VO(Hshed)(dtb)] at 0, 1, 5, and 24 h time points in supernatant fraction.

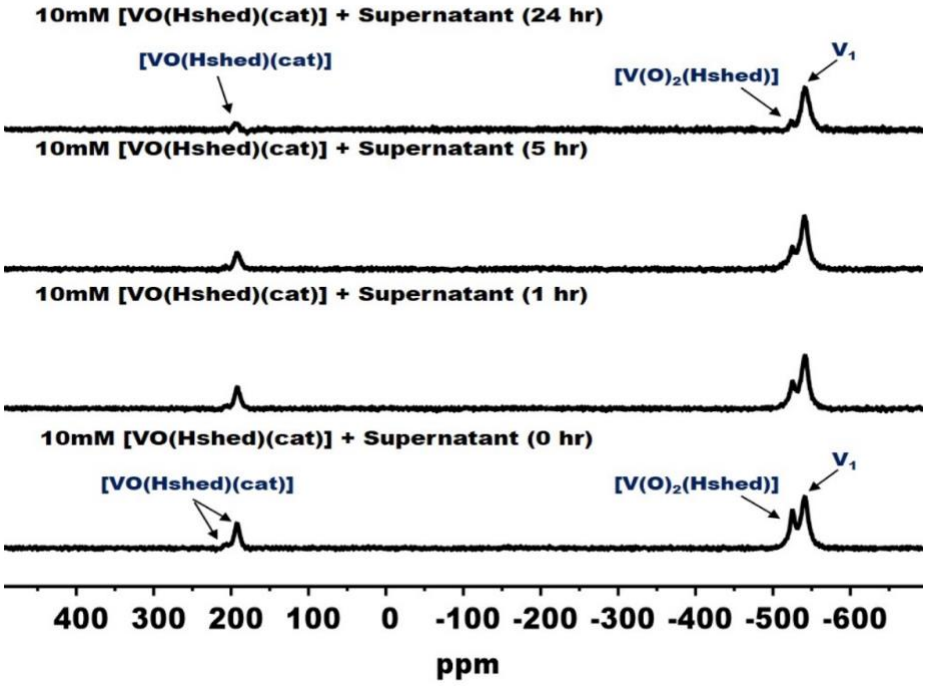

Figure A3.S10. The ^{51}V NMR spectra of 10mM [VO(Hshed)(cat)] at 0, 1, 5, and 24 h time points in supernatant fraction.

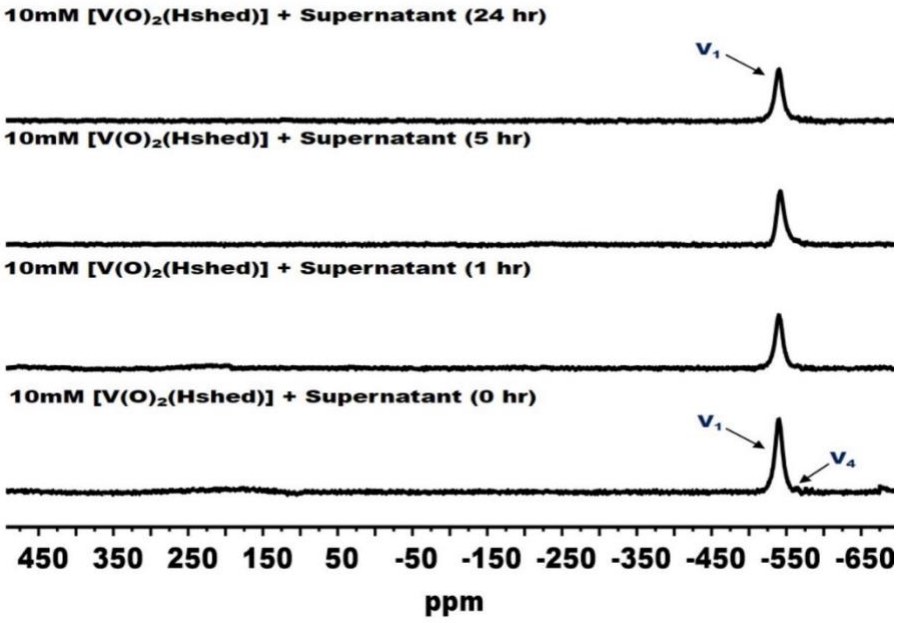

Figure A3.S11. The ^{51}V NMR spectra of 10mM $[V(O)_2(Hshed)]$ at 0, 1, 5, and 24 h time points in supernatant fraction.

Appendix IV: In Silico/In Vitro Hit-to-Lead Methodology Yields SMYD3 Inhibitor That Eliminates Unrestrained Proliferation of Breast Carcinoma Cells

This manuscript is published in the International Journal of Molecular Sciences in collaboration with the first author Ilham Alshiraihi. This work describes a study that aimed to identify and develop a small molecule inhibitor targeting a protein called SMYD3, which has been linked to the progression of breast cancer. In this study, we used a combination of computational modeling (in silico) and laboratory experiments (in vitro) to screen and optimize candidate compounds. Ultimately, they identified a potent SMYD3 inhibitor that was able to suppress the uncontrolled growth of breast cancer cells in culture and stimulate apoptosis. In conclusion, these findings suggest that the inhibitor could have potential as a therapeutic agent for breast cancer treatment.

Reference

Alshiraihi, I.M., Jarrell, D.K., Arhouma, Z., Hassell, K.N., Montgomery, J., Padilla, A., Ibrahim, H.M., Crans, D.C., Kato, T.A. and Brown, M.A., 2020. In silico/in vitro hit-to-lead methodology yields smyd3 inhibitor that eliminates unrestrained proliferation of breast carcinoma cells. *International Journal of Molecular Sciences*, *21*(24), p.9549.

International Journal of
Molecular Sciences

IMPACT FACTOR 6.208

Indexed in: PubMed

Article

In Silico/In Vitro Hit-to-Lead Methodology Yields SMYD3 Inhibitor That Eliminates Unrestrained Proliferation of Breast Carcinoma Cells

Ilham M. Alshiraihi, Dillon K. Jarrell, Zeyad Arhouma, Kelly N. Hassell, Jaelyn Montgomery, Alyssa Padilla, Hend M. Ibrahim, Debbie C. Crans, Takamitsu A. Kato and Mark A. Brown

Special Issue
Drug Discovery and Development 2.0

Edited by
Prof. Dr. William C. (Trey) Putnam

MDPI

https://doi.org/10.3390/ijms21249549

International Journal of
Molecular Sciences

MDPI

Article

In Silico/In Vitro Hit-to-Lead Methodology Yields SMYD3 Inhibitor That Eliminates Unrestrained Proliferation of Breast Carcinoma Cells

Ilham M. Alshiraihi [1,2], Dillon K. Jarrell [3], Zeyad Arhouma [1,4], Kelly N. Hassell [1], Jaelyn Montgomery [5], Alyssa Padilla [5], Hend M. Ibrahim [6,7,8], Debbie C. Crans [1,4], Takamitsu A. Kato [1,7] and Mark A. Brown [1,8,9,10,11,*]

1 Cell and Molecular Biology Program, Colorado State University, Fort Collins, CO 80523-1005, USA; alshiraihi@gmail.com (I.M.A.); zkrahuma@rams.colostate.edu (Z.A.); khassell@colostate.edu (K.N.H.); debbie.crans@colostate.edu (D.C.C.); tkato@rams.colostate.edu (T.A.K.)
2 Department of Biology, University of Tabuk, Tabuk 47713, Saudi Arabia
3 Department of Bioengineering, University of Colorado Anschutz Medical Campus, Aurora, CO 80045-7109, USA; dillom.jarrel@cuanschutz.edu
4 Department of Chemistry, Colorado State University, Fort Collins, CO 80523-1872, USA
5 Department of Biomedical Sciences, Colorado State University, Fort Collins, CO 80523-1617, USA; Jaelyn.Montgomery@rams.colostate.edu (J.M.); aepad20@rams.colostate.edu (A.P.)
6 Department of Medical Biochemistry, Zagazig University, Zagazig 44511, Egypt; hendibrahim1@gmail.com
7 Department of Environmental & Radiological Health Sciences, Colorado State University, Fort Collins, CO 80523-1618, USA
8 Department of Clinical Sciences, Colorado State University, Fort Collins, CO 80523-1678, USA
9 Epidemiology Section, Colorado School of Public Health, Fort Collins, CO 80523-1612, USA
10 Institute for Learning and Teaching, Colorado State University, Fort Collins, CO 80523-1052, USA
11 Department of Ethnic Studies, Colorado State University, Fort Collins, CO 80523-1790, USA
* Correspondence: mark.brown@colostate.edu

Received: 30 October 2020; Accepted: 11 December 2020; Published: 15 December 2020

Abstract: SMYD3 is a lysine methyltransferase that regulates the expression of over 80 genes and is required for the uncontrolled proliferation of most breast, colorectal, and hepatocellular carcinomas. The elimination of SMYD3 restores normal expression patterns of these genes and halts aberrant cell proliferation, making it a promising target for small molecule inhibition. In this study, we sought to establish a proof of concept for our in silico/in vitro hit-to-lead enzyme inhibitor development platform and to identify a lead small molecule candidate for SMYD3 inhibition. We used Schrodinger® software to screen libraries of small molecules in silico and the five compounds with the greatest predicted binding affinity within the SMYD3 binding pocket were purchased and assessed in vitro in direct binding assays and in breast cancer cell lines. We have confirmed the ability of one of these inhibitors, Inhibitor-4, to restore normal rates of cell proliferation, arrest the cell cycle, and induce apoptosis in breast cancer cells without affecting wildtype cell behavior. Our results provide a proof of concept for this fast and affordable small molecule hit-to-lead methodology as well as a promising candidate small molecule SMYD3 inhibitor for the treatment of human cancer.

Keywords: hit-to-lead; in silico drug development; SMYD3; methyltransferase; Inhibitor-4; breast cancer; cell proliferation; cell cycle; apoptosis

1. Introduction

SMYD (SET and MYND domain-containing) protein family members constitute a class of methyltransferases that regulate a wide range of normal cellular processes [1–3] and are also involved

in several tumorigenic pathways [3–5]. SMYD3, the third member of the SMYD family, transfers methyl groups to lysine 4 on histone H3 (H3K4) and lysine 5 on histone 4 (H4K5), a residue that was previously thought to only undergo acetylation [1–3]. Overexpression of SMYD3 results in increased cell proliferation and activates many genes associated with cancer cell transformation [6] and metastasis [7]. Several studies have revealed that lung, breast, pancreatic, colorectal, and hepatocellular carcinoma are highly associated with SMYD3 overexpression [3,8,9]. In vitro studies using NIH3T3 cells have demonstrated that SMYD3 involvement in uncontrolled proliferation is one of the crucial stages in tumorigenesis. Furthermore, the growth of breast, hepatocellular, and colorectal carcinoma cell lines have been impaired significantly through SMYD3 knockdown [3,8]. These studies demonstrate that the oncogenic impact of SMYD3 is mediated in part by its histone methylation activity and the resulting impact on the expression of oncogenes. These downstream genes include NKX2.8 [3], WNT10B [8], TERT [10], cMET [11], and CDK2 [12]. SMYD3 is also known to regulate cancer cell proliferation and viability through its interaction with vascular endothelial growth factor receptor 1 (VEGFR1) [13] and estrogen receptor (ER) [14], both of which are non-histone proteins. The role of SMYD3 in ER-mediated transcription through its histone methyltransferase activity is not fully known. SMYD3 acts as a cofactor of ERα and promotes its efficacy in response to bound ligands. In addition, SMYD3 interacts with ER in the ligand binding domain and activates the transcriptional machinery of downstream genes [14]. Collectively, these studies indicate SMYD3 as a potential therapeutic target for cancer treatment.

The small molecule drug development process is notoriously expensive, time consuming, and inefficient. After target identification, identifying hit compounds with significant activity requires enormous small-molecule libraries and hours of experimentation. Optimizing hit compounds to identify leads that have activity in cells and that meet initial in vitro toxicity criteria often requires several rounds of iteration and molecular synthesis. Because of the difficulty and cost of this process, scientific literature is saturated with studies that identify proteins that are "promising therapeutic targets" but that proceed no further towards actual therapeutic development. In this study, we sought to establish a simple and affordable hit-to-lead methodology that could be implemented by average research laboratories that have elucidated druggable proteins. Using in silico screening to identify initial hits and restricting the initial library to purchasable compounds, we implemented the Small Molecule Drug Discovery Suite (Schrodinger, Inc., NY, USA) to predict the binding affinity of a library of 137,990 molecules [15–17] and thus have demonstrated the ability to identify lead small molecule inhibitors without the need for physical compound libraries or in-house chemical synthesis.

Using SMYD3 as a target protein, we implemented our screening methodology and report a novel small molecule SMYD3 inhibitor (Inhibitor-4) that impairs breast cancer cell proliferation without affecting normal cells, illustrating the potential of SMYD3 inhibitors in the clinical management of breast cancer as well as a proof of concept for this drug development platform. We used two breast cancer cell lines (MCF7 and MDA-MB-231) that were previously shown to overexpress SMYD3 [8,14,18–20] compared with the wild type breast epithelial cell line MCF10A [18,19] (Table 1). After initial hit identification in vitro, we purchased and tested five novel small molecule SMYD3 inhibitors and discovered that Inhibitor-4 significantly reduces breast cancer proliferation, arrests the cell cycle, and induces apoptosis without impacting wild type cells. In all experiments, we used a previously-identified SMYD3 small molecule inhibitor, BCI-121, as a positive control [21].

Table 1. Summary of SMYD3 availability and activity in the cell lines used in this study.

Cancer Cell Lines	Origin	SMYD3 Expression	Assay	Methylation Activity	References
MCF7/MDA-MB-231	Human epithelial breast cancer cells	High	Western blot, RT-qPCR	H4K5, H3K4	[8,14,18–20]
MCF10A	Human epithelial breast cells	Very low	Western blot, RT-qPCR	H4K5, H3K4	[18,19]

2. Results

2.1. Inhibitor-4 Decreases SMYD3-Mediated H3 Methylation

After our iterative in silico screening using Schrodinger software (Glide®, Maestro®, LigPrep®, and Epik®), we purchased the top five hit compounds for testing. Hits were defined as the drug-like small molecules with the lowest free binding energy when docked in the protein-target binding pocket of SMYD3. The predicted free binding energies of the five lead compounds ranged from −7.2 kJ/mol to −9.1 kJ/mol, compared to the natural protein ligand's predicted free binding energy of only around −1 kJ/mol (fragment of VEGFR1). We used an in vitro methylation assay using purified Histone 3 (H3) to assess the ability of the five lead in silico-designed SMYD3 inhibitor candidates to decrease SMYD3 enzymatic activity. We demonstrated that Compound 4 (Inhibitor-4) significantly reduces SMYD3-mediated Histone 3 methylation (70% reduction), while the other novel compounds did not show significant differences. H3 was chosen because of previous studies that demonstrated SMYD3 methylates H3 preferentially (Figure 1) [3].

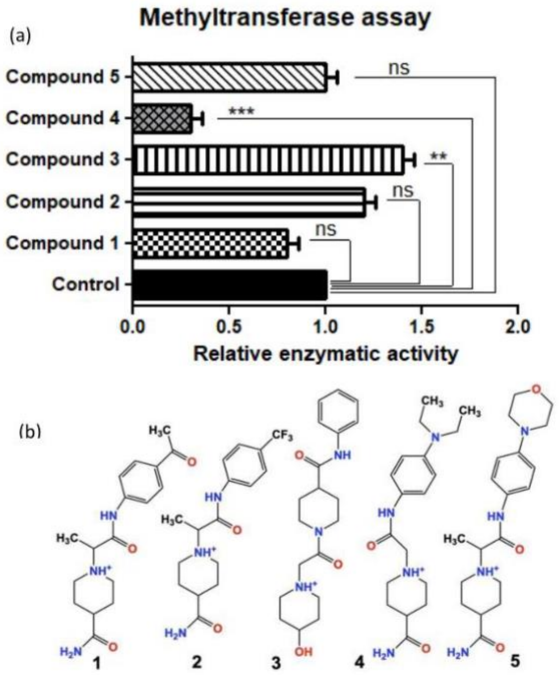

Figure 1. (**a**) Relative SMYD3 activity (top) with the top 5 candidates from in silico testing (bottom) using an in vitro methyltransferase assay (Colorimetric assay). (**b**) Compounds 1–5 drawn in ChemDraw. Compound 4 is from here on referred to as Inhibitor- 4. Error bars display standard error of means. Statistically significant differences from control are indicated by ** $p < 0.01$, *** $p < 0.001$ or ns $p > 0.05$.

2.2. Inhibitor-4 and BCI-121 are Stable in d_6-DMSO Solution

Because of the limited solubility of selected molecules in aqueous solution and in media, we dissolved BCI-121 and Inhibitor-4 in d_6-DMSO solution to record and analyze the 1D ^{1}H NMR spectra of both compounds. The major species attributed to Inhibitor-4 and BCI-121 were observed at time 0 and 24 h, as shown in Figure S1a (BCI-121) and Figure S1b (Inhibitor-4). The ^{1}H NMR peaks of the fresh and aged samples for Inhibitor-4 showed no observable difference in the presence of the

major component (67%) and minor component (33%) peaks as a function of time, suggesting that no hydrolysis is taking place during the experiment for Inhibitor-4. For BCI-121, 70% of the major species was present at time 0, however after 24 h this decreased slightly to 68%, suggesting that the positive control may be slightly less stable than Inhibitor-4.

2.3. SMYD3 Is Overexpressed in Breast Cancer Cells

Western blot and immunocytochemistry were carried out to test the expression levels of SMYD3 using anti-SMYD3 antibody in normal and breast cancer cell lines. Western blot data have indicated that SMYD3 was highly expressed in breast cancer cell lines (1.8-fold in MCF7 and 2.6-fold in MDA-MB-231) compared to normal cell line (Figure 2).

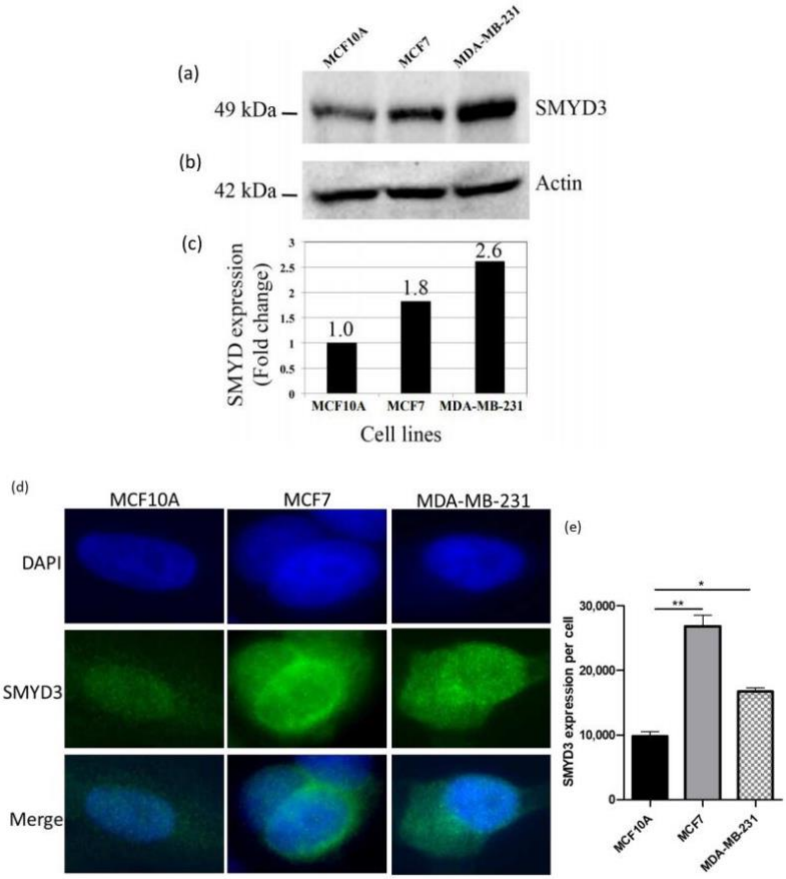

Figure 2. SMYD3 expression using western blot and immunocytochemistry: (**a**) Expression of SMYD3 protein in human cell lines using Western blot. (**b**) Expression of actin served as a quantitative control. (**c**) Western blot analysis shows fold change in SMYD3 expression in the cell lines. (**d**) Expression of SMYD3 protein using immunocytochemistry. (**e**) immunocytochemistry analysis shows SMYD3 intensity in the cell lines. Values are mean ± standard error of the means. Statistically significant differences from control are indicated by * $p < 0.05$, ** $p < 0.01$.

Additionally, immunocytochemistry data have shown elevated levels of SMYD3 expression in breast cancer cell lines comparing to normal cell line (Figure 2a,b). Therefore, increased SMYD3 expression could be correlated with breast carcinogenesis.

2.4. Inhibitor-4 Inhibits Growth of Breast Cancer Cells

The impact of SMYD3 inhibitors on growth of breast cancer cells was tested by adding 50, 100 and 200 μM of Inhibitor-4 or BCI-121 to breast cancer cell lines (MCF7 and MDA-MB-231) and normal breast epithelial cell line (MCF10A). The number of cells was determined daily and the population doubling times were quantified (Figure 3). For MCF7 (breast cancer) cells, the basal doubling time for MCF7 was 38 h, while 40 h for MDA-MB-231. Using the positive control inhibitor, a concentration of 200 μM caused approximately 2-fold suppression of MCF7 cellular growth (Figure 3a). Using Inhibitor-4, however, a clear dose-dependent suppression in growth was observed with the first significant reduction observed at a concentration of 50 μM (Figure 3b). In the MDA-MB-231 cell line, a significant delay in the cellular growth was observed with 200 μM BCI-121 and only 50 μM Inhibitor-4 (Figure 3c,d).

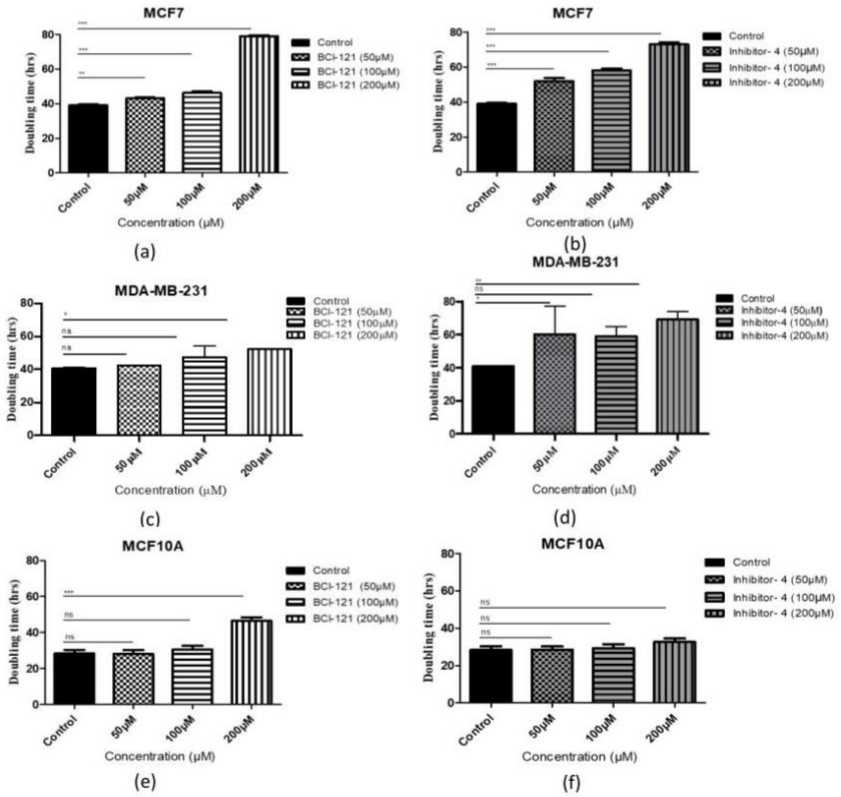

Figure 3. Cell population doubling time with SMYD3 inhibitor treatment. (**a**,**c**,**e**) Cells with BCI-121 as a positive control inhibitor. (**b**,**d**,**f**) Cells with SMYD3 Inhibitor-4. Values are mean ± standard error of the means. Statistically significant differences from control are indicated by * $p < 0.05$, ** $p < 0.01$, *** $p < 0.001$ or ns $p > 0.05$.

For MCF10A (normal) cells, the effect of the SMYD3 inhibitors was limited. The basal doubling time for MCF10A was 28 h. Interestingly, no delay was noticed with 50, or 100 μM concentrations

of either inhibitor. Treatment of the normal cells with 200 μM of Inhibitor-4 resulted in a minor, not significant, growth delay (approximately 5%), while treatment with 200 μM BCI-121 resulted in a major growth delay (Figure 3e,f). These results suggest that Inhibitor-4 shows more growth inhibition than BCI-121 and causes significant inhibition in cancer cell growth while only modestly impacting healthy cells.

2.5. Inhibitor-4 Suppresses Breast Cancer Cell Colony Formation

To determine the effects of Inhibitor-4 on the colony formation of breast cancer cells and normal cell lines, the cells were treated with various concentrations of Inhibitor-4 and BCI-121 (10, 50, 100, 150 and 200 μM) and incubated for 2 weeks. Treatment with Inhibitor-4 significantly suppressed clonogenic activity in MCF7 and MDAMB-231 cells at concentrations of 50, 100, 150 and 200 μM (Figure S2b,d) compared to normal MCF10A cell line (Figure S2f). Similarly, BCI-121 suppressed colony formation on MCF7 at nearly all concentrations (Figure S2a) and MDA-MB-231 cells at 150 and 200 μM concentrations (Figure S2c). Surprisingly, a significant decrease in colony formation of MCF10A (normal) cells was also observed at 200 μM concentration of BCI-121 (Figure S2e) compared to Inhibitor 4, which did not affect MCF10A survival (Figure S2f). This result again suggests the improved inhibition effect of Inhibitor-4 compared to BCI-121.

2.6. Inhibitor-4 Reduces Cell Viability in MCF7 Cells

The effect of Inhibitor-4 on the viability of wild type and cancer cell lines was evaluated using an MTT assay at different time points (24, 48, 72, and 96 h). Cells were treated with the vehicle (DMSO 0.1%, 0.15% and 0.2%), BCI-121, or Inhibitor-4 (Figure S3). Treatment with BCI-121 caused significant decreases in cell viability in both breast cancer (MCF7 and MDA-MB-231) and wild type (MCF10A) cell lines at multiple time points, particularly at concentrations of 150 and 200 μM (Figure S3a,c,e). However, Inhibitor-4 caused significant decreases in cell viability only in the cancer cell lines (MCF7 at 150 and 200 μM, MDA-MB-231 at 200 μM; Figure S3b,d). No concentration of Inhibitor-4 impacted MCF10A cellular viability (Figure S3f). Collectively, these data suggest that Inhibitor-4 is a promising, cancer-specific inhibitor that reduces cancer cell line viability and growth without affecting normal cells.

2.7. Inhibitor-4 Induces Cell Cycle Arrest in Breast Cancer Cells

To investigate whether the growth inhibitory effect of Inhibitor-4 on breast cancer cells was due to cell cycle arrest, we conducted cell cycle analysis using Propidium Iodide (PI) staining. Cells were treated with 200 μM of BCI-121 or Inhibitor-4 for 24 h. As shown in Figure 4 and Figure S4, treatments with both the positive control inhibitor and Inhibitor-4 induced G1 arrest and reduced S phase in MCF7 cells (Figure S4b,c and Figure 4a,b) compared to MCF7 control (Figure S4a). Also, both treatments led to G1 arrest in MDA-MB-231 (Figure S4e,f and Figure 4c,d) compared to MDA-MB-231 control (Figure S4d). Therefore, BCI-121 and Inhibitor-4 prompted an increase in G1 fractions. However, treatments with BCI-121 and Inhibitor-4 did not induce cell cycle arrest (Figure S4h,i) compared to control (Figure S4g) or show statistical differences in normal MCF10A cells (Figure 4e,f).

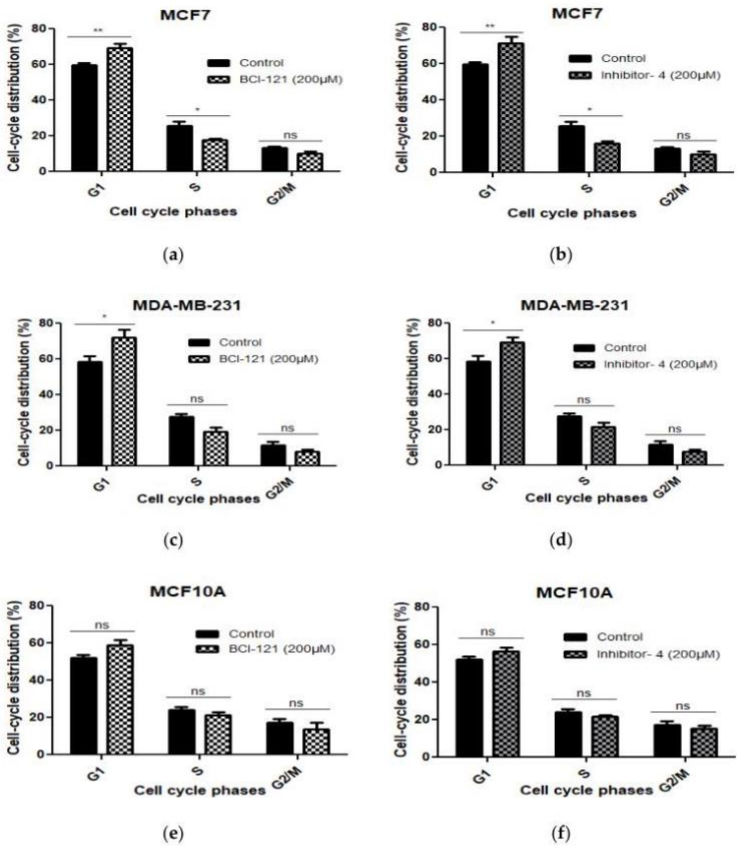

Figure 4. The cell cycle distribution was assessed using PI in MCF7, MDA-MB-231 (breast cancer cell lines) and MCF10A cells (normal breast epithelial cell line) with SMYD3 inhibitor treatments for 24 h and was investigated by flow cytometry. (**a**,**c**,**e**) indicate statistical significant differences on cell cycle phases of the three cell lines treated with BCI-121. (**b**,**d**,**f**) show statistically significant differences on cell cycle phases of the three cell lines treated with Inhibitor-4. Values are mean ± standard error of the means. Statistically significant differences from control are indicated by * $p < 0.05$, ** $p < 0.01$ or ns $p > 0.05$.

2.8. Inhibitor-4 Promotes Apoptosis in Breast Cancer Cells

To reveal whether Inhibitor-4 induce apoptosis on breast cancer cell line or not, we performed apoptosis assay using APC Annexin V/PI followed by flow cytometry analysis. After 48 h of Inhibitor-4 treatment, the percentage of live cells decreased to 71% in both breast cancer cell lines (from 91% in MCF7 and 95% in MDA-MB-231) as demonstrated by flow cytometry (Figure S55d,f,j,l and Figure 5b,d). Also, treatment with Inhibitor-4 showed increase in late apoptosis and necrosis percentages in MCF7 (Figure S5d,f and Figure 5b), while MDA-MB-231 showed early apoptosis with treatment of Inhibitor-4 (Figure S5j,l and Figure 5d). BCI-121 caused late apoptosis in MCF7 and both early and late apoptosis in MDA-MB-231 cells, in addition to necrosis in MCF7 cells (Figure S5e,k and Figure 5a,c). Neither treatment caused significant differences in apoptosis nor necrosis in MCF10A cells (Figure S5q,r and Figure 5e,f).

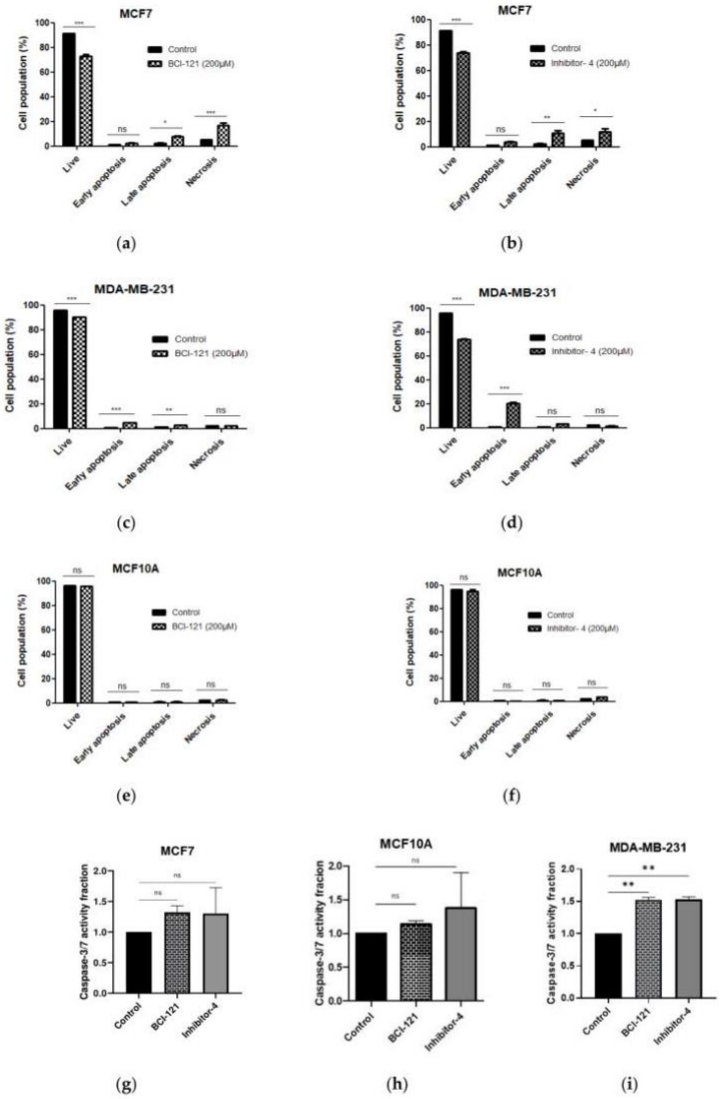

Figure 5. Cell apoptosis was assessed using APC Annexin V/PI and flow cytometry. (**a**,**b**) MCF7 (breast cancer), (**c**,**d**) MDA-MB-231 (breast cancer) and (**e**,**f**) MCF10A (normal breast) cell lines were treated with SMYD3 inhibitors for 48 h. (**a**,**c**,**e**) Apoptosis after 48 h of BCI-121 treatment on each cell line. (**b**,**d**,**f**) Apoptosis after 48 h of Inhibitor-4 treatment on each cell line. (**g**–**i**) Cell apoptosis was investigated with SMYD3 inhibitors using Caspase-3/7 activity assay. Values are mean ± standard error of the means. statistically significant differences from control are indicated by * $p < 0.05$, ** $p < 0.01$, *** $p < 0.001$ or ns $p > 0.05$.

Apoptosis induction through SMYD3 inhibitors was also tested using Caspase-3/7 activity assay. The data have shown increases in Caspase-3/7 activity in MDA-MB-231, however, no significant differences in MCF7, which is Caspase-3/7 independent apoptosis pathway, and MCF10-A.

3. Discussion

Aberrant expression of SMYD3 has been shown to be oncogenic and is essential for the proliferation of most colorectal, hepatocellular, and breast carcinomas, as well as prostate cancer [3,8]. Over 80 genes (including highly regulated homeobox genes, cell cycle regulators, and oncogenes) display altered expression because of aberrant upregulation of SMYD proteins [1–3]. Specifically, SMYD3 over-expression is highly associated with cancer development by regulating tumor proliferation, metastasis, invasion, and apoptosis [22]. Several studies have shown that SMYD3 regulates the oncogenic RAS signaling pathway by integrating a cytoplasmic-kinase signaling cascade, resulting in accelerated cell proliferation and differentiation [9]. Another study demonstrated that SMYD3 is essential for estrogen receptor-mediated transcription in breast cancer cells by down-regulating SMYD3 via RNA interference [14]. SMYD3 mediated-H2A.Z methylation has also been shown to trigger cyclin A1 gene expression, leading to cell cycle activation in breast cancer cells [23]. Knock down of SMYD3 in ovarian cancer tissues leads to upregulation of CDKN2B (p15INK4B), CDKN2A (p16INK4), CDC25A and CDKN3 as members of cyclin-dependent kinase inhibitors (CDK) [24]. Inducing apoptosis via silencing of SMYD3 has also been observed in ovarian cancer in vivo and has been accredited to the upregulation of CD40LG and downregulation of BIRC3 [24]. BIRC3 is a member of the inhibitors of apoptosis proteins (IAP) family and relates to many cancers in cases of aberrant overexpression because it can prevent apoptotic signals [25,26]. Therefore, it is likely that SMYD3 inhibitors can trigger apoptosis by down-regulating BIRC3. In addition, another study demonstrated that the MCF7 cell line lacks Caspase 3, which is essential for apoptosis, however in the absence of Caspase 3, Caspase 6 can be activated as an alternative mechanism to trigger apoptosis. As a result, under cellular stress, MCF7 cells undergo apoptosis in response to Caspase 6 and necrosis in response to TNF-α stimulation [27–29]. Despite the connection between SMYD3-overexprssion and several types of carcinogenesis, few studies have targeted SMYD3 inhibition in the context of breast cancer through the design of the inhibitors.

In this study, we sought to design small molecule inhibitors for the inhibition of SMYD3-mediated methylation (Figure 1), proliferation (Figure 3), colony formation (Figure S2), and viability (Figure S3) in breast cancer cells. Specifically, we demonstrated that in silico enzyme models can predict effective competitive enzyme inhibitors by screening vast molecular libraries and predicting binding energies. This approach to small molecule design significantly reduces the time, expense, and equipment that have been required for traditional benchtop small molecule screening until now.

Using Schrodinger® software and several in vitro assays, we demonstrated that one of the hit compounds identified in silico (Inhibitor-4) was able to reduce breast cancer cellular growth and viability without affecting normal breast epithelial cells. In vitro, Inhibitor-4 was shown to inhibit SMYD3-mediated histone methylation. In breast cancer cells, Inhibitor-4 extended cell doubling time (Figure 3). We also demonstrated that Inhibitor-4 arrests the cell cycle in breast cancer cells without affecting normal cells (Figure 4 and Figure S4), which demonstrates an improvement over BCl-121, a previously-developed SMYD3 inhibitor. Finally, the novel SMYD3 inhibitor presented here caused apoptosis in breast cancer cell lines without affecting the normal breast cell line (Figure 5 and Figure S5). However, testing the in vivo SMYD3 specificity of Inhibitor-4 needs to investigate the impacts of Inhibitor-4 on SMYD3-knockdown cells. This could be performed for future characterization and validation.

4. Conclusions

In conclusion, we have successfully used in silico compound screening to identify a small molecule that inhibit SMYD3 activity in vitro and reduced cancer cell growth and proliferation. Future work will involve the application of this approach to other therapeutic targets and the continued development and optimization of therapeutics for SMYD3-related cancers.

5. Materials and Methods

5.1. In Silico Screening

We implemented the Small Molecule Drug Discovery Suite (Schrodinger, Inc., New York, NY, USA) to predict the binding affinity of a library of 137,990 molecules [15–17]. This library of molecules was downloaded from the free ZINC15 database, and included all "purchasable" molecules with reported or predicted activity in vitro [30]. The 3D structure of SMYD3 used for in silico docking was uploaded from the Protein Data Bank (PDB) under PDB identification code 5EX3 [31]. After an initial simulation which docked each molecule into SMYD3's protein-target binding pocket (not its s-adenosylmethionine binding pocket), the top ten hits (most-negative binding energy) were entered into the ZINC15 molecular similarity search engine, and the 50 most-similar compounds to each of the ten leading candidates were again scored using the Schrodinger software (500 total compounds). From this iteration, the top five compounds were purchased and assessed in vitro using SMYD3 methyltransferase assays. After initial experiments, Inhibitor-4 was found to be the most promising and, consequently, it advanced to the cell line experiments described below.

5.2. Chemical Compounds

All screened compounds were dissolved in dimethyl sulfoxide (DMSO) as 5, 10 or 100 mM stock solutions. The positive control, BCI-121, is a previously-reported SMYD3 inhibitor shown to reduce the cellular proliferation of colorectal and ovarian cancer [21,24]. It was purchased from Millipore Sigma (1817, Burlington, MA, USA) and dissolved in DMSO at 10 and 100 mM. BCI-121 was used in all experiments to investigate its impacts against breast cancer cell lines and as a positive control inhibitor. All compounds were stored at −20 °C until used for the experiments. Some d_6-dimethyl sulfoxide (D, 99.9%) containing 0.05% *v/v* TMS were used for the ^{1}H NMR stability study and the d_6-dimethyl sulfoxide was purchased from Cambridge Isotope Laboratories, Inc. and used as is. The stock solutions of 10.0 mM of BCI-121 and Inhibitor-4 were prepared immediately before use in d_6-DMSO.

5.3. In Vitro Methylation Assay

In vitro methylation was investigated using a colorimetric assay (BioVision, K986-100, Milpitas, CA, USA). SMYD3 inhibitors (160 nM) were incubated with H3 recombinant protein (1.6 μM; Sigma-Aldrich, SRP0177, St. Louis, MO, USA) for 10 min at room temperature. Next, SMYD3 recombinant protein (100 nM; Sigma-Aldrich, SRP0153, St. Louis, MO, USA) and s-adenosylmethionine (SAM) cofactor (500 μM, methyl donor ligand) were added to the SMYD3 inhibitor and H3 solution in the methylation buffer that was provided with the kit. The absorbance was read using a microplate reader (BioTek, Cytation 5, Winooski, VT, USA) at 570 nm in kinetic mode every 30 s at 37 °C for 45 min. The optical density (OD) of the inhibitors was normalized to the optical density (OD) of the control [3].

5.4. NMR Spectroscopy Analysis

The 10.0 mM stock solutions of Inhibitor-4 and BCI-121 were prepared freshly in d_6-DMSO containing 0.05% *v/v* tetramethylsilane (TMS) and diluted to the final concentration of 5.0 mM in d_6-DMSO. The stabilities of Inhibitor-4 and BCI-121 were determined by 1D ^{1}H Nuclear Magnetic Resonance (NMR) spectroscopy on a Bruker 400 MHz NMR spectrometer at 25 °C using routine parameters [32]. 2D-NMR experiment will run to confirm the assignments (data not included) [32]. Chemical shifts were measured against TMS (0 ppm) as an internal reference. The spectra of Inhibitor-4 and BCI-121 were recorded at 0 and 24 h. The spectra were worked up and integrated using Mnova V.14 (MestreLab Research SL, Escondido, CA, USA). The signals in the aromatic region were used to measure the ratio of starting material and hydrolysis product.

5.5. Cell Culture

All cells were purchased from ATCC and cultured according to manufacturer recommendations. The human breast epithelial cell line MCF10A (ATCC CRL-10317, Manassas, VA, USA) was used as a normal cell line and grown in DMEM/F12 (Invitrogen, 11330-032, Carlsbad, CA, USA) supplemented with 5% horse serum (Invitrogen, 16050-122, Carlsbad, CA, USA), 1% antibiotic/antimycotic mixture (Millipore Sigma, A5955, Burlington, MA, USA), insulin (10 µg/mL), EGF (20 ng/mL), cholera toxin (100 ng/mL), and hydrocortisone (500 ng/mL) [33]. The mammary gland breast cancer lines MCF7 and MDA-MB-231 (ATCC HTB-22 and 26, Manassas, VA, USA) were grown in DMEM media (Corning, 29818003, Corning, NY, USA) with 10% FBS (Atlas Biologicals, F-0500-A, Fort Collins, CO, USA) and 1% antibiotic/antimycotic mixture (Millipore Sigma, A5955, Burlington, MA, USA) [34]. All cell lines were grown in a humidified incubator at 5% CO_2 and 37 °C with regular passaging to avoid confluence.

5.6. Protein Extraction and Immunoblotting

Total protein was extracted from frozen cells using RIPA buffer (150 mM NaCl, 5 mM EDTA, 50 Tris-HCl pH 8.0, 1% NP-40, 0.5% Na-catecholate and 0.1% SDS) supplemented with protease inhibitor (PI 87785, Life tech, Carlsbad, CA, USA). Protein concentration was determined according to Bradford (1976) using bovine serum albumin as a standard [35]. Fifty micrograms of total protein were separated by SDS-PAGE, transferred to nitrocellulose membrane by electroblotting as described by [36] and probed with the antibodies specific for the indicated proteins [36]. Actin was used as an internal control for normalization. Antibodies for immunoblot detection of SMYD3 (Rabbit monoclonal antibody to SMYD3, ab183498, Abcam, Cambridge, MA, USA) and β-Actin (A5316-100 UL, Sigma-Aldrich, St. Louis, MO, USA) have been used as the primary antibodies. Bound antibodies on blots were detected by HRP–conjugated secondary antibodies (ab205718, Abcam, Cambridge, MA, USA). Detection was done using Clarity Western ECL Substrate (Bio-Rad, Hercules, MA, USA) and visualized using Image Lab Software (Bio-Rad). Densitometric evaluation was performed by ImageJ software (Version 2.0.0).

5.7. Immunocytochemistry

Exponentially growing cells were fixed with 4% paraformaldehyde for 15 min at room temperature. After PBS wash, cells were permeabilized with 0.1% SDS, 0.5% Triton X-100 in PBS for 10 min at room temperature. 10% goat serum in PBS was used for blocking for 30 min at room temperature. Primary antibody was diluted in 1:300 and treated for 1 h at 37 °C. Secondary antibody (Alexa488 conjugated anti-rabbit IgG) was diluted for 1:500 and treated for 30 min at 37 °C. DAPI in Vectashield antifade solution was used for mounting. The images were capture by Zeiss Axiophot microscope with Qimaging Exi Aqua camera with Qcapture pro software. Blue signal was obtained with 50 millisecond exposure. Green signal was obtained with 200 millisecond exposure. Signals were quantified by densitometry using ImageJ2 software (Version 2.0.0).

5.8. In Vitro Cell Growth Inhibition Assay

Normal and breast cell lines were plated at a density of 20,000 cells/well onto a 6-well plate with different concentrations of Inhibitor-4 and BCI-121. After trypsinization, cell numbers were counted and scored as the number of proliferating cells after treatments at different time points (24, 48, 72 and 96 h) using a Coulter Counter Z2 (Beckman-Coulter Z2 Coulter Particle Count Counter and Size Analyzer, Brea, CA, USA). Data were analyzed and cell doubling time was calculated using GraphPad Prism 6 software (Graph Pad Software, La Jolla, CA, USA) through the exponential growing equation using the exponential growing stage [37].

5.9. Clonogenic Cell Survival

A colony formation assay was used to determine cell sensitivity to SMYD3 inhibitors. The self-renewal and proliferative capacities of cells were measured. To form colonies, cells were seeded onto 6 well plates and were treated with varying concentrations of BCI-121 and Inhibitor-4. The plated cells were incubated in a humidified incubator at 5% CO_2 and 37 °C for two weeks. Then, colonies were fixed with 100% ethanol and allowed to dry for 20 min at room temperature before staining. Colonies were stained using 0.1% crystal violet and allowed to dry before counting. Reproductively viable surviving cells were counted based on the microscopic colonies containing more than 50 cells. From the cell survival fraction, survival curves were drawn using Graph Pad Prism 6 software (Graph Pad Software, La Jolla, CA, USA). At least three independent experiments for each cell line were conducted [38].

5.10. MTT Assay

Cells were plated at a density of 5000 cells/well in 96 well plates. After seeding, cells were treated with the vehicle (DMSO 0.1%, 0.15% and 0.2% *v/v*) or various concentrations of the screening inhibitors. The plated cells were incubated in CO_2 and treated for 24, 48, 72 and 96 h. Then, 10 µL MTT solutions (5 mg/mL) were added to each well followed by a 4 h incubation in CO_2 in the dark. Formazan crystals formed were dissolved in 100 µL of SDS followed by a second 4 h incubation in CO_2. The absorbance was read using a microplate reader (BioTek Instrument, Cytation 5, Winooski, VT, USA). The optical density (OD) of each sample was subtracted from the optical density (OD) of the background and the Formazan standard curve was determined. Cellular viability of all samples was calculated using the ratio of the inhibitor treated-groups versus vehicle-treated group. Graph bars were obtained using GraphPad Prism 6 software (Graph Pad Software, La Jolla, CA, USA) [39].

5.11. Cell Cycle Assay

Cell cycle distributions were analyzed using PI flow cytometry. Cells were plated at density of 5×10^5 cells per well onto 6-well plate. Cells were treated with 200 µM of Inhibitor-4 or BCI-121 and incubated in a humidified incubator at 5% CO_2 and 37 °C for 24 h. Following incubation, detached cells were collected, washed two times with phosphate buffered saline (PBS). Then, cells were fixed with 70% ethanol in PBS overnight at 4 °C. The fixed cells were washed with PBS twice to remove ethanol thoroughly. The cells were resuspended in propidium iodide staining solution consisting of 20 µg/mL propidium iodide and 200 µg/mL RNase in 0.1% Triton X-100. The stained cells were incubated for 15 min in an incubator at 37 °C. DNA contents were measured subsequently using CyAn ADP analyzer flow cytometry (Beckman Coulter, Fort Collins, CO, USA). Each cell line was gated at 10,000 events and the cell cycle distributions were determined using FLOWJO 10.6 software (FlowJo LLC, Ashland, OR, USA) [40].

5.12. Apoptosis Assays

Cell apoptosis was detected using Annexin V, which binds to translocated phosphatidylserine (PS) in the plasma membrane as previously described [41]. Necrosis and late apoptosis were detected using PI to test loss of cell membrane integrity. Briefly, cells were plated and treated with 200 µM of either BCI-121 or Inhibitor-4 for 48 h. Then, the cells were washed with PBS, trypsinized, pelleted, and resuspended in Annexin binding buffer. The cells were stained first with APC Annexin V for 15 min and then with 2.5 µL of PI. The cell mixture was analyzed using a Cytek 4-laser Aurora instrument (Cytek, Fremont, CA, USA). From each sample, a minimum of 3×10^4 events was collected. SpectroFlo software (Cytek, Fremont, CA, USA) was used to analyze the multivariate data. APC Annexin V+/PI+, APC Annexin V-/PI-, APC Annexin V+/PI- or APC Annexin V-/PI+ represented late apoptotic cells, viable cells (intact), early apoptotic cells or necrosis, respectively [42].

In addition to, apoptosis induction by SMYD3 treatments was also assessed using Caspase 3/7 activation. Exponentially growing cells were treated with 200 µL of BC1-121 and Inhibitor-4. After 48 h of incubation, the early apoptosis was measured with the activation of Caspase 3/7 by Caspase-Glo 3/7 kit (Promega, Madison, WI, USA). Glow luminesce of 15,000 cells was measured by Lumat LB9507 (Berthold technologies, Oak Ridge, TN, USA).

5.13. Statistical Analysis

The statistical significance of the results in this study was analyzed using GraphPad Prism 6 software (Graph Pad Software, La Jolla, CA, USA) for two-way ANOVA analysis. p value of less than 0.05 were considered statistically significant for all analyses.

Supplementary Materials: The following are available online at http://www.mdpi.com/1422-0067/21/24/9549/s1, Figure S1: 1H NMR spectra, Figure S2: Clonogenic cell survival curve, Figure S3: Cell viability using MTT assay, Figure S4: The cell cycle distribution, Figure S5: Cell apoptosis.

Author Contributions: I.M.A., D.K.J., H.M.I., D.C.C., T.A.K., and M.A.B. designed the research. I.M.A., D.K.J., Z.A., K.N.H., J.M., A.P., and H.M.I. performed research. I.M.A., D.K.J., Z.A., H.M.I., D.C.C., T.A.K., and M.A.B. analyzed the data. I.M.A., D.K.J., H.M.I., D.C.C., T.A.K., and M.A.B. wrote the manuscript. All authors have read and agreed to the published version of the manuscript.

Funding: Support for this work was provided by NSF Grant 1930417 to MAB.

Acknowledgments: The authors would like to thank the laboratory of Elizabeth P. Ryan at Colorado State University for the contribution of support and resources. The authors would also like to thank the flow cytometry core facility at Colorado State University.

Conflicts of Interest: The authors declare no conflict of interest.

References

1. Brown, M.A.; Sims, R.J.; Gottlieb, P.D.; Tucker, P.W. Identification and characterization of Smyd2: A split SET/MYND domain-containing histone H3 lysine 36-specific methyltransferase that interacts with the Sin3 histone deacetylase complex. *Mol. Cancer* **2006**, *5*, 26. [CrossRef] [PubMed]
2. Gottlieb, P.D.; Pierce, S.A.; Sims, R.J.; Yamagishi, H.; Weihe, E.K.; Harriss, J.V.; Maika, S.D.; Kuziel, W.A.; King, H.L.; Olson, E.N. Bop encodes a muscle-restricted protein containing MYND and SET domains and is essential for cardiac differentiation and morphogenesis. *Nat. Genet.* **2002**, *31*, 25–32. [CrossRef] [PubMed]
3. Hamamoto, R.; Furukawa, Y.; Morita, M.; Iimura, Y.; Silva, F.P.; Li, M.; Yagyu, R.; Nakamura, Y. SMYD3 encodes a histone methyltransferase involved in the proliferation of cancer cells. *Nat. Cell Biol.* **2004**, *6*, 731–740. [CrossRef] [PubMed]
4. Brown, M.A.; Foreman, K.; Harriss, J.; Das, C.; Zhu, L.; Edwards, M.; Shaaban, S.; Tucker, H. C-terminal domain of SMYD3 serves as a unique HSP90-regulated motif in oncogenesis. *Oncotarget* **2015**, *6*, 4005. [CrossRef]
5. Komatsu, S.; Imoto, I.; Tsuda, H.; Kozaki, K.-I.; Muramatsu, T.; Shimada, Y.; Aiko, S.; Yoshizumi, Y.; Ichikawa, D.; Otsuji, E. Overexpression of SMYD2 relates to tumor cell proliferation and malignant outcome of esophageal squamous cell carcinoma. *Carcinogenesis* **2009**, *30*, 1139–1146. [CrossRef]
6. Cock-Rada, A.M.; Medjkane, S.; Janski, N.; Yousfi, N.; Perichon, M.; Chaussepied, M.; Chluba, J.; Langsley, G.; Weitzman, J.B. SMYD3 promotes cancer invasion by epigenetic upregulation of the metalloproteinase MMP-9. *Cancer Res.* **2012**, *72*, 810–820. [CrossRef]
7. Luo, X.-G.; Zhang, C.-L.; Zhao, W.-W.; Liu, Z.-P.; Liu, L.; Mu, A.; Guo, S.; Wang, N.; Zhou, H.; Zhang, T.-C. Histone methyltransferase SMYD3 promotes MRTF-A-mediated transactivation of MYL9 and migration of MCF-7 breast cancer cells. *Cancer Lett.* **2014**, *344*, 129–137. [CrossRef]
8. Hamamoto, R.; Silva, F.P.; Tsuge, M.; Nishidate, T.; Katagiri, T.; Nakamura, Y.; Furukawa, Y. Enhanced SMYD3 expression is essential for the growth of breast cancer cells. *Cancer Sci.* **2006**, *97*, 113–118. [CrossRef]
9. Mazur, P.K.; Reynoird, N.; Khatri, P.; Jansen, P.W.; Wilkinson, A.W.; Liu, S.; Barbash, O.; Van Aller, G.S.; Huddleston, M.; Dhanak, D. SMYD3 links lysine methylation of MAP3K2 to Ras-driven cancer. *Nature* **2014**, *510*, 283–287. [CrossRef]

10. Liu, C.; Fang, X.; Ge, Z.; Jalink, M.; Kyo, S.; Björkholm, M.; Gruber, A.; Sjöberg, J.; Xu, D. The telomerase reverse transcriptase (hTERT) gene is a direct target of the histone methyltransferase SMYD3. *Cancer Res.* **2007**, *67*, 2626–2631. [CrossRef]
11. Zou, J.-N.; Wang, S.-Z.; Yang, J.-S.; Luo, X.-G.; Xie, J.-H.; Xi, T. Knockdown of SMYD3 by RNA interference down-regulates c-Met expression and inhibits cells migration and invasion induced by HGF. *Cancer Lett.* **2009**, *280*, 78–85. [CrossRef] [PubMed]
12. Ren, T.-N.; Wang, J.-S.; He, Y.-M.; Xu, C.-L.; Wang, S.-Z.; Xi, T. Effects of SMYD3 over-expression on cell cycle acceleration and cell proliferation in MDA-MB-231 human breast cancer cells. *Med. Oncol.* **2011**, *28*, 91–98. [CrossRef] [PubMed]
13. Kunizaki, M.; Hamamoto, R.; Silva, F.P.; Yamaguchi, K.; Nagayasu, T.; Shibuya, M.; Nakamura, Y.; Furukawa, Y. The lysine 831 of vascular endothelial growth factor receptor 1 is a novel target of methylation by SMYD3. *Cancer Res.* **2007**, *67*, 10759–10765. [CrossRef]
14. Kim, H.; Heo, K.; Kim, J.H.; Kim, K.; Choi, J.; An, W. Requirement of histone methyltransferase SMYD3 for estrogen receptor-mediated transcription. *J. Biol. Chem.* **2009**, *284*, 19867–19877. [CrossRef]
15. Friesner, R.A.; Murphy, R.B.; Repasky, M.P.; Frye, L.L.; Greenwood, J.R.; Halgren, T.A.; Sanschagrin, P.C.; Mainz, D.T. Extra precision glide: Docking and scoring incorporating a model of hydrophobic enclosure for protein−ligand complexes. *J. Med. Chem.* **2006**, *49*, 6177–6196. [CrossRef] [PubMed]
16. Greenwood, J.R.; Calkins, D.; Sullivan, A.P.; Shelley, J.C. Towards the comprehensive, rapid, and accurate prediction of the favorable tautomeric states of drug-like molecules in aqueous solution. *J. Comput. Aided Mol. Des.* **2010**, *24*, 591–604. [CrossRef] [PubMed]
17. Shelley, J.C.; Cholleti, A.; Frye, L.L.; Greenwood, J.R.; Timlin, M.R.; Uchimaya, M. Epik: A software program for pK a prediction and protonation state generation for drug-like molecules. *J. Comput. Aided Mol. Des.* **2007**, *21*, 681–691. [CrossRef]
18. Liu, L.; Kimball, S.; Liu, H.; Holowatyj, A.; Yang, Z.-Q. Genetic alterations of histone lysine methyltransferases and their significance in breast cancer. *Oncotarget* **2015**, *6*, 2466. [CrossRef]
19. Ma, S.-J.; Liu, Y.-M.; Zhang, Y.-L.; Chen, M.-W.; Cao, W. Correlations of EZH2 and SMYD3 gene polymorphisms with breast cancer susceptibility and prognosis. *Biosci. Rep.* **2018**, 38. [CrossRef]
20. Van Aller, G.S.; Reynoird, N.; Barbash, O.; Huddleston, M.; Liu, S.; Zmoos, A.-F.; McDevitt, P.; Sinnamon, R.; Le, B.; Mas, G. Smyd3 regulates cancer cell phenotypes and catalyzes histone H4 lysine 5 methylation. *Epigenetics* **2012**, *7*, 340–343. [CrossRef]
21. Peserico, A.; Germani, A.; Sanese, P.; Barbosa, A.J.; Di Virgilio, V.; Fittipaldi, R.; Fabini, E.; Bertucci, C.; Varchi, G.; Moyer, M.P. A SMYD3 small-molecule inhibitor impairing cancer cell growth. *J. Cell. Physiol.* **2015**, *230*, 2447–2460. [CrossRef] [PubMed]
22. Huang, L.; Xu, A.-M. SET and MYND domain containing protein 3 in cancer. *Am. J. Transl. Res.* **2017**, *9*, 1. [PubMed]
23. Tsai, C.-H.; Chen, Y.-J.; Yu, C.-J.; Tzeng, S.-R.; Wu, I.-C.; Kuo, W.-H.; Lin, M.-C.; Chan, N.-L.; Wu, K.-J.; Teng, S.-C. SMYD3-mediated H2A. Z. 1 methylation promotes cell cycle and cancer proliferation. *Cancer Res.* **2016**, *76*, 6043–6053. [CrossRef] [PubMed]
24. Jiang, Y.; Lyu, T.; Che, X.; Jia, N.; Li, Q.; Feng, W. Overexpression of SMYD3 in Ovarian Cancer is Associated with Ovarian Cancer Proliferation and Apoptosis via Methylating H3K4 and H4K20. *J. Cancer* **2019**, *10*, 4072. [CrossRef] [PubMed]
25. Deveraux, Q.L.; Reed, J.C. IAP family proteins—Suppressors of apoptosis. *Genes Dev.* **1999**, *13*, 239–252. [CrossRef] [PubMed]
26. Kempkensteffen, C.; Hinz, S.; Christoph, F.; Köllermann, J.; Krause, H.; Schrader, M.; Schostak, M.; Miller, K.; Weikert, S. Expression parameters of the inhibitors of apoptosis cIAP1 and cIAP2 in renal cell carcinomas and their prognostic relevance. *Int. J. Cancer* **2007**, *120*, 1081–1086. [CrossRef]
27. Jänicke, R.U.; Sprengart, M.L.; Wati, M.R.; Porter, A.G. Caspase-3 is required for DNA fragmentation and morphological changes associated with apoptosis. *J. Biol. Chem.* **1998**, *273*, 9357–9360. [CrossRef]
28. Kagawa, S.; Gu, J.; Honda, T.; McDonnell, T.J.; Swisher, S.G.; Roth, J.A.; Fang, B. Deficiency of caspase-3 in MCF7 cells blocks Bax-mediated nuclear fragmentation but not cell death. *Clin. Cancer Res.* **2001**, *7*, 1474–1480.

29. Tewari, M.; Quan, L.T.; O'Rourke, K.; Desnoyers, S.; Zeng, Z.; Beidler, D.R.; Poirier, G.G.; Salvesen, G.S.; Dixit, V.M. Yama/CPP32β, a mammalian homolog of CED-3, is a CrmA-inhibitable protease that cleaves the death substrate poly (ADP-ribose) polymerase. *Cell* **1995**, *81*, 801–809. [CrossRef]
30. Sterling, T.; Irwin, J.J. ZINC 15–ligand discovery for everyone. *J. Chem. Inf. Modeling* **2015**, *55*, 2324–2337. [CrossRef]
31. Fu, W.; Liu, N.; Qiao, Q.; Wang, M.; Min, J.; Zhu, B.; Xu, R.-M.; Yang, N. Structural basis for substrate preference of SMYD3, a SET domain-containing protein lysine methyltransferase. *J. Biol. Chem.* **2016**, *291*, 9173–9180. [CrossRef] [PubMed]
32. Koehn, J.T.; Magallanes, E.S.; Peters, B.J.; Beuning, C.N.; Haase, A.A.; Zhu, M.J.; Rithner, C.D.; Crick, D.C.; Crans, D.C. A synthetic isoprenoid lipoquinone, menaquinone-2, adopts a folded conformation in solution and at a model membrane interface. *J. Org. Chem.* **2017**, *83*, 275–288. [CrossRef] [PubMed]
33. Debnath, J.; Muthuswamy, S.K.; Brugge, J.S. Morphogenesis and oncogenesis of MCF-10A mammary epithelial acini grown in three-dimensional basement membrane cultures. *Methods* **2003**, *30*, 256–268. [CrossRef]
34. Roger, S.; Besson, P.; Le Guennec, J.-Y. Involvement of a novel fast inward sodium current in the invasion capacity of a breast cancer cell line. *Biochim. Biophys. Acta BBA Biomembr.* **2003**, *1616*, 107–111. [CrossRef]
35. Bradford, M.M. A rapid and sensitive method for the quantitation of microgram quantities of protein utilizing the principle of protein-dye binding. *Anal. Biochem.* **1976**, *72*, 248–254. [CrossRef]
36. Chiacchiera, F.; Matrone, A.; Ferrari, E.; Ingravallo, G.; Sasso, G.L.; Murzilli, S.; Petruzzelli, M.; Salvatore, L.; Moschetta, A.; Simone, C. p38 α blockade inhibits colorectal cancer growth in vivo by inducing a switch from HIF1 α-to FoxO-dependent transcription. *Cell Death Differ.* **2009**, *16*, 1203–1214. [CrossRef]
37. Maeda, J.; Yurkon, C.R.; Fujisawa, H.; Kaneko, M.; Genet, S.C.; Roybal, E.J.; Rota, G.W.; Saffer, E.R.; Rose, B.J.; Hanneman, W.H. Genomic instability and telomere fusion of canine osteosarcoma cells. *PLoS ONE* **2012**, *7*, e43355. [CrossRef]
38. Kato, T.A.; Okayasu, R.; Bedford, J.S. Signatures of DNA double strand breaks produced in irradiated G1 and G2 cells persist into mitosis. *J. Cell. Physiol.* **2009**, *219*, 760–765. [CrossRef]
39. Van Meerloo, J.; Kaspers, G.J.; Cloos, J. Cell sensitivity assays: The MTT assay. In *Cancer Cell Culture*; Springer: Berlin/Heidelberg, Germany, 2011; pp. 237–245.
40. Krishan, A. Rapid flow cytofluorometric analysis of mammalian cell cycle by propidium iodide staining. *J. Cell Biol.* **1975**, *66*, 188–193. [CrossRef]
41. Vermes, I.; Haanen, C.; Steffens-Nakken, H.; Reutellingsperger, C. A novel assay for apoptosis flow cytometric detection of phosphatidylserine expression on early apoptotic cells using fluorescein labelled annexin V. *J. Immunol. Methods* **1995**, *184*, 39–51. [CrossRef]
42. Aubry, J.P.; Blaecke, A.; Lecoanet-Henchoz, S.; Jeannin, P.; Herbault, N.; Caron, G.; Moine, V.; Bonnefoy, J.Y. Annexin V used for measuring apoptosis in the early events of cellular cytotoxicity. *Cytom. J. Int. Soc. Anal. Cytol.* **1999**, *37*, 197–204. [CrossRef]